INFORMATION TO USERS

This manuscript has been reproduced from the microfilm master. UMI films the text directly from the original or copy submitted. Thus, some thesis and dissertation copies are in typewriter face, while others may be from any type of computer printer.

The quality of this reproduction is dependent upon the quality of the copy submitted. Broken or indistinct print, colored or poor quality illustrations and photographs, print bleedthrough, substandard margins, and improper alignment can adversely affect reproduction.

In the unlikely event that the author did not send UMI a complete manuscript and there are missing pages, these will be noted. Also, if unauthorized copyright material had to be removed, a note will indicate the deletion.

Oversize materials (e.g., maps, drawings, charts) are reproduced by sectioning the original, beginning at the upper left-hand corner and continuing from left to right in equal sections with small overlaps.

Photographs included in the original manuscript have been reproduced xerographically in this copy. Higher quality 6" x 9" black and white photographic prints are available for any photographs or illustrations appearing in this copy for an additional charge. Contact UMI directly to order.

Bell & Howell Information and Learning
300 North Zeeb Road, Ann Arbor, MI 48106-1346 USA
800-521-0600

Sub-seasonal wind variability and El Niño

by

Gabriel Andrés Vecchi

A dissertation submitted in partial fulfillment of the
requirements for the degree of

Doctor of Philosophy

University of Washington

2000

Program Authorized to Offer Degree: School of Oceanography

UMI Number: 9976078

Bell & Howell Information and Learning Company
300 North Zeeb Road
P.O. Box 1346
Ann Arbor, MI 48106-1346

Doctoral Dissertation

In presenting this dissertation in partial fulfillment of the requirements for the Doctoral degree at the University of Washington, I agree that the Library shall make its copies freely available for inspection. I further agree that extensive copying of the dissertation is allowable only for scholarly purposes, consistent with "fair use" as prescribed in the U.S. Copyright Law. Requests for copying and reproduction of this dissertation may be referred to Bell and Howell Information and Learning, 300 North Zeed Road, P.O. Box 1346, Ann Arbor, MI 48106-1346, or to the author.

Signature 

Date April 25, 2000

University of Washington
Graduate School

This is to certify that I have examined this copy of a doctoral dissertation by

Gabriel Andrés Vecchi

and have found that it is complete and satisfactory in all respects,
and that any and all revisions required by the final
examining committee have been made.

Chair of Supervisory Committee:

Don E. Harrison

Reading Committee:

Mitsuhiro Kawase

Luanne Thompson

Date: April 25, 2000

University of Washington

Abstract

Sub-seasonal wind variability and El Niño

by Gabriel Andrés Vecchi

Chairperson of the Supervisory Committee

Affiliate Professor D.E. Harrison
School of Oceanography

The role of sub-seasonal western and central Pacific surface zonal wind variability in the evolution of El Niño sea surface temperature anomaly (SSTA) is examined. The surface wind structure and atmospheric convection variability of tropical Pacific westerly wind events (WWEs) is described. The average tropical Pacific SSTA variability following and in the absence of equatorial WWEs is examined over the period 1986-1998. The surface wind structure of the Madden-Julian Oscillation is examined (MJO), along with relationships between the MJO and WWEs. The response of an ocean general circulation model (OGCM) to composite MJO and WWE surface wind stress forcing is explored.

WWEs can be classified into eight types based on the location of the maximum zonal wind anomalies. WWEs are found to be compact in space and time, exhibiting little translation during their lifetime. Typical scales for WWEs are derived over the period 1986-1995. It is found that certain WWE types exhibit significant seasonality, and some have a significant correlation with the Troup Southern Oscillation Index.

In the absence of equatorial WWEs, tropical Pacific SSTA tends to remain at or return towards climatology. Following equatorial WWEs, tropical Pacific SSTA warms towards or remains at El Niño type conditions.

WWEs are significantly associated with atmospheric convection. The MJO surface wind stress anomaly fields exhibit two regimes in the equatorial Pacific. In the western equatorial Pacific there are both easterly and westerly anomalies with the westerlies dominating, in the central and eastern equatorial Pacific the main anomalies are easterlies. The WWEs which occur during the MJO are modulated by the convective variability of the MJO. West-of-dateline WWEs exhibit a strong relationship to tropical cyclone activity.

Following a composite MJO, the tropical Pacific SSTA in the OGCM does not tend to warm; the composite MJO does not provide a simple mechanism for El Niño waveguide warming. Idealized WWEs drove tropical Pacific SSTA warming in the OGCM; enhanced WWE activity provides a mechanism for the onset of El Niño.

TABLE OF CONTENTS

LIST OF FIGURES

LIST OF TABLES

DEDICATION

I dedicate this dissertation to my grandparents: Anne Kosikowski Hudak, Maria Angela Vecchi Pantaleoni, Frank Kosikowski and Carlo Vecchi.

ACKNOWLEDGMENTS

I would like to thank the following for their help and encouragement during the completion of the work in this dissertation:

My family.

My thesis advisor:
Ed Harrison.

My advisory committee:
Marshall Baker, Mitsuhiro Kawase, Jim Murray and Luanne Thompson.

The TMAP group at NOAA/PMEL:
Steve Hankin, Kevin O'Brien, Joe Sirott, Jonathan Callahan, Ansley Manke, Sim Larkin, Jerry Davison, David McDermott, Harilaos Loukos, and Rick Romea.

Meghan Cronin, Greg Johnson, Dennis Moore, Jody Klymak, Weimin Wang, Eric Maloney, Zuojun Yu, Billy Kessler, Chidong Zhang, Mike McPhaden, Dai McClurg and Linda Mangum.

Della Rogers.

Vallapha Cass.

Jen Jungfleisch, Doug Jongeward, Rob Stewart and Ryan Whitney without whom this would have been written by hand.

Ferret analysis and visiualization package. (*http://wrc.pmel.noaa.gov/~ferret/*)

Sebastian the Dog.

Chapter I:
Introduction and Summary

The tropical Pacific coupled ocean/atmosphere system exhibits large-scale variability on both the seasonal and interannual timescales. The primary mode of tropical Pacific interannual variability is related to the El Niño/Southern Oscillation (ENSO) phenomenon (Weare et al. 1976, Rasmusson and Carpenter 1982, Cane 1983, Harrison and Larkin 1996, 1998.a). The ENSO phenomenon is associated with large-scale changes on local biological productivity (Barber and Chavez 1983, Chavez *et al.* 1998) and global weather patterns (Donguy and Henin 1980, Rasmusson and Wallace 1983, Nicholls and Kariko 1993, Harrison and Larkin 1998.b). The air-sea interactions that bring about El Niño equatorial Pacific sea surface temperature (SST) changes are the focus of much interest at present (See the special issue of Journal of Geophysical Research (1998) for reviews on the range of recent El Niño research); understanding of these coupled mechanisms is essential to improving our understanding and prediction of El Niño. Ever since Wyrtki (1975) suggested that a collapse of the easterly trade winds led to the onset of El Niño warming, there has been interest in the types of atmospheric forcing that can cause this warming. I here examine the roles of two modes of sub-seasonal surface wind variability - the Madden-Julian Oscillation and westerly wind events - on the evolution of El Niño SST anomalies (SSTA).

Since Bjerknes (1961, 1966, 1969) suggested that the atmospheric circulation changes known as the Southern-Oscillation, and the central and eastern Pacific SST changes known as El Niño were fundamentally related, there has been much work in developing a dynamical framework to understand the two phenomena and their coupling. At present there are two main paradigms of the evolution of coupled ENSO system, one viewing the system as deterministic the other as fundamentally stochastic. One paradigm involves deterministic evolution of coupled ocean/atmosphere anomaly modes, as in the "Delayed-Oscillator"

theory (*e.g.* Battisti 1988, Schopf and Suarez 1988 , Suarez and Schopf 1988, Battisti and Hirst 1989, Neelin *et al.* 1998) or the model of Cane and Zebiak (1985). The view that ENSO results from stochastic forcing in the tropical Pacific has been developed more recently (Penland and Magorian 1993, Penland and Sardeshmukh 1995, Penland *et al.* 1995, Thompson and Battisti 2000). There have been suggestions that seasonal and higher frequency wind variability, particularly "sub-seasonal" wind variability, is fundamental to the evolution of the ENSO cycle (Keen 1982, Lau and Chan 1986, 1988, Harrison and Giese 1988, Giese and Harrison 1990, 1991, Weickman 1991, Kessler *et al.* 1995, Harrison and Vecchi 1999, Moore and Kleeman 1999, Vecchi and Harrison 2000)

The spectrum of western and central equatorial Pacific surface winds is distinctive, with about half the zonal wind variability occurring in the sub-seasonal period band (Harrison and Luther 1990). Within the sub-seasonal band close to two thirds the variance is in periods between 3 and 30 days and about one third in periods between 30 and 90 days (Harrison and Luther 1990). At the high frequency end of the sub-seasonal band, pulses of equatorial westerly wind anomaly (westerly wind events or WWEs; Luther *et al.* 1983, Harrison and Giese 1991, Hartten 1996, Harrison and Vecchi 1997) have been suggested as a mechanism for the onset of El Niño waveguide warm anomalies. Ocean general circulation model (OGCM) experiments have suggested that equatorial WWEs can drive El Niño eastern and central equatorial Pacific SST changes (Harrison and Giese 1988, Giese and Harrison 1990, 1991).

It has also been suggested that 30-90 day surface wind variability in the western and central Pacific, driven by the Madden-Julian Oscillation (MJO; see Madden and Julian 1994 for a review), may be important to the onset of waveguide SST warming during El Niño (Lau and Chan 1986, 1988, Lau and Shen 1988, Weickman 1991, Kessler *et al.* 1995, Moore and Kleeman 1999). The MJO is the dominant mode of sub-seasonal tropospheric wind variability over the tropical Indian and Pacific oceans, having a characteristic east-

ward propagating signal in free-tropospheric winds and convection (e.g. Madden and Julian, 1972, 1994, Rui and Wang 1991, Hendon and Salby 1994, Maloney and Hartmann 1998). Interestingly, no correlation has been found between MJO activity indicators and El Niño indices (Slingo et al. 1999, Hendon *et al.* 2000, Harrison and Vecchi 2000).

The air-sea interactions which bring about the termination of El Niño are also of interest. Prior to the return of SST to normal at the end of recent El Niño events, there has been a shoaling of the eastern equatorial Pacific thermocline to normal or shallower than normal depths (Harrison et al. 1990, Kessler and McPhaden 1995, Harrison and Vecchi 1999, 2000, McPhaden 1999, McPhaden and Yu 1999). This thermocline shoaling might be due to "delayed-oscillator" type mechanisms (see Suarez and Schopf 1988, Battisti and Hirst 1989, Neelin et al. 1998), or to the interaction of the seasonal cycle with anomalous El Niño conditions (Harrison and Vecchi 1999), or a combined effect of the two. The shoaling of the thermocline at the end of recent El Niño events pre-conditioned the termination of El Niño, by making cool water available to be upwelled into the surface layer by equatorial easterly winds (Harrison et al. 1990, Kessler and McPhaden 1995, McPhaden 1999, McPhaden and Yu 1999). In weak El Niño events, such as 1986-8 and 1991-2, weakened easterly trades were present through the event; these easterly winds quickly cool the surface once the thermocline shoals and makes the cool water available (Kessler and McPhaden 1995). In strong El Niño events, such as 1982-3 and 1997-8, the easterly trades completely disappear; though the thermocline has shoaled for months, the surface does not cool until the return of easterlies of enough strength to upwell the cool water (Harrison et al. 1990, McPhaden 1999, McPhaden and Yu 1999, Takayabu et al. 1999). Takayabu et al. (1999) suggest that easterly winds in the eastern and central Pacific, driven by the passage of an MJO event in May 1998, resulted in the termination of the 1997-8 El Niño event.

In the chapters that follow I examine the role of sub-seasonal wind variability in the evolution of El Niño. I develop the roles of WWEs and the MJO on the evolution of El Niño

SSTA changes by: examining the surface wind structure of the two phenomena, analyzing statistical relationships to test recent suggestions that WWEs are the surface expression of the MJO, exploring the relationships the phenomena exhibit with El Niño waveguide warming, and finally by forcing an OGCM with the characteristic zonal stress fields of equatorial WWEs and the MJO to determine mechanisms for their role in El Niño.

In Chapter II, I examine the surface wind (x,y,t) structure of WWEs using a compositing technique, and the European Centre for Medium Range Weather Forecasts (ECMWF) 12-hourly gridded operational surface wind analysis (ECMWF 1989). I also examine the seasonal and inter-annual distribution of WWEs, and some relationships of WWEs to each other. I am able to classify WWEs into eight types based on the location of the maximum surface westerly wind anomalies, and derive a quantitative definition for a WWE based on the classifying scheme. Using the classifying scheme, I generate composites of surface wind anomaly for each of the WWE types, and find that the zonal wind anomalies of each type are compact in space and time, exhibiting little translation during the lifetime of the event. I model the WWE zonal wind anomaly field using a Gaussian structure in space and time, and derive characteristic scales for each event. WWEs have an average duration between 5.5 and 7 days, an average zonal width of roughly 30° longitude, and an average meridional width close to 10°. Equatorial WWEs display a statistically significant inter-annual correlation with the Troup Southern Oscillation Index (normalized sea level pressure difference at Darwin minus Tahiti; Troup-SOI), adding to the suggestion of a relationship between equatorial WWE types and El Niño.

In Chapter III, I build upon the WWE identification scheme developed in Chapter II, and use a compositing technique to examine the evolution of SSTA following equatorial WWEs. I begin by examining the evolution of SSTA in the absence of WWEs, and find that, in the absence of equatorial WWEs, tropical Pacific SST tends towards climatology. I examine the evolution of SSTA following WWEs separately for periods of warm eastern equa-

torial Pacific SST and periods of near-normal eastern equatorial Pacific SST. Following equatorial WWEs, the eastern equatorial Pacific SST tends to warm (when SST initially close to climatology) or tends to remain warmer than normal (when ST initially warmer than normal). These results suggest that equatorial WWEs are a fundamental mechanism for El Niño warming and maintenance.

In Chapter IV, I explore the convective and surface wind anomaly fields associated with WWEs and with the MJO. The composite wind anomaly fields associated with the MJO do not much resemble the idealized structures generally used to discuss their role in ENSO. The MJO surface wind anomaly field in the equatorial Pacific extend beyond the convective regime over the western Pacific warm pool. Models of the role of the MJO in El Niño waveguide warming developed using anomalies confined to the western equatorial Pacific are not consistent with these composite results.

WWEs tend to be convective features, however they do not resemble any single atmospheric mode of variability. WWEs of most types which occur during the MJO are modulated by the convective variability associated with the MJO. Less than half of all WWEs occur during the westerly phases of the MJO, and many MJO events do not have any WWEs associated with them. Tropical cyclones are strongly associated with west-of-dateline WWEs: the westernmost WWE Types (those west of 150°E) are associated with tropical cyclones over 90% of the time, the WWE Types occurring between the Dateline and 150°W are associated with tropical cyclones over 60% of the time.WWEs are associated with a variety of large-scale circulation structures, and are not the surface expression of any one mode of atmospheric variability.

In Chapter V, I use an OGCM to attempt to and reproduce the statistical associations between sub-seasonal surface wind variability and tropical Pacific SSTA. The composite MJO developed here does not provide a mechanism for equatorial Pacific waveguide warming in the onset of El Niño events. Because the MJO is associated with both easterlies and

westerlies, it provides a potential mechanism for the return of normal SST at the end of major El Niño events (such as 1982-3 and 1997-8).

Experiments using the realistic zonal scales of WWEs qualitatively reproduce the results of Harrison and Giese (1988) and Giese and Harrison (1990,1991). Multiple WWEs reproduce much of the composite SSTA changes following WWEs; individual WWEs do not reproduce the composite SSTA changes. Sequential equatorial WWEs provide a mechanism for the onset and maintenance of El Niño. The OGCM, without atmospheric coupling, is unable to reproduce the aplitude of the composite SSTA changes following WWEs.

Sub-seasonal surface zonal wind variability over the tropical Pacific is a component of the ocean/atmosphere interactions which bring about El Niño SSTA changes. Equatorial WWEs are been a mechanism for the onset and maintenance of warm El Niño SST. Central and eastern equatorial Pacific zonal wind variability related to the MJO provides a mechanism for the return of SST to normal at the end of major El Niño events. Improved understanding of the various modes of sub-seasonal wind variability, including WWEs, the MJO, tropical cyclones, mid-latitude cold surges and convective super-clusters, and of the interactions between these modes of sub-seasonal variability and the tropical Pacific circulation, will lead to improved understanding and predictability of the ENSO cycle.

Chapter II:
Surface structure of westerly wind events.

II.1. Introduction

In this chapter I explore the spatial and temporal characteristics of westerly wind events (WWEs) over the Western and Central Tropical Pacific Ocean, from 1986 through 1995. This work has been described in Harrison and Vecchi (1997), with Vecchi and Harrison (1997) serving as a complementary Technical Memorandum containing a comprehensive set of figures and tables which detail all the results. The results outlined here are the first rigorous statistical analysis of the 3-D space-time evolution of WWEs. These results, especially the WWE classification and definition scheme, are the main foundation upon which the rest of the work described in this Dissertation builds.

WWEs are a dominant mode of the sub-seasonal surface wind variability over the tropical Pacific Ocean (Luther *et al.* 1983, Harrison and Luther 1990) characterized by large amplitude (10-20 ms^{-1}), short timescale (6-20 day) westerly wind anomalies in a system where the main surface wind anomalies are weak easterlies throughout most of the time (ie. the distribution of surface wind anomaly is skewed). There have been detailed descriptions of the evolution of the wind fields during individual WWE periods (*e.g.* Keen 1982, Love 1985a, Eldin *et al.* 1994, Chen and Houze 1995, Lin and Johnson 1996), however it is important to develop a view of the mean characteristics of WWEs for any general discussion. Harrison and Giese (1991) used 30 years of near-dateline island wind data to develop a description of the meridional-time structure of WWEs which occur near the dateline. Due to the limited zonal extent of the islands, Harrison and Giese (1991) were unable to describe the zonal scales of the WWEs, nor determine whether these WWEs exhibited zonal translation during their lifetime. Hartten (1996) used the U.S. Navy NOGAPS operational surface wind product to described the surface wind characteristics of west-of-dateline westerly wind

bursts. Hartten (1996) developed a subjective classification scheme for westerly wind bursts based on the circulation patterns of the westerly wind bursts; 90% of the westerly wind bursts in the period 1985-1994 fit into the 9 categories. However, the subjective nature of the classification scheme did not lend itself to rigorous statistical analysis of the data. It has been noted that there is a significant tendency for near-Dateline WWEs to be associated preferentially with warm El Niño-Southern Oscillation (ENSO) periods and with particular seasons (Luther *et al.* 1983, Harrison and Giese 1991, Hartten 1996).

The purpose of this work was to use the European Centre for Medium Range Weather Forecasts (ECMWF) operational surface wind analysis for the years 1986-1995 to develop a 3-D (latitude, longitude and time) characterization of WWEs. Since the early-1980s, the operational surface wind analysis product of the ECMWF has improved considerably; after extensive analysis of the ECMWF data I consider it to be plausible enough after 1986 to use as my surface wind dataset. Using the global gridded ECMWF operational wind data, the structure and existence of WWEs beyond the dateline could be explored, and tendencies for WWEs to translate could be determined.

I determined that it was possible to classify the WWEs into eight types based on the location of the maximum zonal wind anomalies of the WWEs. Using this classification scheme, an unambiguous WWE definition was developed, and intensity measures defined. Using the WWEs identified in the record, the composite surface wind fields were evaluated for each type of WWE. Using the composite wind fields as a guide, I developed a simple analytical model to further summarize the basic properties of each type of event. The TOGA-COARE Intensive Observation Period (November 1992 through February 1993) was used to test the applicability of the composite model to individual wind events. Finally, the temporal distribution was studied on monthly and inter-annual time scales of both the frequency and intensity of the WWEs.

In the following sections I describe the main results of the analysis of the surface

wind strunture of WWEs for the period 1986-1995. Section II.2 describes the data sets used; Section II.3 describes the classification scheme and the compositing technique used in this study. The composite results are presented and a simple mathematical model structure for these composite WWEs is described in Section II.4. The westerly wind variability during the TOGA-COARE Intense Observation Period and the ability of the composite events to characterize the IOP variability is presented in Section II.5. Section II.6 discusses the seasonal and inter-annual distribution of WWEs and their correlation with the Southern Oscillation Index, and describes the extent to which WWEs occur in particular sequences. Section II.7 offers some summary and discussion.

I.2. Data

The wind data set used is the ECMWF 10-m operational 12 hourly wind analysis, on their 2.5°x2.5°global grid. Attention was on the region from 100°E to 100°W, by 30°S to 30°N and over the years 1986-1995. The ECMWF analysis was significantly improved in the middle 1980s, hence the choice of 1986 for the beginning of this analysis effort. A monthly climatology was constructed from the 12-hourly ECMWF surface wind analysis of the entire ten years of record (1986-1995), using a time axis centered on the mid-day of each month. Anomalies were defined as the difference between the instantaneous wind and the climatology, linearly interpolated in time.

In order to assess the utility of the ECMWF 10m wind field, two comparisons were carried out. First the large time and space scale aspects of the circulation were determined by comparing the ECMWF monthly climatology to the COADS monthly climatology of ship observations from 1946 through 1993 (Woodruff *et al.* 1987). Then, to examine the short time scale variability, ECMWF time series is compared with data from the TOGA-TAO buoys (McPhaden 1993).

To summarize the results of comparing the ECMWF climatology with the COADS

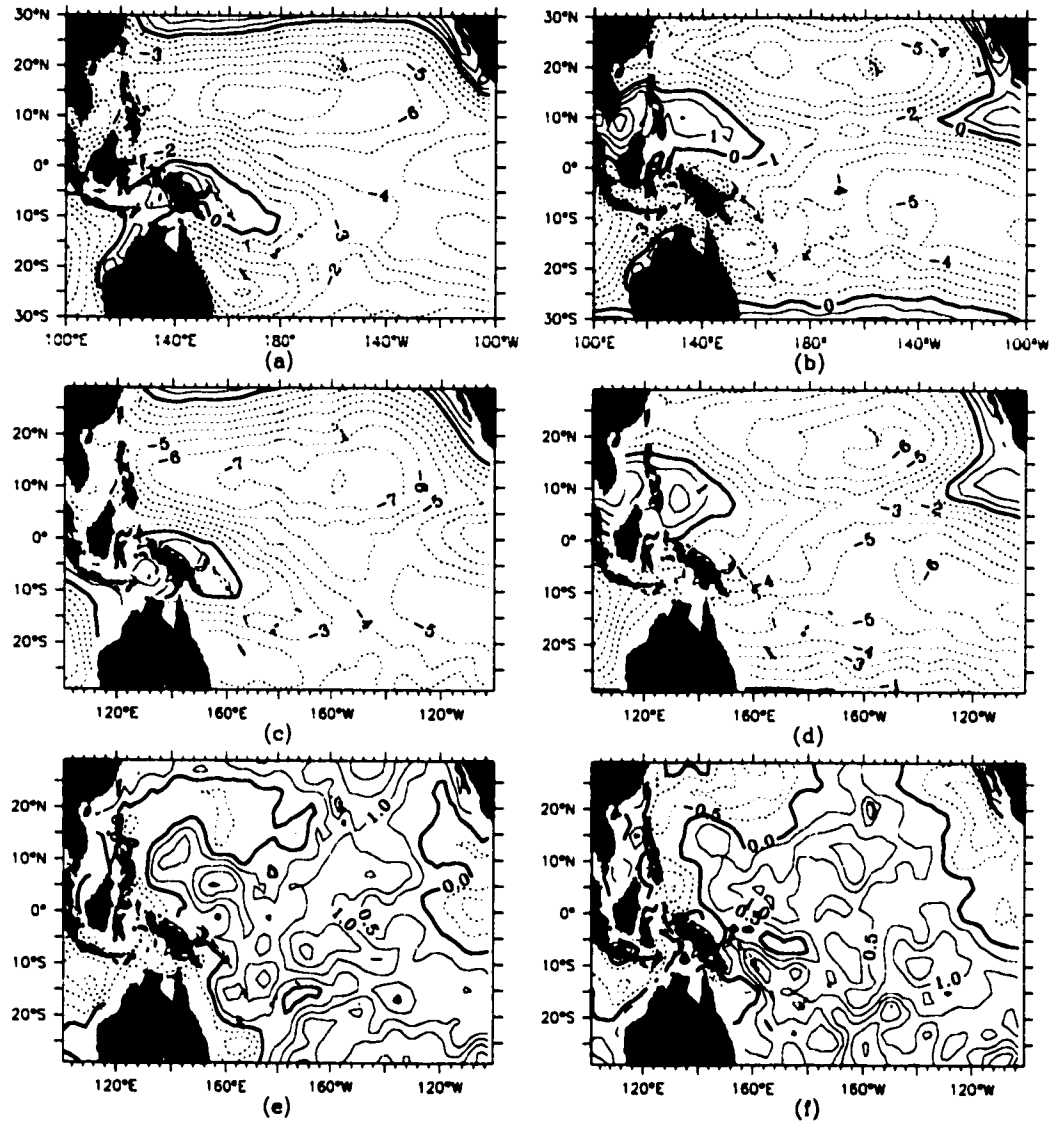

Figure II.1. Contours of (a) March and (b) September 10-m climatological zonal wind from ECMWF (1986-1995), (c) March and (d) September 10-m climatological zonal wind from COADS (1946-93), and (e) March and (f) September difference (ECMWF-COADS) 10-m climatological zonal wind. Dashed contours indicate negative values. COADS climatology data is smoothed using a five-point triangle filter in the zonal direction and a three-point triangle filter in the meridional direction. Contour interval is 1.0 ms^{-1} for (a)-(d), and 0.5 ms^{-1} for (e)-(f).

climatology, the wind data are shown for March and September (Figures II.1-.3). Contour plots are shown for the ECMWF climatology from 1986 through 1995, for the COADS climatology from 1946 through 1993 and for the difference ECMWF - COADS, for zonal wind (Figure II.1), meridional wind (Figure II.2) and wind divergence (Figure II.3). For all these plots the COADS climatology is smoothed with a 5-point triangle filter (half power

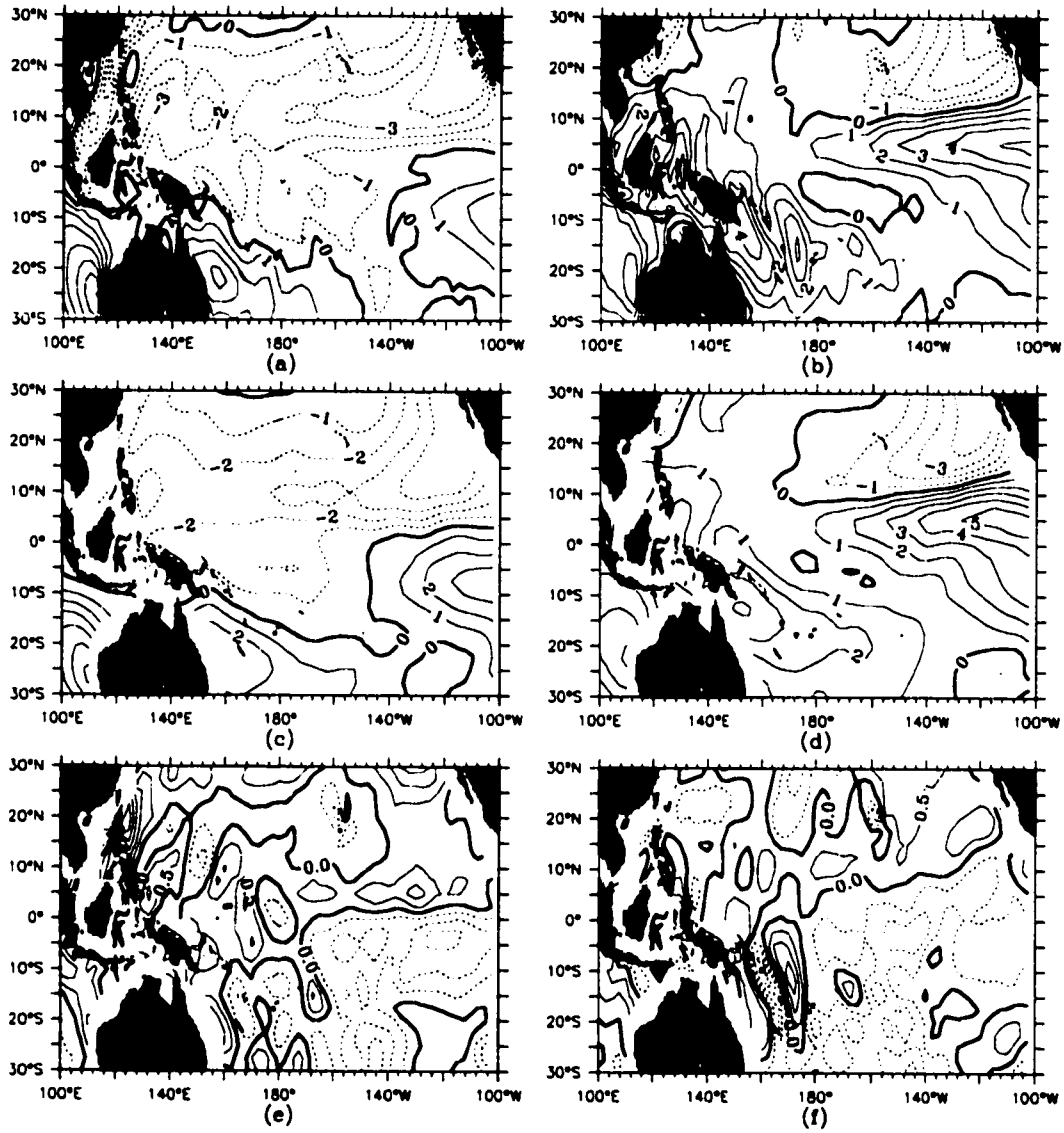

Figure II.2. Same as Figure 1, except for 10-m meridional wind.

point at 18°) in the zonal direction and a 3-point triangle smoother (half power point at 11°) in the meridional direction.

The ECMWF climatology reproduces the main aspects of the large scale circulation appropriately (Figures II.1, .2). The zonal wind cores of the SE and NE trade winds are clear in Figure II.1, and their magnitudes are comparable to the ship-based winds of COADS. The small area of western Pacific equatorial westerlies in March, and the comparable band of westerlies from SE Asia to 160°W along 10°N in September are present in the ECMWF

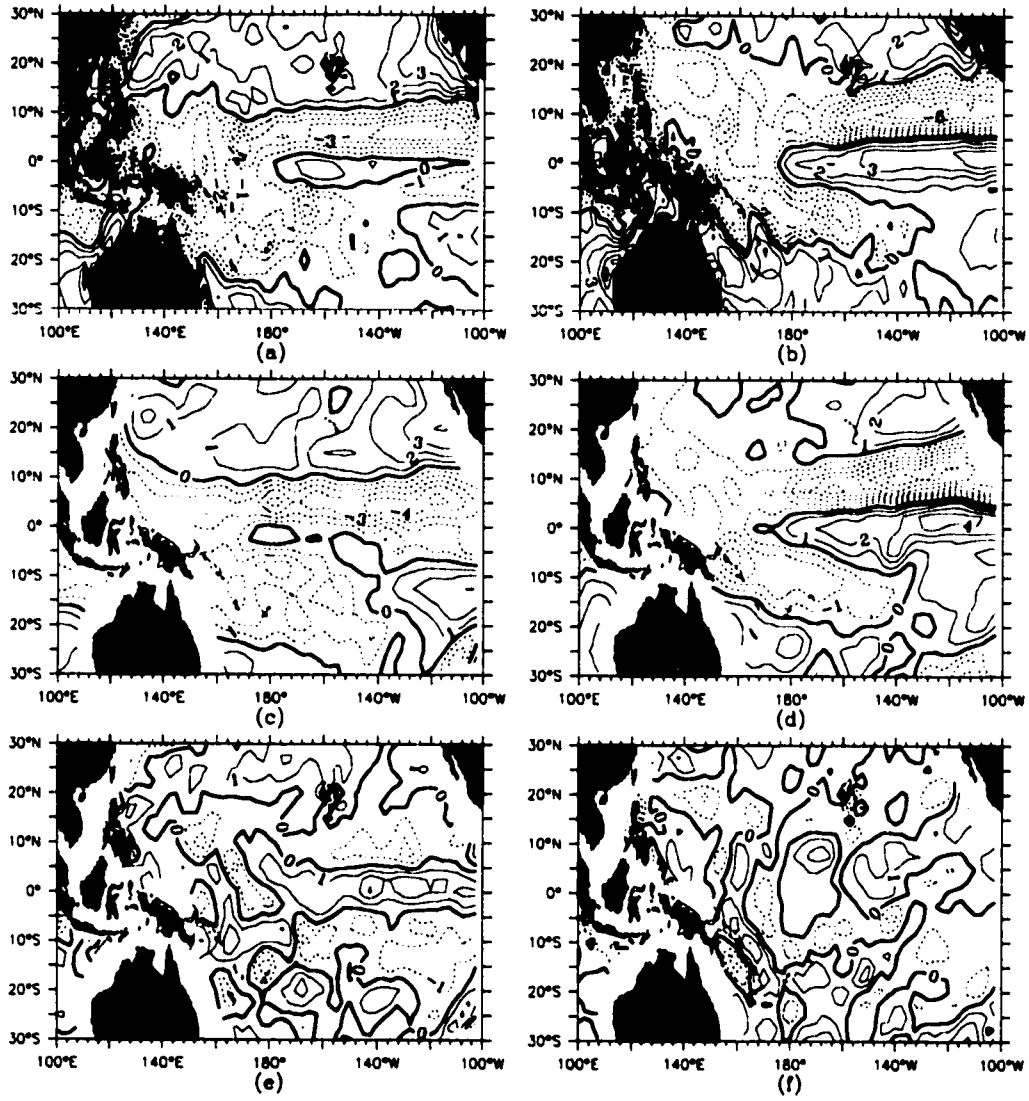

Figure II.3. Same as Figure 1, except for 10-m wind divergence. Contour interval is 10^{-6} s.

fields. The difference fields of zonal wind (Figure II.1-e,f) show considerable spatial structure, but the large scale difference is seldom more than 1.5ms^{-1} and is typically closer to 1ms^{-1}. Near the equator ECMWF winds tend to be weaker (less easterly) than the COADS winds west of 120°W and stronger (more easterly) east of 120°W. The SE trades tend to be weaker (less easterly) in ECMWF, but the NE trades are some places weaker and others stronger in ECMWF. The meridional wind comparisons of Figure II.2 also show considerable large scale similarity. The strong seasonal variations between 10°S and 15°N east of

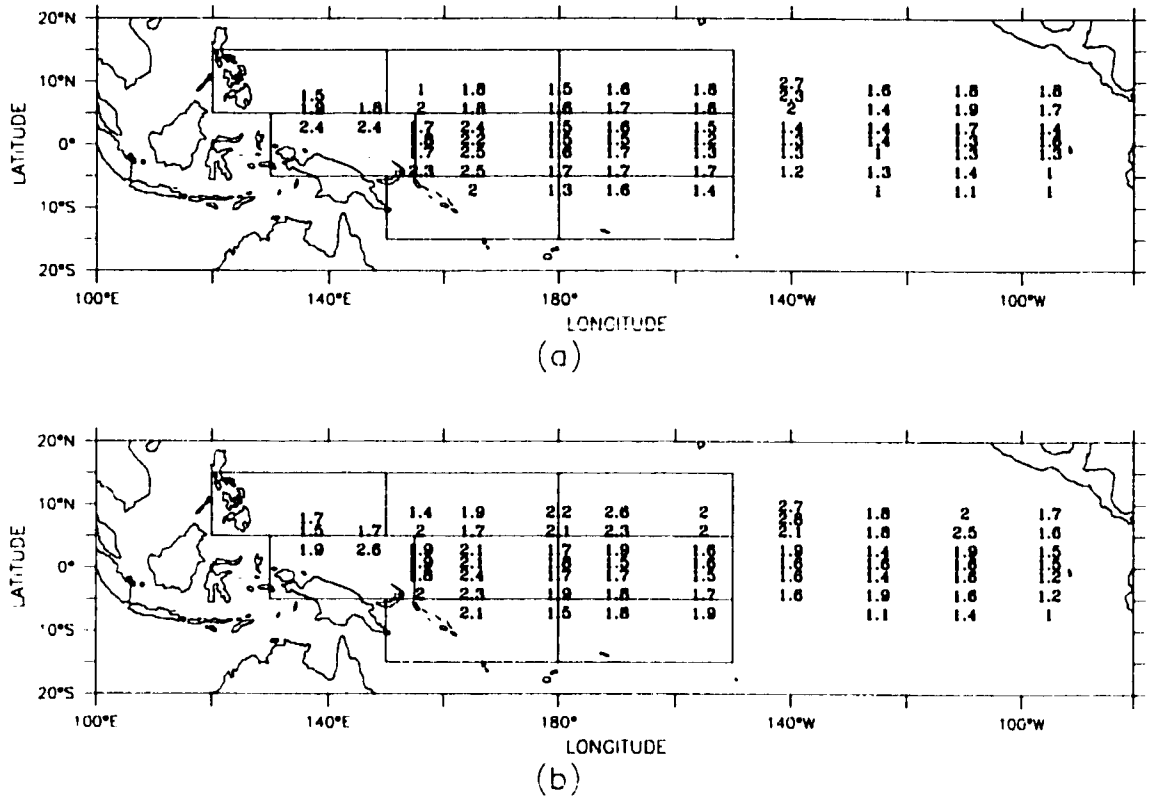

Figure II.4. Values of the rms difference (TAO-ECMWF) at selected TAO buoy locations for daily (a) surface zonal wind and (b) surface meridional wind. Units are ms^{-1}. The time period over which TAO data are available varies for each buoy. Supperimposed are the outlines of the WWE classifying regions.

the Dateline are well reproduced, as is the broad area of southerly wind east of Australia. However, there is much small space scale structure in ECMWF in the western tropical Pacific that has no counterpart in the COADS climatology. This is particularly evident in the meridional wind difference results (Figure II.2-e,f). The large scale meridional wind differences are typically less than $1ms^{-1}$, but NE of Australia they can exceed $1.5ms^{-1}$. The ECMWF climatology in general overestimates the meridional wind speed north of the Inter Tropical Convergence Zone (ITCZ) and underestimates it to the south, compared to COADS.

It is possible that the generally weaker near-equatorial easterlies in ECMWF result from their being a recent average, over a period in which ENSO conditions have been prominent. I have not pursued this possibility, because I judge the differences found here to be small enough to be of little concern for the topic of interest. WWEs typically have peak

zonal wind anomalies in excess of 10 ms^{-1} over a large area, so a 2 ms^{-1} difference is does not significantly affect the analysis or its main conclusions.

Another measure of the large scale aspects of the ECMWF analysis is the monthly mean divergence field. The March and September divergence patterns for the ECMWF and COADS climatologies are compared in Figure II.3. The two climatologies have similar divergence patterns, with maximum convergence in the ITCZ and the South Pacific Convergence Zone (SPCZ). Generally the location and meridional scale of each convergence zone are similar, but the ECMWF convergence is substantially weaker than COADS. The divergence patterns along the equator are rather different in March, with ECMWF indicating a clear band of divergence from the Dateline to about 110°W, but with COADS indicating a broad area of weak equatorial convergence east of 140°W. There are no large scale differences in the central and western tropical Pacific sufficient to merit concern.

The RMS difference between the daily averaged ECMWF wind analysis, interpolated to each buoy location (when necessary), and the daily averaged TAO buoy winds were computed. No trends were removed. Note that the period over which it was possible to compute the RMS difference varies from buoy to buoy, so there can be significant change from one buoy to another. The buoys along 110°W, 140°W and 165°E had the longest time series; other buoys had data for as little as a year, because they were recently deployed. The results for a large sampling of the buoys are presented in Figure II.4. Overall, the zonal and meridional wind results were comparable. Maximum RMS differences were about 2.5 ms^{-1} and minimum differences about 1ms^{-1}. The largest values tended to be in the ITCZ and SPCZ regions, although the differences along 165°E were 2 ms^{-1} or more from 5°N to 9°S. The smallest values tended to be in the eastern south-easterly trade winds.

The implication of these values comes following comparison with the magnitude of the WWE signal (which I later shall show is 8 to 20 ms^{-1}) and with the accuracy of the TAO measurement. The wind sensors themselves are claimed to be accurate to about 0.2 ms^{-1}

pre-deployment and are estimated to drift by up to 0.5 ms^{-1} during 1 year of activity (Mangum, Freitag and McPhaden 1994). It should also be noted that the wind measurements on the buoys are done at 4m from the surface, while the ECMWF winds are at 10m. According to a stability correction algorithm developed by W.G. Large (Large and Pond 1981) to adjust wind speed from a height z to a height of 10m., I found that the wind speed correction is typically 10% or less. Thus without height adjustment I may expect errors of about 0.5 ms^{-1} on a wind of 5 ms^{-1} or 1 ms^{-1} for 10ms^{-1} wind. Since I cannot height-adjust the TAO winds because the information required to make the stability correction is typically not available, I suggest a plausible expected mean error on the TAO data to be 0.7 to 1.5 ms^{-1} under typical moderate WWE conditions. Thus the disagreement between the TAO data and the ECMWF data is similar to the uncertainty in the TAO data; and, since WWEs typically have maximum zonal winds in excess of 10ms^{-1}, use of the ECMWF analysis gives us an acceptable signal to noise ratio.

I am unable to determine the accuaracy of the ECMWF high-frequency data outside the region spanned by the TOGA/TAO array. Since the ECMWF incorporates TAO data into its analysis, an agreement with TAO is not surprising. Since the main signals in the analysis are in the regions covered by the TAO array, and the signals are large relative the seasonal variance, I expect the ECMWF analysis to be satisfactory. The ECMWF, because of its grid-spacing and time sampling (2.5° and 12 hours) should be expected to deviate from observed winds expecially in the region of the ITCZ. These differences could be large instantaneously. In the TAO buoys nearest the ITCZ (bouys along 8°N, 180°-140°W), the zonal wind rms difference between ECMWF and TAO is not noticeably different from that in other regions, however the meridional wind rms difference is. Because of this, I am most cautious about subtle results in and near the ITCZ region, especially those relating to variations in meridional winds.

Ideally, the TAO array would be dense enough to permit characterization of the

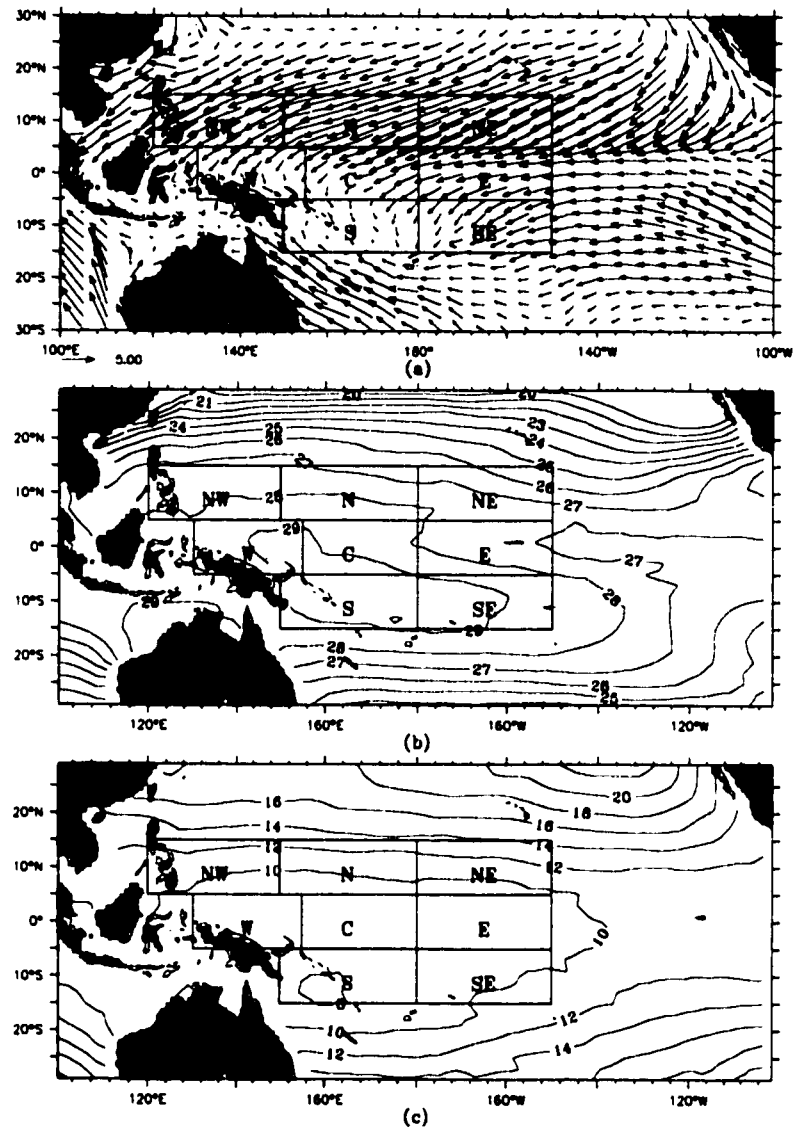

Figure II.5. Classification regions supperimposed on the March (a) ECMWF climatological winds (1986-95), (b) COADS climatological SST, (c) COADS cliamtological SLP-1000. Scale vector is 5ms^{-1} for (a); contour intervals are 1°C for (b) and 2 mbar. for (c).

structure of WWEs itself. However the area coverage and the spatial separation of buoys significantly limit its ability to provide the needed spatial resolution. In its present configuration the TAO array is useful in that it provides data to the wind analyses (and thus should improve their realism) and it provides the information needed to define the likely errors in the analysis. But the ECMWF wind analysis itself is required to carry out the work described below.

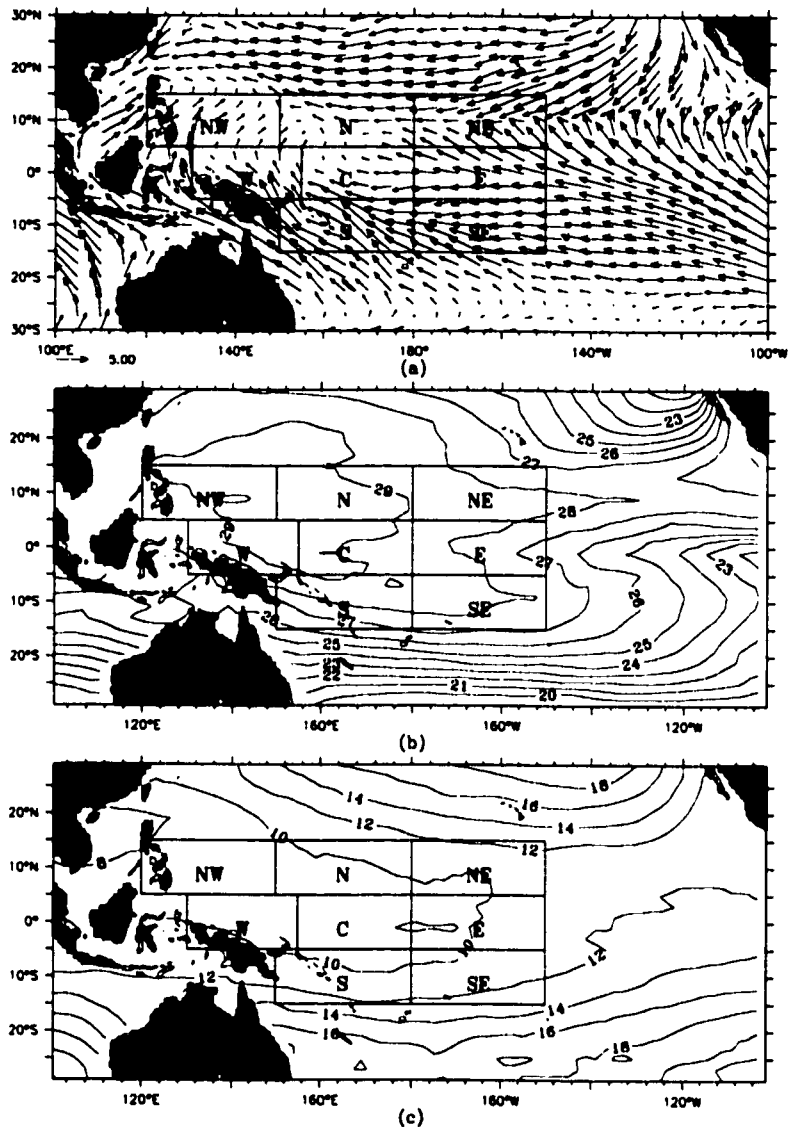

Figure II.6. Same as Figure II.5 except for the month of September.

II.3. Methods

This section describes how the WWEs are classified and how the composite WWEs are computed. First how I came to define the different types of WWEs is described; then the quantitative classification criteria used for each are described. The number of events of different types that follow from the application of these classification criteria to the 1986-1995 ECMWF wind anomaly fields is shown. Finally, the details of the WWE compositing technique are discussed. Description of the analysis to determine the statistical significance of the features of the composites is included in Appendix A.

a. Classification

I began by looking at vector plots of the wind and wind anomalies over the tropical Pacific, for every 12 hour analysis period in the data set. I then highlighted the vectors with westerly anomaly and looked at all the anomaly plots again. I found that westerly wind anomalies of substantial scale tended to occur in particular regions, and not to show major translation during their lifetimes. This suggested that a good classification scheme could be based upon the location of maximum westerly wind anomaly.

Based on the wind anomaly patterns I saw, I defined eight regions to serve as the framework for the classification scheme. These regions, which cover most of the ocean from 120°E to 150°W and 15°S to 15°N, were named according to their location relative to each other. The zonal dimension of these regions is about 30° of longitude, and the meridional dimension is 10° of latitude. Each contains five ECMWF grid-points in the meridional direction, and twelve to thirteen points in the zonal direction. To help place them in the context of the large scale environment of the region, the regions are superimposed upon the COADS climatological (1946-1995) mean winds, SST and SLP for March (Figure II.5) and for September (Figure II.6). Note that there are substantial changes in the environment in each region between March and September.

In order to systematically identify and analyze WWEs, it is useful to introduced a quantitative definition for their existence, within the context of the classification scheme. A WWE of type ***X*** is defined as any period of three or more days for which the 10-m zonal wind anomaly, averaged over region ***X*** and smoothed by a three point triangle filter in time (half-power point at 2.75 days), exceeded 2 ms^{-1}. To label and organize the events, an event's center day was defined to be the day for which the zonal wind anomaly, averaged over the region, was greatest. With these classification criteria all the westerly wind events identified, by region (type) and center date.

It is useful to describe the intensity of the WWEs according to their "duration",

"maximum averaged anomaly", "maximum point anomaly" and "wind measure". The duration of each WWE is defined to be the time span between when the identification criteria are first met and when the identification criteria are no longer satisfied. The maximum averaged anomaly is defined to be the zonal wind anomaly averaged over the classifying region on the center day of the event. The maximum point anomaly is the maximum zonal wind anomaly within the classifying region, on the center date. The wind measure is defined as the time integral of the zonal wind anomaly, averaged within the classifying region and smoothed by a three point triangle filter in time (half-power point at 2.75 days), over the event duration.

Not every period of westerly wind anomalies fit perfectly into the classification scheme. In particular, sometimes substantial westerly wind anomalies occurred in adjacent regions at the same time. This led to an additional sub-classification of WWEs into overlapping and non-overlapping events. Overlapping events were defined to be events which were identified in two regions which shared more than half an edge and whose center dates were within three days of each other. For each pair of overlapping events, the maximum averaged anomaly for each event was compared, and the event was classified as an event of the type for which the maximum averaged anomaly was greatest. There were then two lists of dates, one with all the events, which shall be referred to as the "complete event list", and another with all the non-overlapping events plus the overlapping events classified according to the secondary classification scheme, which shall be referred to as the "non-overlapping event list". Table II.1 summarizes the number of events identified for each type of event in each list.

Table II.1: Number of WWEs identified duirng 1986-95, in each of the classifying regions, for the complete event list and for the non-overlapping event list. (see Section 3.a)

List	NW	N	NE	W	C	E	S	SE
Complete event list	58	28	36	35	62	42	39	51
Non-overlapping event list	51	25	28	28	49	34	29	43

b. Compositing

The basis of the compositing is the identification of the center day (day (0)) for each event of a type "X". The day(0) field for the composite type "X" event is computed by averaging together the wind or wind anomaly field for all the type "X" event days(0). Composite day(±n) is computed similarly from each of the days(±n) for type "X" events. The composites are evaluated for day(-9) through day(9) for each of the eight types of WWEs, resulting in a 20 day composite event. The composites are evaluated using all the events from each type of WWE.

For each type of event, then, the composite is evaluated according to:

$$\vec{U}(x,y,t_n) = \frac{\sum_{i=1}^{N} \vec{u}(x,y,t_n + \tau_i)}{N}$$

Where **U** is the composite vector wind anomaly, **u** is the instantaneous vector wind anomaly, x is the zonal location, y is the meridional location, $\{\tau_i\}$ are the center days for the individual events, $t_n \in [-9,10]$ is the event day, and N is the number of events to be composited. To study the effect of event overlap in the averaging process, two sets of composite westerly wind events were generated: one using the dates in the complete event list, the other using the dates in the non-overlapping event list. The two composites were not different in any significant qualitative aspect, so I present only the composites generated from the complete event list. The composite wind fields for each type of event were similarly computed.

II.4. Composite results

In this section I present the results of the composite analysis. I show vector wind anomaly maps for selected days of each type of event. I also present vector maps of the wind field on the center day (day(0)) for each type of event. I shall show that a simple model structure provides a convenient way to define the zonal, meridional and temporal scales of

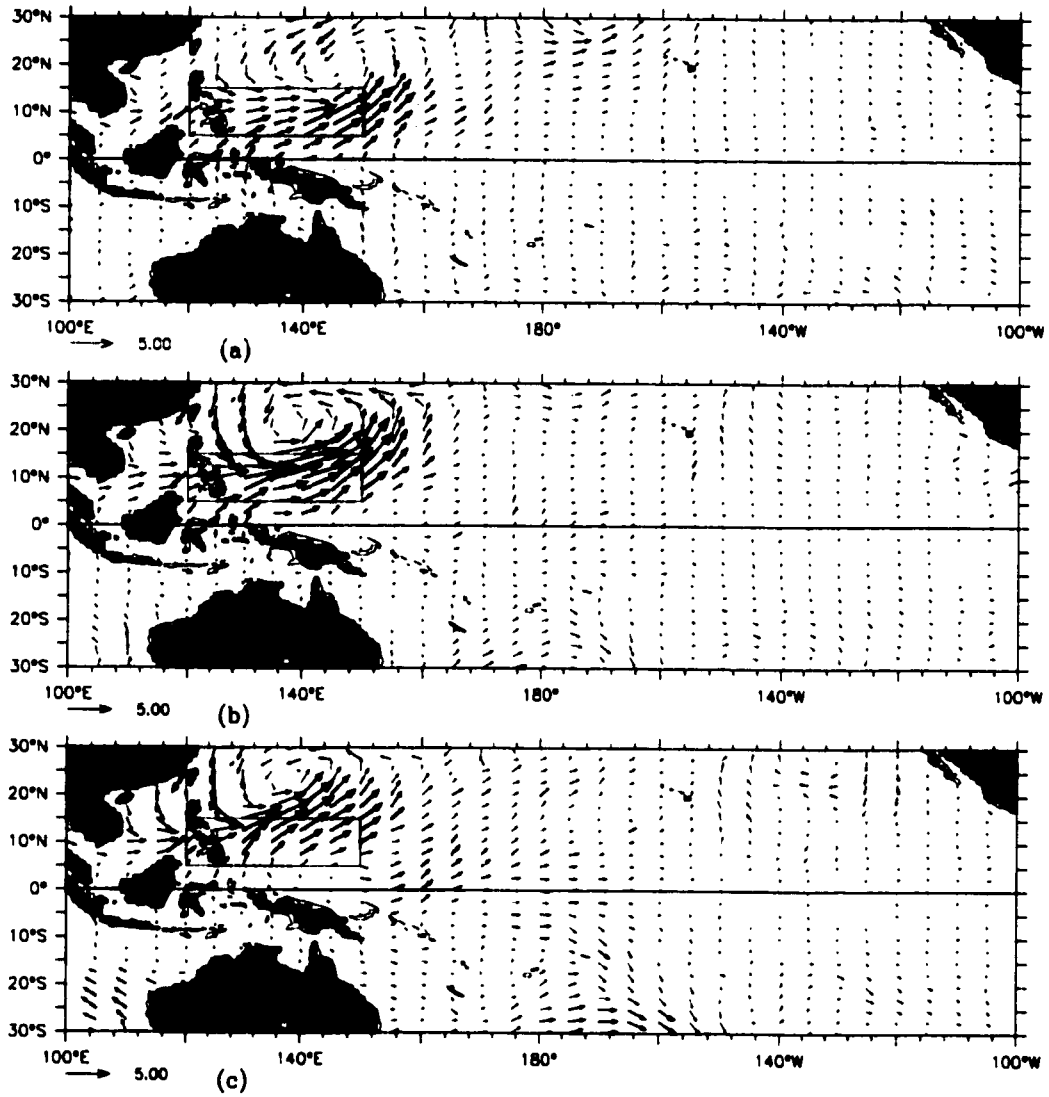

Figure I.I.7. Type NW composite wind anomalies for (a) Day (-2), (b) center day, and (c) Day (2). Classifying region is indicated by thin lined box. Bold vectors (shading) indicate the zonal (meridional) component is significant at the 95% level. Scale vector is 5 ms^{-1}.

the zonal wind anomalies for each of the composites and I present the scales of each event from this perspective.

a. Vector maps

Daily wind anomaly vector maps for days (-9) through (+9) for each of the eight types of WWEs were generated, the full set of maps is shown in Vecchi and Harrison (1997). Here I present only selected maps to illustrate the patterns when the wind anomalies are substantial. For each type of event I show the wind anomaly on day(-2), day(0) and day(+2)

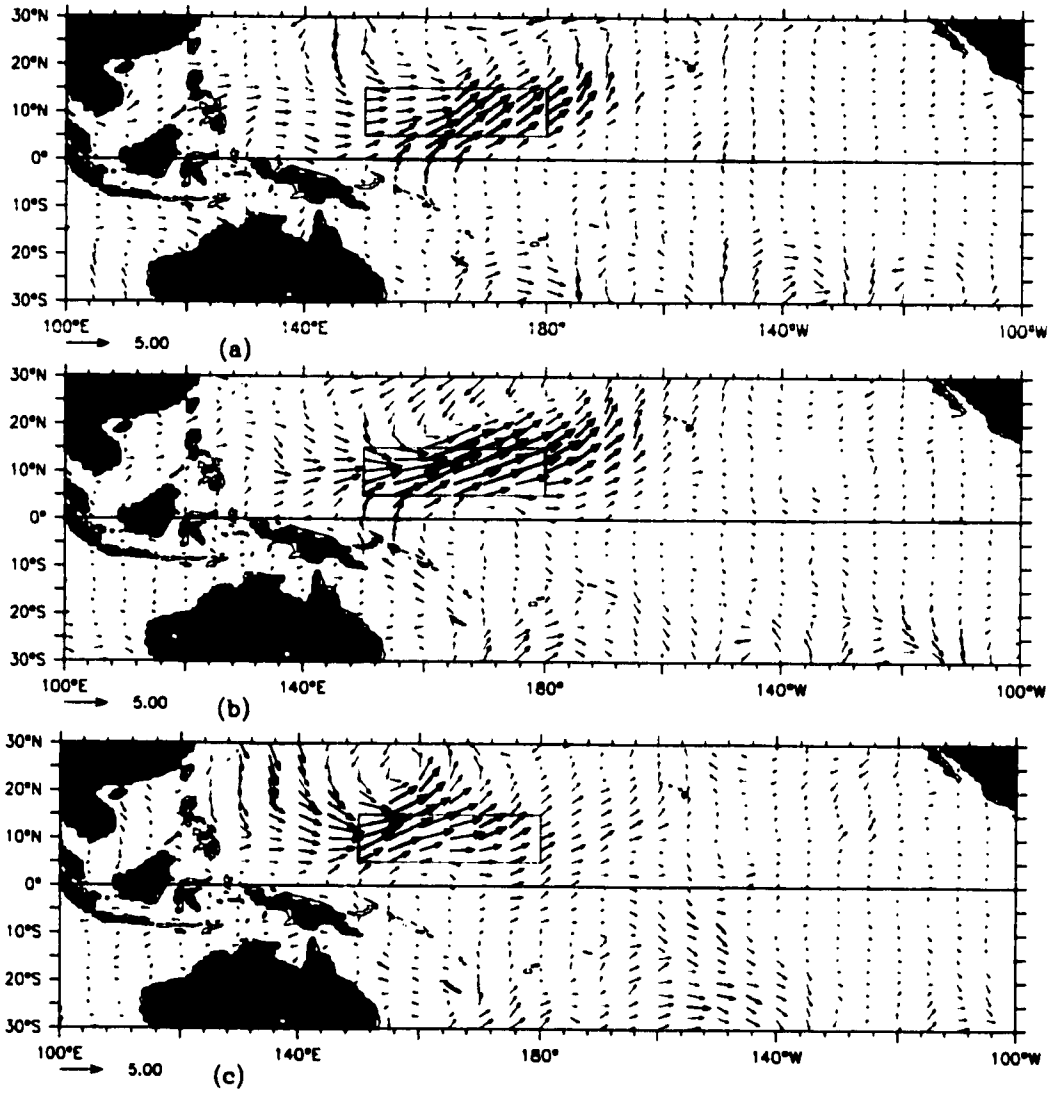

Figure II.8. Same as Figure II.7, except for type N composite.

(Figures II.7 through II.14). Note in these figures that the region used to define the featured type of event is outlined. The anomalies highlighted as bold vectors have zonal component significant at the 99% level, and those highlighted by a shaded background have meridional wind component comparably significant. Statistical significance was determined by a Student's-*t* test (Appendix A).

I describe qualitatively the features of the patterns that merit note, and follow the atmospheric convention that an easterly wind is a wind from the east, etc. It is helpful to introduce composite wind magnitude labels as follows: weak (u£2 ms^{-1}), moderate (2ms

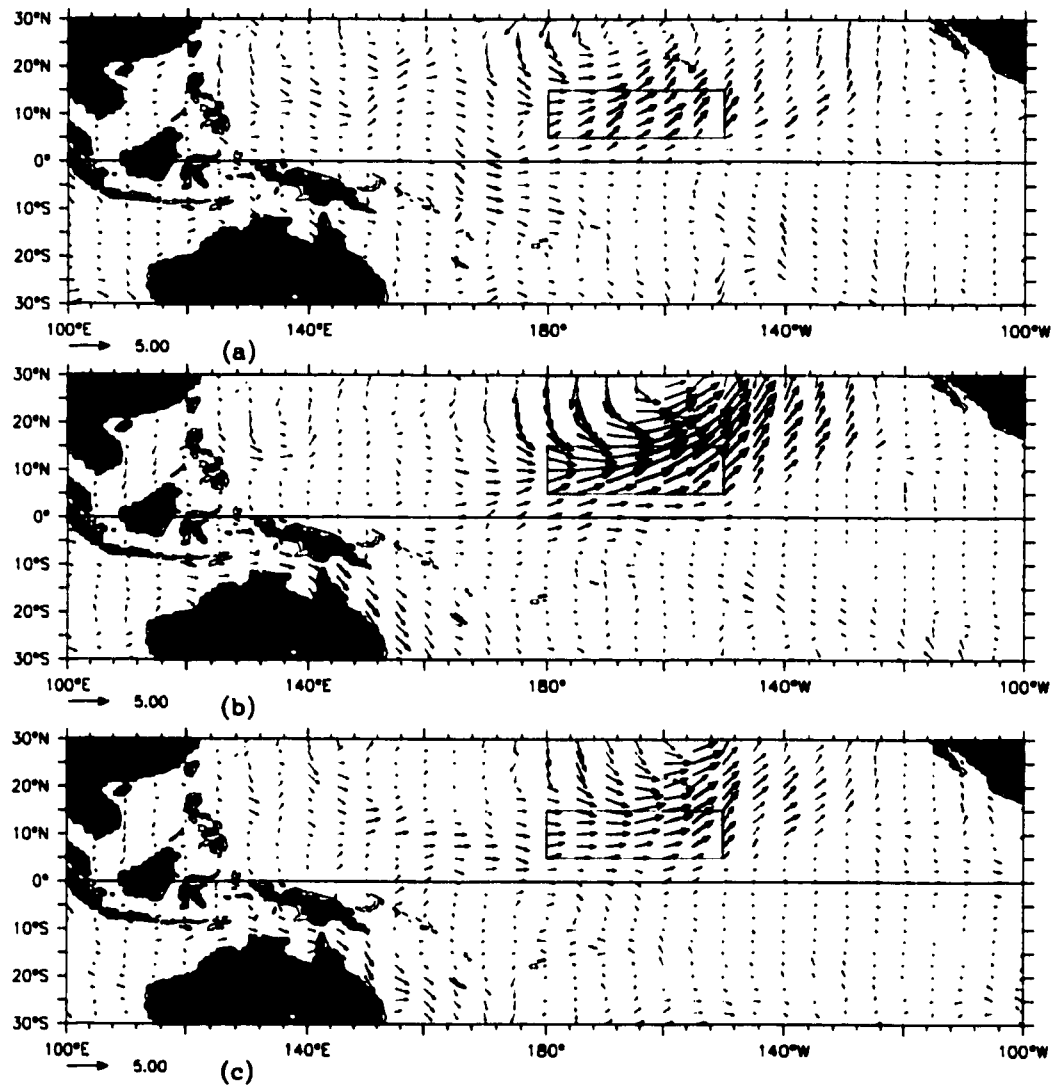

Figure II.9. Same as Figurel I.7, except for type NE composite.

^{1}<u£ 4 ms^{-1}) and strong (u>4 ms^{-1}). It is simplest to identify common elements in the Composite events by sorting them into Northern Regions (NW, N and NE); the Equatorial Regions (W, C and E); and the Southern Regions (S and SE).

i) NORTHERN REGIONS: NW, N AND NE (Figures II.7, .8 and .9):

Each of these events has strong meridional and zonal wind anomalies. Although the areas of maximum significance are principally occupied by moderate to strong westerly and south-westerly anomalies, there are clear suggestions that these events are associated with anomalously cyclonic circulations, with moderate to strong easterlies and northerlies

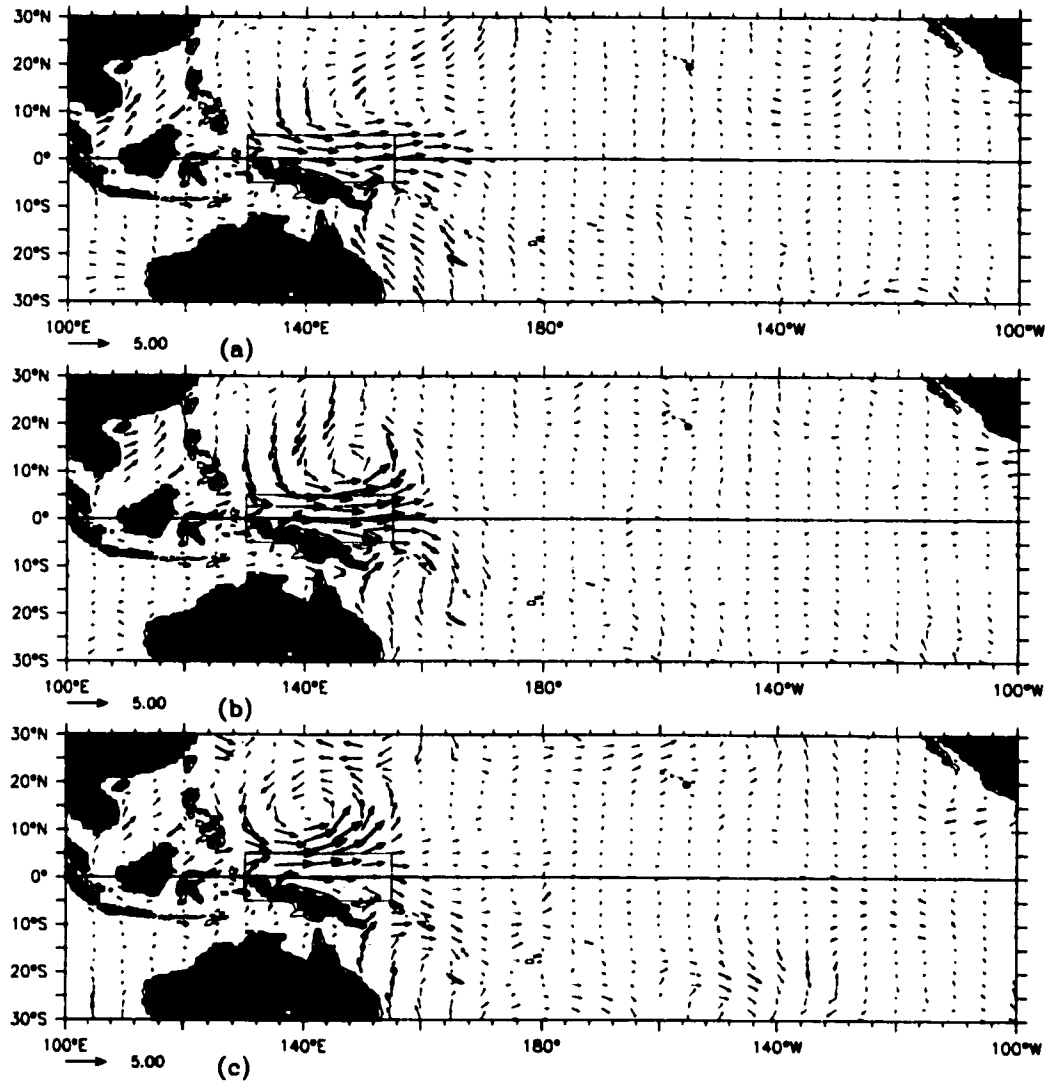

Figure II.10. Same as Figure II.7, except for type W composite.

to the north and west of the regions. All of these events also show a modest translation of the area of maximum anomalies during the event. The type N and NW events show northwestward displacement throughout the event, while the type NE event shows an eastward displacement throughout the event.

The NW and N type events share additional common features. Both types of events have periods of distinct weak to moderate cross-equatorial inflow from day(-3) until day(2) for the type NW event, and from day(-3) until day(0) for the type N event. There is also well defined inflow from west of the cyclonic feature from day(-2) to day(3) for the type NW

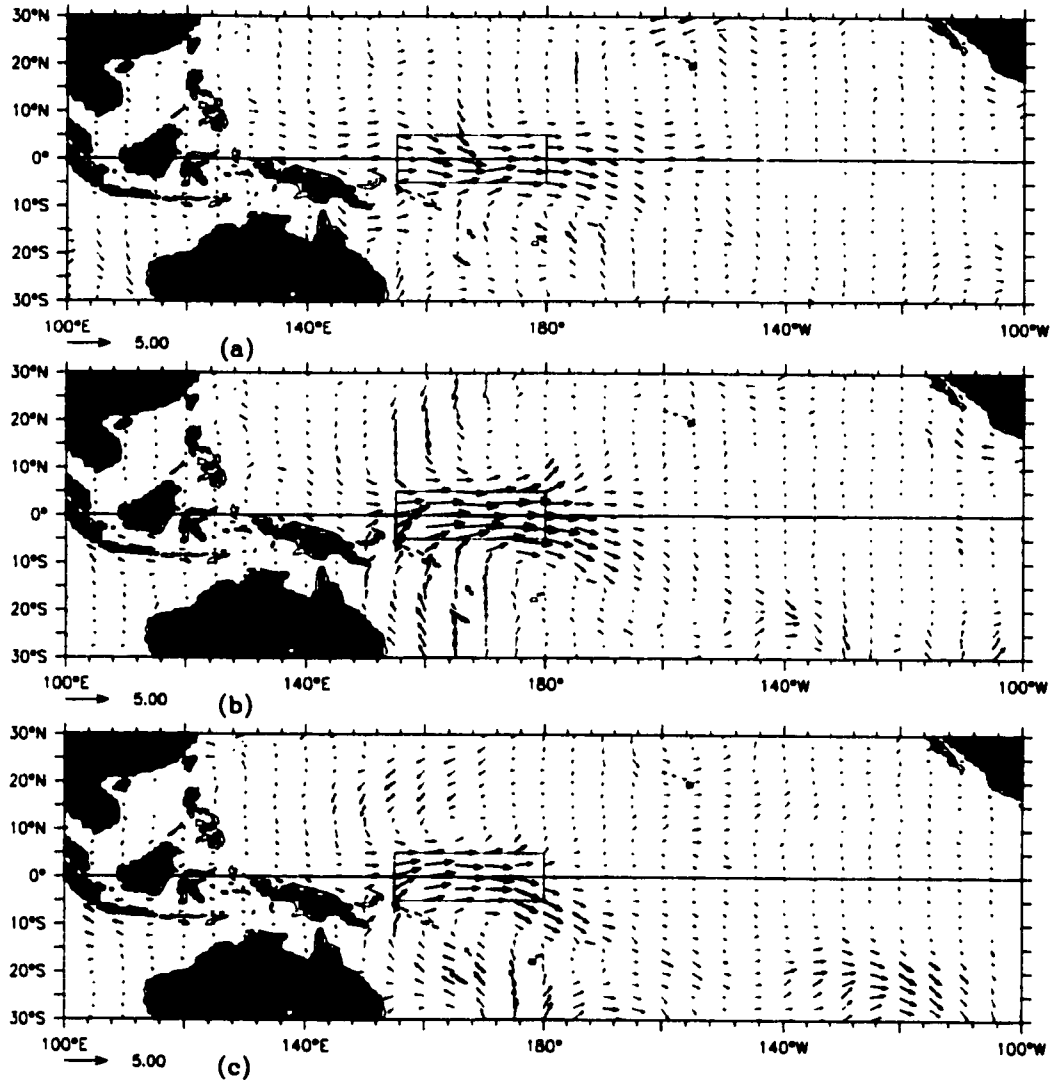

Figure II.11. Same as Figure II.7, except for type C composite.

event, and from day(-2) to day(2) for the type N event. The circulation is more complicated than a simple cyclonic flow.

The NW and NE type events share periods of weak to moderate equatorial westerly anomalies. For the NW type events, there is a period of equatorial westerlies to the south of the classifying region prior to the center day, lasting eight days, centered around day(-5), when the maximum equatorial westerlies occur; there are also weak equatorial westerlies from day (2) through day(5), to the southeast of the region. For the type NE events, equatorial westerlies to the south of the classifying region occur during the period of maximum

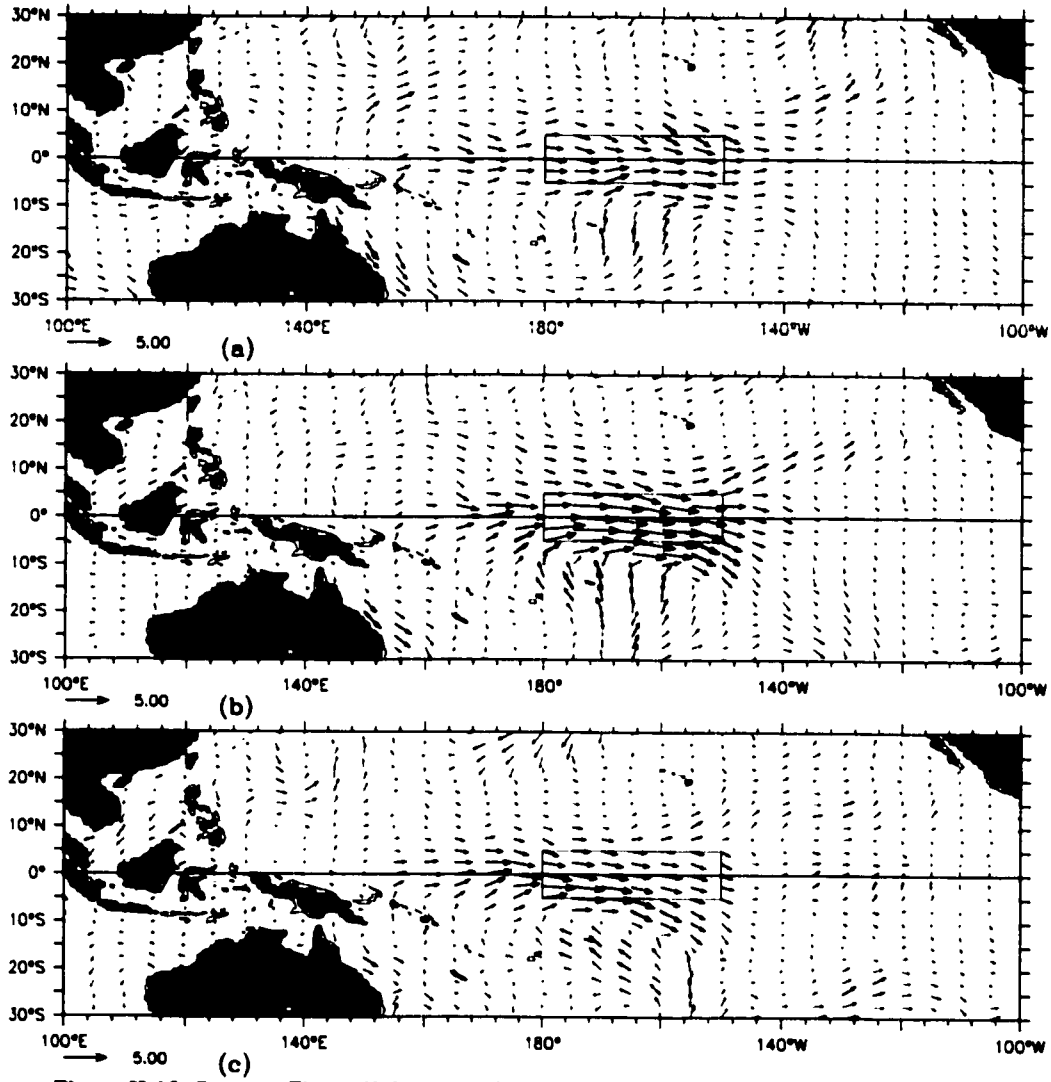

Figure II.12. Same as Figure II.7, except for type E composite.

anomaly in the region, last for three days and have their peak amplitude on the center day of the event.

ii) EQUATORIAL REGIONS: W, C AND E (Figures I10, .11 and .12):

For each of the equatorial WWEs the maximum anomalies are primarily zonal, with periods of moderate meridional inflow to the western part of the regions. The equatorial westerlies in all three events are meridionally contained within the defining region, but their zonal extent can be substantially larger than the defining region. The meridional inflow typically can be found at least 20 degrees away from the equator, but can extend as far

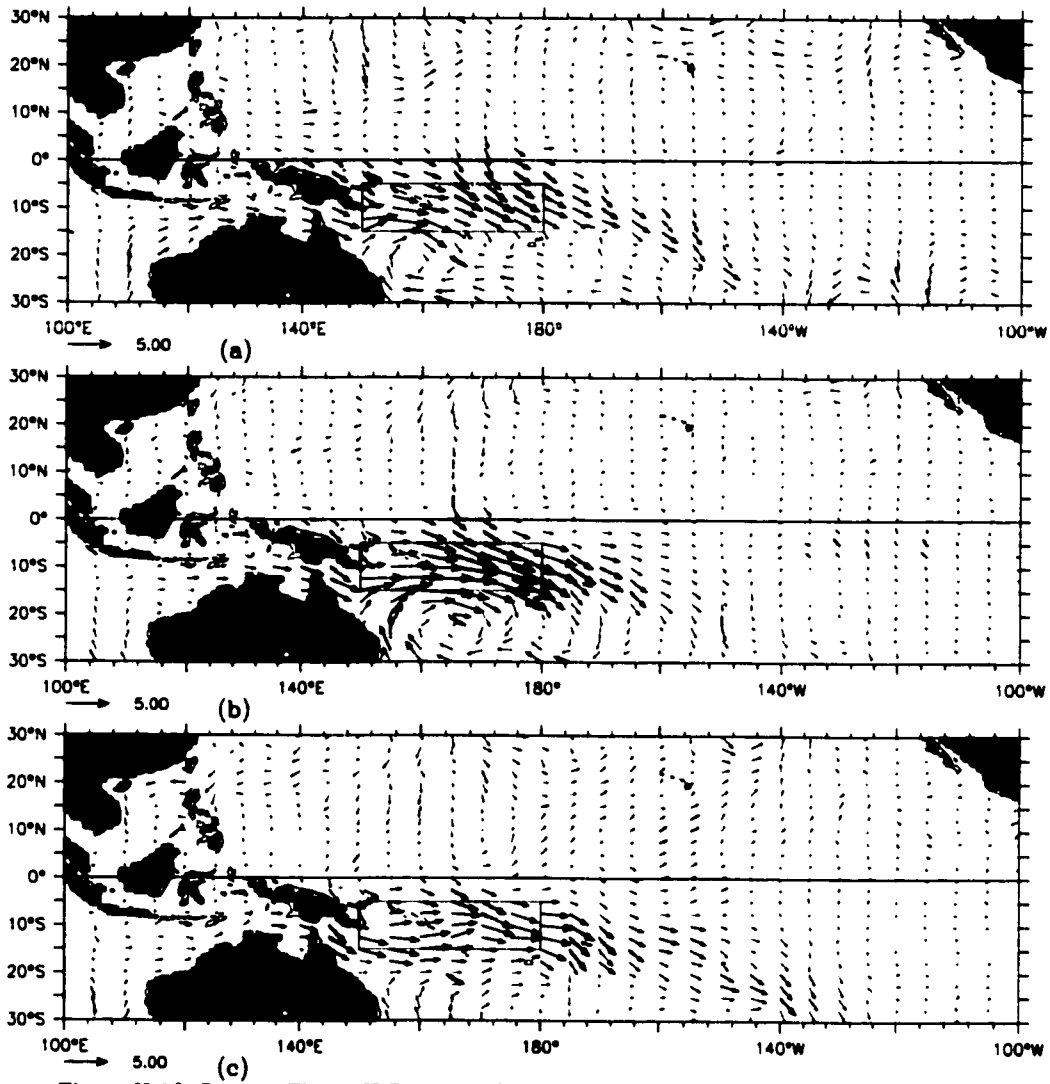

Figure II.13. Same as Figure II.7, except for type S composite.

as 30 degrees (the southerly inflow on day(0) of the type C event). For the type C composite event, the zonal wind anomalies are close to symmetric with respect to the Equator, while for the types W and E event there is a pronounced asymmetry. The type W composite event has symmetric anomalies in the early part of its evolution, while as day(0) is approached the anomalies become more pronounced to the north of the Equator. The type E composite event has its largest anomalies to the south of the Equator.

For the type W event there is moderate southerly inflow during event days(-5) and (-4) (Vecchi and Harrison 1997), followed by a moderate northerly inflow that begins on the

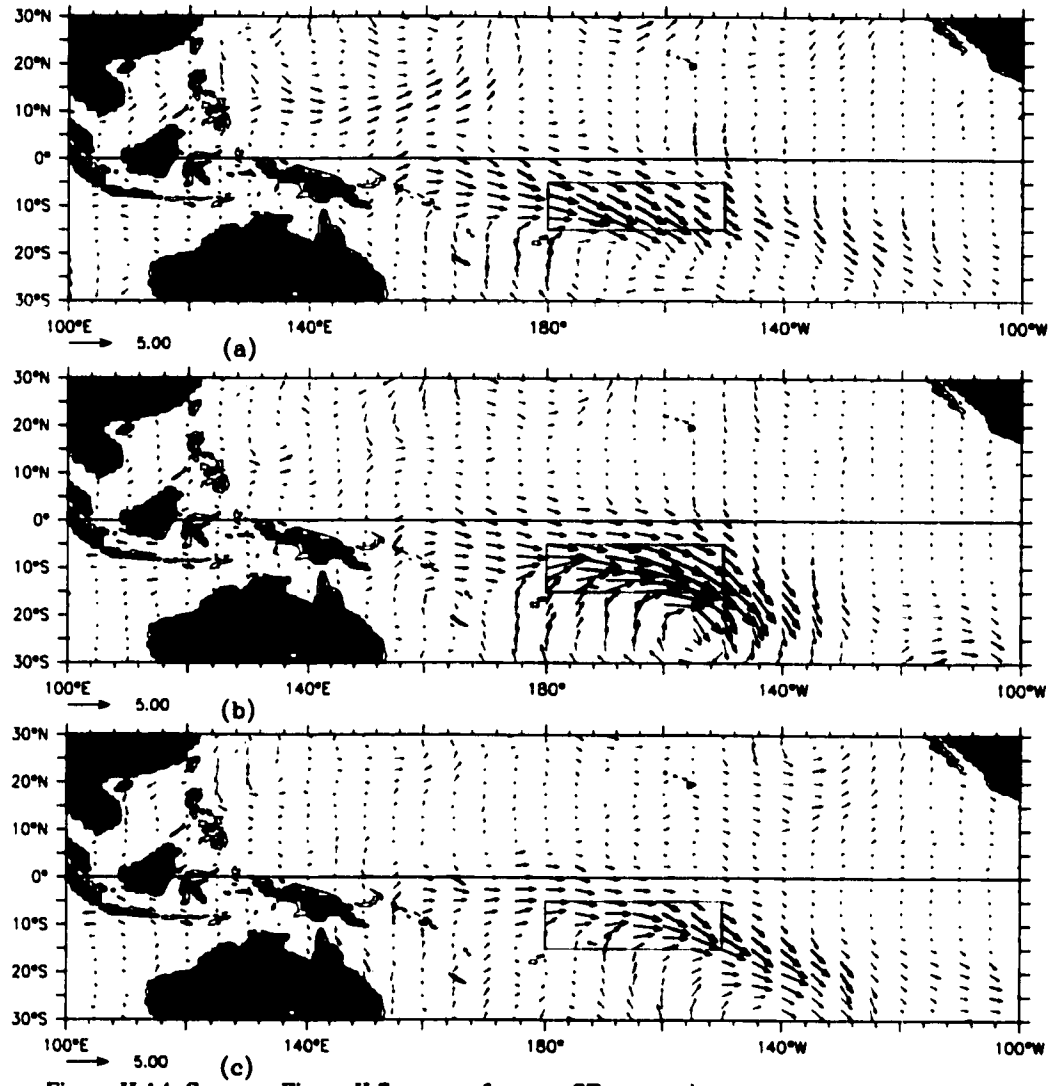

Figure II.14. Same as Figure II.7, except for type SE composite.

center day and an anomalous cyclonic circulation subsequently develops. For the type C event there is moderate northerly and southerly inflow beginning on day(-1) and ending after day(1). For the type E event, there is moderate southerly inflow beginning on day(-2) that continues until the center day. Both the type W and the type E events exhibit a translation of the area of maximum anomaly. The W type event has a translation towards the northwest after the center day. The type E event has a westward translation after the center day.

iii) SOUTHERN REGIONS: S AND SE (Figures II.13 and .14):

Both of these composite events have a moderate to strong meridional component as well as strong westerly anomalies near day(0). Although most of the significant anomalies are westerly and northwesterly, there are also moderate to strong easterly and southerly anomalies suggesting a pattern of anomalously cyclonic flow. The events also exhibit eastward translation of the area of maximum anomaly throughout the event.

Both of the composite events exhibit moderate cross-equatorial inflow on and immediately preceding the center day. The cross-equatorial inflow for the type S event occurs through the northwestern corner of the region as well as the eastern half of the northern edge of the region, from day(-2) through day(0). For the type SE event, the cross-equatorial flow is most persistent north of the eastern corner of the region, from day(-2) through day(0). Both events exhibit strong inflow from the west on the days before and during the period of maximum anomaly. The westerly inflow for the type S event, begins on day (-9) and extends as far west as the Indian Ocean. So the structure of the circulation of these events, like that of the type N and NW events, is not just a simple cyclonic one.

The type SE event has persistent weak to moderate equatorial westerly anomalies on the days surrounding the center day. The equatorial westerlies are stronger to the south of the equator than to the north of it. The type SE event also has moderate southerly inflow from higher latitudes on the days preceding and on the center day.

b. Center day wind maps

Figures II.15 through II.17 show vector plots of the center day of the total wind composite, for each type of WWE. As before, it is helpful to discuss the composites by grouping the events by northern, equatorial and southern regions. I shall refer to many of the features described in the previous section; see Figures II.7 through II.14 as needed.

i) NORTHERN REGIONS: NW, N AND NE (Figure II.15):

The anomalously cyclonic circulations in the type NW and N anomaly composites manifest themselves as cyclonic wind patterns in the wind composites. The type N wind

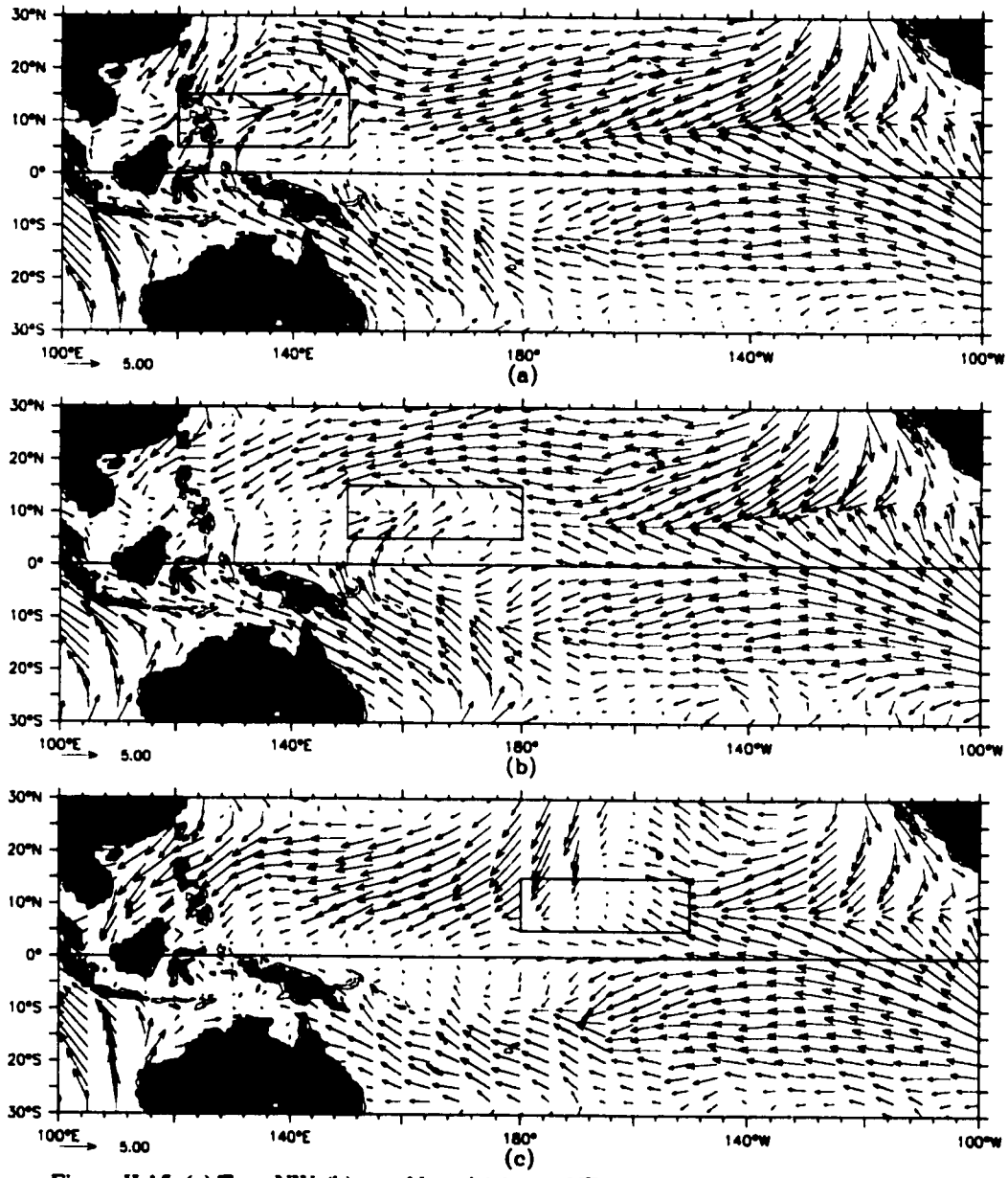

Figure II.15. (a) Type NW, (b) type N, and (c) type NE composite WWE 10-m wind vector map, for event center day. Scale vector is 5 ms^{-1}. Classifying region is indicated by the box.

pattern indicates a reversal of the north-easterly trades within the classifying region. The situation differs for the type NE event, for which the wind composite indicates a trade wind break, but not a cyclonic wind pattern, because of the strength of the north-easterly trades in that region. The translation of the area of maximum anomaly noted in the anomaly plots, is also apparent in the full sequence of wind composite figures (Vecchi and Harrison 1997).

The cross-equatorial inflow noted in the type NW and N event anomalies is also

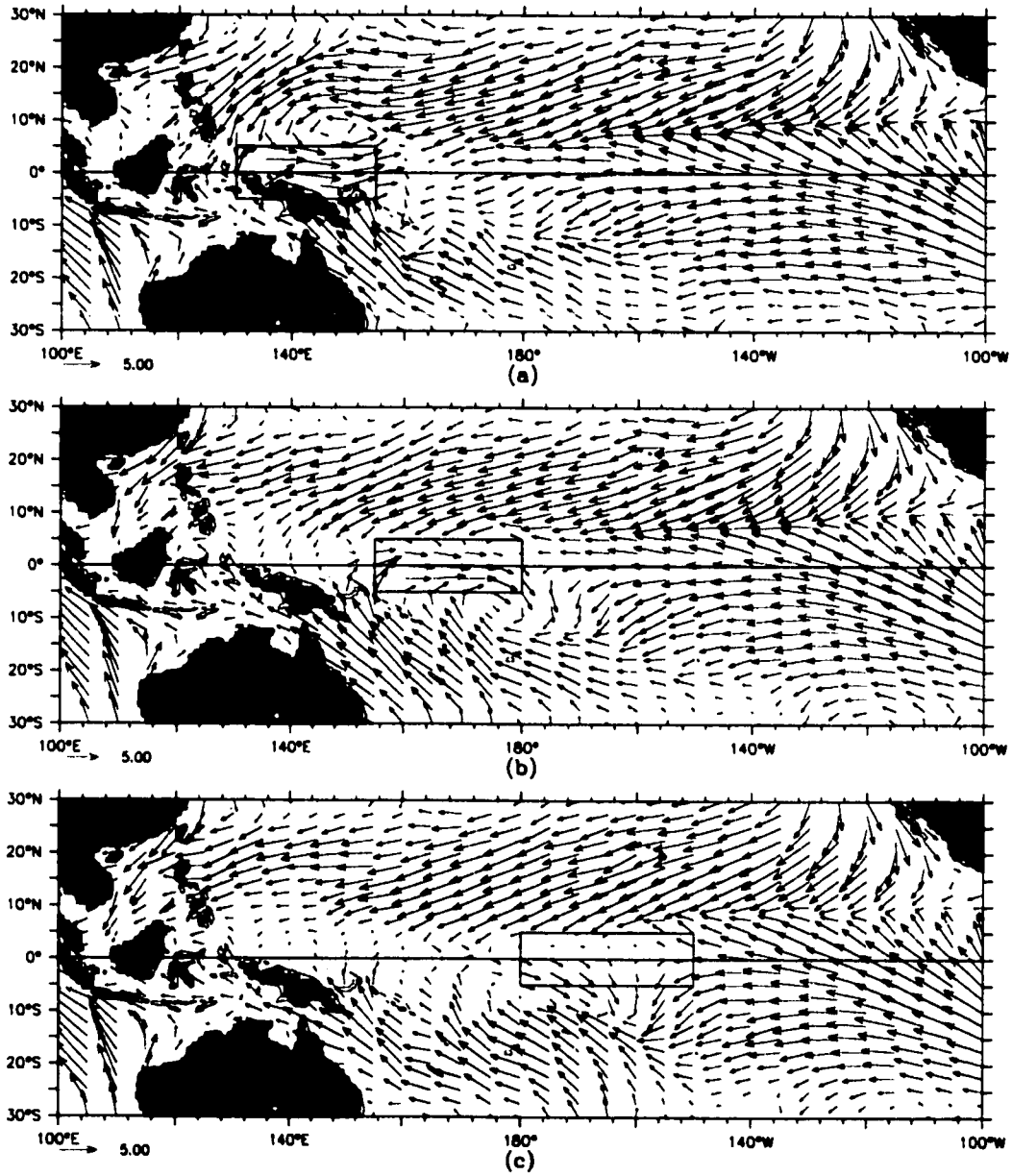

Figure II.16. (a) Type W, (b) type C, and (c) type E composite WWE 10-m wind vector map, for event center day. Scale vector is 5 ms^{-1}. Classifying region is indicated by the box.

apparent in the wind composites, but the anomaly inflow from the west is not clear in the winds themselves. The equatorial westerly anomalies in the type NW event appear as actual equatorial westerly winds to the south of the region. The equatorial westerly anomalies noted in the type NE events do not appear as equatorial westerly winds here.

ii) EQUATORIAL REGIONS: W, C, AND E (Figure II.16):

For the type W and C events, the primarily zonal westerly anomalies in the region

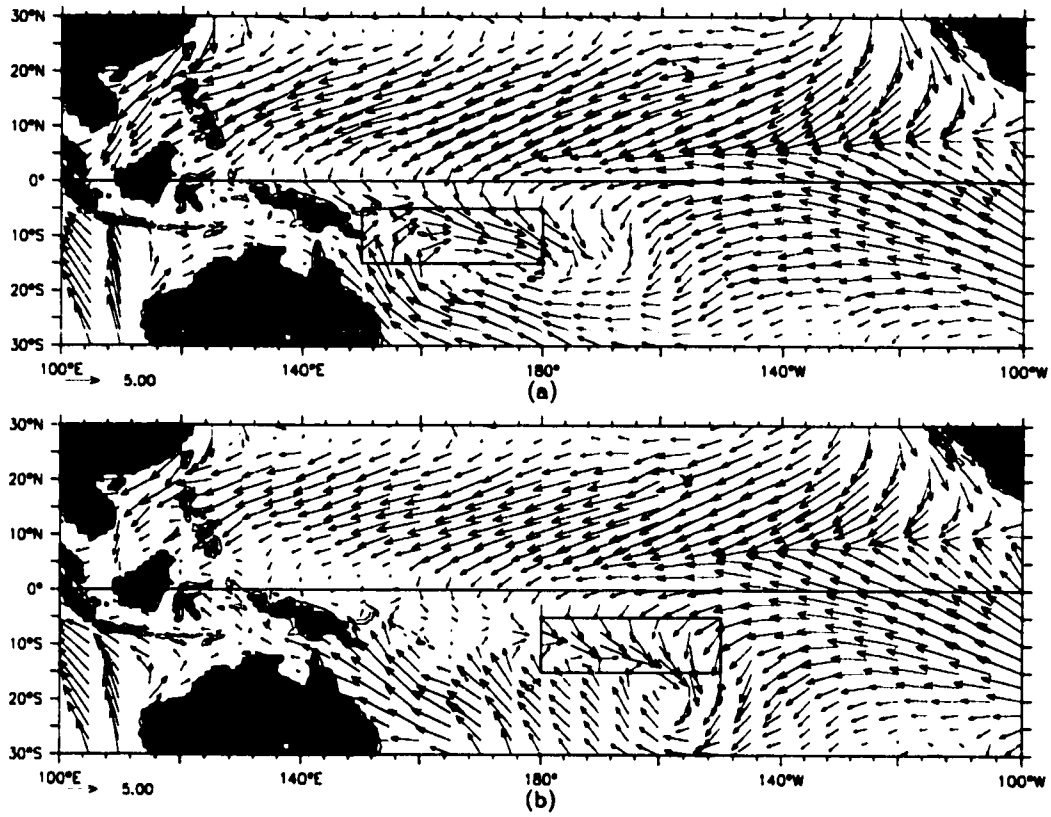

Figure II.17. (a) Type S, and (b) type SE composite WWE 10-m wind vector map, for event center day. Scale vector is 5 ms^{-1}. Classifying region is indicated by the box.

appear as primarily zonal westerly winds. However, for the type E event, the wind field has a noticeable meridional component. Also, while the anomalies for the type C event were centered about the equator, the winds are asymmetrical with the greatest westerly amplitudes south of the equator (this is due to the seasonality of the strong type C events (Section 6.a), which tend to occur in austral winter when the climatological winds south of the equator are westerly). The equatorial asymmetry of the type E zonal wind anomalies is also noticeable in the wind composite.

The southerly inflow anomaly in the type W and C events appears as a strengthening of the already prominent south-easterly trade winds to the east of Australia. For the type E event, southerly inflow in apparent, and is linked to a cyclonic circulation pattern to the south-west of the region, which translates westward. For the type W event the northerly inflow anomaly is discernible in the winds, so is the cyclonic anomaly circulation which

tends to move north-westward. For the type C event the northerly inflow anomaly is overwhelmed by the strong trade winds, but a cyclonic wind circulation forms, centered to the south of the region, which does not propagate from day (-4) when it first appears to day (4) when it dissipates.

iii) SOUTHERN REGIONS: SE AND S (Figure II.17):

Both of these composite events display strong meridional winds, as well as zonal winds in the classifying regions. The type SE composite winds shows a reversal of the south-easterly trades. The winds also have a cyclonic pattern to them, which translates to the east as it decays for the type S events, and decays quickly for the type SE event. The cross equatorial inflow anomaly for the type S event produces cross-equatorial flow in the winds. For the type SE event, there is no cross-equatorial flow in the area of cross-equatorial anomalies. For the SE type event the anomalously southerly inflow enhances the south-easterly trade winds to the west of the trade wind reversal.

c. Scales

Now I turn to the problem of defining the scales of the composite WWEs. Table II.2 shows the duration, maximum averaged anomaly, wind measure and maximum point anomaly for each of the composite WWEs (Section II.3.a). The events have a duration in the range of 4.5-5.5 days, except the type NE event (4 days). The maximum averaged anomaly is in the

Table II.2. Duration, maximum averaged anomaly, wind measure and maximum point anomaly for each composite WWE. Quantities as defined in Section 3.a.

Region	Duration (days)	Maximum averaged anomaly (ms^{-1})	Wind measure (10^6 m)	Maximum point anomaly (ms^{-1})
NW	5	4.0	1.3	7.2
N	5.5	4.6	1.6	6.6
NE	4	4.2	1.1	6.3
W	4.5	3.9	1.1	6.9
C	5.5	4.4	1.4	6.4
E	4.5	4.1	1.2	5.5
S	5	4.4	1.4	6.4
SE	5	4.7	1.4	6.7

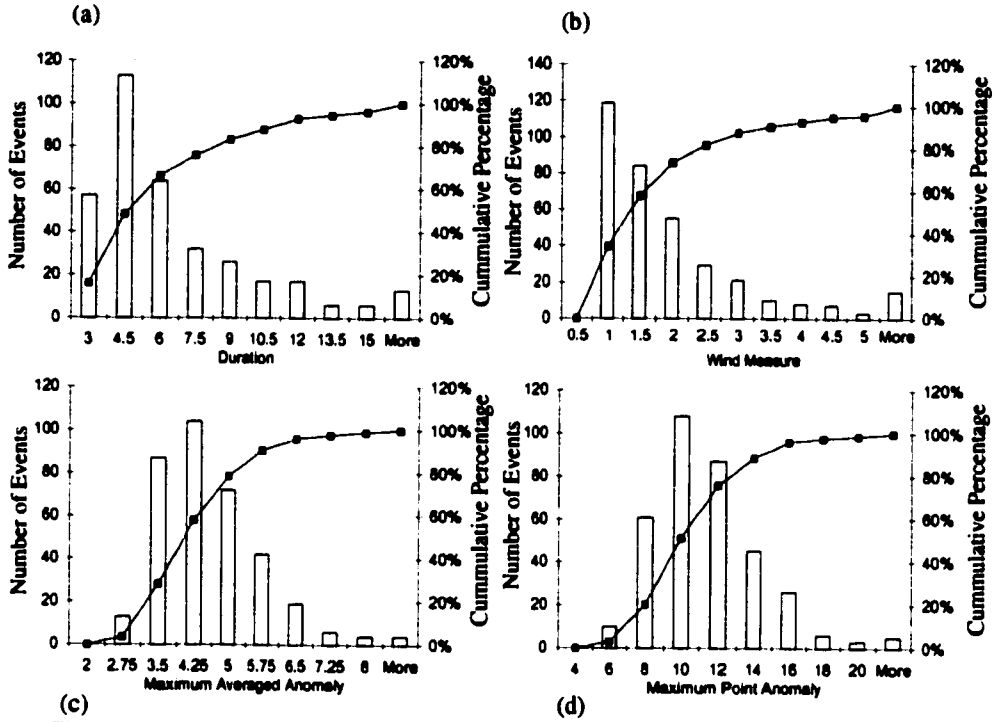

Figure II.18. Histograms of WWE (a) duration, (b) wind measure, (c) maximum averaged anomaly, and (d) maximum point anomaly, for WWEs of all types occuring during the 1986-1995 period. Bar graph indicates the number of WWEs occurring within the labeled bins, and the line graph indicates the cumulative percentage of events at each bin. Units are days for duration, 10^6 m for wind measure, and ms^{-1} for maximum point anomaly and maximum averaged anomaly. Quantities as defined in Section 3.a.

range of 3.9 to 4.7 ms^{-1}; the strongest events are type SE (4.7 ms^{-1}) and type N (4.6 ms^{-1}), and the weakest is type W (3.9 ms^{-1}). The wind measure for all the events is between 1.1 and 1.6 x 10^6 m; the strongest event is type N (1.6 x 10^6 m). The events have maximum point anomaly between 6.3-7.2 ms^{-1}, except the type E event (5.5 ms^{-1}).

Histograms for duration, maximum point anomaly, maximum averaged anomaly and wind measure for all the events over the entire record are shown in Figure II.18. The frequency distributions for the individual events are similar to those for the entire record, so I do not present distributions for each type of event; see Vecchi and Harrison (1997) for breakdown by event type. From Figure II.18 it can be seen that approximately 50% of the WWEs in the record have a duration greater than 3 and less than 6 days (recall the composite WWE durations vary between 4 and 5.5 days). For maximum averaged anomaly, ap-

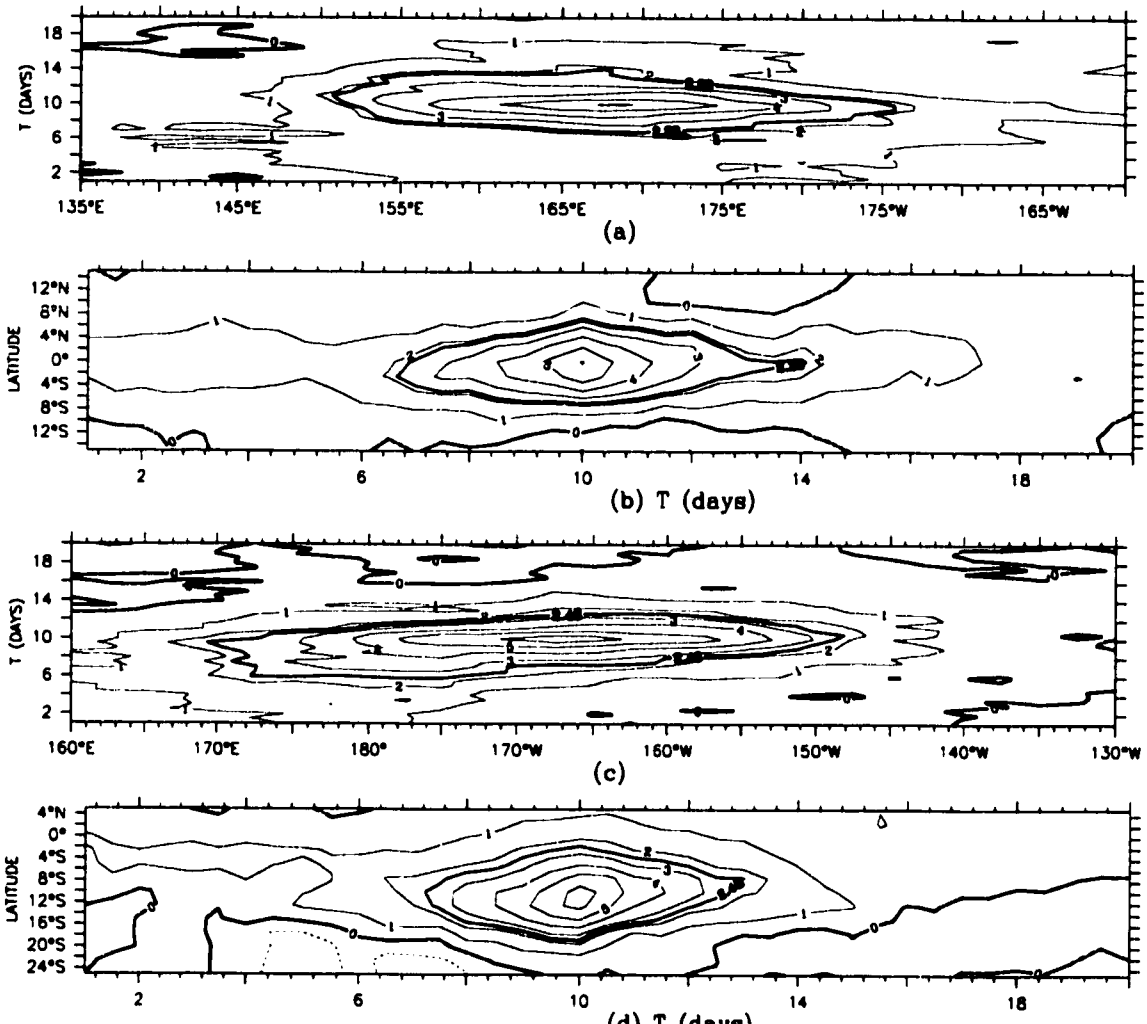

Figure II.19. (a) Longitude vs. time and (b) latitude vs. time contour plots of the 10-m zonal wind anomaly for the type C composite WWE; and (c) longitude vs. time and (d) latitude vs. time contour plots for the type SE composite WWE. Contour intervals are 1 ms^{-1} and the dark contour indicates the e^{-1} level of the zonal wind anomaly. Center day of the event is day 10 on the time axis.

proximately 50% of the events have values greater than 3.5 ms^{-1} and less than 5 ms^{-1}, and the composite WWE values are between 3.9 and 4.7 ms^{-1}. For wind measure, approximately 40% of the events have wind measure between 1 x 10^6 m and 2 x 10^6 m (composite WWE wind measures vary between 1.1 and 1.6 x 10^6 m). Since the previous three quantities are large space scale linearly averaged quantities, they are not affected a great deal by the smoothing effects of compositing. For the maximum point anomaly the smoothing effects of the averaging process are evident. The maximum point anomaly of the composite events

varies between 5.5 and 7.2 ms^{-1}, but fewer than 20% of the WWEs had maximum point anomaly values which are that low; this is because much of the small scale structure of the individual events has been smoothed out by the averaging.

To characterize the behavior of the zonal wind anomaly field as simply as possible, I formulated a simple analytical model for it. I constructed x-t and y-t contour plots of the zonal wind anomaly for each type of event (see Vecchi and Harrison (1997) for the full set of these plots), and found the zonal wind anomaly to be sharply bounded in space and time. Examples of Type C and SE composite suffice to illustrate the typical situation (Figure II.19).

$$U(x,y,t) = U_o \exp\left[-\left(\frac{x - X_o - c_x t}{L_x}\right)^2\right] \times \exp\left[-\left(\frac{y - Y_o - c_y t}{L_y}\right)^2\right] \times \exp\left[-\left(\frac{t}{T}\right)^2\right]$$

A Gaussian in (x,y,t) with translating center to is used define the scales of the events: Where U is the model zonal wind anomaly field, U_o is the maximum point anomaly, (X_o, Y_o) is the geographic center, (c_x, c_y) is the translational velocity, (L_x, L_y) are the spatial e-folding scales, T is the temporal e-folding scale, and x,y and t_n are as in Section II.3.b. The scales for the Gaussian model were computed as follows. The geographic center of the event is identified as the location of the maximum zonal wind anomaly on the center day. The spatial e-folding scales were calculated as half the distance between the two closest e-folding points

TableII. 3. Table of scales for the composite WWEs according to the simple Gaussian model described in section 4.b.

Region	U_o (ms^{-1})	X_o	Y_o	L_x (10^6m)	L_y (10^6m)	T (days)	c_x (ms^{-1})	c_y (ms^{-1})
NW	7.2	132.5°E	12.5°N	1.4	0.6	3.5	-3.8	2.6
N	6.6	185°E	10°N	2.5	0.7	3	-5.1	0.3
NE	6.3	165*W	12.5°N	1.6	1.1	2.5	1.3	
W	6.9	142.5°E	0°	1.7	0.4	3.5	-1.3	1.3
C	6.4	170°E	0°	1.8	0.6	3		
E	5.5	172.5°E	2.5°S	1.9	0.7	3	-1.3	
S	6.4	170°E	10°S	2.2	0.7	2.5	2.5	
SE	6.7	167.5°W	10°S	1.6	0.7	3.5	3.8	

on either side of the center, along the axis in the direction of interest. Since the center of the event generally moves in time through the region, the instantaneous center of the event is defined as the point with the largest zonal wind anomaly within 50° in the zonal and 30° degrees in the meridional direction from the geographic center. The temporal *e*-folding scale was half the time between the two closest *e*-folding points on either side of the center day. Using the instantaneous centers as 'path' data, the translational velocity is the mean velocity with which the instantaneous center moved, during the time when the zonal wind anomalies at the instantaneous centers were above the *e*-folding level.

The characteristics of the events are summarized in Table II.3, presented are the maximum point anomaly, geographic center on day(0), spatial and temporal *e*-folding scales, and translational velocities, for each composite WWE. Using the parameters in the table, the maximum point anomaly (U_o) is between 6 and 7 ms^{-1} and the time scale (T) is close to 3 days for each type of event. All but two types of events have meridional length scale (L_Y) of about 700 km (NE has $L_Y \sim 1{,}100$ km and W has $L_Y \sim 400$ km) and zonal length scale (L_X) between 1,400 and 1,900 km (NW has $L_X \sim 2{,}500$ km and S has $L_X \sim 2{,}200$ km). Note that the atmospheric baroclinic Rossby radius of deformation varies from (assuming a wave speed of 20-80 ms^{-1}) 650 to 1300 km (Gill 1982), which is in general agreement with the meridional length scales summarized in the table. All but one type of event (C) has zonal translation of its center (values ranging from -5.1 for N and 3.8 for SE); only type NW, N and W events have meridional translation (northward in each case). For the type of events which appear clearly associated with northern hemisphere cyclonic circulation patterns (NW, N and W) the translational direction is consistent with the direction expected of a northern hemisphere tropical cyclone. (Lau and Lau 1992; Joint Typhoon Warning Center 1994a,b; Tsutsui and Kasahara 1996, see Figure IV.4.a)

II.5. WWEs and the TOGA-COARE intensive observations period

So far I have concentrated on describing the composite WWEs (Section II.4.a,b) and have proposed a simple descriptive model for them (Section II.4.c). A natural subsequent question is the extent to which the composite WWEs usefully describe the wind field when particular WWEs are taking place. The TOGA-COARE Intensive Observations Period (IOP) (Webster and Lukas 1992; Lukas *et al.* 1995) offers an example period (November 1992 - February 1993) when WWEs were the focus of a major oceanographic and meteorological field program. The IOP occurred at the end of the warm phase of ENSO, ISOs passed over the western pacific during the program (Chen and Houze 1996; Lin and Johnson 1996), and there were some tropical cyclones as well (McBride *et al* 1995). So conditions were very favorable for the appearance of WWEs.

Table 4 lists the WWEs that occurred during the IOP according to the classification scheme. There were three type NE and C events, two type NW, N, E and SE events, and one

Table II.4. List of WWEs occurring during the TOGA/COARE IOP (November 1992 through February 1993). Quantities are as defined in Section 3.a. Events whose wind measure statistic exceeds 2.5×10^6 m are highlighted by bolding.

Region	Date	Maximum point anomaly (ms^{-1})	Duration (days)	Maximum averaged anomaly (ms^{-1})	Wind measure (10^6 m)
N	31 October 1992	12.6	3	4.3	0.8
E	10 November 1992	11.9	4	4.5	1.2
NE	19 November 1992	14.4	4	5.6	1.2
NW	***20 November 1992***	***12.1***	***10***	***4.4***	***3.0***
NE	25 November 1992	13.0	3	5.4	0.9
E	29 November 1992	11.5	4	2.8	0.8
N	9 December 1992	15.7	3	3.9	0.8
S	***1 January 1993***	***19.3***	***8.5***	***10.4***	***3.8***
C	***2 January 1993***	***14.8***	***11.5***	***6.4***	***4.2***
SE	***3 January 1993***	***14.0***	***7***	***4.4***	***2.5***
NE	***5 January 1993***	***14.8***	***9.5***	***4.0***	***2.5***
NW	27 January 1993	15.3	4	3.5	0.9
W	29 January 1993	11.3	4.5	3.9	1.3
C	***31 January 1993***	***11.0***	***10***	***5.0***	***2.5***
SE	***6 February 1993***	***15.1***	***12***	***6.2***	***4.0***
C	10 February 1993	9.5	4.5	3.7	1.2

type W and S events during the IOP. Maximum point anomalies are ≥ 15 ms^{-1} in six events, between 10 and 15 ms^{-1} in nine events and less that 10 ms^{-1} in one event. The maximum averaged anomaly offers another indicator of the overall intensity of the event. By this standard the 1-Jan-1993 type S (10.4 ms^{-1}) and the 2-Jan-1993 type C (6.4 ms^{-1}) events are the most intense of the IOP. The next most intense are the 19-Nov-1992 type NE and the 6-Feb-1993 type SE events. The remaining events have maximum averaged anomalies of 5 ms^{-1} or less.

The final column of Table II.4 lists the wind measure of each event, as defined in Section 3. Three "primary" events have wind measure values near $4x10^6$ m, four "secondary" events have values between $2.5x10^6$ m and $3x10^6$ m, and the rest have values less than or equal to $1.3x10^6$ m. The three primary events are the type S and C events centered on 1 and 2-Jan-1993, and the type SE event centered on 6-Feb-1993. The secondary events are the type NW event centered on 20-Nov.-1992, the type SE event centered on 3-Jan-1993, the type NE event centered on 5-Jan-1993 and the type C event centered on 31-Jan-1993. Late December 1992 and early January 1993 was the period of primary WWE activity according to the wind measure. The next most active period was late January 1993 through early February 1993.

These WWE statistics are consistent with westerly wind periods that have been discussed elsewhere. Eldin *et al.*(1994) reported strong westerly winds and found large eastward surface currents from their ship track along 156°E, during early January 1993 and early February 1993. The large westerly wind activity during early January 1993 and during early February 1993 coincided both times with the passage of the convectively active phase of an ISO (Lin and Johnson 1996; Chen and Houze 1996). Three WWEs seem to be associated with named tropical cyclones: the 31-Oct-1992 type N event (cyclones Dan and Carrie), the 20-Nov-1992 type NW event (cyclone Hunt), the 6-Feb-1993 the SE event (cyclone Mick) (McBride *et al* 1995).

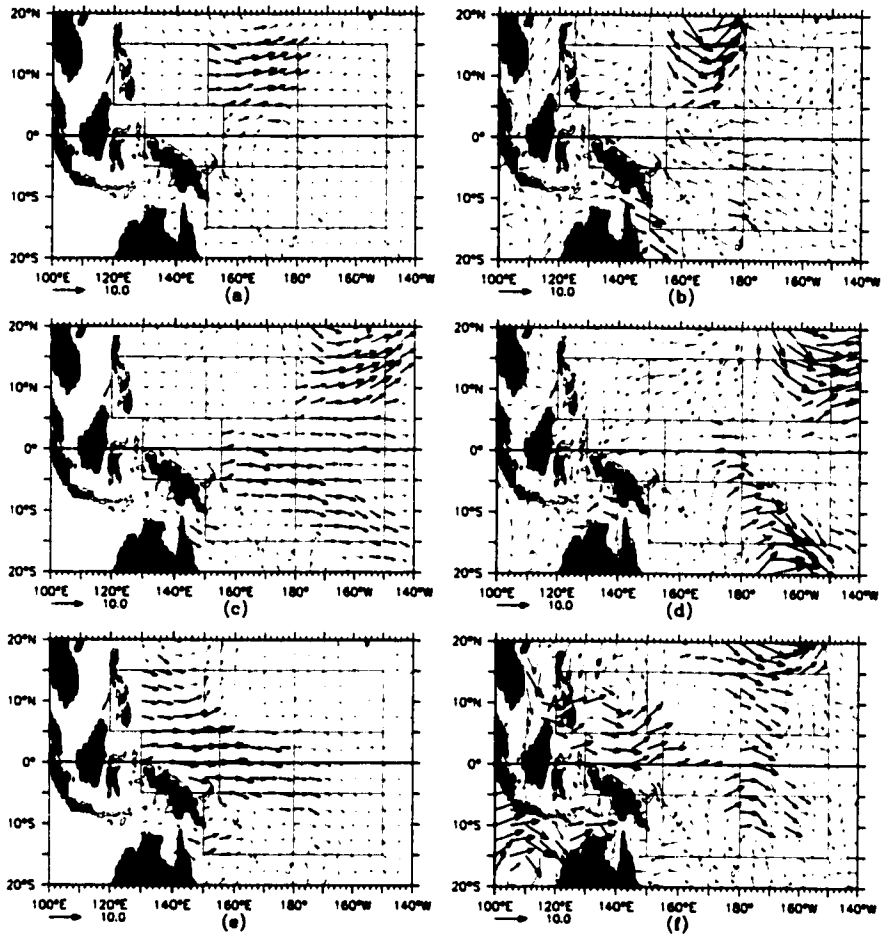

Figure II.20. Vector plots of the wind fields for the composite WWE modeled wind anomaly field on (a) 9 Dec. 1992, (c) 5 Jan. 1993, and (e) 29 Jan. 1993; and ECMWF daily wind anomaly field on (b) 9 Dec. 1992, (d) 5 Jan. 1993, and (f) 29 Jan. 1993. These are three WWE periods occurring during the TOGA/COARE IOP that are well represented by the composite WWE model. Bold wind anomaly vectors indicate zonal wind anomaly exceeding 3 ms^{-1}. Classifying regions are shown by the thin-lined boxes.

How well do the composite WWEs describe the periods of WWEs during the IOP? I have compared the IOP anomaly fields with the wind anomaly fields obtained by simply superimposing the composite anomaly WWEs for the events listed in Table II.4. Vecchi and Harrison (1997) show the results of this comparison for the full IOP period. There are a number of instances in which the simple composite anomaly field is a good first approximation to the real anomaly field, and several instances where the simple field is not so satisfactory. In the interest of brevity I present here only three examples of each. These six event center days are shown for both the modeled anomaly wind field and the daily wind

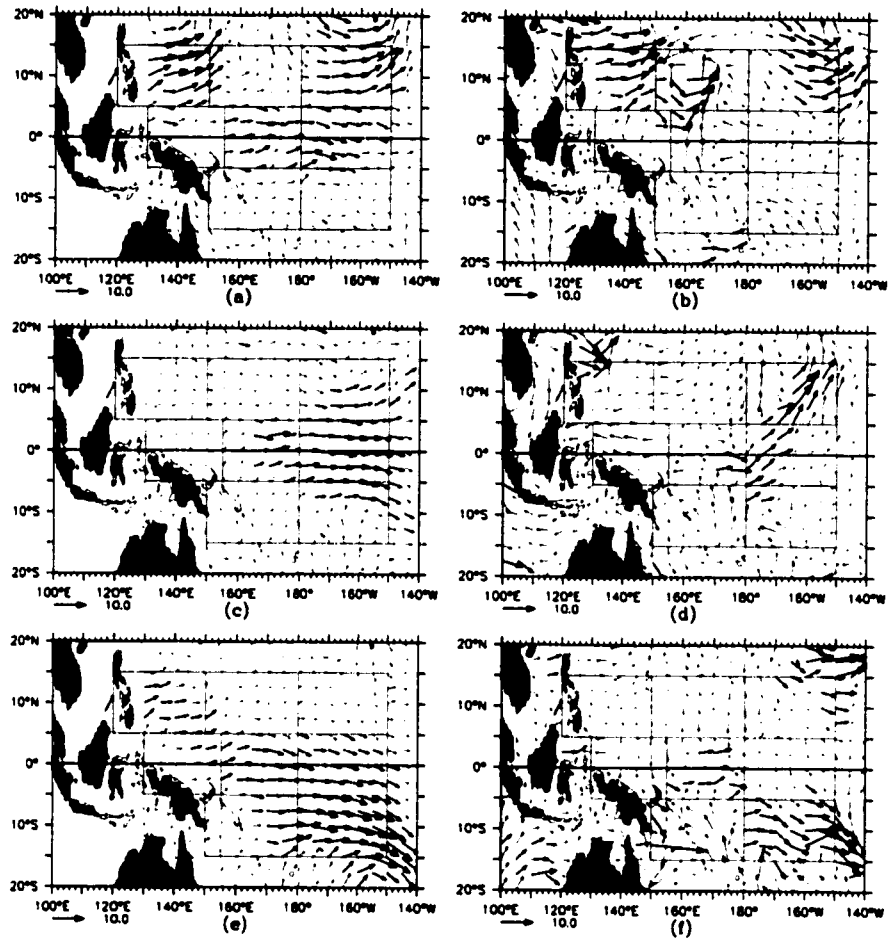

Figure II.21. Same as Figure I.20, except for (a) and (b) 20 Nov. 1992, (c) and (d) 29 Nov. 1992, and (e) and (f) 6 Feb. 1993 These are the three WWE periods occurring during the TOGA/COARE IOP that are most poorly represented by the composite WWE model.

anomaly field, with bold vectors indicating zonal component greater than 3 ms^{-1} (Figures I.20 and .21).

First, consider the three center days when the composite description is a reasonable approximation to the actual anomaly field (9-Dec-92, N; 5-Jan-93, NE and SE; and 29-Jan-93, W and C). Figure II.20 shows that generally the composite description is more diffuse than the daily wind anomaly fields; amplitudes are somewhat reduced and length scales are somewhat larger, even in the defining regions. Outside the defining regions there can be substantial differences, but in these areas the wind anomalies are substantially smaller than in the defining regions.

Now consider the three examples in which the composite fit is least satisfactory (20-

Nov-92, NW and NE; 29-Nov-92, E; 6-Feb-93, SE), shown in Figure II.21. The 29-Nov-92 type E event is quite weak and has substantial ($\geq 3ms^{-1}$) westerly anomalies only in the western third of the defining region; the composite type E event has westerlies over a much greater zonal extent. This is the only situation in the IOP when the composite does not reproduce the basic features of the wind within the defining region. This is also the weakest event during the IOP, based on the wind measure, and its maximum averaged anomaly is only barely over the identification threshold of $2ms^{-1}$. In the other two examples the substantial shortcoming of the composite fit concerns the winds outside the defining regions, particularly near the equator. These IOP off-equatorial events have less equatorial westerly wind than one would expect from the composite WWEs.

More than half the IOP WWEs had a duration shorter than the composite events, so the composite fit produces near equatorial westerly wind anomalies when they were not present in the wind fields. During periods when the WWEs have a duration more like that of the composite events, the fit is much better. This is because while the WWEs identified and averaged to generate the composite WWEs have similar general characteristics, the differences in the details result in a smudged composite WWE.

II.6. Temporal distribution

In this section I describe various temporal relationships for WWEs. I present the climatological distribution of WWEs by month, and define seasonality for each WWE type when applicable. I also show the year to year variation of WWE occurrence and intensity. Finally, I offer some statistics on the extent to which WWEs occur in particular relationships to each other.

a. Single event distributions

Consider first the climatological distribution by month. Figure II.22 shows, for each region, the ten year (1986-95) total number of WWEs that occurred during each calendar

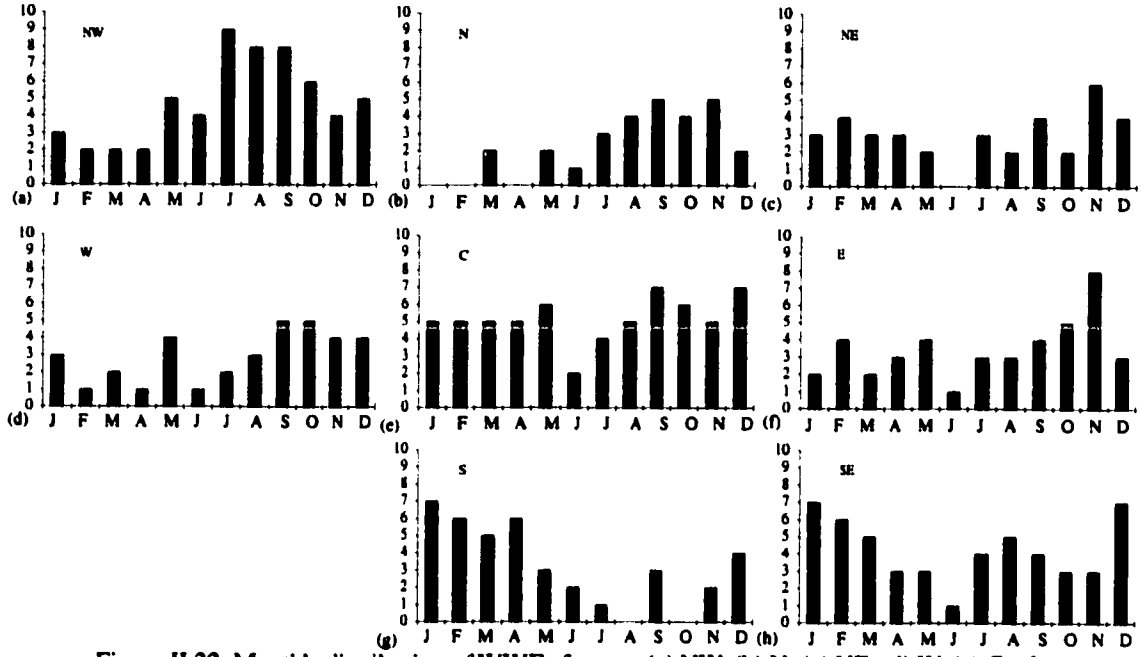

Figure II.22. Monthly distribution of WWEs for type (a) NW, (b) N, (c) NE, (d) W, (e) C, (f) E, (g) S, and (h) SE.

month. No striking variation is seen in the month-by-month comparison, but there is a clear seasonal preference for types NW, N and S, which is statistically significant to the 99% level using the test described in Appendix 1. A seasonal description for the distribution of the type NW WWEs is that of an "on" season from July through October, two transition seasons (May-June and November-December) and an "off" season from January through April. For the type N and S WWEs the simplest seasonal description is that of a six month "on" season, and a six month "off" season. The "on" seasons are July through December for the type N event, and December through May for the type S event. I cannot define an "on" or "off" season for type NE, W, C, E or SE events that is statistically significant at the 90% level.

The distribution of moderate or stronger WWEs is somewhat more striking; defining a moderate or stronger event as an event whose wind measure (see Section II.3.a) exceeds 2×10^6 m, leads to Figure II.23. Boreal summer and fall are the primary seasons for the type NW (July-December) and N (July-October) events; November through January is the primary season for type C events; and boreal winter and spring are the primary seasons for

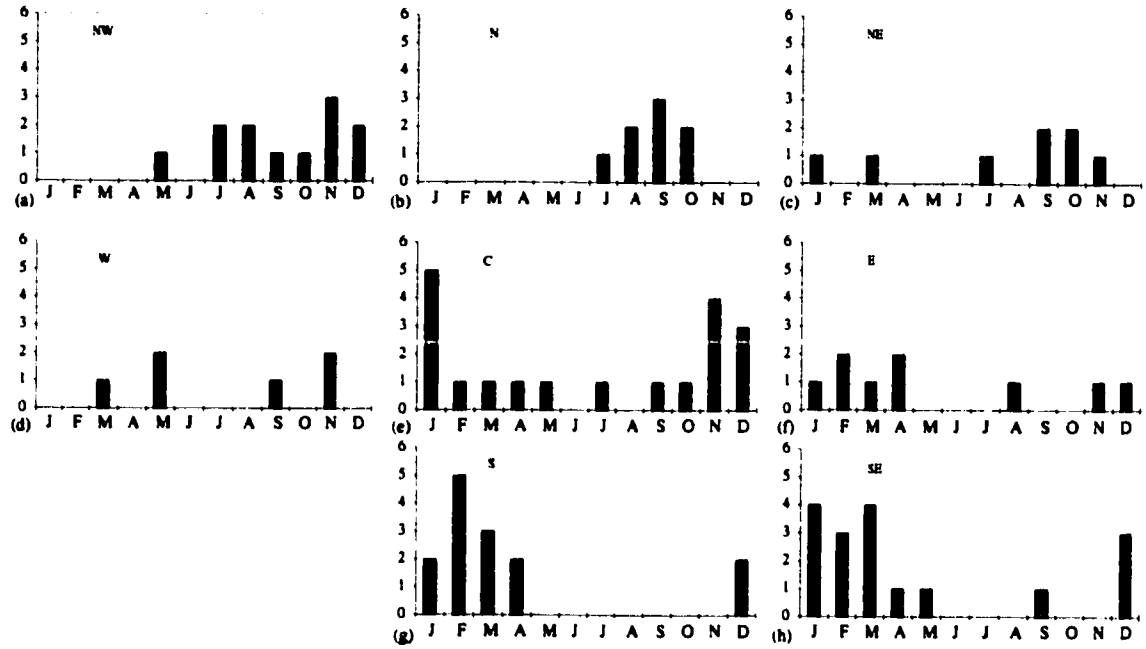

Figure II.23. Monthly distribution of WWEs with mind measure in excess of 2.0×10^6 m for type (a) NW, (b) N, (c) NE, (d) W, (e) C, (f) E, (g) S, and (h) SE.

type S (December-April) and SE (December-March) events. While the type C events are evenly distributed across the months, most of the events that occur between November and February are of moderate or greater strength. All these seasonal distributions are significant to the 97% level. No seasonal distribution, significant even at 70%, exists for the strong type NE, W and E events.

Now consider the year-to-year distribution of WWEs. Figure II.24 shows the number of each type event, year by year from 1986 through 1995. The mean number of events is indicated by the thick horizontal line. It is also instructive to compare these distributions with the Troup Southern Oscillation Index (SOI). The twelve month running mean of (-1)xSOI is plotted along with the mean (-1)xSOI for the 10 year period 1986-95, as the lower left hand panel of Figure II.24. SOI values have been negative much of this period, indicating warm (ENSO) conditions for the tropical Pacific; the ten year average is -4.5.

The fewest number of events occurred in 1988 for every type of event, and in most regions 1989 was also a year of few events. 1988-89 was the only period of persistently positive SOI in this record. There is no comparably strong connection between years of

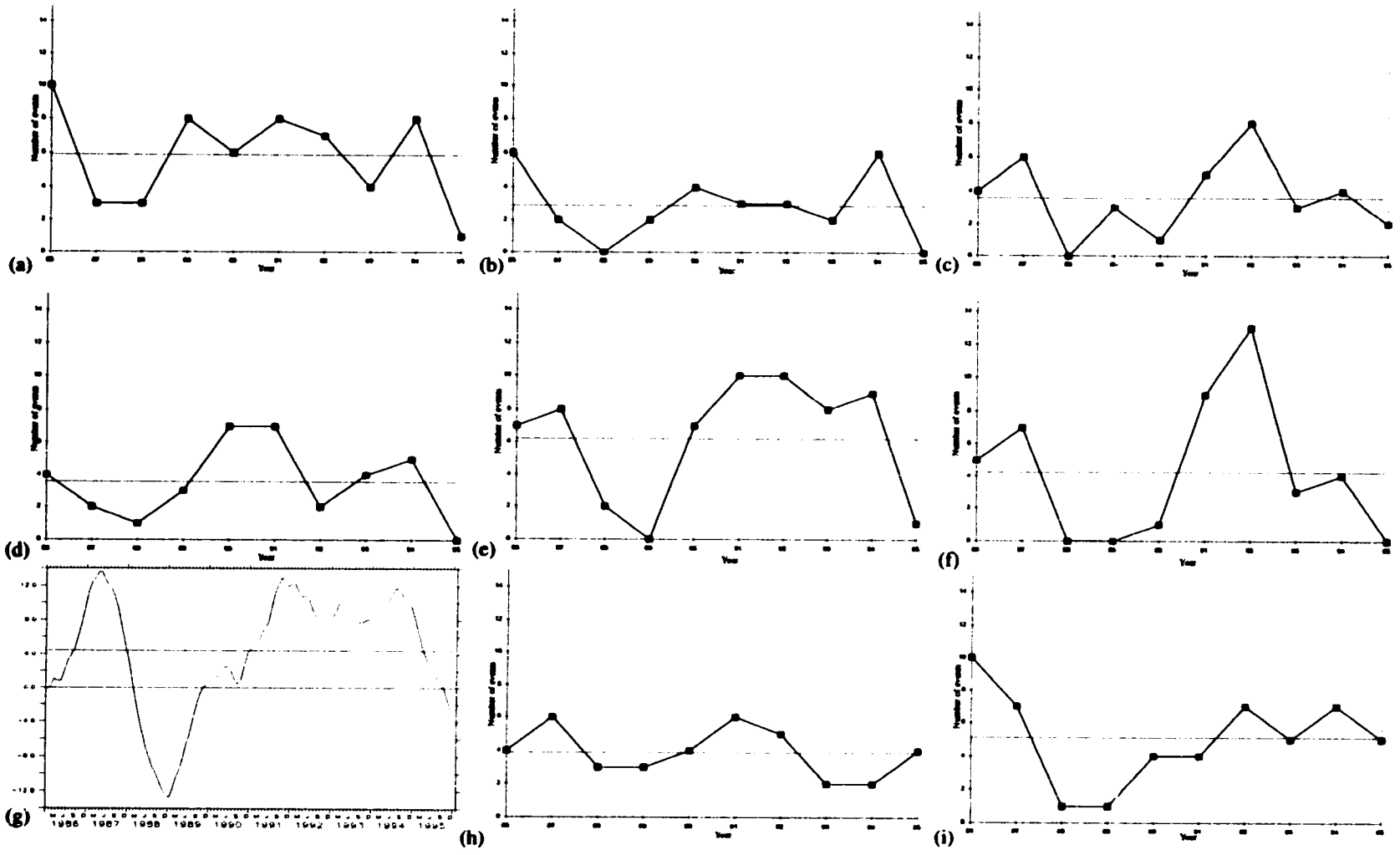

Figure II.24. Plots of yearly distributions of WWEs for type (a) NW, (b) N, (c) NE, (d) W, (e) C, (f) E, (h) S, and (i) SE. Also shown is (g) the 12-month running mean of the quantity (-1)×Troup SOI Superimposed on all the panels is the 10-yr-(1986-95) mean of each quantity.

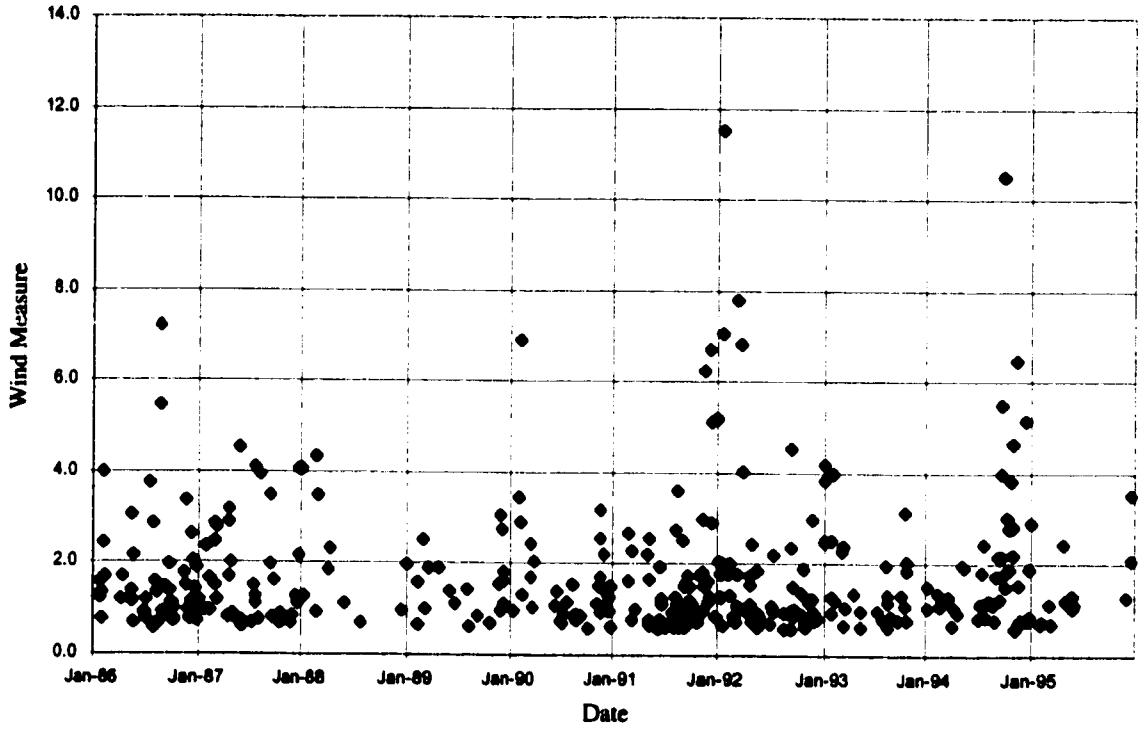

Figure II.25. Scatterplot of wind measure vs. center date of WWE, for all the WWEs in the period 1986-1995. Wind measure is as defined in Section 3.a, and units are 10^6 m.

negative SOI and more than normal total number of WWEs. However lagged correlations between the SOI and the number of events in each region revealed that some statistically significant relationships exist. The strongest correlation (-0.85) exists for type C events at zero lag, and is 99% significant. Zero lag correlations significant at the 95% level exist for type NE(-0.69), E(-0.69) and SE(-0.68) events. Type NW and W regions have 90% significance level correlation (-0.61 and -0.59 respectively) but they lead the SOI by one year. Overall, WWEs in the easternmost three regions and the C region are negatively correlated with zero lag to SOI. WWEs in the westernmost regions are negatively correlated at a one year lead with SOI. Only type N and S events do not show a significant correlation with SOI.

There is another WWE-SOI relationship of interest, which is evident in Figure II.25. In this figure I have plotted a scatter plot of the wind measure of all the events in the10 year record. It is clear that strong events (wind measure > $3x10^6$ m) associate well with periods

of most negative SOI, and that no strong events occur when SOI is positive (see Figure II.24).

b. Multi-event distributions

I have implied an independence of WWEs throughout this study. Typically WWEs form, develop and decay without any strong relationship with other events. I base this on a study of the sequencing of events with center days within three days of each other, looking to determine if there were any statistically significant patterns. In a few instances of substantial statistical significance (99%) different types of WWEs seem to be related. For example, 18% of the time a type N event will evolve into a type NW event (5 times), 17% of the time a type W event will evolve into a type NW event (6 times) and 18% of the time a type S event will evolve into a type SE event (7 times). These three relationships are consistent with the translation speed of the original event. It must be noted that it is not typical for the second event to form out of the first. Two other statistically significant relationships exist in the record, for which I cannot propose mechanisms. In the record 18% of the time a type N event will precede a type SE event (5 times) and 14% of the time a type E event precedes a type NE event (6 times). These last relationships might be coincidental, or there might be some mechanism which accounts for their occurrence. Longer records, containing additional WWEs are needed to determine the robustness of these relationships; only a very few instances exist in the 10-year record.

Another aspect of interest in the frequency distribution of westerly winds was identified by computing the average zonal wind anomaly over the area spanned by all eight of the WWE regions. Recall that a WWE is defined to exist in any one of the WWE regions when the area average zonal wind anomaly exceeds $2ms^{-1}$ for three days. Defining a "Mega"-WWE (MWWE) to exist when the average over all eight regions meets the WWE criterion; there are eleven MWWEs in the analysis period. Figure II.26 provides a cartoon of the spatial structure and wind measure of each MWWE.

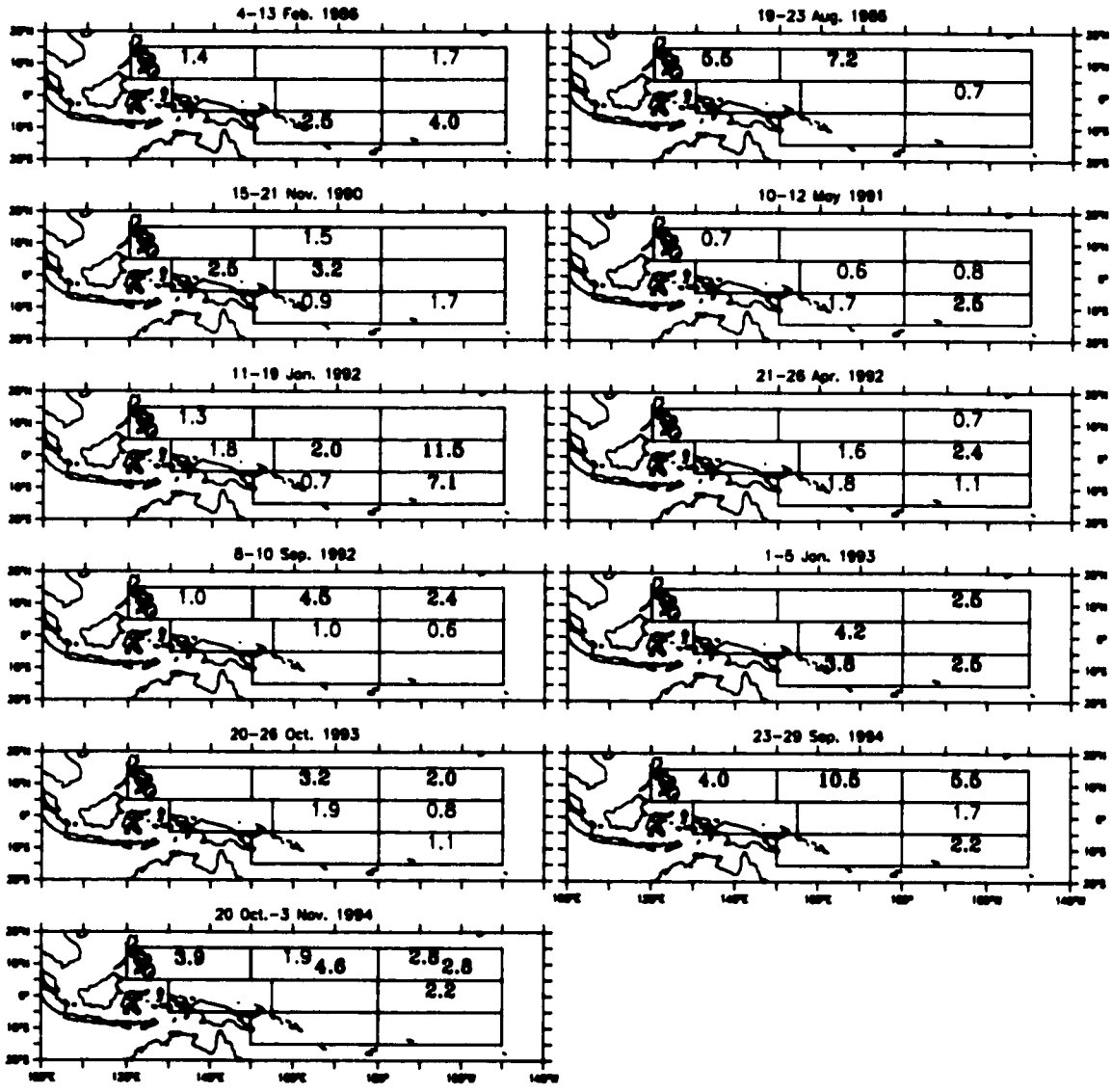

Figure II.26. Cartoon description of the mega-WWEs (MWWEs) in the record. The dates of the MWWEs appear on the top of each figure. Inside the regions involved in the MWWE is listed the wind measure for the particular WWEs. Wind measure values are bolded if greater than 2×10^6 m. Units for wind measure are 10^6 m.

The number of MWWEs by year is: 2-86, 1-90, 1-91, 3-92, 2-93, 2-94; MWWEs only occur during years when the annual average SOI was negative. Of the eleven MWWEs one involves three regions, two involve four regions, six involve five regions and two involve six regions. One MWWE does not involve any of the three equatorial regions, four involve only one, five involve two and one involves all three equatorial regions. In the MWWEs the component WWE of largest wind measure occurs five times in a northern

region, four times in an equatorial region and two times in a southern region. In none of the MWWEs does the W or NW region have the event of largest wind measure. Apart from having events of strongest measure in the central or eastern regions, no clear geographical patterns emerge for MWWEs.

There is a suggestion of seasonality in the meridional frequency of the component WWEs in each MWWE. The five MWWEs for which the dominant component WWEs were northern hemisphere WWEs occurred between the middle of August and the beginning of November; the three MWWEs which had southern hemisphere WWEs as their primary component WWEs all occurred between January and May; the three MWWEs which had equatorial WWEs as their main component WWEs occurred between late November and late April. However there are too few MWWEs for us to do meaningful statistics.

The TOGA COARE IOP contained one MWWE, composed of WWEs with center days between 1-Jan-1993 and 9-Jan-1993. Only this IOP MWWE and one other had each type of WWE in it with wind measure greater than 2.0×10^6 m. Most MWWEs have several types of WWEs with wind measure less than 2.0×10^6 m. The TOGA-COARE IOP thus represented an extreme period of westerly wind variability.

II.7 Summary and discussion

I have examined ECMWF 10m surface wind analyses every 12 hours between 1986 and 1995, to characterize the space and time scales of westerly wind events (WWEs) in the tropical Pacific ocean. I found that Pacific WWEs can be classified satisfactorily according to the region in which they attain their maximum zonal wind anomalies, and that eight adjoining regions are needed to describe the different WWEs in the wind fields. The events are named by the region used to define their existence; regions are named according to their position relative to each other and to the equator (Figures II.5 and II.6): NW, N and NE are

north of the equator; W, C and E straddle the equator; S and SE are south of the equator. With a quantitative measure to define the existence of a WWE, there were 351 events in this period: 58- NW, 28-N, 36-E, 35-W, 62-C, 42-E, 39-S and 51-SE.

I generated a composite event for each type by averaging and find that the zonal wind anomalies associated with each type of event are quite compact in space and time. The structure of each event is modeled as a uniformly translating Gaussian in space and time (Table II.3). The typical amplitude is between 6 and 7 ms^{-1}; the typical *e*-folding time scale is about 3-days (duration is six days between the times of e^{-1} amplitude). The time-scales found by Harrison and Giese (1991) are longer (5-10 days), but the amplitudes obtained in this study compare well to theirs. The meridional *e*-folding scale varies between event types from 400 km to 1,100 km, but values are mostly in the 600-700 km range; these meridional *e*-folding scales are slightly larger to those found by Harrison and Giese (1991). Zonal *e*-folding scales vary from 1,400 km to 2,500 km, while the equatorial events have *e*-folding scales of 1,700 to 1,900 km; Giese and Harrison (1991) estimated a zonal length scale of 20°, that is an *e*-folding scale of about 1,000 km, from the island wind data. Some events translate slowly (largest speed is about 5 ms^{-1}) and others show no significant translational motion. In Section 2 four additional quantities to characterize WWE were defined: duration, maximum point anomaly, maximum averaged anomaly and wind measure; Table II.2 summarizes these characteristics for each type of composite WWE.

This classification method is similar to an extension of that used by Harrison and Giese (1991), except that a two dimensional surface wind field that covers the entire western and central Pacific has been used, instead of a distribution of islands. The analysis can be extended to the zonal scales and translation characteristics of WWEs throughout the entire tropical Pacific. Hartten (1996) used a subjective classification scheme based on the circulation patterns that are observed in association with westerly wind activity, which is defined in terms of wind and not wind anomaly. Hartten's analysis, which covers the area

west of the Dateline, finds many of the circulation patterns seen in the composite WWE analysis; such as cross-equatorial flow, cyclonic circulation patterns and inflow from the west. However, where the trade winds are a strong and persistent feature of the tropical atmospheric circulation, the strong anomalies that are seen in the studies will not usually satisfy her westerly wind burst criterion of 5 ms^{-1} westerly winds. Also, west of the dateline, climatological winds are westerly at 2-3 ms^{-1} in the equatorial western Pacific from November through February, and in the northwestern tropical Pacific (120°E to 145°E, 5-15°N) from July through September. So Hartten's definition identifies as westerly wind bursts situations in which the winds are nearly climatological and does not identify all periods where the wind anomalies are strongly westerly.

Composites like these are most useful when they reasonably well represent the characteristics of typical events in their region. The TOGA-COARE Intensive Observing Period (IOP) provided a four month period (November 1992-March 1993) which contained at least one event of each of the types. The WWEs of the IOP period are summarized in Table II.4. There were 16 WWEs during the IOP; the events with the largest wind measure values occurred late December 1992, early January 1993 and toward the end of January 1993. Another period of strong westerly wind activity was the third week of November 1992. Nine IOP events had wind measure less than $1.3x10^{6}$ m., and seven of the events had wind measure greater than $2.5x10^{6}$ m. Most events had maximum point anomaly values between 11 and 16 ms^{-1}; one event had maximum point anomaly greater than 19 ms^{-1} and one less than 10 ms^{-1}. There was a MWWE in early January 1993, involving four different types of WWEs (S, C, SE and NE) in rapid sequence (center days between 1-Jan-1993 and 5-Jan-1993); this was one of the most intense periods of westerly wind variability in the ten year record. The strong WWEs occurring at the beginning of January 1993 and the beginning of February 1993 were associated with the convectively active phase of an MJO (Lin and Johnson 1996; Chen and Houze 1996). Three WWEs were associated with named tropical

cyclones, two in the northern hemisphere and one in the southern hemisphere

The wind anomaly fields produced simply by superimposing the composite anomalies in place of the particular WWEs of the IOP were compared with the actual wind anomalies. In many cases the composite representation is reasonable. The most common shortcoming is that the weaker WWEs during the IOP typically were of shorter duration than the composites, particularly near the equator. This means that the composite representation tended to have more near-equatorial westerlies than the IOP wind anomalies indicate. It is not simple to characterize the events that are not well modeled by the composites; some had a small wind measure and others a large one, and there were no event types which were dramatically better (or worse) represented by their composite.

Overall, the composite WWEs offer a useful first characterization of the structure of substantial westerly wind anomalies in this region. The composite events are representative of many WWEs, according to the intensity criteria (Figure II.18). However there are events more extreme than the composite events. Because aspects of the oceanic response to WWEs depend on the wind stress or some higher power of the wind stress magnitude, it may turn out that these extreme events must be examined separately in order to understand the full range of ocean response to WWEs. The idealized WWEs used in the response studies of Harrison and Giese (1988) and Giese and Harrison (1991) in their WWE experiments were conservative; indicating that WWEs might force the ocean more strongly than suggested by their idealized experiments.

The distribution of WWEs by year, by climatological month and relative the Troup Southern Oscillation Index (SOI) were also examined. Moderate to strong events (those with wind measure greater than 2×10^6 m) show distinct seasonality for some WWE types (see Section I.6), with off equatorial events tending to favor local summer and fall seasons, and type C events tending to favor boreal winter; while no seasonality is apparent in either the type NE, W or E events. These seasonal distributions are consistent with those found by

Harrison and Giese (1991) and by Hartten (1996). Correlation of annual distribution with SOI is less simply summarized, in part because the SOI was predominantly negative during the period of study - only mid 1988 through mid 1989 and late 1995 had SOI persistently positive. Overall there is a 95% statistically significant negative correlation between SOI and type C, NE, E and SE events at zero lag, and 90% significant negative correlation between SOI and type NW and W events with the events leading the SOI by a year. The type C event is the only event whose correlation with Troup SOI is significant to the 99% level.

The relationships between the existence, preferred location, and intensity of WWEs and the large scale environment of the atmosphere remain to be uncovered. Because the MJO is prominent in tropical convection and free atmosphere zonal wind anomalies (Madden and Julian 1972,1994; Rui and Wang 1990), and because WWEs are often associated with enhanced convection (Kiladis *et al* 1994; Meehl *et al* 1996), a relationship between WWEs and the MJO (particularly the convectively active phase of the MJO) has been suggested (Lau *et al* 1989; Sui and Lau 1992). In particular, the two most intense periods of surface westerly wind variability during the TOGA-COARE IOP occurred in association with the convectively active phase of the MJO. In Chapter IV, I examine the relationships that have been evident in the period 1986-1995 between WWEs, and the MJO and tropical cyclones.

WWEs are an unusual mode of tropical atmospheric variability. According to this analysis the off-equatorial events appear associated with tropical cyclonic systems, but the period in which substantial westerly wind anomalies exist over regions of any significant extent is not characterized by strong translation of the cyclonic system. In this sense, it would seem that these Pacific systems are rather different from their tropical Atlantic counterparts, which usually propagate over large distances once they form. I found nothing similar to WWEs in the ECMWF analyses over the tropical Atlantic or tropical Indian Oceans. In four of the off-equatorial composite WWEs (types NW, N, S and SE) I find moderate (2-

4 ms^{-1}) cross-equatorial inflow and as well as moderate (2-4 ms^{-1}) inflow from the west during the days surrounding the center day (see Section 4.a); Hartten (1996) also has identified cross equatorial circulations into her sort of westerly wind bursts north of the equator, as well as inflow from the west. I are not able to identify a consistent source of alternate-hemispheric flow; the tropical extra-tropical connection remains unclear.

The near-equatorial WWEs are sometimes associated with cyclonic circulations on either (or both) hemisphere. In many instances events of these types appear to be simple down-gradient pressure flows, with meridional scale determined by the atmospheric first radius of deformation. The near equatorial events in the analysis seem also to have a mid-latitude connection, with cross equatorial inflows similar to those described by Love(1985a), Chu(1988), and Chu and Frederick(1990). An interesting feature is the moderate to strong (>2 ms^{-1}) meridional inflow generating poleward of 20° on the days preceding and on the center day of the event (see Section II.4.a).

The near-equatorial events are the primary events to force the ocean east of their location, and it is most likely these events which help to cause warm water to be advected eastward and downward by Kelvin-wave type surges during ENSO events. This type of behavior has been modeled (Schopf and Harrison 1983, Harrison and Schopf 1984, Giese and Harrison 1991) and observed (McPhaden *et al* 1992, Delcroix *et al* 1993) in the equatorial Pacific. Because the SST changes associated with the remote forcing of modest amplitude WWEs is modest - typically 0.5°C over a couple of months, according to Giese and Harrison (1991) - it is not simple to observe clearly in an ocean full of variability on many frequencies. Chapter III deals with the analysis of the SSTA variability associated with each equatorial WWE type, while Chapter V describes the observed eastern Pacific SST warming with an ocean general circulation model (OGCM).

Chapter III
Tropical Pacific SSTA and Equatorial Westerly Wind Events

III.1 Introduction:

This chapter examines global statistical relationships between westerly wind events (WWEs) and sea surface temperature anomaly (SSTA) variability, using a compositing technique for the period 1986-1998. I describe the extent to which equatorial WWEs are associated with central and eastern equatorial Pacific waveguide warming and with local SSTA changes under the WWE. The work described in this chapter will appear in a forthcoming issue of the Journal of Climate (Vecchi and Harrison, 2000 - henceforth VH00), and builds on the WWE identification scheme outlined in Chapter II. The goal is to quantify the extent to which equatorial WWEs are fundamental to the onset and maintenance of warm El Niño/Southern Oscillation (ENSO) conditions. In order to understand the effect of WWEs on SSTA evolution, I begin by examining how SSTA changes in the absence of equatorial WWEs. I find that SSTA tends towards climatology in the absence of equatorial WWEs, whether the eastern equatorial Pacific has close to normal SSTA or warmer than normal SSTA.

There are significant SSTA changes under the main WWE wind anomalies for all three equatorial WWE types. The two equatorial WWE types whose main surface wind anomalies are west of the dateline (W and C) are associated with weak local surface cooling. The equatorial WWE type that has equatorial westerly wind anomalies east of the dateline (E) is associated with weak warming under those anomalies, when the eastern equatorial Pacific SSTA is close to normal.

When the tropical Pacific has near normal eastern equatorial Pacific SST, each of the equatorial WWE types are followed by substantial equatorial waveguide warming in the

central and eastern Pacific (composite warming as large as 1.0°C); also more than 50% of the large amplitude WWEs were followed by NIÑO3 SSTA warming in excess of 0.5°C. These changes are of similar amplitude and spatial structure as those seen in the onset of El Niño, and are consistent with the predicted oceanic response to WWE forcing. When the eastern equatorial Pacific is initially warmer than usual, the two westernmost equatorial WWE types (W and C) are associated with the maintenance of warm El Niño eastern and central Pacific SSTA; these warm anomalies tend to disappear in the absence of those WWE types. The main result of this work is that WWEs, or some mechanism strongly correlated with WWEs, represent a fundamental process for waveguide warming in the onset of El Niño, and for eastern and central Pacific warm SSTA maintenance during El Niño.

Linear theory predicts that equatorial westerly wind anomalies in the western and central Pacific will drive current and temperature changes across the tropical Pacific through the excitation of eastward propagating Kelvin pulses (Godfrey 1975, Anderson and Gill 1976, McCreary 1976, Moore and Philander 1977, Giese and Harrison 1990). These Kelvin pulses will generally be associated with eastward surface currents, and warming of the surface ocean through anomalous advection of the background zonal temperature gradient. The first two vertical modes will generally lead to thermocline deepening, and subsequent surface warming due to vertical advection of anomalously warm sub-surface water. The details of the background ocean temperature and density field, and the structure of the wind forcing determines the details of the expected response. Though the first baroclinic mode is the one generally discussed, modes higher than the first are a significant part of the predicted linear response (Harrison and Giese 1989, Giese and Harrison 1990).

Modeling studies of the oceanic response to WWEs have shown that WWEs can force large surface and sub-surface temperature changes by modifying the zonal current structure in the central and eastern equatorial Pacific (Harrison and Giese 1988, Giese and Harrison 1990, 1991, Harrison and Craig 1993, Kindle and Phoebus 1995). It has also been

suggested that interaction between the WWE forced eastward propagating current pulse and the tropical instability wave (TIW) field in the central and eastern tropical Pacific can lead to enhanced waveguide warming (Harrison and Giese 1988, Giese and Harrison 1990,1991). In modeling studies the background state of the model oceans can greatly influence the response to anomalous forcing (Schopf and Harrison 1983, Harrison and Schopf 1984, Harrison and Giese 1990); it is important to consider the background state of the ocean when determining the effect of anomalous forcing.

Case studies have found large amplitude local and remote changes to the oceanic temperature, current and sea surface height fields, related to the WWEs. Local response to WWEs involves surface cooling and freshening, a deepening of the mixed layer and strengthening of the thermocline, along with an eastward surface and westward subsurface current jet (McPhaden et al. 1988, McPhaden et al. 1992, Delcroix et al. 1993, Eldin et al. 1994, Smyth et al. 1996.a-b, Cronin and McPhaden 1997, Ralph et al. 1997, Feng et al. 1998). Remote changes observed to follow WWEs include eastward propagating increase in sea surface height, eastward surface current, net eastward equatorial transport, deepening of the thermocline, an increase in SST and upper ocean heat content (Eriksen et al. 1983, McPhaden et al. 1988, Kessler and McPhaden 1995, McPhaden 1999). There has been an indication of a relation between eastern Pacific biological productivity and Kelvin pulses related the westerly wind variability (Chavez et al. 1998). Analysis of the recent 1997-8 El Niño event has suggested that the genesis of the event can be traced to a series of periods of westerly wind in the western and central Pacific (Yu and Rienecker 1998, McPhaden, 1999). Strong westerly wind variability has occurred without leading to El Niño warming: one of the strongest periods of WWE activity in 1986-1998 occurred during the TOGA/COARE IOP in January 1993 (HV97); in spring 1993 eastern equatorial SSTA increased and briefly produced strong anomalies but SSTA then returned to normal and remained so for the rest of the year (see Fig. III.1.a). According to the BEI index of Harrison and Larkin (1998),

1993 was not an El Niño year.

Some statistical relationships between equatorial westerly wind variability and SSTA changes across the tropical Pacific were examined to help assess the theoretical, modeling and anecdotal evidence for a relationship between westerly wind variability and SSTA changes. The analysis was performed separately for periods in which the eastern tropical Pacific SSTA was initially close to normal and when it was warmer than normal. The WWE associated SSTA variability was compared with the SSTA variability when no equatorial WWEs occurred, to determine which features were associated with the WWEs and which showed no special relation to WWEs.This has been the first systematic statistical analysis to suggest that WWEs are a fundamental mechanism in the onset and maintenance of El Niño.

In the following sections I summarize the methods and results, and discuss some of the implications of the results. Section III.2 describes the datasets used and the statistical analysis method. The results of compositing SSTA for each WWE type are described in Section III.3. Section III.4 offers a summary and discussion of the main results.

III.2. Datasets and Methods

The European Centre for Medium Range Weather Forecasts (ECMWF) 12-hourly 2.5°¥2.5° gridded 10-meter wind operational analysis (European Centre for Medium Range Weather Forecasts 1989), and the method described in Chapter II were used to identify all the WWEs in the period 1986-1997. The SST analysis used the Reynolds/NCEP weekly 1°×1° gridded SST product (Reynolds and Smith 1994). A monthly climatology of SST was generated using the weekly SST data from 1984 through 1996 (those years are chosen to exclude the very anomalous periods of 1982-3 and 1997-8); SSTA was computed from this monthly climatology. Note that the analysis was repeated using other SST climatologies, and none of the principal results were affected.

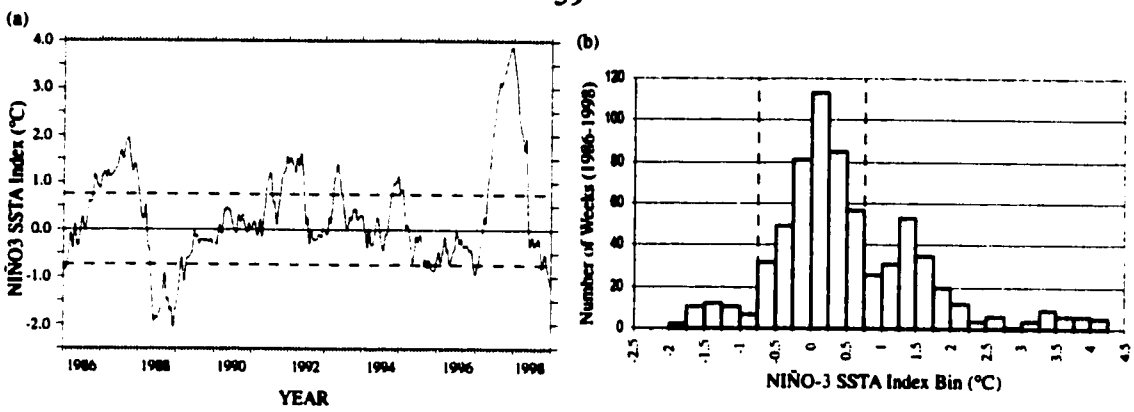

FIGURE III.1: (a) Weekly time-series of the NIÑO3 SSTA index used in this study, for the period 1986-1998. Dashed lines indicate the cutoffs for the three ENSO regimes (as defined in Section 2). Note how the El Niño events of 1986-88, 1991-92 and 1997-98, and the La Niña event of 1988-89 are identified by the index. (b) Histogram of the NIÑO3 SSTA index used in this study, for the period 1986-1998. The bin width is 0.25°C; the dashed lines indicate the cutoffs for the three ENSO regimes (as defined in Section 2). Notice how there appear to be three distinct modes in this period.

To summarize the SSTA evolution following WWEs it is useful to consider separately events that occurred in different ocean/atmosphere states. Ideally, one would examine the evolution of the ocean in different periods of the seasonal cycle and in different phases of ENSO. Due to the limited data available (13 years), I only considered the different phases of ENSO separately. A widely used quantity to categorize the ENSO state of the ocean is the NIÑO3 SSTA index, defined as SSTA averaged over the region 150°W-90°W, 5°S-5°N. Figure III.1 shows the time-series and histogram of the NIÑO3 index used here; the index identifies the El Niño events of 1986-8, 1991-2 and 1997-8 clearly, and the La Niña of 1988-9 is also evident. The distribution of NIÑO3 SSTA, shown in figure III.1.b, can be described as having three main states (cold, normal and warm), with a long tail on the warm side; this tail results from the large El Niño of 1997-8.

For the analysis, I describe the ocean as having 3 main states: COLD (NIÑO3 < -0.75°C), REG (-0.75°C ≤ NIÑO3 ≤ 0.75°C), and WARM (NIÑO3 > 0.75°C). Table III.1 shows the breakdown of WWEs by event type and NIÑO3 state 20 days before the WWE center day. Note that no equatorial WWEs occurred when the system was initially in a COLD state. Further discussion is limited to the REG and WARM states. The results de-

scribed in this paper are qualitatively unaffected by using thresholds between WARM and REG in the range 0.25°C to 1.25°C; nor are they affected by ignoring the separation between COLD and REG states. Testing against a binomial distribution with probabilities determined by the total number of REG and WARM days, the Type C and E events have a distribution which shows a preference for the WARM periods, significant at the 99% level. This distribution is consistent with the interannual distribution of WWEs relative the Troup-SOI discussed in Chapter II, Section 6.a.

To examine the evolution of the SSTA field following the WWEs a series of composites were generated as in HV97. To quantify the composite SSTA evolution, I defined the SSTA change (ΔSSTA) relative to the WWEs as the difference between the SSTA at a given time and the SSTA 20 days before the center day of the WWE (Day (–20)). I generated both REG and WARM composites of SSTA and DSSTA for each WWE type from Day (-30) (30 days before center day) to Day (120) (120 days after center day). Since the distributions of the SSTA and DSSTA field are not normal, to test for statistical significance we use a bootstrap method (Efron and Tibshirani 1991), using 1000 bootstraps samples. The composite SSTA and ΔSSTA fields are tested at the 95% level, for difference from a mean of zero.

TABLE III.1: Number of WWEs identified in the period 1986-1998, broken down by NIÑO3 SSTA condition 20 days before the WWE center day. The final row shows the percentage of all days which fall into each of the NIÑO3 SSTA condition bins. WWE types identified as in HV97, see Section 2 for a description of the NIÑO3 SSTA conditions. Bolding indicates the NIÑO3 SSTA state with a singificant number of WWEs.

WWE Type	Total (1986-1998)	COLD (NIÑO3 < -0.75°C)	REGULAR (-0.75°C ≤ NIÑO3 ≤ 0.75°C)	WARM (NIÑO3 > 0.75°C)
W	41		**30**	11
C	72		39	**33**
E	56		19	**37**
Percentage of total days		11.0	60.6	28.4

To correctly interpret the relationship between SSTA variability and WWEs, it is necessary to understand how the evolution of SSTA following a WWE compares with the evolution of SSTA when there are no WWEs of that type. In order to interpret the SSTA/WWE associations, for each WWE type I constructed a series of WWE non-event composites, using a bootstrap method. First, all the dates that were not within 10 days of a center day for a particular WWE type were identified; those days were labeled as "non-event center days" for that particular WWE type. I then generated 1000 WARM and REG non-event SSTA and ΔSSTA composites for each WWE type by randomly sampling (with replacement) the non-event center day list, the non-event composites go from Day (-30) through Day (120). At each location, for each composite day, the SSTA and ΔSSTA non-event composite value was taken as the mean of the 1000 random non-event composites. Also computed were the percentage of non-event composites that had SSTA or ΔSSTA values as large or larger than the corresponding event composite, which were used to compute the significance of the event composite relative to the non-event composite.

To explore the evolution of the SSTA field following periods when no WWEs of any of the three equatorial types occurred ALL/WARM and an ALL/REG non-event composites were generated, by excluding all equatorial WWE periods. The ALL non-event composites were computed from Day (-30) through Day (120) by using all days that were not within 10 days of any WWE center day as the non-event center days. The composites were computed using a bootstrap method (Efron and Tibshirani 1991), with 1000 bootstrap samples, and tested against a mean of zero at the 95% level.

III.3. Results

Here I summarize the results from compositing SSTA and ΔSSTA for each of the three equatorial WWE types, both for events and non-events (see Section III.2). Only those features in the composites that are significant at the 95% level are discussed. I first describe

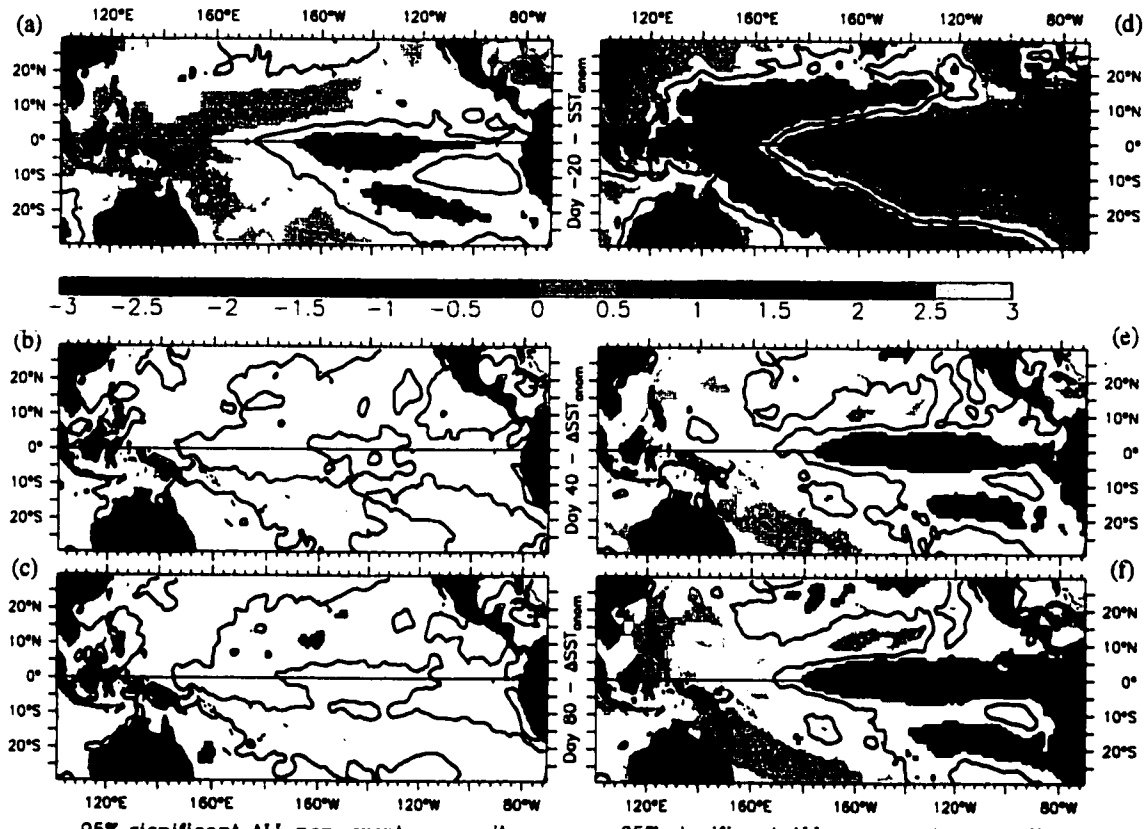

FIGURE III.2: ALL/REG non-event composite: (a) Day (–20) SSTA, and (b) Day (40), (c) Day (80) ΔSSTA. ALL/WARM non-event composite: (d) Day (20) SSTA, and (e) Day (40), (f) Day (80) ΔSSTA. Color shading indicates values which are significantly different (at the 95% level) from zero. Units are degrees centigrade, contour interval is 0.25°C, shading interval is 0.5°C.

the results of compositing SSTA and ΔSSTA for non-WWE periods; these composites are viewed as the control experiments against which to compare the WWE event composites. The results of compositing for the three equatorial WWE types (W, C and E) are then described. The equatorial WWE event composites generally have SSTA changes significantly different (at the 95% level) from those in their respective non-event composites.

a. Non-WWE Composites:

The non-event composites for each individual WWE type had the same general characteristics. The individual/REG non-event composites are characterized by sparse areas of significance in the SSTA and DSSTA fields. Most individual/REG non-event com-

posites have only one significant SSTA feature; every individual/WARM non-event composites, on the other hand, has large regions of significant SSTA and a strong ΔSSTA signal along the Pacific equatorial waveguide. Both the ALL/REG and ALL/WARM non-event composites have large-scale SSTA and ΔSSTA patterns throughout the tropical Pacific, but the amplitude of the fields in the ALL/REG composite is much smaller than that of the ALL/WARM composite (Figure III.2). For both the ALL/WARM and individual/WARM non-event composites, the principal ΔSSTA feature is cooling in the central and eastern Pacific equatorial waveguide.

The main feature for each of the individual/REG non-event composite Day (–20) SSTA field was weak warm (<0.25°C) values centered around 10°N, between 160°E and 160°W. The C/REG non-event composite also had weak cool (>-0.5°C) anomalies covering most of the NIÑO-3 region (see Figure III.4.b). None of the individual/REG non-event composites had any large-scale significant anomalies outside the Tropical Pacific basin. For none of individual/REG non-event composites were any ΔSSTA fields significant (even at the 90% level).

Figure III.2.a-c shows the Day (–20) SSTA and the Day (40) and (80) ΔSSTA field for the ALL/REG non-event composites, the features significant at the 95% level are highlighted by shading. The SSTA for the ALL/REG non-event composite tends to be close to normal across the basin, with slightly cooler than normal values in the central equatorial Pacific. When no WWEs occurred in the period 1986-1998, and NIÑO3 SSTA was initially close to zero, there was no tendency for eastern and central Pacific warming; none of the SSTA changes exceed 0.25°C. In the absence of WWEs and NIÑO3 SSTA was close to zero, tropical Pacific SST tended to remain near climatology.

The features of the individual/WARM non-event composite contrast sharply with the individual/REG non-event composite: the Day (-20) SSTA amplitudes are large, there are large-scale ΔSSTA values in the tropical Pacific as well as SSTA features outside the

tropical Pacific region. The Day (–20) individual/WARM non-event composite SSTA field is dominated by El Niño type anomalies in the tropical Pacific, and weak warm (<0.5°C) anomalies in the Indian and northern tropical Atlantic Oceans. The tropical Pacific has strong (>1.5°C) composite anomalies between 5°S and 5°N east of the dateline, and along the northwest coast of South America. There are weak cold anomalies poleward and west of the warm El Niño anomalies. The individual/WARM non-event composite ΔSSTA fields for the individual WWE types are confined to the tropical Pacific, and are dominated by moderate to strong cooling of the central and eastern equatorial waveguide. By Day (80), the waveguide cooling exceeds –0.75°C in all the individual non-event composites. The composites also show weak cooling in the southeast Pacific, and weak warming in the southwest Pacific; the amplitude of these changes are all less than 0.5°C.

Figure III.2.d-f shows the ALL/WARM non-event composite Day (–20) SSTA, and the Day (40) and (80) DSSTA fields, highlighting significant values by shading. The fields are all qualitatively similar to the individual/WARM non-event composites, however the amplitude of the changes is larger in the ALL/WARM non-event composite. In the Day (–20) SSTA field, the El Niño type features are apparent, with strong warm eastern and central equatorial Pacific anomalies, and weak cold anomalies poleward and west of these. The warm anomalies in the Indian and northern tropical Atlantic Oceans are present in the ALL/WARM non-event composite. The cooling of the central and eastern equatorial waveguide is pronounced in the Day (40) and (80) ΔSSTA fields, as is the weak warming of the southwestern and cooling of the southeastern part of the basin. The changes by Day (40) are generally of the opposite sign as the anomalies on Day (–20). For the period 1986-1998, when NIÑO3 SSTA was initially warm and no WWEs occurred, the tropical Pacific tended to return towards climatological SST.

b. Equatorial WWE Composites:

I now examine the SSTA composites for each of the three equatorial WWE types

(W, C and E). The composite SSTA evolution for each of the equatorial WWE composites are shown in Figures III.3, III.5 and III.6; the panels on the left (right) half of each figure show the evolution of the REG (WARM) composite. Color shading indicates statistically significant SSTA or ΔSSTA values. The contour interval is 0.25°C, positive (negative) values are indicated warm (cold) colors, and the dark contour indicates the zero line. The upper panels (Fig. III.3.a, III.3.g) show composite SSTA on Day (-20). The lower panels (Fig. III.3.b-.3.f, III.3.h-.3.l) show the evolution of the ΔSSTA in 20 day increments, from the center day (Fig. III.3.b) to Day (+80) (Fig. III.3.f). For reference, in all the panels the WWE classifying region is indicated by a blue box.

i) W/REG Composite

The composite initial SSTA structure for the W/REG event composite (Fig. III.3.a) exhibits weak cold anomalies in the southeast tropical Pacific, weak warm anomalies extending to the northeast from the central equatorial Pacific and cold anomalies poleward and westward of the warm anomalies. None of the anomalies exceed 0.75°C in the composite. Compared to the W/REG non-event composite, the W/REG event composite SSTA field on Day (–20) is warmer in the region 160°E -120°W, 5°S-5°N by 0.5°C, and cooler poleward and west of the warm waveguide deviations from the W/REG non-event composite. Outside the Pacific basin there are also anomalies and deviations from the non-event anomalies. The eastern Indian ocean south of Indonesia is cool; and the anomaly is cooler than that of the W/REG non-event composite by –0.25°C. There is also a broad region of weakly cold water (cooler than the non-event composite as well) covering the southern hemisphere tropical Atlantic Ocean. Both extra-Pacific Day (-20) SSTA patterns appear when the anomalies are masked at the 99% level.

The composite ΔSSTA structure is characterized by cooling in the W region, warming along the equatorial waveguide and the northwest coast of South America, and warming in the southeastern Pacific (Fig. III.3.b-III.3.f). The cooling under the main WWE appears

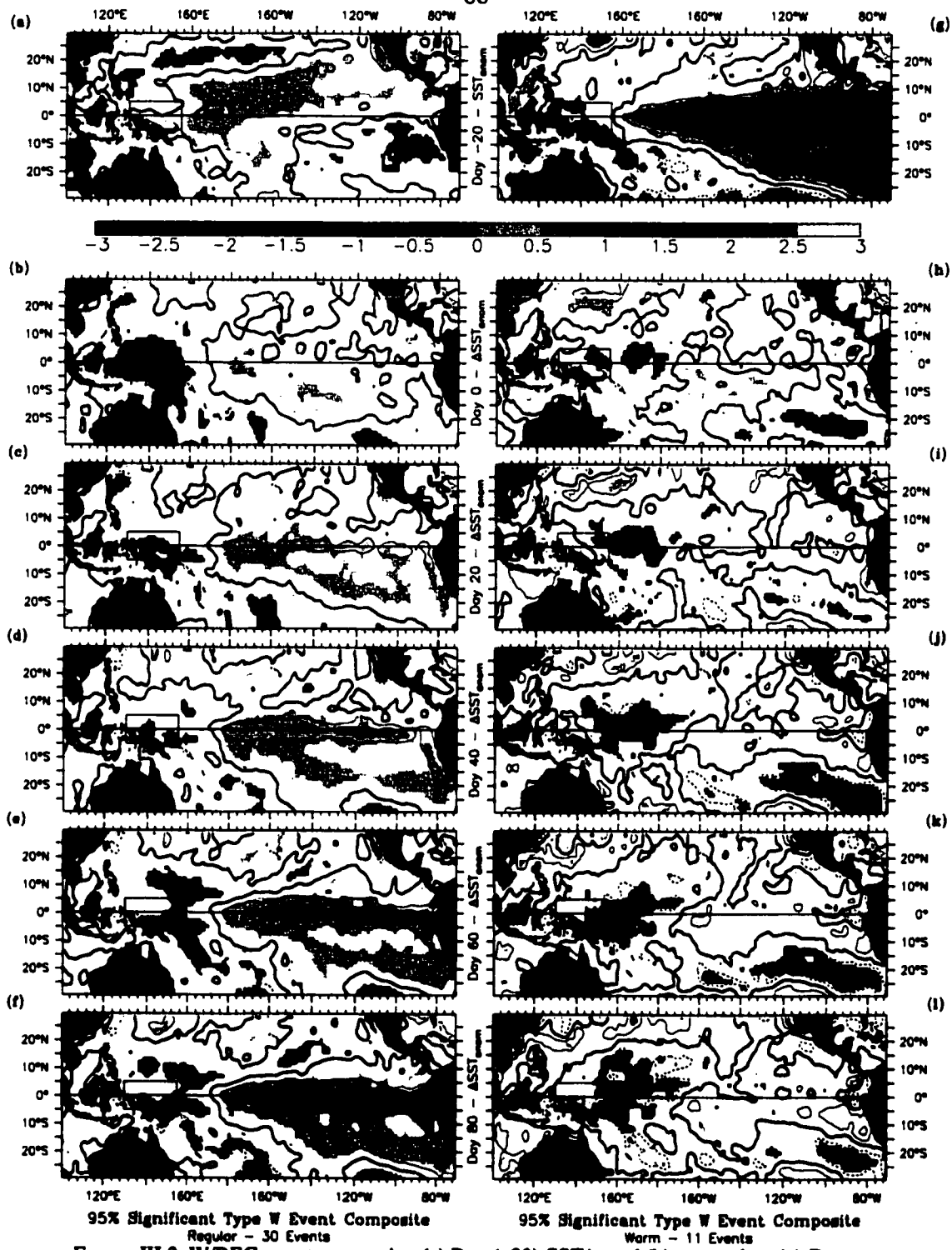

FIGURE III.3: W/REG event composite: (a) Day (–20) SSTA, and (b) center day, (c) Day (20), (d) Day (40), (e) Day (60), (f) Day (80) ΔSSTA. W/WARM event composite (g) Day (–20) SSTA, and (h) center day, (i) Day (20), (j) Day (40), (k) Day (60), (l) Day (80) ΔSSTA. Values significantly different than zero at the 95% level are highlighted by color shading. Units are degrees centigrade, contour interval is 0.25°C, shading interval is 0.5°C. The classifying region is indicated by the purple box in each figure.

during the lifetime of the WWE and remains through Day (80); the cooling is less than 0.5°C. The equatorial waveguide warming is apparent by Day (20), and it expands and increases in amplitude through Day (80). The main warming is contained between 130°W and the South American coast, and exceeds 0.75°C by Day (80); the warming leads to warm anomalies along the equatorial waveguide and the South American coast by Day (60). There is no conspicuous propagation to the ΔSSTA pattern, rather a general spreading and amplification. The warming in the southeast Pacific happens by Day (20) and expands through the compositing period, the amplitude is between 0.25°C and 0.5°C. There is a minimum in composite ΔSSTA amplitude between the waveguide warming and the southeast Pacific warming. The cooling in the classifying region, the waveguide warming and the southeast Pacific warming are all different from the changes in the W/REG non-event composite.

ii) W/WARM Composite

The SSTA structure in Day (–20) of the W/WARM composite event is similar to that seen in the ONSET and PEAK phases of ENSO (Rassmusson and Carpenter 1982, Harrison and Larkin 1998). There is warm SSTA east of 160°E, along the northwest coast of South America and in the southeastern Pacific (Fig. III.3.g). There are weak cold anomalies in the eastern Indian Ocean and the western Pacific Ocean. The cold anomalies do not exceed 0.25°C, while the equatorial warm anomalies exceed 1.0°C east of the dateline. There is an area of minimum in the SSTA amplitude in the southeast Pacific between the warm coastal and waveguide anomalies, and the southeast Pacific Ocean anomalies. The W/WARM event SSTA field in the tropical Pacific basin is not different from the non-event SSTA field on Day (–20), except for slightly warmer anomalies between 150°E and the dateline, and 5°S and 5°N. On Day (-20) there are deviations from the W/WARM non-event composite outside the Pacific basin: the warm Indian Ocean anomalies are smaller and actually become negative close to the maritime continent, and there are moderate (>0.5°C) cool anomalies in the Gulf of Guinea in the Atlantic Ocean.

Following the W/WARM WWE, there is very little structured ΔSSTA, the main feature being cooling in the W region (Fig. III.3.h-.3.l). The cooling under the main wind anomalies is between 0.25°C and 0.5°C and persists through Day (80). There is weak cooling in the southeast Pacific by the center day, which disappears by Day (20). There is some warming near the Equator in the central Pacific, but it is not persistent nor does it exceed 0.25°C. The SSTA changes in the W/WARM event composite are seen to be primarily local to the wind event region. When compared with the W/WARM non-event composite, an interesting pattern emerges. While the waveguide ΔSSTA values in the composite are not significantly different from zero, compared with the non-event composite there is large amplitude reduced cooling. By Day (80), the waveguide DSSTA values in the event composite exceed those in the non-event composite by over 0.5°C from the dateline to the coast of South America. The cooling in the Type W classifying region is significantly larger than that which appears in the non-event composite.

iii) C/REG Composite

The Day (-20) composite SSTA field for the C/REG composite shows some large-scale extra-tropical SSTA features similar to those in the W/REG composite. I show the Day (-20) SSTA field for the C/REG event, non-event and the difference (event minus non-event) in Figure III.4.a-c to illustrate the features. The large-scale central Pacific warm anomalies, and the western Pacific, eastern Indian and southern hemisphere Atlantic cold SSTA is evident in figure III.4.a. It is clear from figures III.4.b and III.4.c that these features are quite different from those in the C/REG non-event composite. Figure III.5.a focuses on the Day (-20) tropical Pacific SSTA features of the C/REG event composite. The band of warm water extending to the northeast of the warm water core just east of the classifying region is clear, as is the cool water poleward and west of it.

The event ΔSSTA composite shows three main patterns: cooling under the main WWE wind anomalies, warming along the equatorial waveguide and the northwest coast of

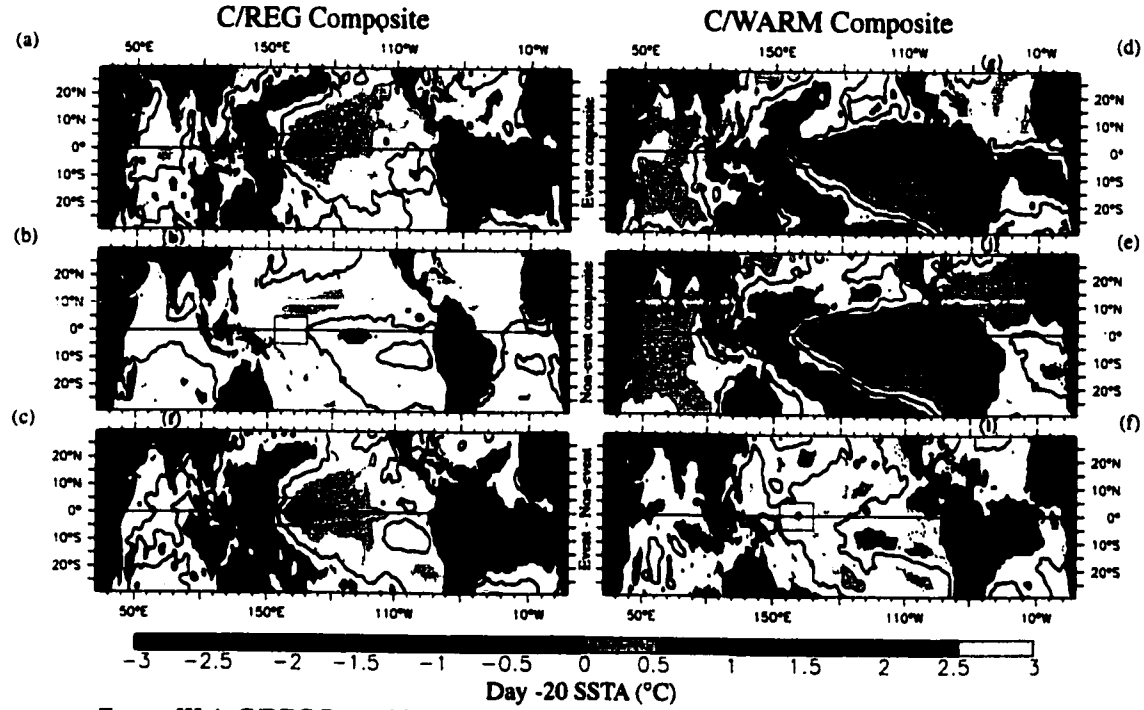

FIGURE III.4: C/REG Day (-20) SSTA for the (a) event composite and (b) non-event composite, and (c) difference between the Day (-20) event composite SSTA and the Day (-20) non-event composite SSTA. C/WARM Day (-20) SSTA for the (d) event composite and (e) non-event composite, and (f) difference between the Day (-20) event composite SSTA and the Day (-20) non-event composite SSTA. Units are degrees centigrade, contour interval is 0.25°C, shading interval is 0.5°C. The classifying region is indicated by the purple box in each figure

South America, and warming in the southeast Pacific (Fig. III.5.b-III.5.f). The cooling under the event happens during the period of maximum westerly anomalies and exceeds 0.25°C. The warming in the southeast Pacific happens by Day (20) and remains through Day (80). The equatorial waveguide and South American coastal warming is evident on Day (40), and remains through Day (80) intensifying and expanding with time. The warming exceeds 0.5°C east of 160°W by Day (80), and close to the northwest coast of South America it exceeds 1.0°C. The warming along the waveguide and the coast of South America leads to warm anomalies by Day (60) east of 120°W. The waveguide and South American coast warming exceeds that in the non-event composite by over 0.5°C by Day (80), the southeast Pacific warming exceeds that in the non-event composite by 0.25°C from Day (20) on, and the cooling under the WWE is significantly different from the non-event composite changes.

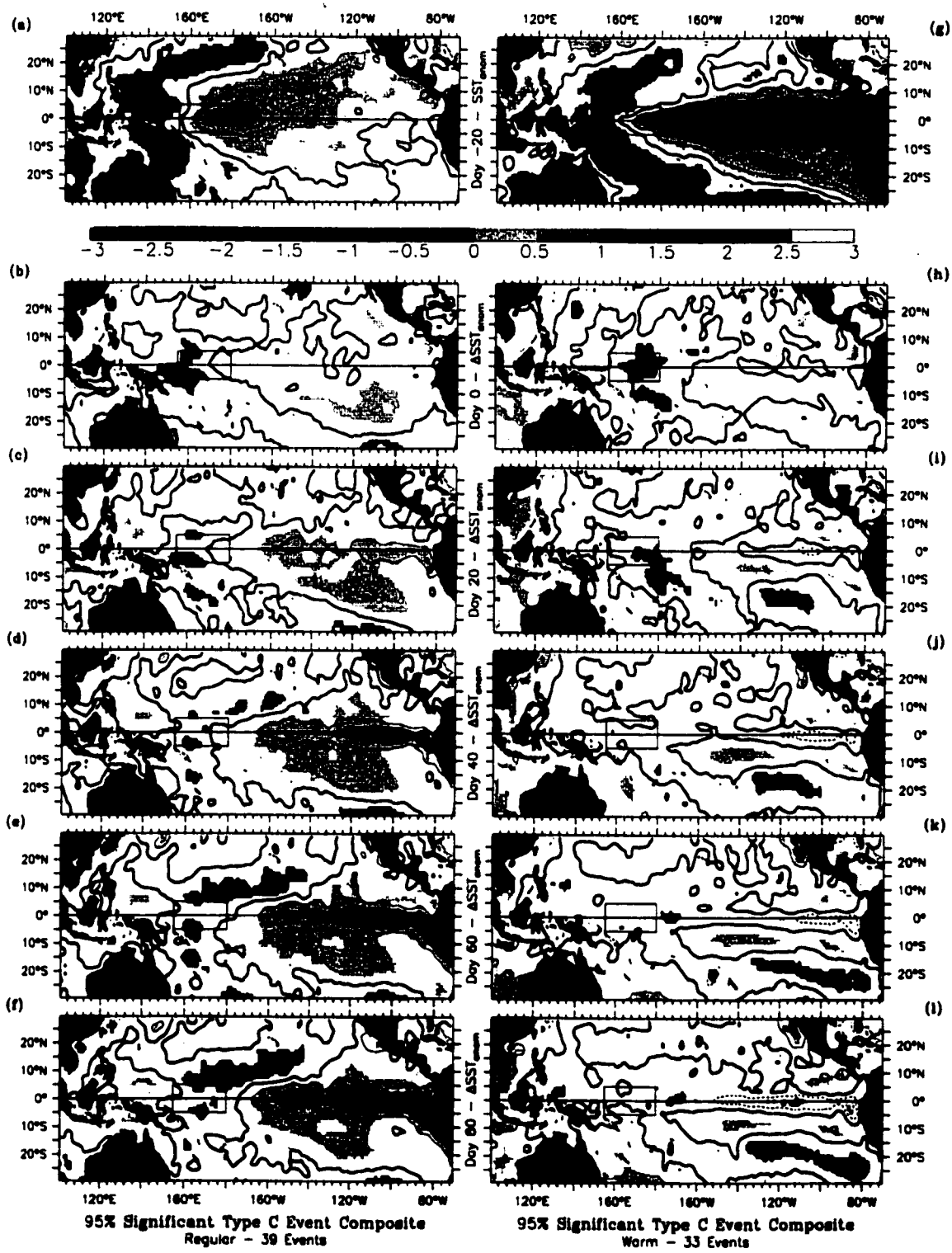

FIGURE III.5: As in Figure III.3, except for the C/REG (a)-(f) and C/WARM (g)-(l) event composites.

iv) C/WARM Composite

The Day (-20) SSTA field across all tropical oceans for the C/WARM event, non-event and difference (event minus non-event) is shown in Figure III.4.d-f. Figure III.5.g shows the Day (-20) C/WARM event composite SSTA field in the tropical Pacific. The initial tropical Pacific SSTA structure for the C/WARM event composite is qualitatively similar to the type C/WARM non-event composite, but there are areas of small amplitude differences between the two. On Day (–20) the composite SSTA exceeds 1.0°C east of 170°W along the equator to the northwest coast of South America. The C/WARM event composite SSTA on Day –20 is significantly cooler than the non-event composite along the northwest coast of South America and in the South China Sea – the differences are all less than 0.5°C. Extra-Pacific SSTA patterns, similar to those which appear in the W/WARM event composite are evident in Figure III.4: the SSTA in the Gulf of Guinea and in the eastern Indian Ocean are both weakly cooler than zero and than the C/WARM non-event composite.

The ΔSSTA event composite (Fig. III.5.h-III.5.l) has almost no large-scale features, and the amplitude of the changes is generally less than 0.25°C. The main cooling pattern is underneath the main WWE surface wind anomalies; it occurs during the period of maximum westerly anomalies, and disappears by Day (40). There is weak warming south of the equatorial waveguide beginning Day (20), remaining there through Day (80). There is a patch of warm water off the west coast of Mexico, which appears in Day (60). Even though there are no equatorial waveguide changes in the C/WARM event composite, the ΔSSTA values are different from those of the C/WARM non-event composite. Relative to the non-event composite, the C/WARM composite is characterized by reduced waveguide cooling that extends from the dateline to the coast of South America by Day (60), and exceeds 0.5°C east of 140°W.

v) E/REG COMPOSITE:

The E/REG composite has an initial structure (Fig III.6.a) similar to the W/REG and C/REG event composites. On Day (-20) the western Pacific is cooler than in the E/REG non-event composite (by more than 0.25°C) and the central equatorial Pacific is warmer than in the non-event composite by over 0.25°C from 160°E-120°W. There are also weak extra-Pacific SSTA features which are less than zero and than the E/REG non-event composite. The tropical Atlantic Day (-20) SSTA is less than zero (SSTA exceeds –0.5°C in Gulf of Guinea) and than the non-event composite; the SSTA in the eastern Indian Ocean is less than -0.25°C, and is cooler than the non-event composite SSTA. Both extra-Pacific features are significant at the 99% level.

The ΔSSTA composite (Fig. III.6.b-III.6.f) exhibits an evolution similar to that seen in the C/REG and W/REG composites, except the SSTA changes under the WWE are warming rather than cooling. There is warming in the classifying region, occurring during the lifetime of the WWE, the warming remains through the compositing period and by Day (20) exceeds 0.5°C. There is warming in the southeast Pacific, appearing by the center day, and intensifying following Day (60). The equatorial waveguide warms following the event, the warming slowly spreads east. There is some warming in the western Pacific, peaking near Day (80) at 0.25°C. The waveguide, southeast Pacific and western Pacific warming are all greater in the event composite than in the non-event composite.

vi) E/WARM COMPOSITE:

None of the SSTA or ΔSSTA patterns for the E/WARM composite are different from the E/WARM non-event composite. The initial SSTA structure (Fig. III.6.g) shows the same El Niño anomalies that were seen in all previous WARM composites. The main feature of the ΔSSTA field (Fig. III.6.h-III.6.l) is cooling along the eastern and central equatorial waveguide, which exceeds –0.5°C by Day (60). There is also weak warming in the eastern Indian Ocean. The cooling in the central Pacific basin, while not distinguishable

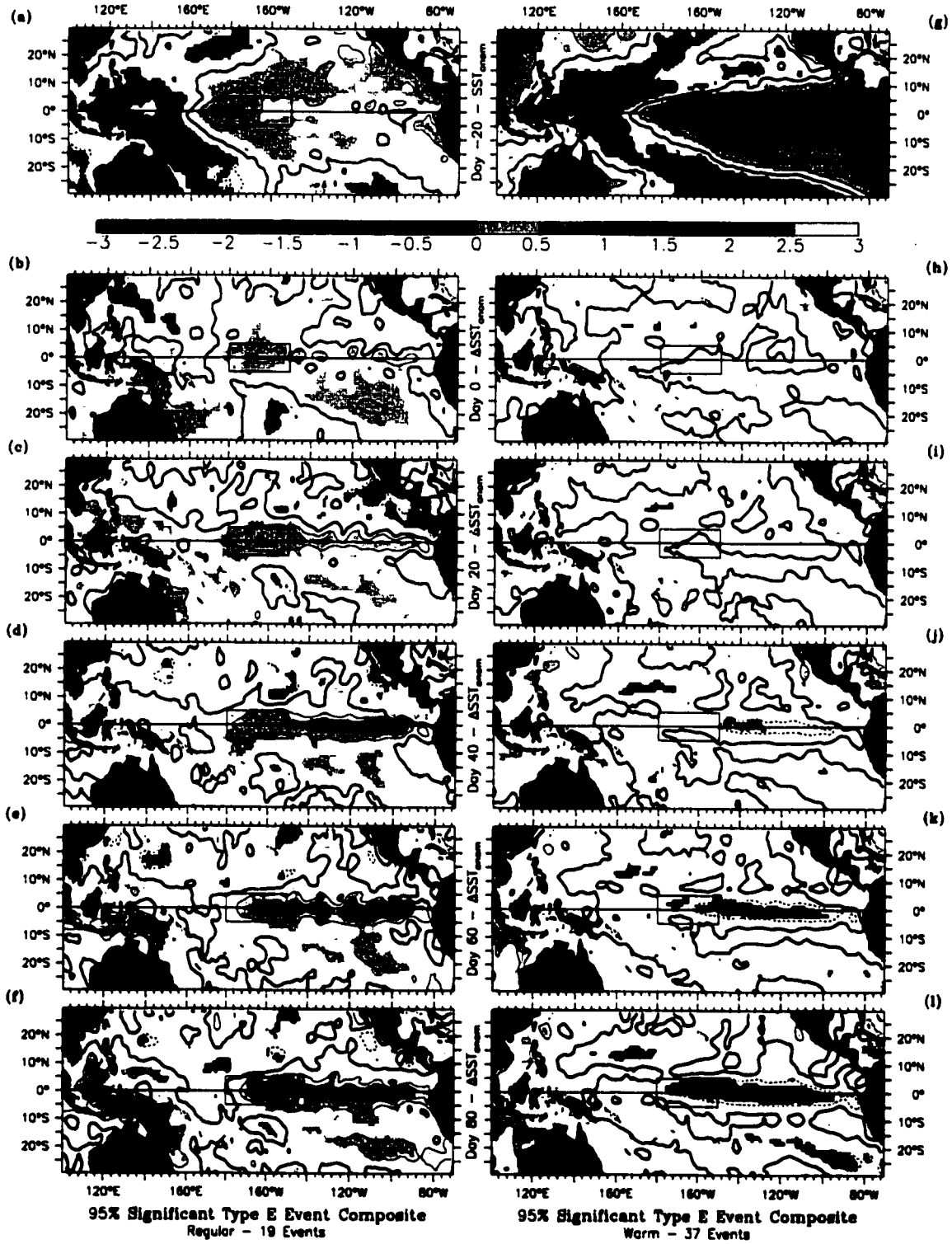

FIGURE III.6: As in Figure III.3, except for the E/REG (a)-(f) and E/WARM (g)-(l) event composites.

from that which is seen in the E/WARM non-event composite, is of smaller amplitude than that of the ALL/WARM non-event composite.

III.4. Summary and Discussion

Using the WWE classification scheme of HV97 and the Reynolds/NCEP weekly global SST analysis (Reynolds and Smith 1994), I have composited the SSTA changes following the three equatorial types of WWEs (W, C and E), between 1986 and 1998. These changes were compared with those occurring in the absence of WWEs. The focus is on the tropical Pacific because of our interest in the role(s) of equatorial WWEs in the onset and maintenance of ENSO warm SSTA. I argue that WWEs are a fundamental part of the appearance of warm conditions in the central and eastern equatorial Pacific, and for the maintenance of warm conditions during El Niño events.

In this section I summarize the results of our compositing analysis, and discuss the relation of these results to previous theoretical, modeling and observational studies. I first summarize the SSTA evolution in the absence of equatorial WWEs, followed by a summary of the local and remote SSTA evolution following different types of WWEs, and conclude by connecting these results to the dynamical mechanisms proposed for WWE/ocean interaction.

a. SSTA Evolution in the Absence of WWEs:

In the absence of equatorial WWEs, the tropical Pacific ocean SST field tended to remain at or return toward climatological values (Section III.3.a). When NIÑO3 SST is initially close to climatology, tropical Pacific SST remains near climatology (see Fig. III.2.b-c). When the NIÑO3 SSTA was initially warmer than normal, there was moderate to strong cooling (as much as −1.0°C in the composite) of the central and eastern equatorial Pacific waveguide surface waters. This cooling tended to reduce the pre-exiting warm El Niño type anomalies (see Fig. III.2.e-f).

b. Local SSTA Changes following WWEs:

By local SSTA changes I mean those which occur under the composite WWE wind anomalies, both inside the WWE identification region and adjacent to it. The second and third columns of Table III.2 summarize the character of the local SSTA changes following each of the WWE types and their departures from the non-event composite. Local changes that were significantly different from zero were also significantly different from the non-event composites.

The Type W and C WWEs exhibited local SSTA cooling during the lifetime of the WWE. The composite cooling was generally less than 0.25°C, and everywhere less than 0.5°C; the cooling occurred irrespective of the initial eastern Pacific SSTA (see Figs. III.3,.5). Although small, this cooling was a significant feature of the composites at the 99% confidence level.

The Type E WWEs have a different local SSTA change than that of the western equatorial WWEs. Following Type E events, when NIÑO3 SST is initially close to climatology, there is SSTA warming in the WWE defining region (see Fig. III.6). When NIÑO3

TABLE 2: Summary of the principal ΔSSTA values and departures from the non-event composites for each of the equatorial WWE types, for both REG and WARM event composites. Plus signs (+) indicate that the ΔSSTA value or departure from the non-event composite was significantly greater than zero. Minus signs (-) indicate that the SSTA change or departure from the non-event composite was significantly less than zero. Double plusses (++) indicates that the dominant changes or departures had an amplitude greater than 0.5°C.

NIÑO-3 SSTA	Event Type	Local		Central and Eastern Pacific Waveguide		SE Tropical Pacific	
		Value	Departure	Value	Departure	Value	Departure
REGULAR	W	-	-	++	++	+	+
(-0.75°C≤ and	C	-	-	++	++	+	+
≥0.75°C)	E	+	+	++	++	+	+
WARM	*W*	-	-		++	-	
(>0.75°C)	*C*	-	-		++	-	
	E		+	-		-	

was warmer than normal there were no local SSTA changes; however the E/WARM event SSTA change composite exhibits less cooling than is seen in the E/WARM the non-event composite.

c. Remote SSTA Changes following WWEs:

The period following some WWE types exhibited large-scale SSTA changes and departures from the evolution of the non-event composites far from the main WWE wind anomalies; these also are summarized in Table III.2. The remote SSTA changes depended on the initial NIÑO3 SSTA. Generally the central and eastern Pacific equatorial SSTA field warmed or remained warm.

When the NIÑO3 SST was initially close to climatology, the WWEs centered on the equator were followed by large-scale remote SSTA changes. The main features were: warming of the central and eastern equatorial Pacific along the equatorial waveguide and the northwest coast of South America; cooling in the western Pacific; and warming in the southeastern Pacific (see Figs. III.3,.5,.6). The composite waveguide warming following the Type W and C WWEs exceeded 1.0°C 80 days after the event, while the western Pacific cooling and southeast Pacific warming was of small amplitude (0.25-0.5°C). The amplitude of these SSTA changes is of the same general structure as that seen in the onset of El Niño, and the amplitudes are large enough to account for a large part of the observed composite El Niño warming (see Rasmusson and Carpenter 1982, Harrison and Larkin 1998).

There is no waveguide warming associated with the WARM event composites for any equatorial WWE type; nonetheless these represent significant departures from the non-event composites (since the expected change in the absence of a WWE is for waveguide cooling). The W/WARM and C/WARM event composites had no cooling of central and eastern waveguide SSTA, which when compared with the non-event composite amounted to maintenance of the warm waveguide SSTA values (recall that the departures from the non-event composite exceeded 0.5°C). The timing of these departures is similar to the changes

and departures seen in the W/REG and C/REG composites; however the departures are much more pronounced in the central equatorial Pacific than in the eastern Pacific. Also, the maximum amplitude of the deviations from the non-event composite in these two equatorial WARM composites is only 66% of the maximum deviation in the respective REG event composites.

d. Discussion:

The local cooling seen in the Type C and W event composites is in agreement with the available case studies of the evolution of local SST following WWEs in the western Pacific warm pool (McPhaden et al. 1988, McPhaden et al. 1992, Delcroix et al. 1993, Eldin et al. 1994, Smyth et al. 1996, Cronin and McPhaden 1997, Feng et al. 1998). The range of the amplitude of the observed local cooling under individual WWEs has been 0.2°C-0.6°C over the period of a week (McPhaden et al. 1988, McPhaden et al. 1992, Delcroix et al. 1993, Eldin et al. 1994); recall the composite amplitudes were between 0.25°C and 0.5°C. Observations of SST evolution under a series of WWEs which quickly follow each other has shown larger cooling, between 0.8°C and 1.0°C, over a period of a few weeks (Smyth et al. 1996.b, Cronin and McPhaden 1997); unsurprisingly, a sequence of WWEs in succession impact the local ocean more strongly than individual WWEs. The agreement between the various observations of local SST changes following individual WWEs, and with the composite behavior over 13 years, suggests that the local changes observed in the case studies were representative of the local SST evolution following WWEs.

There have been many mechanisms suggested for local SST cooling under strong winds in the western equatorial Pacific. During the TOGA/COARE Intensive Observational Period, the evolution of the western equatorial Pacific during a series of WWEs was observed more thoroughly than ever before; this allowed exploration of the factors controlling SST variability during the observed WWE periods. In a 1-D analysis of the heat balance at (156°E, 0°), Cronin and McPhaden (1997) argue that the local warm pool SST

variability under WWE conditions was controlled by decreased incoming short-wave radiation and increased latent heat-flux; they note that zonal advection also plays an important role. Feng et al. (1998) did a 3-D heat and salinity budget in the western Pacific during the same period, centered at (156°E, 2°S); and found that both zonal and meridional advection of heat and salt played an important in the budgets under WWE conditions, and acted both to increase the surface salinity and to reduce surface temperature. According to Feng et al. (1998), cooling through meridional advection dominated warming due to zonal advection during the January 1993 western Pacific WWE. Evidently there remains some uncertainty about the processes responsible for local cooling under Type C and W WWEs; no single process is expected to apply to every event.

I am not aware of any case studies of the local response to Type E WWEs. I suggest that the character of the local SSTA evolution following a Type E WWE is due to the Type E classifying region being dominated by strong and persistent trade winds. These trade winds lead to equatorial upwelling through Ekman divergence at the surface, as well as to a generally strong westward surface current. Climatologically, both the upwelling and the westward current act to cool the local SST by advection of cooler waters (the zonal temperature gradient is generally negative, except during the most extreme of El Niño events). Westerly anomalies in this region would lead to reduced Ekman divergence and upwelling, and reduced westward surface current; both of which would contribute to warm the surface waters. The latent surface fluxes of heat would be reduced since the WWEs, in all but the most extreme cases, result in reduction of the wind speed (HV97). Reductions in easterly trade winds should be expected to lead to local SST warming, as is seen in the Type E composite.

Only one case study of the remote changes in SST following WWEs is known to me: McPhaden *et al.* (1988) describe an eastward propagating current pulse generated by a western Pacific WWE during May 1986. This pulse was associated with warming of 1°C at

(110°W,0°N) in mid-June 1986 (30 days after the WWE); according to McPhaden *et al.* (1988) the warming pulse following the WWE had little effect on the evolution of the subsequent 1986-7 El Niño event. Harrison and Giese (1989) offer a different interpretation of the same event; they agree that the June-1986 warming at 110°W is the result of the first baroclinic mode Kelvin pulse excited by the May WWE, and is short lived. However, using current data from moorings on the Equator at 140°W and 110°W, they argue that a second phase of warming occurring in mid-July 1986 was the result of the second baroclinic mode Kelvin pulse forced by the WWE; this pulse was related to SST warming of over 2.0°C at the onset of the 1986-7 El Niño. Both McPhaden *et al.* (1988) and Harrison and Giese (1989) argue that zonal and meridional advection of heat played an important role in the eastern Pacific SST warming forced by the WWE.

Though WWEs have been suggested as an important mechanism in the evolution of ENSO, there have been no other observational attempts at describing the remote SST changes following WWEs. Some observational studies have found eastern and central Pacific thermocline (as defined by the depth of the 20°C isotherm) and sea surface height changes following WWEs, and have suggested a relationship between ENSO warming and WWEs (Eriksen *et al.* 1983, Hayes *et al.* 1991, Kessler and McPhaden 1995, Chavez *et al.* 1998, Yu and Rienecker 1998, McPhaden 1999). This present study is the first to systematically describe the remote SSTA changes that occur following equatorial WWEs.

The composite remote SSTA changes reported here when NIÑO3 SST is close to climatology are consistent with the results from ocean general circulation model (OGCM) experiments described in the literature. Examining the response of the OGCM to idealized WWE forcing, Harrison and Giese (1988), and Giese and Harrison (1990, 1991) found that WWEs drove warming in the eastern and central equatorial Pacific in excess of 0.5°C; the warming appeared at 140°W within a month of the anomalous forcing and continued for over three months. The SST warming in the OGCM was driven primarily by zonal advec-

tion by equatorially trapped eastward propagating current pulses, and by meridional advection due to interaction of these pulses with the background tropical instability wave (TIW) field. Note that the WWE forcing used in those model experiments had an estimated zonal extent of 10° longitude, which is about 1/3 the average zonal extent of WWEs; the response to a WWE of larger zonal extent would be more than that described in the mentioned experiments. The large amplitude composite response relative to the OGCM experiments (1.0°C vs. 0.5°C) could be the result of the underestimation of the WWE zonal extent by Harrison and Giese (1988), and Giese and Harrison (1990,1991) or due to some ocean/atmosphere coupling which would be absent in their model; the timing and structure of the SSTA composite changes when NIÑO3 SST is initially close to climatology are consistent with those of the OGCM experiments. Chapter V further explores the ability of the model to reproduce the composite SSTA changes.

The composite remote changes to the SSTA fields when NIÑO3 SST is initially warmer than climatology, for the Type W and C events, is not like that described in the literature. The sensitivity of the SSTA associations with WWEs to initial state of the ocean/atmosphere is not unexpected. Schopf and Harrison (1983) and Harrison and Schopf (1984) found that the eastern Pacific temperature response following a period of westerly wind anomaly was larger when the forcing was in the northern winter months than in the northern summer months. The difference in response in the two cases was due the equatorial zonal temperature gradients and the TIW activity being much stronger in boreal winter than in boreal spring. The difference in amplitude of the maximum departures from non-event SSTA changes between the WARM and REG events could be similarly explained.

The warming associated with El Niño leads to a reduced magnitude of the equatorial zonal temperature gradients; in extreme cases such as the peak of the 1997-8 El Niño the zonal temperature gradient disappears or even reverses. For the period 1986-1998, when the NIÑO3 SSTA index was close to normal (within 0.75°C of climatology) the mean zonal

SST gradient on the equator was: -7.0×10^{-7} °C/m at 170°W, -5.5×10^{-7} °C/m at 140°W, and -5.7×10^{-7} °C/m at 110°W; but for periods where the NIÑO3 SSTA index exceeded 0.75°C, the equatorial zonal temperature gradient was: -1.6×10^{-7} °C/m at 170°W, -5.3×10^{-7} °C/m at 140°W, and -4.0×10^{-7} °C/m at 110°W. Even though the magnitude is reduced in warm NIÑO3 periods, the average zonal SST gradient across the equator is negative both in periods of near normal and warm NIÑO3 SST. If the current response following the WWE were comparable when the NIÑO3 SST is close to and warmer than climatology, the temperature response due to zonal temperature advection when NIÑO3 was initially warm would be smaller.

It has been suggested that that an important mechanism leading to eastern equatorial Pacific SST warming following a WWE, is anomalous meridional advection of heat due to interaction between the WWE forced Kelvin pulse and the tropical instability waves (Harrison and Giese 1988, Giese and Harrison 1990,1991). In the absence of TIWs that process would not be able to increase the equatorward surface heat flux, and the SST response would be smaller than in the presence of TIWs. Decreased TIW activity during El Niño is a possible contributing factor to the decrease in eastern Pacific SSTA changes to following WWEs in initially warm NIÑO3 conditions.

This compositing study describes the average SSTA changes that follow the various WWE types, however the SSTA changes following any individual WWE may be different from the composite. Figure III.7 shows scatter plots of the NIÑO3 SSTA on Day (-20) vs. the NIÑO3 DSSTA on Day (60) for the equatorial WWE types and for non-event periods, the horizontal lines show the composite values for both eastern Pacific SSTA regimes. Figure III.7 highlights those WWEs of strong intensity by using red marks on the plots; we define strong events to be those events whose wind measure statistic exceeds $1.5\text{¥}10^{6}$m (wind measure is a time integral of the spatially averaged zonal wind anomaly of each WWE; see Chapter II, HV97). It is apparent in these scatter plots that the changes to eastern

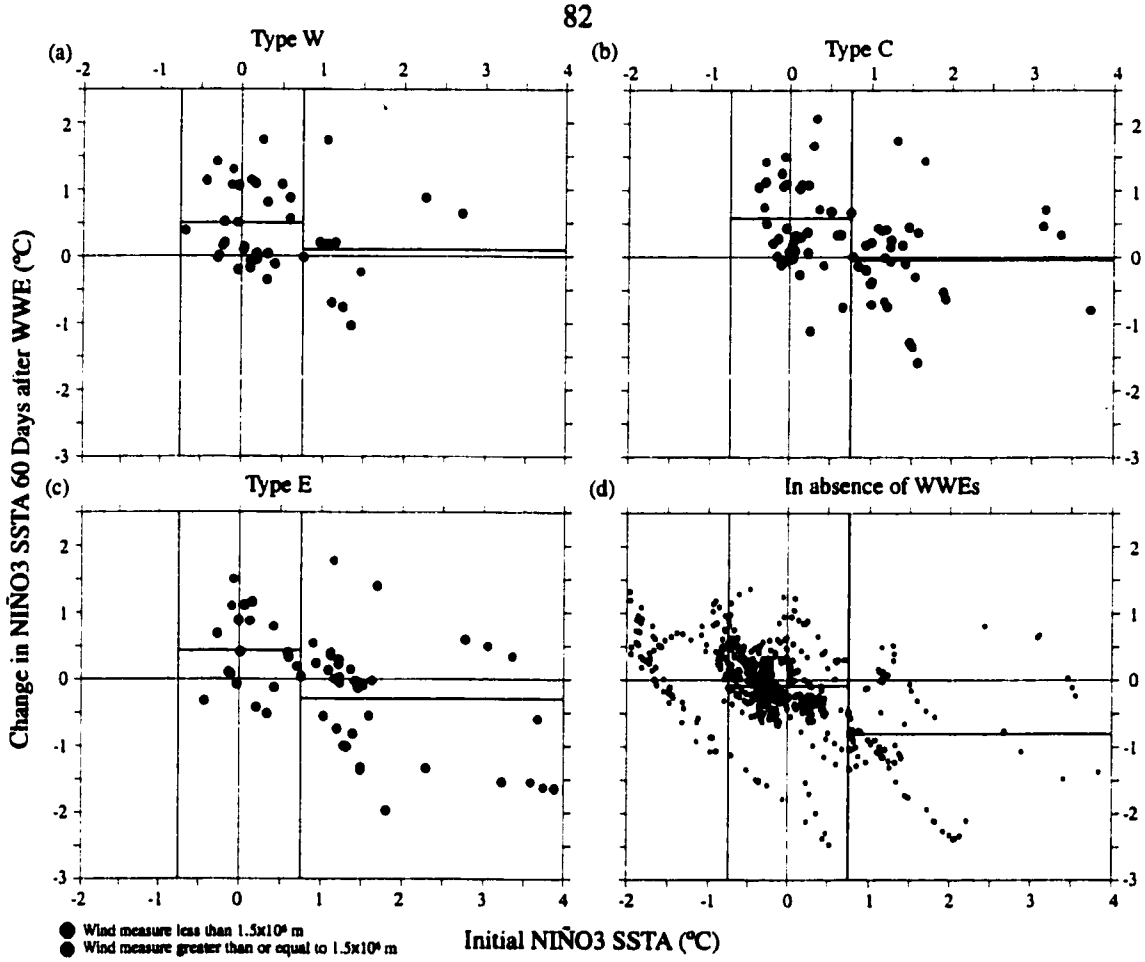

FIGURE III.7: Scatter plots of the NIÑO3 SSTA on Day(-20) vs. the NIÑO3 DSSTA on Day(60) for (a) Type W, (b) Type C and (c) Type E WWEs, and (d) for periods without WWEs. The units are °C, the vertical lines indicate the boundaries of the NIÑO3 SSTA regimes (COLD, REG, WARM), and the horizontal green lines indicate the composite values inside the REG and WARM regimes. Red marks highlight WWEs whose wind measure exceeds 1.5×10^6m.

equatorial Pacific SSTA in the absence of WWEs are very different from those when WWEs occur. Most notably, in the REG temperature regime there is a much greater likelihood for warming following WWEs than in the absence of WWEs, and a corresponding decrease in likelihood of eastern Pacific cooling.

Table III.3 summarizes the percentage of events in the REG SSTA regime which were followed by Day (60) NIÑO3 SSTA changes in various ranges, for all three equatorial WWE types, for equatorial WWE types of strong intensity (wind measure statistic in excess of 1.5×10^6m; HV97), and for non-event periods. Notice that the probability of extreme NIÑO3 warming following WWEs (>1.0°C) is between 10 and 15 times that in the absence

of WWEs; and there is a greater than 50% chance of moderate (>0.5°C) warming following strong WWEs. In addition, no strong equatorial WWEs were followed by cooling of more than –0.5° (in Fig. 8 this relation is also evident), and a total of three weak WWEs (one Type E and two Type C) WWEs were followed by moderate cooling.

This observational study provides support to the previous model and theoretical suggestions that equatorial westerly wind events are a fundamental mechanism in the appearance and maintenance of warm eastern equatorial Pacific SST anomalies. In the absence of WWEs the tropical Pacific SST tends to return toward or remain at climatological values, in the presence of WWEs the evolution is quite different. When the eastern equatorial Pacific SST is close to climatological values, equatorial WWEs are associated with strong warming of the equatorial waveguide of similar amplitude and structure as that associated with the onset of El Niño conditions. When eastern equatorial Pacific SST was warmer than climatology, some WWE types were associated with maintenance of the warm eastern and central equatorial Pacific SSTA values. Given the agreement between these statistical results and previous modeling and theoretical work on ocean response to WWE forcing, I

TABLE III.3: Percentage of WWEs and non-event periods with Day (-20) NIÑO3 SSTA in the range ±0.75°C which have NIÑO3 SSTA change on Day (60) in the ranges indicated. Strong events indicates WWEs whose wind measure (an indicator of WWE strength) exceeded 1.5×10^6 m. Notice the considerable likelihood of NIÑO3 SSTA warming following equatorial WWEs.

WWE Type	Number of events	Percentage of REG events with Day(-60) NIÑO3 ΔSSTA in range:			
		<-0.5°C	>0.25°C	>0.5°C	>1.0°C
W	30		50	47	30
Strong W	13		62	54	38
C	38	5	63	39	32
Strong C	16		81	63	50
E	19	5	58	42	21
Strong E	5		80	80	40
In absence of equatorial WWEs		15	26	10	2

suggest that WWE driven warming of the central and eastern equatorial waveguide is a fundamental mechanism for the onset of warm El Niño conditions in the equatorial Pacific and in the maintenance of warm El Niño conditions in the equatorial Pacific.

In Chapter V the mechanisms responsible for the SSTA changes following WWEs are examined. The next chapter, Chapter IV, describes the relationship between WWEs and atmospheric convection, and between WWEs and certain atmospheric circulation patterns (tropical cyclones and the MJO), in order to further develop an understanding of the coupled mechanisms involved in the evolution of WWEs.

Chapter IV:
Tropical Pacific sub-seasonal convection

IV.1. Introduction

In this chapter I explore the relationship of westerly wind events (WWEs) to atmospheric convection as described by satellite measured outgoing longwave radiation (OLR). I compute the mean surface wind and convective structures associated with the Madden-Julian Oscillation (MJO, see Madden and Julian 1994 for a review). I examine statistical relationships that WWEs exhibit with the MJO and tropical cyclones. The work here builds on the surface wind analysis described in Chapters II and III, Harrison and Vecchi (1997, henceforth HV97) and Vecchi and Harrison (2000, henceforth VH00); and attempts to resolve the relationships that have been observed anecdotally between WWEs, the MJO and tropical cyclones.

Observations of two MJO events during the TOGA-COARE IOP suggest enhanced WWE variability associated with the MJO (Godfrey *et al.* 1998). A relationship between tropical cyclone activity and WWEs has been discussed since the first descriptions of WWEs (Keen 1982, Harrison and Giese 1991, Hartten 1996); I use the identification scheme described in Chapter II and HV97 to explore WWE relationships to the MJO and tropical cyclone activity, for the period 1986-1997. Also shown in this chapter are the results of compositing the surface wind anomaly and OLR anomaly fields for the MJO.

The Madden-Julian Oscillation (MJO; also referred to as the Intra-seasonal Oscillation or ISO) was first identified as a spectral peak in global tropical 850mb and 150mb zonal wind and wind divergence (Madden and Julian 1972) in the 40-50 day range, and has been the subject of much research by the atmospheric science community for the past 30 years. The spectral peak has been found to exist in a much broader range of 30-90 days, and is associated with globally propagating (global wavenumber 1 or 2) variability of tropo-

spheric wind and atmospheric convection (see Madden and Julian 1972, 1974, 1994, Rui and Wang 1990, Hendon and Salby 1994, Maloney and Hartmann 1998). Atmospheric convection related to the MJO is limited to the regions of warmest SST (SST>28°C) in the Indo-Pacific warm pool region, and near the Pacific Intertropical Convergence Zone (ITCZ) and South Pacific Convergence Zone (SPCZ) (see Rui and Wang 1990, Hendon and Salby 1994). The atmospheric convective structures associated with the MJO propagate eastward from the Indian Ocean at 5-10 ms^{-1} (see Rui and Wang 1990, Hendon and Salby 1994, Figures IV.5-.7); while the tropospheric zonal wind structures propagate eastward at a speed between 10 and 20 ms^{-1} (see Madden and Julian 1974,1994, Hendon and Salby 1994, Maloney and Hartmann 1998). While the free-tropospheric wind and atmospheric convection variability associated with the MJO have been previously described, the global surface wind and wind-stress anomalies associated with it merit further examination. Hendon *et al.* (1998) found that equatorial zonal wind-stress anomalies associated with the MJO extend into the central/eastern Pacific, away from the Pacific warm pool convective region.

Tropical atmospheric convection is generally associated with strong surface wind convergence; near the Equator convection usually includes surface westerlies under the convection. The period of WWE activity in Dec 1992-Jan 1993, during the TOGA/COARE IOP, which was one of the most extreme in the period 1986-1995 (see Chapter II, HV97), occurred with the passage of the convectively active phase of the MJO over the western Pacific warm pool (Lin and Johnson 1996, Chen and Houze 1996). Some of the westerly wind variability in the onset of the 1997-8 El Niño event appeared related to the MJO (McPhaden 1999). I use a quantitative definition for MJO variability developed by Maloney and Hartmann (1998, heceforth MH98) to examine MJO related surface wind and atmospheric convection variability.

There is little evidence for a systematic WWE/MJO connection in the WWE composite results described in Chapter II and HV97. None of the equatorial WWEs shows a

translation during its lifetime consistent with being a direct surface expression of the MJO (whose tropospheric with phase translates eastward at 10-20 ms^{-1}, and atmospheric convection phase translates eastward at 5-10 ms^{-1}). Even the southern hemisphere WWEs, which display an average eastward propagation, translate more lowly at 3-4 ms^{-1}. If there is a connection between MJOs and WWEs it is not clear in the average behavior of WWEs, and must be explored carefully before any generalizations are drawn from a few observed connections. Using the MH98 MJO definition, I also describe statistical relationships between the MJO and WWEs.

I also explore the relationship between WWEs and tropical cyclone activity, which has been made possible by the cataloguing of cyclone tracks. The suggestion that there is a relationship between the cyclones and WWEs dates from the early exploration of westerly wind activity in the central equatorial Pacific. Keen (1982) described the relationship between paired cyclones on either side of the equator and extreme periods of surface westerlies. The relationship was examined again by Harrison and Giese (1991) and the conclusion was that for near-dateline WWEs the relationship is not as strong as originally suggested: ~60% of near-dateline WWEs were associated with tropical cyclone activity. The relationship between cyclones and certain WWEs is suggested by the analysis of surface wind structures of WWEs (Hartten 1996, HV97, Chapter II), where certain WWE types exhibited cyclonic circulation patterns and translation consistent with the main cyclone tracks in the respective hemispheres (towards the northwest in the northern hemisphere, towards the east-south-east in the southern hemisphere). This suggested relationship is reemphasized by the OLR analysis shown in Section 3 of this chapter: the westernmost WWE types (NW and W) displayed tight convective signals which propagate northwestward, and the southern hemisphere WWEs displayed some convective structures which translate eastward.

In the remainder of this chapter I will summarize the work into cataloguing the general relationships between WWEs and tropical convection. Section 2 will describe the

data and methods used. The results of compositing OLR anomaly and surface wind anomaly for each WWE type and for the MJO are described in Section 3. Section 4 summarizes the inter-WWE time spacing results, which indicate that the 40-80 day spacing one would expect from an MJO driven phenomenon is not prominent in most WWE types. Section 5 summarizes the co-occurrence between WWEs and the MJO. Section 6 examines relationships between WWEs and tropical cyclones. Finally, Section 7 gives summarizes and discusses the results.

IV.2. Data and Methods.

The European Centre for Medium Range Weather Forecasts (ECMWF) 12-hourly 2.5°×2.5° gridded 10-meter wind operational analysis (European Centre for Medium Range Weather Forecasts 1989), and the method described by HV97 and Chapter II were used to identify all the WWEs in the period 1986-1998 (see Table IV.1 for a summary of the identified WWEs). Daily NOAA Interpolated Outgoing Longwave Radiation (OLR), on a 2.5°×2.5° global grid from 1986-1998 was provided by the NOAA-CIRES Climate Diagnostics Center, Bolder, Colorado (available from their web site: *http://www.cdc.noaa.gov*). The SST used in this analysis is the Reynolds/NCEP weekly 1°×1° gridded SST product (Reynolds and Smith 1994).

Monthly climatologies of SST and OLR were generated using the weekly SST and daily OLR, respectively, data from 1984 through 1996 (those years are chosen to exclude the very anomalous periods of 1982-3 and 1997-8). Monthly climatology of 10-m wind (U) was generated using the 12-hourly data from ECMWF for the period 1986-1995 (for consistency with HV97). SST anomaly (SSTA), OLR anomaly (OLRA) and 10-m wind anomaly (UA) were computed from the corresponding monthly climatology. The analysis was repeated using other climatologies, and none of the principal results were affected.

For reference, the climatological convection and SST fields for the months of March,

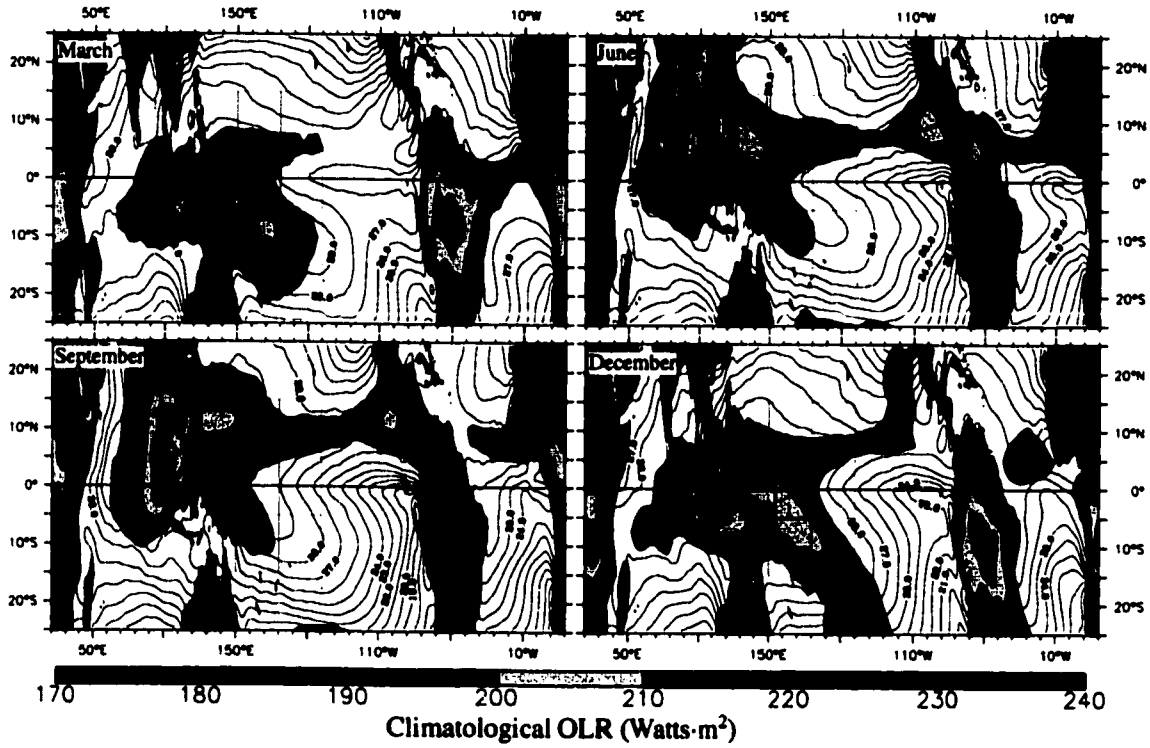

Figure IV.1: Climatological OLR (shading) and SST (contours). Units are °C for SST and Watts·m^{-2}. Contour interval for SST is 1°C, shading interval for OLR is 10 Watts·m^{-2}.

June, September and December are shown Figure IV.1; contoured is SST at 1°C intervals and shaded is OLR values less than 230 Wm^{-2}. Notice the seasonal meridional migration of the warm pool (waters warmer than 28°C) and western Pacific convection fields. Also evident is the seasonal cycle of the eastern Pacific cold tongue in SST, and the Pacific Intertropical and south Pacific convergence zones.

In Chapter III, Section 2, and VH00 the NIÑO3 SSTA distribution was examined over the period 1986-1998, and it was determined that an adequate description of the distribution is of having three states: COOL (NIÑO3 < -0.75°C), REGULAR (|NIÑO3| ≤ 0.75°C) and WARM (NIÑO3 > 0.75°C). Table IV.1 summarizes the number of WWEs of each type identified during the period 1986-1998, and breaks down their distribution based on the NIÑO3 SSTA (SSTA averaged over 150°W-90°W, 5°S-5°N) 20 days prior to the WWE center day.

The bootstrap compositing technique used in Chapter III and VH00 to explore the

SSTA evolution associated with WWEs was applied to the OLR and 10-meter wind data. Because of the large OLRA and UA associated with the ENSO phenomenon, the compositing of OLRA and UA is performed separately for periods of initially near normal and warmer than normal NIÑO3 SSTA (Cases REGULAR and WARM). The compositing analysis is not performed for periods of initially cooler than normal NIÑO3 SSTA (case COOL), since there are not enough WWEs in that state to perform reliable statistics (see Table IV.1). For the period 1986-1998 ,composites of OLRA are generated for each WWE type, and for each initial NIÑO3 state; the composites go from event Day(-20) to Day(20). As in Chapter III and VH00, I also generated NON-WWE composites, by bootstrap sampling all those dates which are more than 10 days from a given WWE-type center day. Each WWE composite is compared to the corresponding NON-WWE composite, to determine the composite OLRA or UA deviation (OLRD, UD) from the expected mean. Statistical significance, against a mean of zero, is determined for all composited quantities using a bootstrap method.

A quantitative definition of MJO events was developed by MH98 using the first two empirical orthogonal functions (EOFs) of 30-100 day bandpassed 850 HPa zonal wind. The

Table IV.1: Number of WWEs and MJOs identified in the period Jan. 1986- May 1998. The number of events for each type are listed, along with the breakdown based on NIÑO3 SSTA state 20 days before the WWE center day (or on Phase 4 for the MJOs). The final row lists the percentage of total time in each NIÑO3 SSTA case.

WWE Type	All Time	Case Warm (NIÑO3>0.75°C)	Case Regular (|NIÑO3|≤0.75°C)	Case Cool (NIÑO3 < -0.75°C)
NW	72	24%	68%	8%
N	37	32%	62%	5.4%
NE	44	39%	50%	9%
W	41	27%	73%	
C	72	42%	58%	
E	51	62%	37%	
S	51	35%	55%	10%
SE	61	44%	48%	8%
MJO	70	29%	63%	8.6%
Percentage of Time in each NIÑO3 State		28%	61%	11%

global MJO definition and index derived by MH98, using the first two empirical orthogonal functions (EOFs) of the intraseasonal filtered 850-mb zonal wind from the NCEP/NCAR reanalysis wind product (Kalnay et al. 1996). The first EOF (which explains 32% of the variance) has a maximum over the central Indian Ocean; the second EOF (which explains 23% of the variance) has a maximum over the Maritime Continent and the western Pacific Ocean. Their principal component timeseries (PCs) are in quadrature,and together they describe and eastward propagating oscillation of 850-mb zonal winds. The MH98 MJO index is generated by adding the first PC with the backward time-shifted second PC; the index has maximum (minimum) values when Indian Ocean 850-mb westerlies (easterlies) are followined by western Pacific westerlies (easterlies). MJO events are defined by identifying times when the local maximum in the index exceeds one standard deviation and is surrounded by local minima with negative index values. The maximum is labeled Phase 5 and the leading (trailing) minimum is labeled Phase 1 (9); Phases 3 and 7 are at the intervening zero crossings of the index, and the "even" Phases (2,4,6,8) are at the midpoints between the surrounding "odd" Phases. Using the different dates identified for each Phase, composites for various quantities can be generated by averaging (as in MH98). The average length of each Phase is close to five days. See Table IV.1 for a breakdown of the number of MJO events identified. Notice that the distribution of MJO events within the three NIÑO3 SSTA states is not significantly different from a uniform distribution (even at the 85% confidence level).

Defining as an index of MJO-activity the 240-day running count of MJO events, a timeseries of MJO-activity can be generated using the MH98 MJO index (henceforth MH-MJOI) from January 1979 through March 1998. The MJO-activity index is plotted along with the NIÑO3 SSTA index in Figure IV.2 (Note that the results are unaffected if the MJO-activity index is computed using anything from the 380 day to 150 day running count). There is a lack of connection between the two indices, which is evident in the correlation

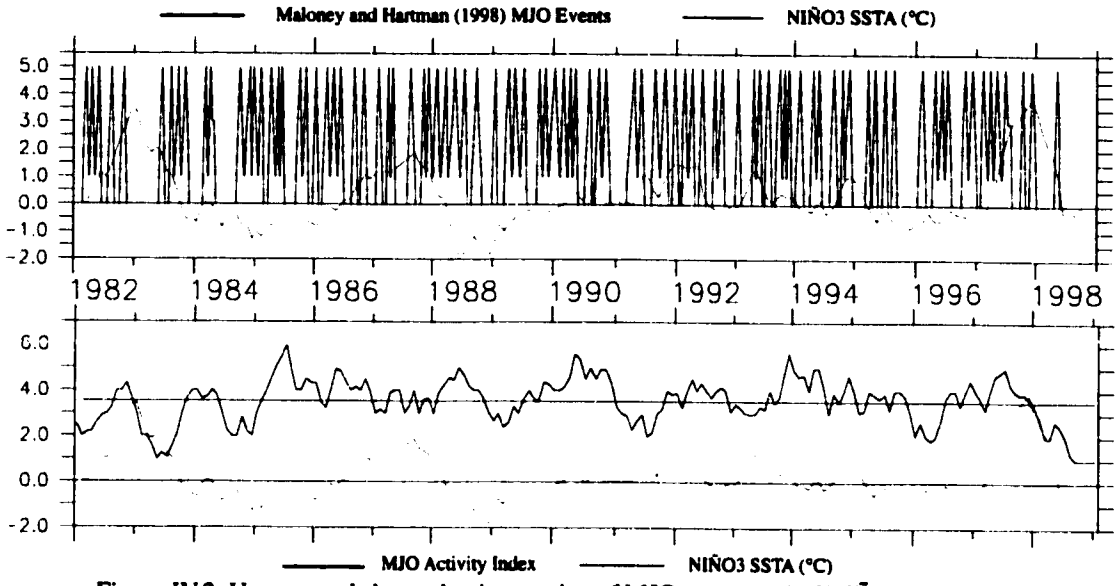

Figure IV.2: Upper panel shows the time-series of MJO events and of NIÑO3 SSTA for the period Jan. 1982-Mar. 1998. Lower panel shows the time-series of MJO activity and of NIÑO3 SSTA for the same period. MJO activity is defined as the 240-day running count of MJO events. Notice the lack of connection between the MJO-activity index and NIÑO3 SSTA.

coefficient of -0.16 at zero lag, which is not significant even at the 85% confidence level. Figure IV.3 shows the 1982-1998 lagged correlation between NIÑO3 SSTA and the MJO Activity Index, with the dashed lines indicating the 90% confidence interval (assuming 24 degrees of freedom and computed as in Appendix A), notice how the only statistically significant correlation (and marginally so) between the quantities is approximately -0.4 at -18 months lag, with increased NIÑO3 SSTA leading reduced MJO activity.

Examining only extreme periods of MJO activity in Figure IV.2, three of the primary maxima of the activity index occur during cold or normal years (cold 1985 and 1988, near-normal 1990), one during a mildly warm year (1994), and one maximum occurs in early 1997 (coincident with the development of the 1997-8 El Niño); the largest minimum occurs during the warm event of 1982. These results are consistent with recent analyses of other MJO indices, which found no significant relationship between increased MJO activity and common El Niño indices (Slingo *et al.* 1999, Hendon *et al.* 2000, Harrison and Vecchi 2000). This should be contrasted with the significant correlations between Troup-SOI and certain WWEs (see HV97 and Chapter II), and with the NIÑO3 SSTA warming

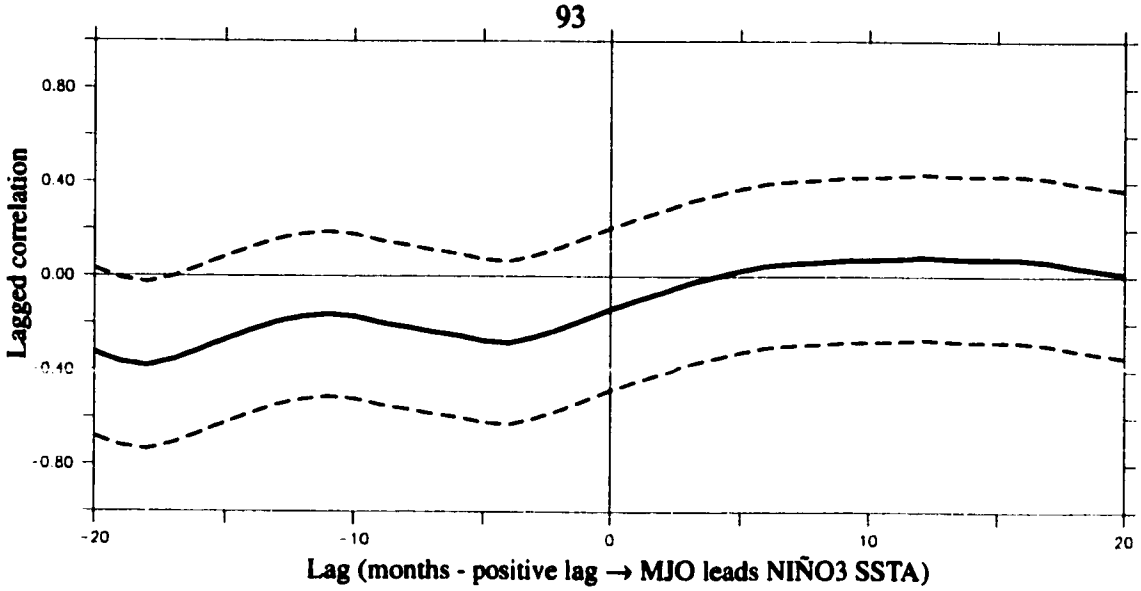

Figure IV.3: Lagged correlation between MJO activity index and NIÑO3 SSTA index. Lag is in months, with positive lag indicating the MJO activity leads NIÑO3 SSTA). Dasshed lines indicate the 90% confidence interval on the correlation.

which tends to follow equatorial WWEs (see VH00 and Chapter III).

Using the MH-MJOI from January 1986 through May 1998 I generated composites of the MJO related atmospheric convection and surface wind fields, for each MJO phase and for both initially WARM and REGULAR conditions. These composites represent the average surface expression of the MJO, and are compared to the WWE OLRA and UA composites (see Section 3). I also explore statistical relationships between the various WWE types and MJO events as defined by the MH-MJOI (see Section IV.5).

Tropical cyclone best track data was used to compare tropical cyclone activity to WWE activity, over the period 1986-1998. Eastern tropical Pacific northern hemisphere data was compiled by Dr. Christopher Landsea at Colorado State University (available on-line at: *http://weather.unisys.com/hurricane/)*. Southern hemisphere and western Pacific northern hemisphere cyclone best track data was compiled by the U.S. NAVPACMETOC Center and the Joint Typhoon Warning Center, and can be found on the web at: *http:// www.npmoc.navy.mil/products/jtwc/best_tracks/*. These hurricane data are used to examine relationships between WWEs and Pacific Ocean tropical cyclones over the period 1986-1998. Intensity groupings of the cyclones was done based on the Saffir-Simpson Scale. The

(a) Northwest Pacific cyclone tracks (1987)

(b) Southwest Pacific cyclone tracks (1987)

Figure IV.4: Tropical cyclone tracks in the western Pacific in 1987. (a) Tracks for north-west Pacific cyclones, (b) for south-west Pacific cyclones. Data from the Global Tropical and Extra-Tropical Cyclone Atlas (GTECCA 1998).

classifications used here are: a *Tropical Cyclone* is any tropical cyclone catalogued in the atlases regardless of intensity, a *Hurricane* is a tropical storm whose maximum hourly averaged surface winds exceed 74 knots at any point, and a *Category 2 Hurricane* is a Hurricane whose maximum hourly averaged surface winds exceed 96 knots. Tropical cyclone tracks from the Global Tropical and Extratropical Cyclone Atlas (GTECCA 1998) in 1987 are plotted in Figure IV.4. Notice how northern hemisphere western Pacific cyclones tend to translate west-north-westward, while southern hemisphere cyclones tend to translate south-eastward.

WWE Type	Northern Hemisphere Cyclones	Southern Hemisphere Cyclones
NW	130°E-155°E; 12°N-25°N	
N	150°E-180°E; 12°N-25°N	
NE	170°W-140°W; 20°N-30°N	
W	135°E-160°E; 0°-15°N	145°E-160°E; 15°S-0°
C	150°E-175°E; 0°-15°N	150°E-175°W; 15°S-0°
E	180°-150°W; 0°-15°N	180°-150°W; 15°S-0°
S		150°E-170°W; 20°S-10°S
SE		170°E-140°W; 25°S-12°S

Table IV.2: List of regions used to compare tropical cyclone activity to WWE activity. These are referred to as "regions of interest" in the text. They are the places where one might expect a relationship to exist between WWEs and tropical cyclones.

To explore the relationship between cyclones and WWEs methodically, cyclone regions of interest for each WWE are defined. These regions of interest are where cyclone activity might be expected to be related to WWE activity, based on the surface wind analysis, the OLR composites and the structure of tropical cyclones (which have westerly circulation equatorward of the eye). The regions of interest for each WWE type are listed in Table IV.2. For off-equatorial WWE types, only cyclones in the corresponding hemisphere are examined; for equatorial WWEs, cyclones on either side of the equator are examined.

In order to be able to discuss the various degrees of statistical association that WWEs have to cyclones and to the MJO, the term "characteristic" will be used to denote a particular statistical relationship. A property X is defined to be *characteristic* of a phenomenon Y if the conditional probability of X being true given Y has occurred is much greater than the conditional probability of X being false given Y has occurred (X is defined as a characteristic of Y if $P(X|Y) >> P(\sim X|Y)$). Since I will be dealing with simple systems where X and Y are exclusively true or false, $P(\sim X|Y) = 1-P(X|Y)$. The definition of characteristic can be simplified to having $P(X|Y) > t$, where t is some threshold. For the remainder of this discussion, t is chosen to be 85%. Note that characteristic as defined here is independent of statistical significance, rather it refers to whether a particular feature is likely to be found associated with a phenomenon. A feature might be significant and not characteristic, or vice-versa.

IV.3. OLR Composite results.

This section summarizes the results of compositing OLRA and UA for the MJO and for each WWE type. Tropical Pacific atmospheric convection and surface wind have large interannual variability associated with ENSO, which should be removed to observe only the WWE or MJO related convective and wind signals. When examining the composite OLR variability associated with each WWE type or the MJO separately for WARM and REGULAR cases we will focus of the OLRA and UA departure from the expected mean in the absence of the particular WWE type or MJO Phase (the quantity defined as OLRD and UD in Section 2).

a. MJO Composites:

First I examine the evolution of the MJO related OLRA and UA fields for all MJO events, regardless of NIÑO3 SSTA. The UA results are analogous to the WWE wind anomaly composites described in Chapter II and HV97. Figure IV.5 shows the 99% significant OLRA and UA all time MJO composite; shaded are values of OLRA significant at the 99% level, vectors indicate UA when either vector component is significant at the 99% confidence level (significance determined using a bootstrap method). The expected anomalies when all time is considered, are close to zero, so OLRD and UD are very similar to OLRA and UA in the all event composite (Figure IV.5). Each Phase of the MJO is as defined in Maloney and Hartmann (1998); the average duration of a Phase is five days.

Phase 1 of the MJO is associated with reduced convection north and south of the equator over the eastern Indian Ocean; there are easterly anomalies west of the convection anomalies. There is also enhanced convection north of the Equator over Central America and northern South America, with weak westerly anomalies generally in the Pacific ITCZ region. During Phase 2 there are no large-scale convection anomalies, but there are large regions of easterly (westerly) in the off-equatorial tropical Indian Ocean (eastern tropical north Pacific). In Phase 3, enhanced convection exists over the western equatorial Indian

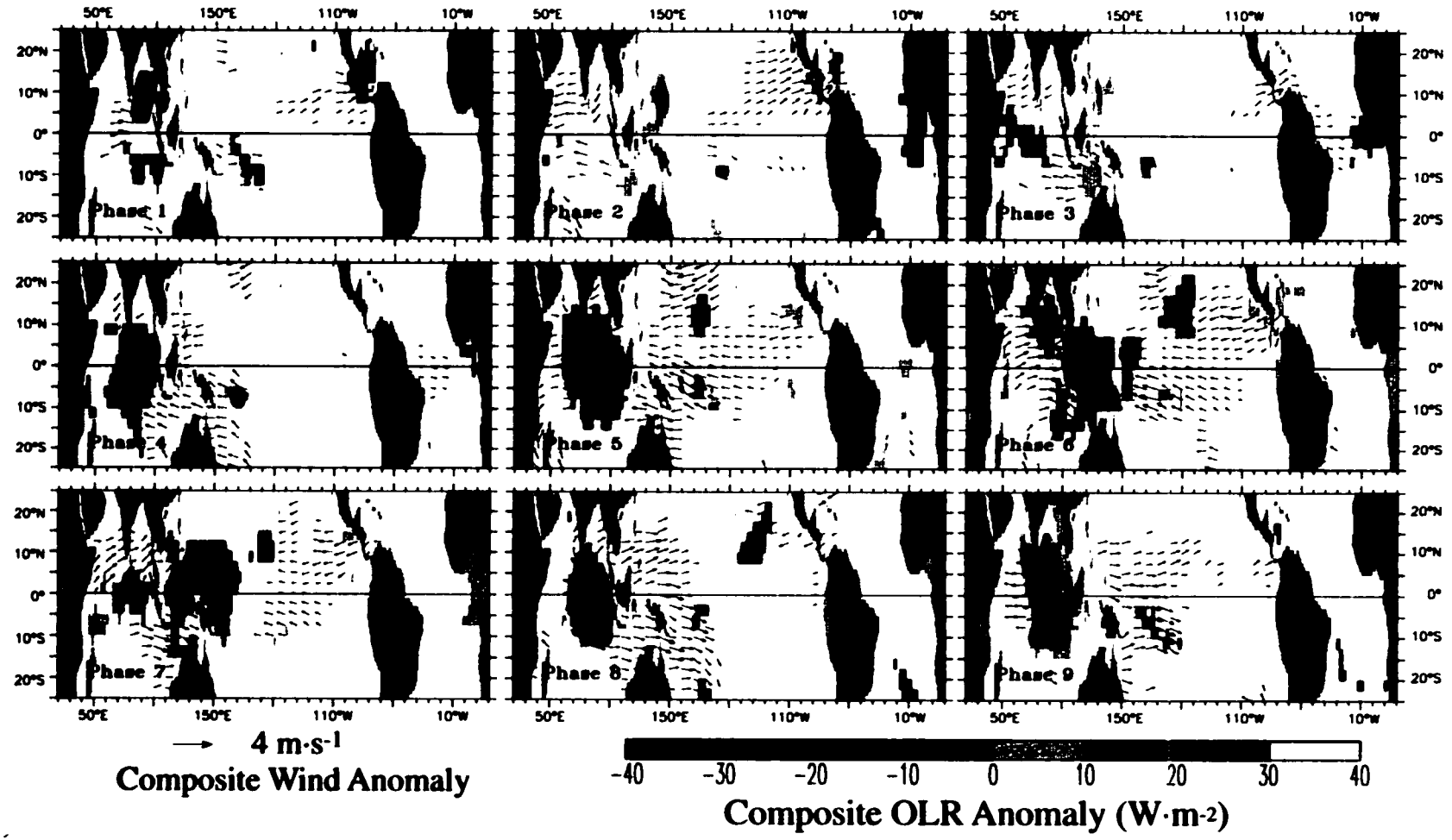

Figure IV.5: All-event composite MJO OLRD and UD for each of the nine MJO Phases. Cool (warm) colors indicate enhanced (reduced) convection. OLRD is shaded if significant at the 99% confidence level. UD vectors are drawn if either the zonal or meridional component is significant at the 99% confidence level.

ocean with easterly anomalies north of it and southeast of it. There are southeasterly anomalies from the Pacific ITCZ across Central American into the southern Caribbean, with no associated convective anomalies.

Phase 4 exhibits enhanced convection over a large part of the eastern Indian Ocean, and easterly anomalies across much of the western Pacific and southeastern Indian Oceans. During Phase 5 (the Phase with maximum central Indian Ocean 850 hPa westerlies – MH98) the Indian Ocean enhanced convection has grown in size and intensity, but its center has not moved much; now there are westerly anomalies west of and within the convection region, and easterly anomalies broadly across the central and western tropical Pacific. Phase 6 has the region of enhanced convection over the Maritime Continent, with westerly anomalies covering much of the tropical Indian Ocean, and easterly anomalies covering much of the eastern and central tropical Pacific. During Phase 7 there is a convective anomaly couplet, with enhanced convection still over the Maritime Continent and reduced convection in the central and eastern equatorial Indian Ocean. Westerly anomalies continue north and south of the region of reduced convection and, weakly, into the region of enhanced convection. Easterly anomalies exist broadly in the central tropical Pacific between 10°N and 10°S. Only during Phases 8 and 9 are the dominant Pacific wind anomalies westerly. In Phases 8 and 9, there is weakly enhanced convection over the central Pacific, and strongly reduced convection over the central and eastern Indian Ocean. There are westerly anomalies generally over the western Pacific between 15°N and 15°S and the flow is generally divergent at the surface, with a northerly (southerly) component north (south) of the equator and with only a small area of equatorial westerly anomalies.

The periods of enhanced convection over the western Pacific are Phases 6 through 8, and there are corresponding periods of reduced convection in Phases 2 through 4. This OLRA field is qualitatively consistent with the MJO OLRA evolution described in the literature (Rui and Wang 1991, Madden and Julian 1994). The convective anomalies propa-

gate at an average speed of 5-10 ms^{-1} (depending on whether the Phase length is between 5 and 10 days).

A feature to notice, and contrast with the OLR evolution and recent models of the MJO surface wind field, is the asymmetry of the surface zonal wind circulation over the tropical Pacific. A prominent surface wind feature are the easterlies across most of the western and central Pacific during MJO Phases 4 through 7. There is no corresponding Phase of strong westerlies across the basin, rather the westerlies tend to be confined to an area west of the dateline. The amplitude of the wind anomalies over the central equatorial Pacific is roughly half that over the western Pacific, but the easterly anomalies tend to occur in a region of strong easterly trade winds, while the westerlies occur over a region of weak climatological winds (see Figure II.3). Since wind stress is proportional to the square of the wind speed, the momentum flux due to the central/eastern Pacific anomalies could be comparable to that associated with the western Pacific anomalies. Notice also how the largest amplitude wind anomalies tend to be far off equator (>5°), beyond the oceanic equatorial waveguide.

Since the interactions which couple the tropospheric MJO circulation with the atmospheric boundary layer circulation are generally a function of the background atmospheric circulation and of SST, I now examine the MJO related surface circulation for periods of near normal NIÑO3 SSTA separately from periods of warm NIÑO3 SSTA. As with the compositing of SSTA following WWEs in Chapter III, one would ideally like to perform the compositing for different seasons as well as for different NIÑO3 SSTA states; however, since there are only 13 years of wind data available, the analysis is performed only for different NIÑO3 SSTA states. This analysis will examine the statistically significant OLRA and UA deviations from the expected anomalies (defined as OLRD and UD in Section 2), for MJO phases when NIÑO3 SSTA is in the REGULAR state (Figure IV.6) and in the WARM state (Figure IV.7). The deviations shown in Figure IV.6 are masked at the

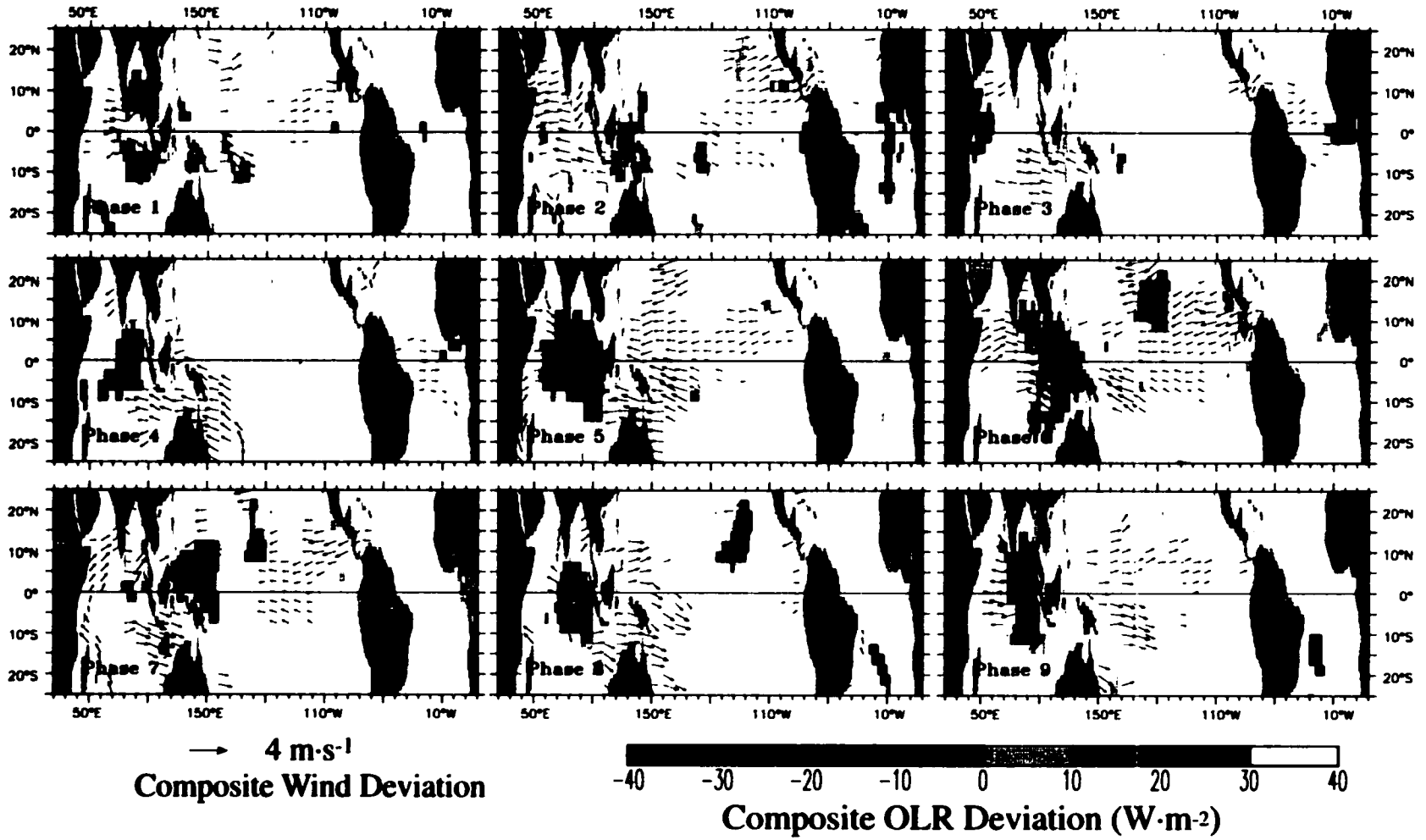

Figure IV.6: REGULAR-event composite MJO OLRD and UD for each of the nine MJO Phases. Cool (warm) colors indicate enhanced (reduced) convection. OLRA is shaded if significant at the 99% confidence level. UD vectors are drawn if either the zonal or meridional component is significant at the 99% confidence level.

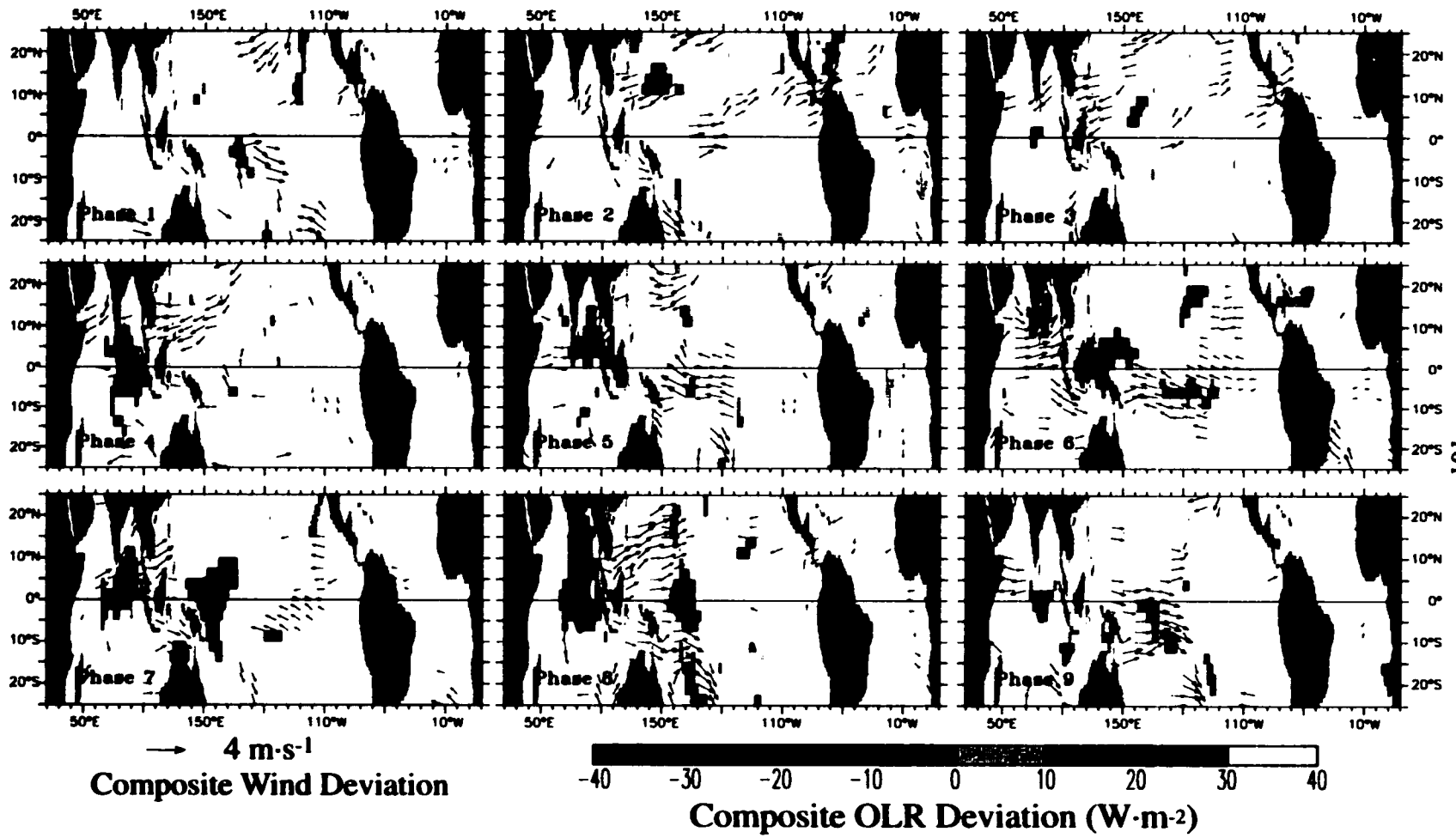

Figure IV.7: WARM-event composite MJO OLRD and UD for each of the nine MJO Phases. Cool (warm) colors indicate enhanced (reduced) convection. OLRA is shaded if significant at the 95% confidence level. UD vectors are drawn if either the zonal or meridional component is significant at the 95% confidence level.

99% confidence level; the deviations shown in Figure IV.7 are masked at the 95% confidence level because of the small number of realizations.

Figure IV.6 shows the evolution of the 99% significant OLRD and UD fields for the case REGULAR MJO composite. Notice how the fields are qualitatively similar to the OLRA and UA fields for the all MJO composite (Figure IV.5). The wind asymmetry in the tropical Pacific is still evident in this composite. Notice how the period of westerlies in the Pacific is MJO phases 6 through 9. The character of the wind and convective deviations in the Case REGULAR composite is essentially that of the convective and surface wind anomalies in the all-event composite.

Figure IV.7 shows the evolution of the OLRD and UD fields for the case WARM MJO composite. The evolution in Figure IV.7 is qualitatively similar to that in Figures IV.5 and IV.4, but the amplitude of the Indian ocean convection is smaller and the peak occurs in Phase 4 rather than Phase 5. Here, again, the MJO phases with westerlies in Pacific are Phases 7 through 9. The main difference between the WARM and REGULAR MJO composite is the more persistent westerlies which extend east past the Dateline. This eastward expansion and persistence of the westerlies is likely due to the eastward migration of the western Pacific warm pool east of the Dateline during El Niño events.

b. WWE Composites:

Figure IV-8 shows the *OLRA* and UA fields from the ALL/NON-EVENT composites, for both case REGULAR and WARM. The NON-EVENT composites for each of the individual WWE types do not differ in any appreciable way from the ALL/NON-EVENT composite. Notice that when the NIÑO3 SSTA index is near normal and there are no WWEs (Fig. IV.8.a) the main anomalies are enhancements of the climatological state, with enhanced convection over the Maritime Continent, reduced convection east of the dateline and enhanced easterlies along the equatorial Pacific and westerlies over the Indian Ocean. These patterns are due to the fact that there were more warm ENSO (El Niño) events in the

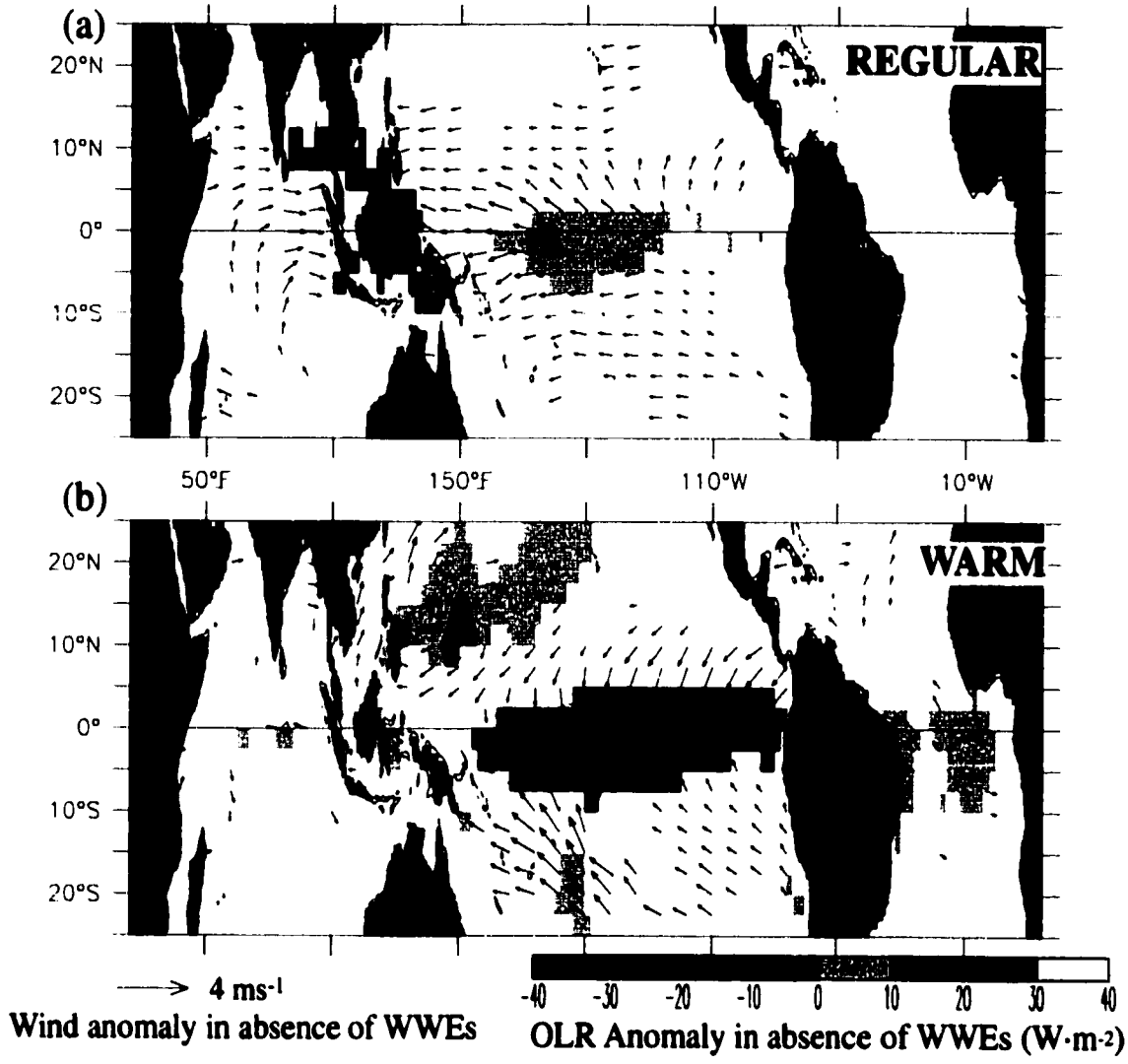

Figure IV.8: 99% significant OLRA and UA in the absence of any WWEs (a) when NIÑO3 SSTA is near normal (Case REGULAR), (b) when NIÑO3 SSTA is warmer than noemal (Case WARM).

period 1984-1996 than cold ENSO (La Niña) events, so the climatology is slightly biased towards the warm state of ENSO (When computing OLRD and UD the bias is removed). When NIÑO3 SSTA is warmer than normal (Fig. IV.8.b), the convective patterns generally associated with ENSO are evident, as are the surface wind anomaly patterns. The enhanced convection east of the dateline is associated with the eastward migration of the warm pool during ENSO, and the weak equatorial westerlies and meridional inflow to the equator have

been described in previous analyses of the average evolution of ENSO (Rasmusson and Carpenter 1982, Harrison and Larkin 1998). There is also reduced convection over the Amazon basin and the northwestern tropical Pacific when NIÑO3 SST is warmer than normal.

Let us now turn our discussion to the composite OLRD and UD evolution associated with the 8 WWE types. Generally, there is reduced OLRA (indicative of enhanced atmospheric convection) in or near the main WWE surface wind anomalies near the WWE center day; there is also enhanced OLRA (indicative of reduced atmospheric convection) over the eastern Indian Ocean and Maritime Continent for many WWE types. The three north-westernmost WWE types (NW, N and W) have propagating convective structures suggestive of a WWE/tropical cyclone connection. The two southern hemisphere (Types S and SE) WWEs have eastward propagating convective structures. The equatorial WWE Type whose main westerly anomalies are just west (Type C) and east (Type E) of the date-line are associated with enhanced convection over the main surface westerlies, with no distinct propagation. The surface wind fields are similar to those described in HV97 and Chapter II.

i) TYPE NW (FIGURE IV.9):

The evolution of the OLRD and UD fields in both the WARM and REGULAR case composites is similar. The surface wind evolution in both cases is as described in HV97 and Chapter II, with a cyclonic structure developing and moving towards the northwest. Prior to the formation of the cyclonic structure there are weak westerlies in the classifying region and weakly enhanced equatorial convection. The OLR deviations grow in amplitude and move towards the northwest as the surface winds develop a cyclonic structure and begin to move with the convective anomalies. By Day (6) the convective and surface wind deviations have disappeared. In both cases (REGULAR and WARM) there is some reduced convection in the eastern Indian Ocean near Day (-3). In both cases there are weak equatorial

westerlies on and following the center day near the dateline. The convective and surface wind structures are suggestive of a link between tropical cyclone activity and the Type NW WWE.

ii) TYPE N (FIGURE IV.10):

The case REGULAR and WARM composite OLRD and UD fields for the Type N WWE have some qualitative differences, although many general features are the same. The surface wind variability in and near the classifying region is similar in both cases. Both composites have enhanced convection poleward of the main surface westerlies. The case REGULAR composite OLRD does not develop the tight structure seen in the case WARM composite. The case REGULAR composite surface wind deviation has weak equatorial westerlies following the WWE center day, which are not present in the case WARM composite. The case REGULAR composite has weak reduced convection over the Maritime Continent through the lifetime of the WWE. The composite OLRD and UD fields are suggestive of a link between Type N WWEs and tropical cyclone activity when the eastern Pacific is warmer than normal.

iii) TYPE NE (FIGURE IV.11):

The convective and wind variability is qualitatively similar in the case REGULAR and WARM Type NE composite WWE. In both cases the main convective structure is a localized region of enhancement, centered near the Hawaiian islands. This convection is evident through the center day, and quickly disappears after it. The wind deviations have a cyclonic structure to them, but the climatological trade winds over the northeast tropical Pacific are so strong that the wind deviations (and anomalies) actually represent near zero winds. The Type NE composite winds are best described as a break in the trade winds.

iv) TYPE W (FIGURE IV.12):

The case REGULAR and WARM composites for the Type W WWE are different in

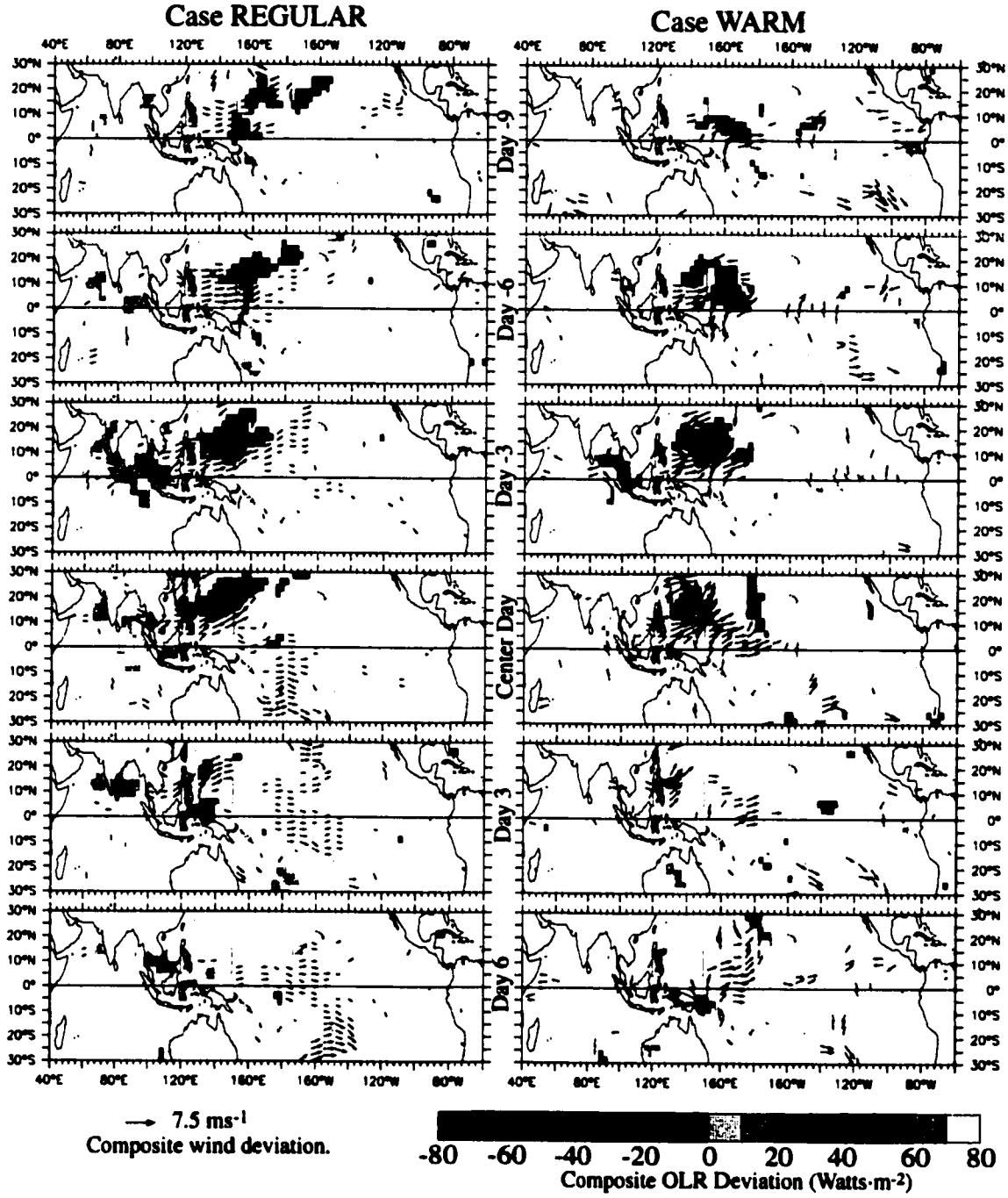

Figure IV.9: Composite evolution of the Type NW OLRD and UD fields for (left column) Case REGULAR, (right column) Case WARM. Composite goes from Day (-9) though Day (6) by 3 day intervals. Shaded is OLRD, with cool (warm) colors indicating enhanced (reduced) convection, masked at the 99% confidence level. Wind deviation vectors are plotted if either the zonal or meridional component is significant at the 99% confidence level.

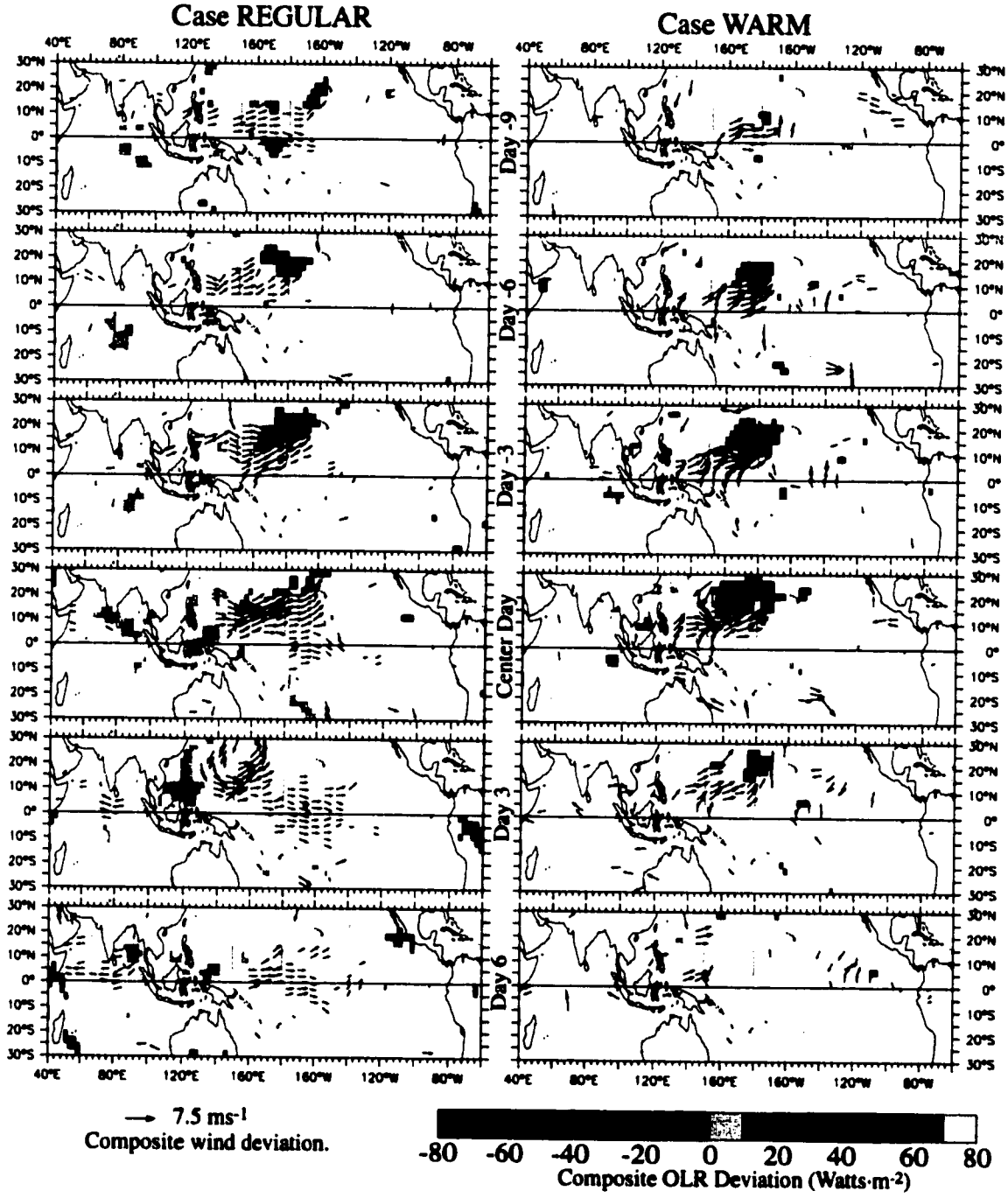

Figure IV.10: Composite evolution of the Type N OLRD and UD fields for (left column) Case REGULAR, (right column) Case WARM. Composite goes from Day (-9) though Day (6) by 3 day intervals. Shaded is OLRD, with cool (warm) colors indicating enhanced (reduced) convection, masked at the 99% confidence level. Wind deviation vectors are plotted if either the zonal or meridional component is significant at the 99% confidence level.

many respects, but both composites are indicative of a relationship between Type W WWEs and tropical cyclone activity. The differences between the two composites might be due to the small number of Type W WWEs occurring during when the eastern Pacific SST is warmer than normal; or it might be due to an actual difference in the evolution of the convection and surface wind fields in either case.

In the case REGULAR composite (Fig IV.12.a-.f) there is weak enhanced convection on Day (-9) along with weak equatorial westerlies. The convection and westerlies intensify as the winds develop a cyclonic structure. North of the Equator the cyclonic structure and enhanced convection concentrate and move towards the northwest (note that there is also a concentration of the southern hemisphere convection to the southeast of the classifying region on before the center day). Near the center day there is a reduction of the convection over the Maritime Continent, which continues through Day (6).

The case WARM composite (Fig. IV.12.g-.l) displays more localized regions of significance. On Day(-9) and Day(-6) there is some weak enhanced convection west of the classifying region, with no significant equatorial westerlies. By Day(-3) a strong, tight convectively enhanced feature off the northeastern corner of the classifying region has formed, along with cyclonic winds surrounding it. There is also some weak convection to the southeast of the classifying region. The northern hemisphere cyclonic circulation / convectively enhanced feature propagates to the northwest and dissipates after Day (3). There is an indication of reduced convection over northern Australia following the center day.

v) TYPE C (FIGURE IV.13):

The case REGULAR and case WARM UD and OLRD composites for the Type C WWE are similar to each other within the WWE classifying region, but there are some striking differences over the Indian Ocean and in the far eastern Pacific off the equator. In the classifying region, the composite for both cases has enhanced convection developing with the equatorial westerlies up to the center day; and disappearing after the center day.

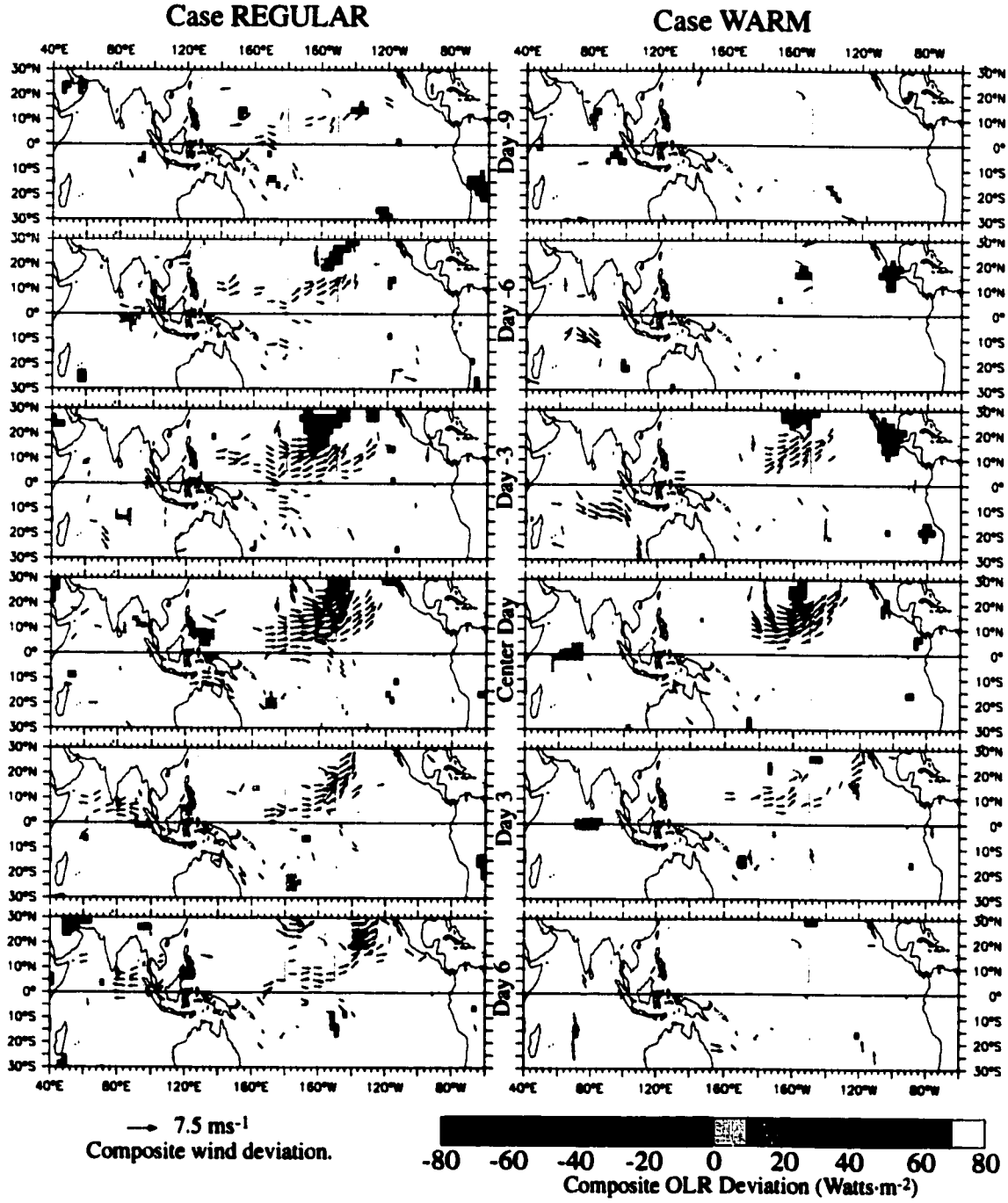

Figure IV.11: Composite evolution of the Type NE OLRD and UD fields for (left column) Case REGULAR, (right column) Case WARM. Composite goes from Day (-9) though Day (6) by 3 day intervals. Shaded is OLRD, with cool (warm) colors indicating enhanced (reduced) convection, masked at the 99% confidence level. Wind deviation vectors are plotted if either the zonal or meridional component is significant at the 99% confidence level.

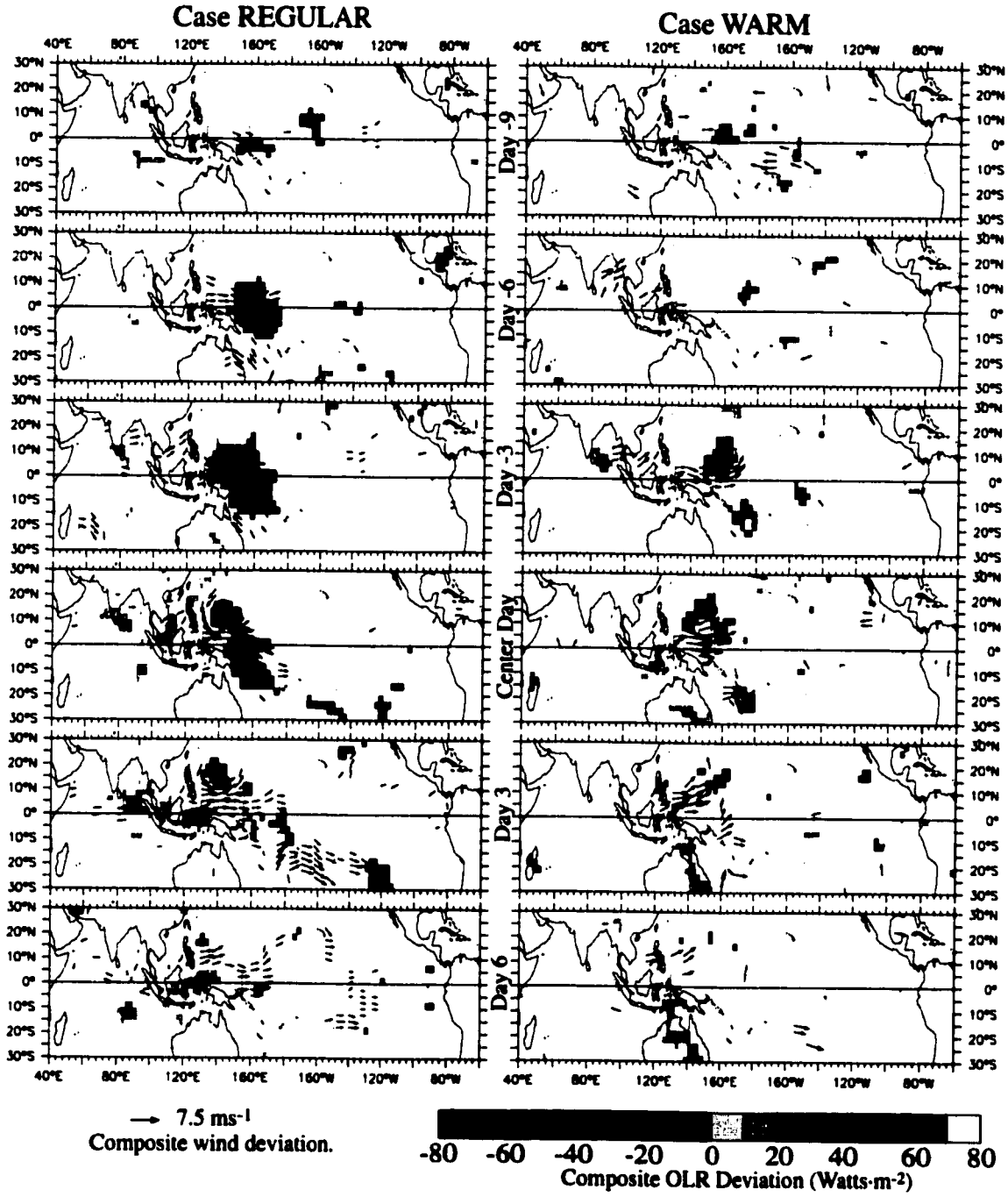

Figure IV.12: Composite evolution of the Type W OLRD and UD fields for (left column) Case REGULAR, (right column) Case WARM. Composite goes from Day (-9) though Day (6) by 3 day intervals. Shaded is OLRD, with cool (warm) colors indicating enhanced (reduced) convection, masked at the 99% confidence level. Wind deviation vectors are plotted if either the zonal or meridional component is significant at the 99% confidence level.

The case WARM composite has only scattered wind and OLR deviation patterns far from the classifying region, the main feature is reduced convection over the Maritime Continent beginning near the center day.

Apart from the main WWE anomalies, the case REGULAR composite has reduced convection over the central Indian Ocean beginning on Day (-9) (see Fig. IV.13.a), which appears to propagate east until it reaches the Maritime Continent on Day (-3) (see Fig. IV.11.c), where it remains through Day (9) (not shown). Also evident in the Type C composite is some reduced OLRA over the southeastern Pacific Ocean, centered near 20°S; this feature might not be representative of variability in atmospheric convection since this area is generally covered by marine stratus clouds (Klein and Hartmann 1993). Evident in the case REGULAR UD composite are two branches of weak to moderate westerlies centered near 20°S and 20°N, between 160°W and 120°W; these off-equatorial westerlies have no counterpart in the WARM event composite.

vi) TYPE E (FIGURE IV.14):

The case REGULAR and WARM Type E composite OLRD and UD fields are similar in and near the classifying region, but there are differences away from the classifying region. The differences between the case REGULAR and WARM OLRD appears to be a matter of amplitude and extent, while the surface wind deviation fields away from the classifying region are qualitatively different.

In the WWE classifying region, significant equatorial westerlies appear by Day (-6) in both cases (see Fig. IV.14.b and IV.14.h), and weakly enhanced convection appears following the westerlies. Reduced convection over the Maritime Continent appears at the same time as the enhanced convection in the classifying region. The reduced convection is of larger extent and amplitude in the case REGULAR composite than in the case WARM composite. In the case REGULAR composite there are moderate westerlies in the northern hemisphere east of the dateline, which appear to propagate eastward beginning on Day (-9)

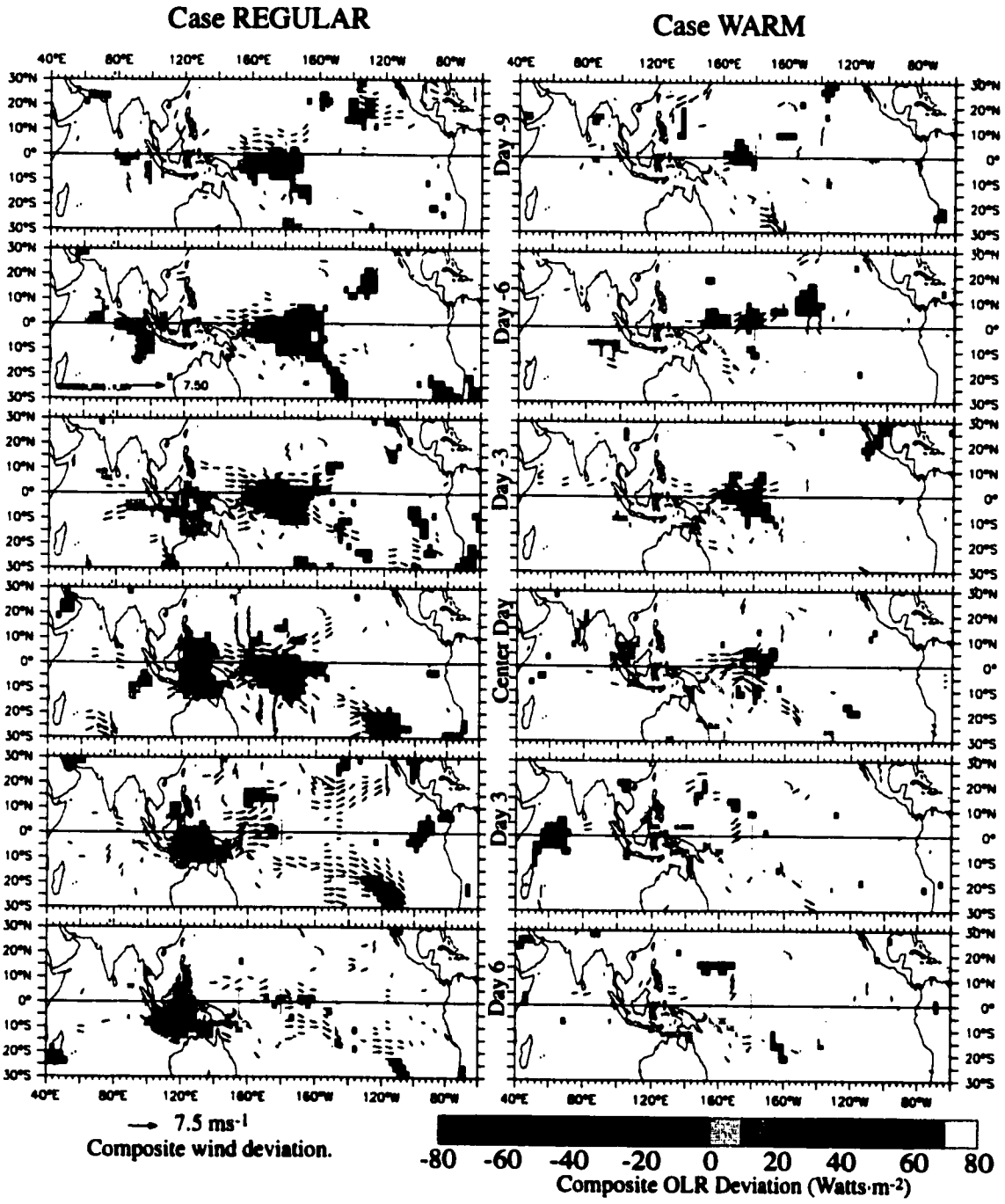

Figure IV.13: Composite evolution of the Type C OLRD and UD fields for (left column) Case REGULAR, (right column) Case WARM. Composite goes from Day (-9) though Day (6) by 3 day intervals. Shaded is OLRD, with cool (warm) colors indicating enhanced (reduced) convection, masked at the 99% confidence level. Wind deviation vectors are plotted if either the zonal or meridional component is significant at the 99% confidence level.

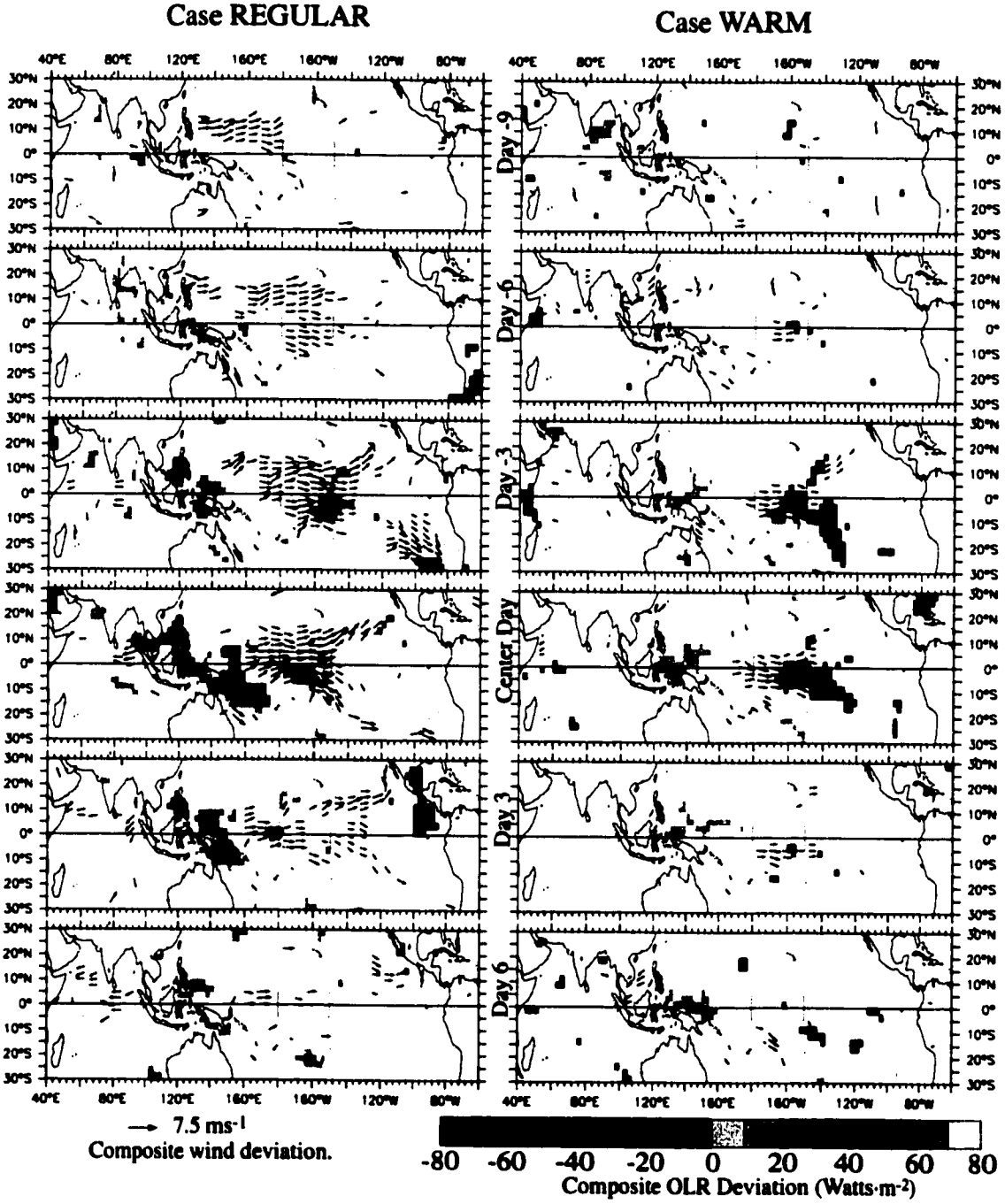

Figure IV.14: Composite evolution of the Type E OLRD and UD fields for (left column) Case REGULAR, (right column) Case WARM. Composite goes from Day (-9) though Day (6) by 3 day intervals. Shaded is OLRD, with cool (warm) colors indicating enhanced (reduced) convection, masked at the 99% confidence level. Wind deviation vectors are plotted if either the zonal or meridional component is significant at the 99% confidence level.

and they appear to meld into the equatorial westerlies by the center day.

vii) TYPE S (FIGURE IV.15):

The case REGULAR and WARM Type S convection and surface wind deviation composites are similar to each other, both having large-scale deviations of both enhanced and reduced convection. The enhanced convection in the case WARM composite extends further into the eastern Pacific and has its peak amplitude later than the case REGULAR composite. In both composites, the reduced convection occurs over the Maritime Continent and peaks in the days following the center day. The surface wind and enhanced convection deviations in both cases are similar, showing an eastward translation somewhere between 5 and 8 ms^{-1}. This translation speed is larger than that discussed in Chapter II, who found a translation between 3-4 ms^{-1} for the Type S WWE. The Chapter II composite analysis did not treat the case REGULAR and WARM composites separately. In the case REGULAR composite, the enhanced convection is evident on Day (-9) in the equatorial western Pacific, and reaches the dateline by the center day, with the enhancement concentrated south of the equator. In the case WARM composite, the enhanced convection is evident as early as Day (-6), increasing in amplitude and extent through Day (3) by when it extends far past the dateline in the southern hemisphere.

viii) TYPE SE (FIGURE IV.16):

The case REGULAR and WARM Type SE composites are similar to each other. The main difference between the two is that the case REGULAR Type SE composite has wind deviations throughout the basin, while the case WARM composite has sparser areas of significance. The main convective patterns in both composites are enhanced convection near the main surface wind deviations in the classifying region, and a region of reduced convection extending to the southeast from the Maritime Continent to the dateline near 30°S.

The surface wind deviations in the case REGULAR composite are evident in the

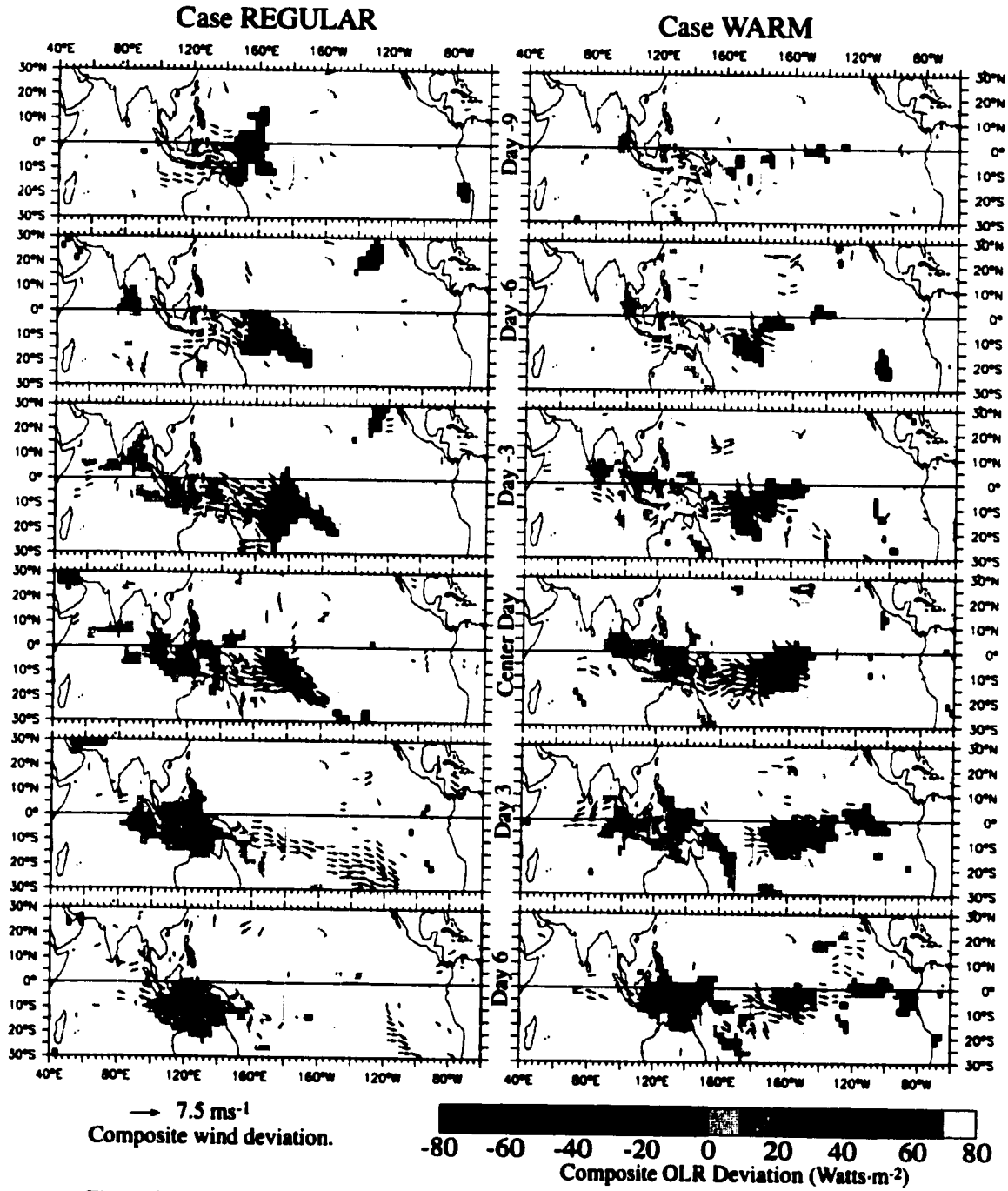

Figure IV.15: Composite evolution of the Type S OLRD and UD fields for (left column) Case REGULAR, (right column) Case WARM. Composite goes from Day (-9) though Day (6) by 3 day intervals. Shaded is OLRD, with cool (warm) colors indicating enhanced (reduced) convection, masked at the 99% confidence level. Wind deviation vectors are plotted if either the zonal or meridional component is significant at the 99% confidence level.

northern hemisphere western Pacific (near the Type NW classifying region) by Day (-9). The surface westerlies appear in the Type SE classifying region following Day (-6); developing a cyclonic circulation structure near the center day. There are equatorial westerlies in the case REGULAR composite. It appears that both the co-occurrence between the Type NW and SE events and the composite equatorial westerlies associated with the Type SE WWE mentioned in HV97 and Chapter II, result from the evolution of the Type SE events when NIÑO3 SST is near normal.

The surface wind deviations in the case WARM composite appear west of the Type SE classifying region by Day (-9) and intensify. By the center day the winds have developed a cyclonic circulation structure. By Day (6) the only large-scale deviations remaining are reduced convection north of New Guinea and to the south of the classifying region.

ix) SUMMARY:

The convective variability associated with each WWE type is complex, and not generally suggestive of a tight association between the WWE types and particular atmospheric circulation phenomena (*ie.* the MJO, tropical cyclones, convective superclusters, etc.). The composites of the Type NW and W WWEs are suggestive of an association between these WWE types and tropical cyclone activity. The eastward propagation seen in the Type S and SE composites, is consistent of a relationship between these event types and both the MJO and tropical cyclone activity (since tropical cyclones in that part of the world generally translate southeastward at ~3-5 ms^{-1}). The propagation speed of these southern hemisphere WWEs is consistent with both the typical translation of southern hemisphere tropical cyclones and with the phase speed MJO convective variability (although not with the phase speed of MJO tropospheric wind variability).

The connection between convection in general and surface westerlies is clear from these composites; yet further analysis is necessary to understand the relationship between WWEs and circulation structures such as the MJO or cyclones. The fact that individual

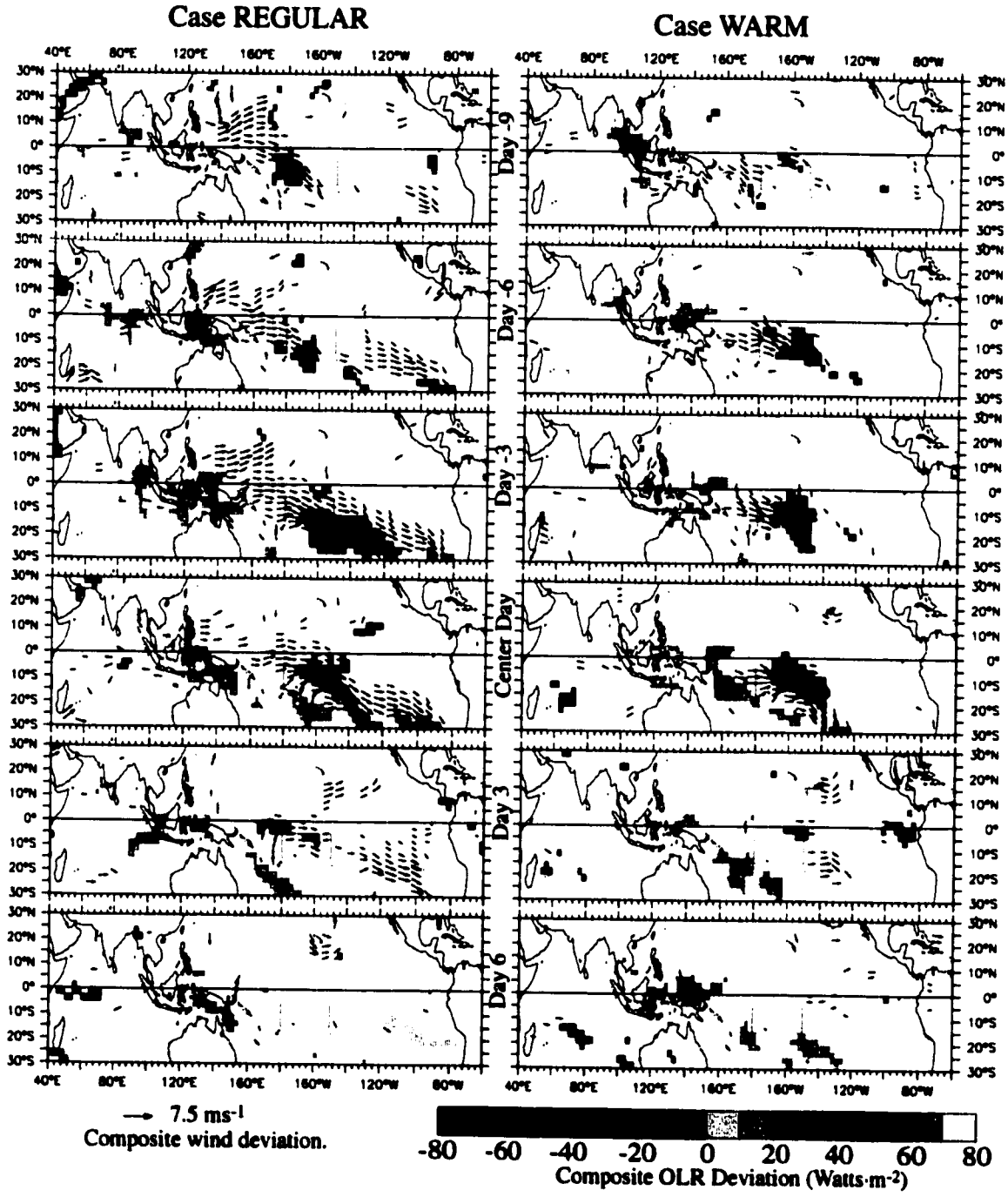

Figure IV.16: Composite evolution of the Type SE OLRD and UD fields for (left column) Case REGULAR, (right column) Case WARM. Composite goes from Day (-9) though Day (6) by 3 day intervals. Shaded is OLRD, with cool (warm) colors indicating enhanced (reduced) convection, masked at the 99% confidence level. Wind deviation vectors are plotted if either the zonal or meridional component is significant at the 99% confidence level.

WWEs have been observed with a variety of atmospheric circulation phenomena (mid-latitude cold surges, paired tropical cyclones, individual tropical cyclones, the convectively active phase of the MJO, convective superclusters, etc.) is consistent with the fact that no single circulation phenomenon appears clearly in the WWE composites. A general relationship between WWEs and any single mode of atmospheric variability cannot be developed from these results. In the next section I examine the "inter-WWE" spacing to explore relationships between WWEs, and between WWEs and the MJO. In sections 5 and 6, I examine relationships between WWEs and these two particular circulation structures: the MJO (in Sections 5) and tropical cyclones (in Section 6).

IV.4. Inter-WWE Spacing:

Exploring the inter-WWE spacing gives an opportunity to understand the "randomness" of WWE occurrence and to explore suggestions of a tight coupling between WWEs and 40-80 day variability. The distribution of inter-WWE spacing can be tested for significant difference from an exponential distribution. If there are no significant departures, WWEs can be thought of as Poisson distributed random phenomena. If there are significant departures, the location of the departures can include hints as to the preferred timescale WWEs.

One of the fundamental features of the MJO, in fact the feature leading to its identification, is its strong spectral peak between 40 and 80 days. A phenomenon strongly associated with the MJO might be expected to have a spectral peak in the 40-80 day range. The duration of WWEs (typically 3-20 days, see Chapter II and HV97) is not consistent with the timescales of the MJO; yet it is possible that the MJO drives episodic variability with WWE timescales, with a typical spacing on the order of the MJO period. In this section, the spacing between successive WWEs of each type is examined to determine whether a suggestion for a relationship between the MJO and WWEs is evidenced in the inter-WWE spacing.

Figure IV.17 shows histograms for the spacing between successive WWEs of each

type for the period 1986-1998. The large bin size is 40 days, and the narrower bins are 10 days wide. Indicated on each 40 day bin is the 95% significant range expected from an exponential distribution with scale parameter fit to each WWE type. An exponential distribution has a probability density function given by:

And the maximum likelihood estimator for the exponential factor is the population average (Rice 1995, Zwillinger 1996). For each WWE type the exponential factor is approximated as the average days between WWEs, and a Montecarlo method is used to compute statistical significance (Rice 1995). The 95% confidence interval for the estimated exponential distribution is indicated by the vertical lines at the center of each bin. When the distribution

$$f(x) = \begin{cases} \lambda e^{-\lambda x} & x \geq 0 \\ 0 & x < 0 \end{cases}$$

is outside the 95% confidence interval in any bin, the distribution is significantly different from an exponential with the calculated factor at the 95% confidence interval.

All the WWEs have a peak in inter-event spacing in the ≤40 day range, roughly consistent with an exponential distribution. However, three WWE types (N, C and E) have significantly more WWEs occurring within 40 days of each other than expected from random. This spacing is consistent with the spectral character of the zonal wind near the dateline which has its largest sub-seasonal peak in the 6-30 day range (Luther *et al.* 1982, Harrison and Luther 1990). None of the event types deviate by having too many (or few) events in the 40-80 day bin.

Limiting the analysis to strong WWEs, the distribution of inter-event spacing is different for some event types. The inter-WWE spacing histograms for the events with zonal wind anomaly averaged over the classifying region exceeding 4 ms^{-1} is shown in Figure IV.18, with bins of 10 and 40 days width. It is clear from Figure IV.18, that the strongest southern hemisphere WWEs tended to be 40-80 days apart from each other. For the Type C and E strong WWEs, the strong event spacing is significantly different (at the

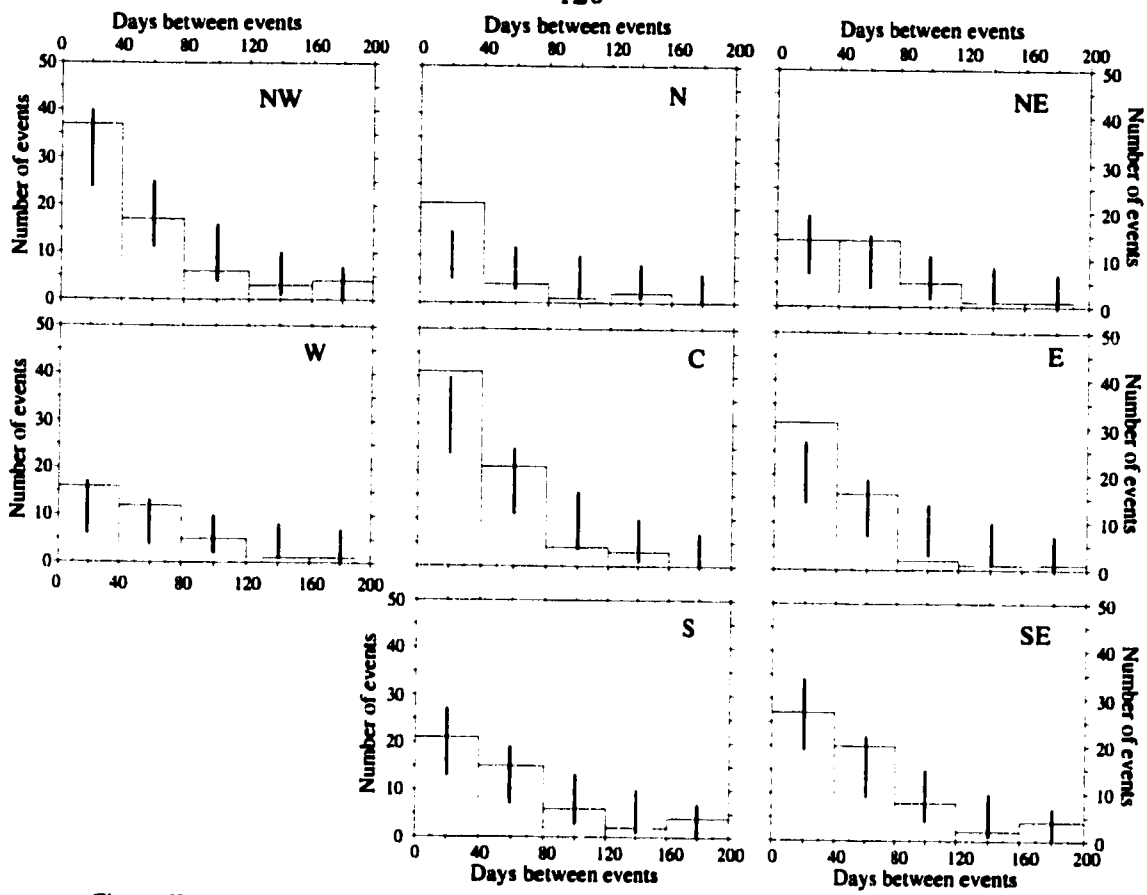

Figure IV.17: Histograms of the spacing between successive WWEs for each of the eight WWE types. Narrow bins are 10 days wide, wide bins are 40 days wide. Notice how no WWE type has a peak inter WWE spacing in the "intra-seasonal" 40-80 days band. Vertical lines indicate the 95% confidence interval for the distribution.

95% confidence level) from an exponential distribution. All other strong WWE types are indistinguishable from Poisson random phenomena.

The histograms shown in Figure IV.17 do not suggest a general relationship between WWEs and 40-80 day forcing. There are secondary peaks in that range for some WWE types, but the main inter-event spacing peak is ≤40 days for all WWE types. The event spacing is for the Type C and E events is consistent with the spectral character of tropical Pacific zonal winds, which have about twice as much energy in the 6-30 day band as in the 30-90 day band (Harrison and Luther 1990). When only strong events are considered (Figure V.18), southern hemisphere WWEs (Types S and SE) have a prominent peak in the 40-80 day period. This spacing, along with the OLR and surface wind composites, is

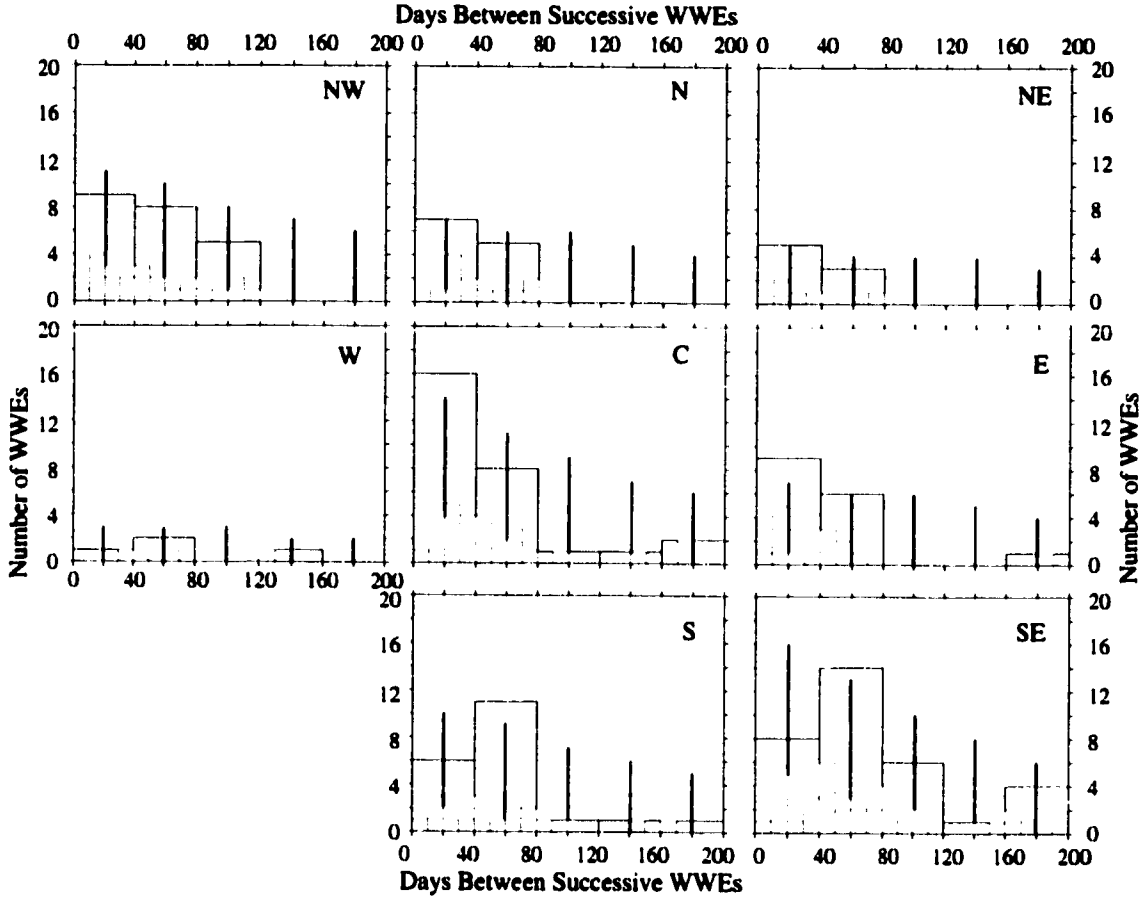

Figure IV.18: Histograms of spcaing between successive strong WWEs for each of the eight WWE types. "Strong" WWEs are those whose maximum zonal wind anomaly averaged over the classifying region exceeds 4 ms^{-1}. Narrow bins are 10 days wide, wide bins are 40 days wide. Notice how southern hemisphere WWEs have a peak in the "intra-seasonal" 40-80 day band, while no other WWE type has such a peak. Vertical lines indicate the 95% confidence interval for the distribution.

suggestive that the strongest southern hemisphere WWEs on record might be related to the MJO. In the next section, I use the MH98-MJOI to explore relationships between WWEs (as identified here) and the MJO (as defined by the MH98-MJOI).

IV.5. WWE/MJO co-occurrence.

In the previous section the inter-event spacing was explored to look for a suggestion of a systematic WWE/MJO relationship. In this section the search for WWE/MJO relationships is carried out using the MH98 MJO Index (MH-MJOI) and the WWE center day list. The MH-MJOI is an index derived independently from the WWE definitions, which uniquely

defines MJO events. These events are divided into 9 Phases, of which Phases 6-9 are the ones with enhanced western and central Pacific convection and surface westerlies (see Maloney and Hartmann 1998, Section 3). According to the MH-MJOI there were 70 MJO events in the period Jan 1986 through May 1998. If we use the NIÑO3 SSTA at the beginning of Phase 4 to separate the MJOs, we find that 20 (29%) occurred in case WARM, 44 (63%) occurred in case REGULAR and 6 (9%) occurred in case COOL; this distribution is not significantly different than a uniform distribution even at an 85% confidence level (see Table IV.1).

In this section, I first examine the distribution of WWEs relative to the Phases of the MJO, and perform two distinct tests of the distribution of WWEs into the MJO Phases. The first test examines whether the number of WWEs occurring when no MJO is present is significantly different from a binomial distribution, with probability given by $(1\text{-}p(MJO))$. This first test will determine whether a WWE is likelier to occur when an MJO is present than when it is not. The second test is whether, for the WWEs occurring inside the MJO, I am able to identify a sequence of Phases within which occur a preferential number of WWEs. If I am able to identify these Phases, they will then be referred to as the "WWE-rich" Phases of the MJO. Two combinations of the results occur in these data, and I interpret them as:

- *MJO modulation of WWE occurrence:* If a given WWE type has a distribution such that the number of WWEs occurring with the MJO is indistinguishable from random, but the events occurring within the MJO exhibit a preference for particular Phases of the MJO; then the MJO can be thought of as modulating the occurrence of WWEs. That is, WWEs are as likely to occur with an MJO as without, but if they happen with an MJO they tend to happen within certain Phases.

- *MJO driving of WWE occurrence*: If a given WWE type has a distribution that shows both a preference for the MJO and for particular Phases of the MJO, the distribution

is consistent with the WWEs occurring during the WWE-rich Phases of the MJO being driven by the MJO. This statistical relationship does not imply causality, but it is consistent with it.

Histograms of the MJO Phase at the beginning of the WWE for each WWE type are shown in Figure IV.19 (IV.19.a-.f, .h and .i), along with the distribution of the MJO phases over all time (IV.19.g). Notice, in Fig. IV.19.g, that about 34% of the time there are no MJOs present and the rest of the time is split pretty evenly among each MJO Phase; Phases 1 and 9 have less time in each of them because some MJOs occur in succession. Identification of the MJO Phases with an increased number of WWEs in them presents a problem in the easternmost regions, since the expected Phases roll over past Phase 9. For the easternmost WWE Types (NE, E and SE), histograms of the MJO Phase 5 days prior to the WWE beginning are shown in Figure IV.19 (shifting by 5 days was chosen because the average length of a Phase was 5 days; note that varying the shift between 5 and 10 days does not alter the principal results). Bars in the non-MJO bin of each WWE type indicate the limits of the 95% confidence interval for a binomial distribution with $p = 0.66$.

None of the WWE types has a statistically significant preference for MJO periods at the 95% confidence level. For the type W WWE, there is significant preference at the 90% level. For none of the other event types is the distribution distinguishable from a binomial even at the 85% confidence level.

The distribution for the various WWEs shows a peak in frequency of occurrence for most WWE types between Phases 6 through 9. This peak tends to move later in the MJO from the westernmost to the easternmost regions (notice the peak for Type W is Phases 6-8, and for Type C it 7-9), this is consistent with the MJO's eastward propagation of 40° longitude per Phase. (360° longitude / 9 Phases). By examining the distribution of MJO Phases for each WWE and performing bootstrap significance analysis on the co-occurrence statistics, a statistically significant "WWE-rich" Phases of the MJO can be defined for each

WWE type, where the number of WWEs occurring in the Phases is significantly different from a uniform distribution.

In Table IV.3 are listed, for each WWE type: the WWE-rich Phases of the MJO, and for all time and for each NIÑO3 SSTA state, the percentage of WWEs in the WWE-rich phases of the MJO. Highlighted by bolding are the statistics for which at least 50% of the WWEs occur in the WWE-rich phases of the MJO. For all time, only the Type W WWE has more than half its events occurring during the WWE-rich phases of the MJO, for the rest of the WWE types the values are between 36% and 45%. For none of the WWE Types is the percentage of WWEs occurring in any NIÑO3 SSTA state significantly different from the

Figure IV.19: Distribution of the MJO Phase in which a WWE begins, for each of the eight WWE types. Phases 1 through 9 refer to the Maloney and Hartman (1998) MJO definition, Phase 0 indicates that the WWE began when no MJO was identified. Bottom left panel shows the all time distribution of MJO phases. Notice how there are "WWE-rich" phases for most WWEs, coincident with the westerly phase of the MJO over the tropical Pacific. Stars indicate the lower limit of the 95% confidence interval of a binomial distribution for the non-MJO periods.

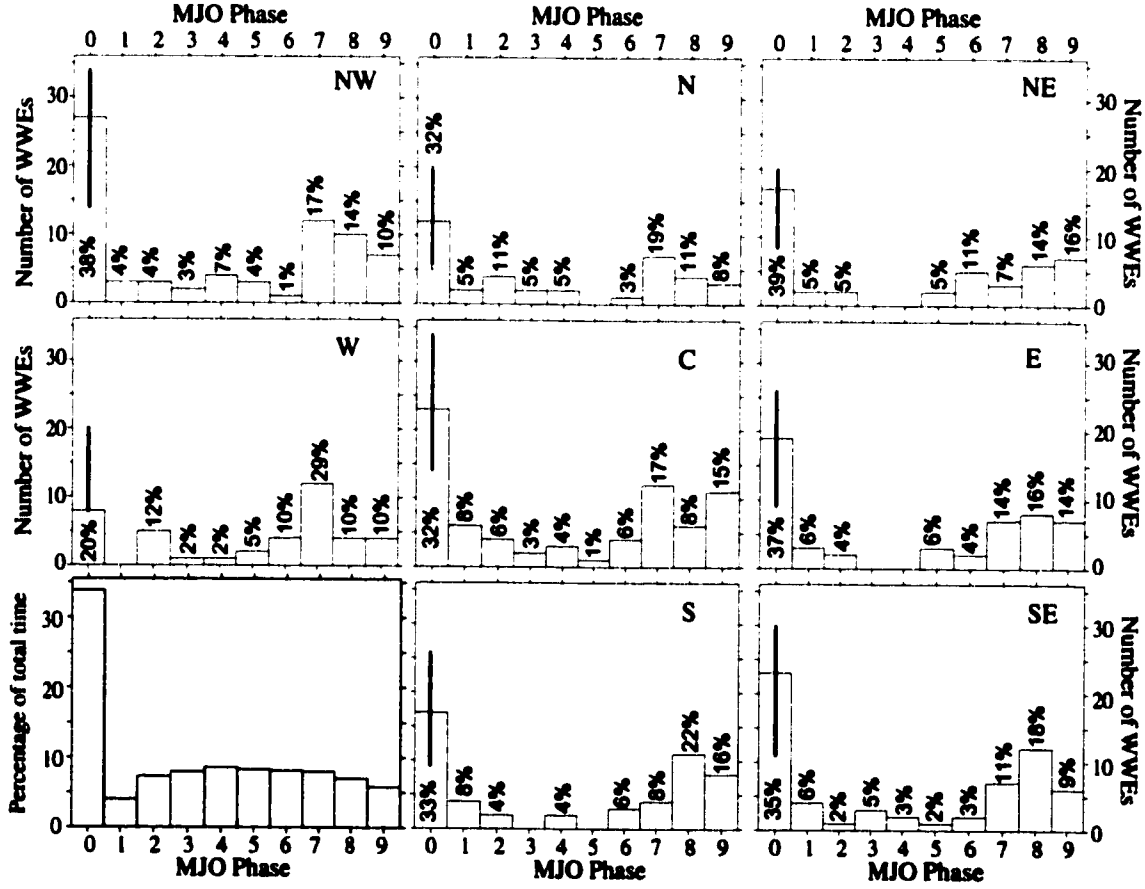

all-event case at the 95% confidence level.

Table IV.4 lists for each WWE type and for each NIÑO3 SSTA case: the percentage of MJOs which had a WWE occurring during the corresponding WWE-rich Phase. Also listed are the collective statistics for the northern hemisphere WWEs, equatorial WWEs, southern hemisphere WWEs, all WWEs, and for Type W and C WWEs (these particular WWEs are those most strongly associated with the onset and maintenance of warm El Niño SST anomaly changes; see VH00 and Chapter III). Percentages higher than 50% are highlighted by bolding.

The number of MJOs with any particular WWE occurring in the corresponding WWE-rich Phases is larger than what would be expected from random, yet over all time there is no individual WWE type which occurs in more than 50% of the MJO events. The highest percentage is for the Type NW WWE, which occurs in 39% of all MJO events. When WWEs are grouped together, the percentages increase, and when all WWEs are considered the percentage of MJOs with a WWE is close to 75%. It is common for MJO events to have a WWE during the corresponding WWE-rich Phases of the MJO, however it is not characteristic (as defined in Section IV.2) of the MJO.

Table IV.3: Percentage of westerly wind events beginning during the WWE-rich phases of the MJO, for the period Jan 1986 - May 1998. The statistics are computed for all time, and also separately for each NIÑO3 SSTA state (as defined in Section 2). The second column lists the WWE-rich phases of the MJO which correspond to each WWE type; for the easternmost WWE types the 5 day shifted statistics are computed (see text for discussion).

WWE Type	WWE-Rich MJO Phases	Percentage of WWEs beginning during WWE-rich phases			
		All Time	CaseWarm (NIÑO3 > 0.75°C)	Case Regular (|NIÑO3| ≤ 0.75°C)	Case Cool (NIÑO3 < –0.75°C)
NW	7,8,9	40%	35%	44%	29%
N	7,8,9	38%	33%	39%	**50%**
NE	7,8,9 (SHF)	36%	24%	**50%**	20%
W	6,7,8	**51%**	36%	**57%**	
C	7,8,9	40%	37%	43%	
E	7,8,9 (SHF)	41%	37%	48%	
S	7,8,9	45%	44%	46%	40%
SE	7,8,9 (SHF)	41%	42%	40%	40%

Examining the distribution of MJOs with WWEs separately for each NIÑO3 SSTA state, a case REGULAR MJO is likelier to have a Type NW or N wind event than a case WARM MJO (at the 95% confidence level). For none of the other event types is the distribution within NIÑO3 SSTA states of WWE/MJO co-occurrence distinguishable from the distribution of the WWEs within NIÑO3 SSTA states.

MJO events have a significant co-occurrence with WWEs, when all WWEs are considered, 74% of MJO events have a WWE occurring during the WWE-rich phases. When only those events most strongly associated with the onset and maintenance of ENSO (Types W and C) are considered: between 47% and 60% of MJO events have WWEs of those types, and between 37% and 57% of those WWEs occur during the WWE-rich phases of the MJO.

Figure IV.20 shows a scatter plot of the NIÑO3 SSTA changes following an MJO, color coded by whether the MJO had an equatorial WWE during its "WWE-rich" phases.

Table IV.4: Percentage of MJO events with a westerly wind event beginning during the WWE-rich phases of the MJO, for the period Jan 1986 - May 1998. The statistics are computed for all time, and also separately based NIÑO3 SSTA state at the beginning of Phase 4 of the MJO. Percentages higher than 50% are hightlighted by bolding.

WWE Type	Percentage of MJOs with a WWE beginning during the WWE-rich phases			
	All Time	Case Warm (NIÑ03 > 0.75°C)	Case Regular (|NIÑ03| ≤ 0.75°C)	Case Cool (NIÑ03 < -0.75°C)
NW	39%	25%	43%	**50%**
N	17%	15%	40%	
NE	21%	15%	25%	17%
W	23%	20%	27%	
C	37%	**60%**	32%	
E	29%	**55%**	20%	
S	33%	45%	30%	17%
SE	34%	**50%**	30%	17%
Northern Hemisphere Type C or W Equatorial	**54%**	45%	**57%**	**67%**
	47%	**60%**	48%	
	54%	**75%**	**52%**	
Southern Hemisphere	44%	**60%**	40%	17%
Any Type	**74%**	**80%**	**73%**	**67%**

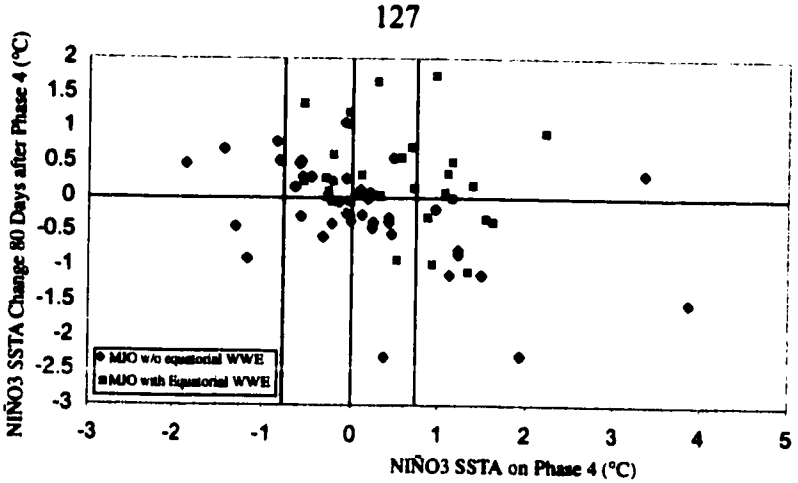

Figure IV.20: Scatter-plot of NIÑO3 SSTA Changes following MJO events. MJO events with equatorial WWEs during their "WWE-rich" Phases are hightlighted by pink squares. Note that the MJOs occurring with equatorial WWEs tend to be followed by warming, while those without WWEs tend not to be.

The NIÑO3 SSTA changes following MJOs in the absence of equatorial WWEs are not significantly different from the population as a whole. However, the SSTA changes following MJO events with an equatorial WWE in them is for significant warming when NIÑO3 SSTA is close to normal and for warm SSTA maintenance when NIÑO3 SSTA is warmer than normal. These expected changes are similar to those following equatorial WWEs. The expected NIÑO3 SSTA changes following MJOs are related to the presence (or absence) of equatorial WWEs.

I now examine the NIÑO3 SSTA changes following the equatorial WWEs, to determine if there is a significant difference between the changes following MJO related WWEs and other WWEs. One of the primary motivations for the study of WWEs has been their potential impact on the evolution of the El Niño cycle. In fact, in Chapter III and VH00, I show equatorial WWEs to be a fundamental mechanism in eastern Pacific SST warming prior to, and of warm SST maintenance during, El Niño. Figure IV.21 shows, for each equatorial WWE, scatter plots of NIÑO3 SSTA 20 days before the WWE center day vs. NIÑO3 SSTA change 60 days after the WWE center day (SSTA change is computed from Day(-20) SSTA), highlighting those WWEs which occurred during the WWE-rich phases of the MJO as stars. Vertical lines indicate the separation between the three NIÑO3 states

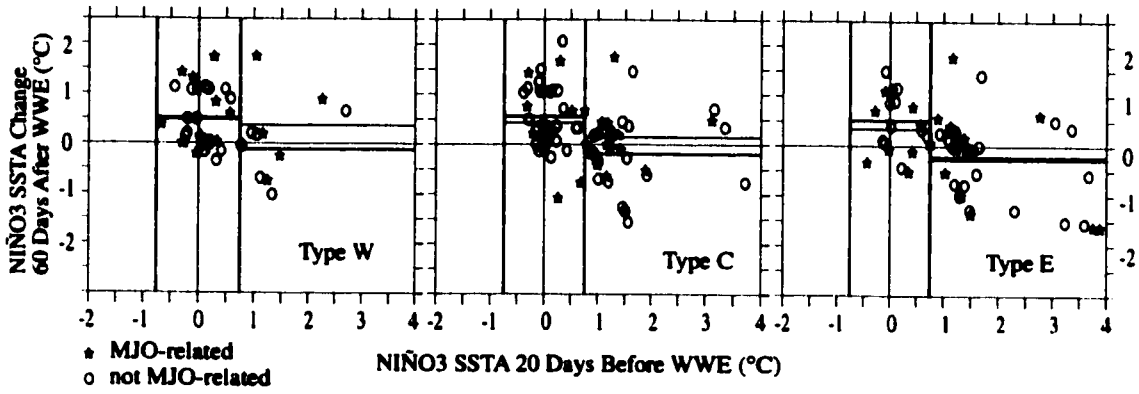

Figure IV.21: NIÑO3 SSTA Change 60 Days after a WWE vs. NIÑO3 SSTA 20 Days prior to the WWE for each of the three equatorial WWE Types. Data for those WWEs which occurred in the "WWE-rich" phase of an MJO are highlighted as stars. Vertical lines indicate the separation between the three NIÑO3 SSTA states (COLD, REGULAR and WARM). Red horizontal line indicates the mean for the MJO-related WWEs, blue horizontal line indicates the mean for the non-MJO-related WWEs. The means are not significantly different from each other.

(COOL, REGULAR and WARM), the red line indicates the mean NIÑO3 SSTA change within each state considering only those WWEs associated with the MJO, and the blue horizontal line in each of the states indicates the mean NIÑO3 SSTA change within each state considering only those WWEs not associated with the MJO.

Testing for significance using a Normal-z test at the 95% confidence level, I find that there is no significant difference in the mean SSTA change whether the event happened in association with the MJO or not, for any of the equatorial WWE types. When the eastern equatorial Pacific SST is warmer than normal, the mean SSTA change following MJO related WWEs is nominally larger than that following non-MJO WWEs, yet the difference is not significant (The difference in the Type W scatter plot appears large, but is not significant due to the small number of realizations). When the eastern equatorial Pacific SST is close to normal the mean SSTA change following non-MJO WWEs is nominally larger than that following MJO related WWEs, yet the difference is not significantly different from zero at the 95% confidence level. As far as warming of SST and maintenance of warm SST in the eastern Pacific during El Niño, MJO related WWEs are no different than non-MJO WWEs.

IV.6. WWE/Tropical Cyclone co-occurrence.

In this section, relationships between tropical cyclone activity and WWEs are explored. The co-occurrence statistics between WWEs and tropical cyclones in the respective regions of interest (as defined in Section 2 and Table IV.2) are summarized in Tables IV.5 and IV.6. Table IV.5 lists, for each WWE type, and for each NIÑO3 SSTA state: the percentage of WWEs for which a tropical cyclone is in the region of interest during the lifetime of the WWE, and the number of tropical cyclones in each region of interest. Table IV.6 lists, for each WWE type, and for each NIÑO3 SSTA state, the percentage of those cyclones which occurred during the lifetime of a WWE.

From the all event statistics in Table IV.5, one can see that this relationship between tropical cyclones and WWEs is strongest for the westernmost WWE types (NW and W), and weakest for the easternmost WWE types (NE, E and SE). Moreover, for the Type NE WWE the co-occurrence with tropical cyclones is not statistically significant even at the 90% confidence level. The relationship is *characteristic* (as defined in Section 2) for westernmost WWE types (NW and W); these statistics are consistent with the strong evidence for such a relationship in the surface wind and OLR composites. A majority (>60%) of the WWEs of each of the three types which are just west of the dateline (N, C and S) have

Table 5: Percentage of WWEs with a tropical cyclone in their respective region of interest during the lifetime of the WWE. The regions of interest are defined in Table 2. The statistics are broken down by NIÑO3 SSTA state on Day(-20) of the WWE.

WWE Type	Percentage of WWEs co-occurring with a Tropical Cyclone			
	All Time	Case Warm (NIÑ03 > 0.75°C)	Case Regular (|NIÑ03| ≤ 0.75°C)	Case Cool (NIÑ03 < -0.75°C)
NW	86%	94%	88%	50%
N	62%	67%	65%	
NE	5%	9%		
W	90%	91%	90%	N/A
C	61%	62%	61%	N/A
E	26%	10%	35%	N/A
S	60%	68%	50%	80%
SE	38%	53%	21%	40%

a tropical cyclone occurring during the event lifetime. Even though the Type E and SE WWEs have a statistically significant relationship with tropical cyclones (at the 95% level), neither of these types has more WWEs occurring with cyclones than without.

Examining each NIÑO3 SSTA state separately in Table IV.5 and testing at the 95% confidence level, the percentage of WWEs associated with cyclones when NIÑO3 SST is close to normal is not significantly different than that when NIÑO3 SST is warmer than normal for the Type NW, N, W and C WWEs. For Types S and SE, there is a significantly greater number of WWEs associated with cyclones when NIÑO3 SST is warmer than normal than when it is close to normal. The WARM state enhanced relationship between cyclones and WWEs is especially prominent for the Type SE WWE, where a majority of case WARM events are associated with cyclones. For the Type E WWE more events occur when NIÑO3 SST is close to normal than when it is warmer than normal; despite the fact that most cyclones in the Type E region of interest occur when NIÑO3 SSTA is warmer than normal. Again, due to the small number of realizations when the eastern Pacific is cooler than normal, the statistics are not significant.

I now examine the number of tropical cyclones which have a WWE related to them. These statistics indicate that, while WWEs are associated with cyclones, the converse is not true. Table IV.6 shows that generally only 34-37% of tropical cyclones occur during a WWE (Type W has 20% and Type S has 43%; the Type NE statistics are not significant at the 95% level). These statistics are all significant at the 95% confidence level (except for Type NE), but in no region do a majority of cyclones co-occur with WWEs. When only cyclones of larger intensity are considered, the statistics for some WWE types become stronger: 54% of Typhoons (out of 46) and 58% of Category 2 Typhoons (out of 26) in the Type C region of interest occur during the lifetime of a Type C WWE, and 50% of Category 2 Hurricanes (out of 12) in the Type SE region of interest occur during the lifetime of a Type SE WWE. However, neither of these statistics gives an overwhelming percentage of cyclones (or ty-

phoons/hurricanes) co-occurring with WWEs. When the different NIÑO3 states are examined separately one finds that most WWE types have a higher cyclones/WWE co-occurrence when the eastern Pacific is warmer than normal that when it is cooler than normal; the exception being Type W event.

Occurring with a cyclone is a characteristic feature of the Type NW and W WWEs. However, most cyclones in the Type NW and W regions of interest are not associated with a WWE. Most west-of-dateline WWEs are associated with cyclone formation, and very few east-of-dateline WWEs are associated with cyclone formation. The WWE-cyclone association for west-of-dateline WWEs is stronger than the WWE-MJO association. For east-of-dateline WWEs the WWE-MJO association is as strong or stronger than the WWE-cyclone association.

IV.7. Summary and Discussion.

In this chapter I computed the surface wind and convective structures associated with the MJO (Section IV.3.a) and WWEs (Section IV.3.b), described statistical relationships which WWEs exhibit with the MJO and tropical cyclones, and examined the inter-WWE spacing statistics for the period 1986-1998. WWEs are generally convective events

Table 6: Characteristics of the cyclones which occurr in the regions of interest of each WWE type. Columns 2 through 5 list the percentage of tropical cyclones in each region of interest which co-occurr with the respective WWE type.

WWE Type	Percentage of Tropical Cyclones co-occurring with a WWE			
	All Time	Case Warm (NIÑ03 > 0.75°C)	Case Regular (|NIÑ03| ≤ 0.75°C)	Case Cool (NIÑ03 < −0.75°C)
NW	37%	47%	36%	13%
N	35%	58%	25%	
NE	13%		17%	
W	20%	20%	21%	15%
C	34%	51%	27%	
E	34%	53%	10%	
S	43%	43%	42%	75%
SE	37%	57%	21%	25%

which do not show much similarity to any individual convective mode of variability. The northwestern-most WWE Types (NW, N and W) are associated with tight convective structures suggestive of a tropical cyclone. Southern hemisphere WWEs are associated with eastward propagating convection near the main wind anomalies. Type C and E WWEs are associated with enhanced convection near the main equatorial westerly anomlies. The MJO is associated with equatorial surface wind anomalies across the entire tropical Pacific. WWEs appear to be modulated by the MJO; west-of-dateline WWEs show a stronger association with tropical cyclone activity than with the MJO.

I computed the convective and surface wind anomaly fields associated with the MJO using a compositing technique based on the Maloney and Hartmann (1998, MH98) MJO identification scheme (see Section IV.3.a). The convective structures identified by this compositing technique very much resemble those previously described in the literature in association with the MJO (*e.g.* Madden and Julian 1994, Rui and Wang 1994, Hendon and Salby 1994): there is an eastward propagating couplet of reduced and enhanced convection over the Indian Ocean and the western Pacific warm pool region. The convective structures propagate eastward at an average speed of ~5 ms^{-1} (based on the mean 5 day Phase length), which is in agreement with previous estimates (Madden and Julian 1994, Rui and Wang 1994, Hendon and Salby 1994). The agreement of the tropospheric circulation patterns described by MH98 and the convective structures described here, with the circulation and convective structures described in previous work gives confidence that the surface wind structures evaluated in the composite are representative of the MJO related surface wind variability.

The surface wind anomaly fields in the MJO composite (Figures IV.3-.5) do not much resemble recent idealizations of the MJO related surface wind variability over the tropical Pacific (Kessler *et al.* 1995, Kessler and Kleeman 2000). Kessler *et al.* (1995) and Kessler and Kleeman (2000) idealize the MJO surface expression based on the observed

convective variability associated with the MJO, which tends to be confined to the warm pool of the western Pacific Ocean. I find that near-equatorial Pacific surface wind anomalies extend beyond the western Pacific warm pool into the central and eastern Pacific. The amplitude of the eastern Pacific variability is smaller than that in the western Pacific, but since the eastern/central equatorial Pacific is dominated by strong and persistent easterly trade winds, the central/eastern Pacific momentum flux (surface stress) might not be negligible. I explore the equatorial Pacific SSTA variability driven by the composite MJO in an OGCM in Chapter V.

The relationship between most WWEs and the MJO appears to be that of the MJO modulating the occurrence of the WWEs within an MJO. For each WWE Type there I am able to define "WWE-rich" phases of the MJO, wherein the number of WWEs occurring is statistically significant, for only one WWE type do the majority of events occur in the "WWE-rich" Phases of the MJO (51% for the Type W WWE). However, one can also define a set of "WWE-poor" Phases of the MJO within which the number of WWEs occurring is significantly lower than expected, these Phases correspond to the convectively suppressed Phases of the MJO. These relationships are not surprising, since WWEs are associated with atmospheric convection (Section 3, Meehl *et al.*, 1995, Kiladis *et al.* 1994), the reduction and enhancement of convection associated with the MJO should be expected to modify WWE distribution. For most WWE Types the convective variability related to the MJO redistributes the probability distribution of WWEs towards the convectively active Phases and away from the convectively suppressed Phases.

There is a weakly significant idication (at the 90% level only) that relationship between Type W WWEs and the MJO is such that MJOs appear to enhance the occurrence of WWEs. This relationship might be due to the enhanced tropical cyclone activity related to the MJO (Liebmann *et al.* 1994), due to an enhancement of westerly wind variability related to the MJO directly, or is might be spurious. Note that the statistical significance of the

relationship between the MJO and Type W WWEs is not robust due to the small number of WWEs, having one more event occurring in the absence of the MJO would reduce the confidence below the 90% level. As the datasets expand in the future, the nature of the statistical relationship should be re-examined.

In examining the NIÑO3 SSTA changes following the MJO, I find that in the absence of equatorial WWEs there is no significant warming (or warm SSTA maintenance) following the MJO (see Figure IV.20). Following MJO events with equatorial WWEs, there is a tendency for NIÑO3 SSTA warming (or warm SSTA maintenance) of a similar character to that following equatorial WWEs (see Figure IV.21). Also, the expected NIÑO3 SSTA changes following equatorial WWEs are independent of their relationship to the MJO (see Figure IV.21). In Chapter V I examine OGCM response to composite MJO and WWE forcing to explore the dynamical aspects of Pacific waveguide SSTA changes following the MJO and WWEs.

In Chapter III and VH00, it was shown that equatorial WWEs are associated with the onset and maintenance of El Niño warming; the global MJO has no significant relationship with El Niño (see Figure IV.2, Table IV.1, Slingo *et al.* 1999, Hendon *et al.* 2000, Harrison and Vecchi 2000). The expected NIÑO3 SSTA changes following equatorial WWEs are independent of whether the WWEs occurred with an MJO or not (see Figure IV.19). Since WWEs are strongly associated with El Niño warming and mechanisms based on the observed surface wind structure of WWEs have been suggested to explain that link (Harrison and Giese 1988, Giese and Harrison 1990,1991, Chapter V), since the MJO shows no significant relation to El Niño, and since WWEs are related to NIÑO3 SSTA warming independent of the relation to the MJO: the connection between surface warming and WWEs seems stronger than with the MJO.

Examining the convective structures associated with WWEs (Section IV.3.b), I find that WWEs are generally associated with convection during the lifetime of the event. The

convective and wind structures of the western-most WWE Types (NW and W) are suggestive of a strong link between these events Types and tropical cyclone activity. This suggested association is confirmed in the WWE/cyclone co-occurrence statistics described in Section IV.6. Over 90% of Type NW and W WWEs are associated with tropical cyclone activity. Further, the relationship between west-of-dateline WWEs and tropical cyclone activity is always stronger than that between the MJO of WWEs.

WWEs and MJOs represent different aspects of tropical Pacific atmospheric variability, both with strong signals in atmospheric convection. The MJO appears to modulate the occurrence of WWEs in the intra-seasonal time-scale; however, the eastern Pacific SSTA changes following equatorial WWEs are independent of their relation to the MJO. Because WWEs are not related to any single atmospheric circulation phenomenon, and because WWEs are strongly linked with El Niño warming and maintenance, improved understanding and prediction of El Niño SSTA changes likely depends on better understanding and prediction of the entire range of atmospheric variability which brings about WWEs. This variability includes paired and individual tropical cyclones, the MJO, mid-latitude cold surges and convective superclusters.

Chapter V
Ocean response to sub-seasonal wind forcing

V.1 Introduction:

In this chapter, I use an OGCM to explore dynamical aspects of the ocean response to sub-seasonal surface wind variability. I examine the response of the central and eastern equatorial Pacific to the Type C WWE and to composite MJO forcing. I use these analyses to understand the dynamical connections which are the source of the statistical associations between SST variability and sub-seasonal wind variability.

In the previous chapters I described the typical surface wind structures associated with WWEs (Chapter II) and with the MJO (Chapter IV). I argued that WWEs and the MJO were distinct modes of variability (Chapter IV); and examined statistical relationships of the MJO and WWEs to El Niño. Equatorial WWEs are associated with warming at the onset of El Niño and warm anomaly maintenance during El Niño (Chapter III); there is no correlation between the MJO and El Niño indicators (Slingo *et al.* 1999, Hendon *et al.* 2000, Harrison and Vecchi 2000, Vecchi and Harrison 2000.b, Chapter IV).

I here attempt to reproduce the statistical associations of the MJO and WWEs to eastern Pacific SSTA, using an OGCM; I also examine the mechanisms responsible for those changes. I find that the composite MJO zonal stress anomalies do not drive central/ eastern equatorial Pacific waveguide warming in the model; the composite MJO does not provide a mechanism for waveguide warming during the onset of El Niño. I find that equatorial WWEs force eastern and central equatorial Pacific SSTA changes which resemble those observed in the composite (see Chapter III); WWEs are a mechanism for the onset of El Niño. I find that superimposing a composite Type C WWE on a composite MJO leads to eastern Pacific SST warming of a similar structure to that following the WWE.

Analyses of OGCM response to idealized WWE zonal wind anomalies have found

that WWE-driven circulation changes produce SST warming in the eastern and central Pacific equatorial waveguide (Harrison and Giese 1988, Giese and Harrison 1990, 1991), with SST changes as large as 0.5°C from a single WWE. Those experiments were performed using idealized WWEs with realistic meridional and time-scales, but the zonal scale was hypothetical; the experiments described in this chapter are done with realistic (x,y,t) scales.

Harrison and Giese (1988) found that while changes in the zonal surface current field tended to coincide with the first baroclinic Kelvin pulse, the SST changes in the eastern equatorial Pacific were dominated by the second baroclinic mode. An unexpected finding of Harrison and Giese (1988) was that anomalous meridional advection of heat has a dominant term in the eastern Pacific SST warming. It was suggested that modulation of the tropical instability wave (TIW) field by the WWE driven Kelvin pulses was a mechanism for the anomalous meridional advection.

It has been suggested that intra-seasonal surface wind variability in the western and central Pacific, driven by the MJO, may be important to the onset of waveguide SST warming during El Niño (Lau and Chan 1986, 1988, Lau and Shen 1988, Weickman 1991, Kessler *et al.* 1995, Moore and Kleeman 1999). Analysis of the potential role of the MJO on tropical Pacific SST have idealized the MJO surface wind variability as a sinusoid confined to the western equatorial Pacific (Kessler *et al.* 1995, Kessler and Kleeman 2000). In the previous Chapter, I argued that the surface wind variability associated with the MJO does not much resemble those idealized models; the near-equatorial surface wind anomalies extend across much of the central and eastern Pacific (see Section IV.3.a). In a recent description of the abrupt termination of the 1997-98 El Niño event, Takayabu *et al.* (1999) argue that easterly stresses driven by the MJO were responsible for the return to normal SST. I explore the potential role of the composite MJO in El Niño using the composite zonal stress anomaly fields and the OGCM.

In the following sections I describe the modeling work done to explore the role of

sub-seasonal variability in El Niño. Section 2 describes the model and the different experiments run. Section 3 discusses the results for the MJO experiments. Section 4 shows the results for the MJO experiment. Finally, Section 5 gives a summary and conclusions.

2. Data and Methods:

To explore to oceanic response to the composite zonal wind stress pattern, I use the NOAA primitive equation OGCM, which has been used in many studies of the tropical Pacific (Philander and Seigel 1985, Harrison and Giese 1988, Philander *et al.* 1987, Philander *et al.* 1989, Giese and Harrison 1991) and is the basis of NOAA's operational tropical Pacific Ocean analysis program (Ji *et al.* 1995). The model grid is an Arakawa-B grid, which spans the tropical Pacific from 130°E to 90°W (by 1° longitude) and 30°S to 50°N (by 1/3° from 10°S to 10°N, stretching to 2.3° at 30°S and 2.9° at 50°N); there are 27 levels in the vertical, with 10 m resolution in the upper 100 meters and stretching to 650m at 3800m depth. The model timestep is 3600 seconds (1 hour). The model topography includes realistic coastlines, but no bottom topography. Vertical mixing is parametrized using the Richardson number dependent scheme of Pacanowski and Philander (1981), with the background wind mixing parameter set at 10 cm^2s^{-1}, the maximum friction coefficient at 50 cm^2s^{-1}, the background mixing and diffusion are set at 1.0 cm^2s^{-1} and 0.1 cm^2s^{-1}, respectively. Horizontal mixing is parametrized as eddy diffusion, with momentum mixed using A_m of 1.0×10^7 cm^2s^{-1}, and heat diffused using A_h of 2.0×10^7 cm^2s^{-1}.

The model is spun up for five years using the annual mean climatological wind stress field of Harrison (1989), a sixth year is run as the control experiment. Surface heat flux is parametrized as in Harrison (1989), using the annual mean air temperature from the COADS climatology (Woodruff *et al.* 1987). Sea surface salinity is restored to the annual mean Levitus climatology using a 50 day restoring timescale. Figure V.1 shows the SST and wind-stress fields for the spin-up run, along with the annual mean SST from COADS.

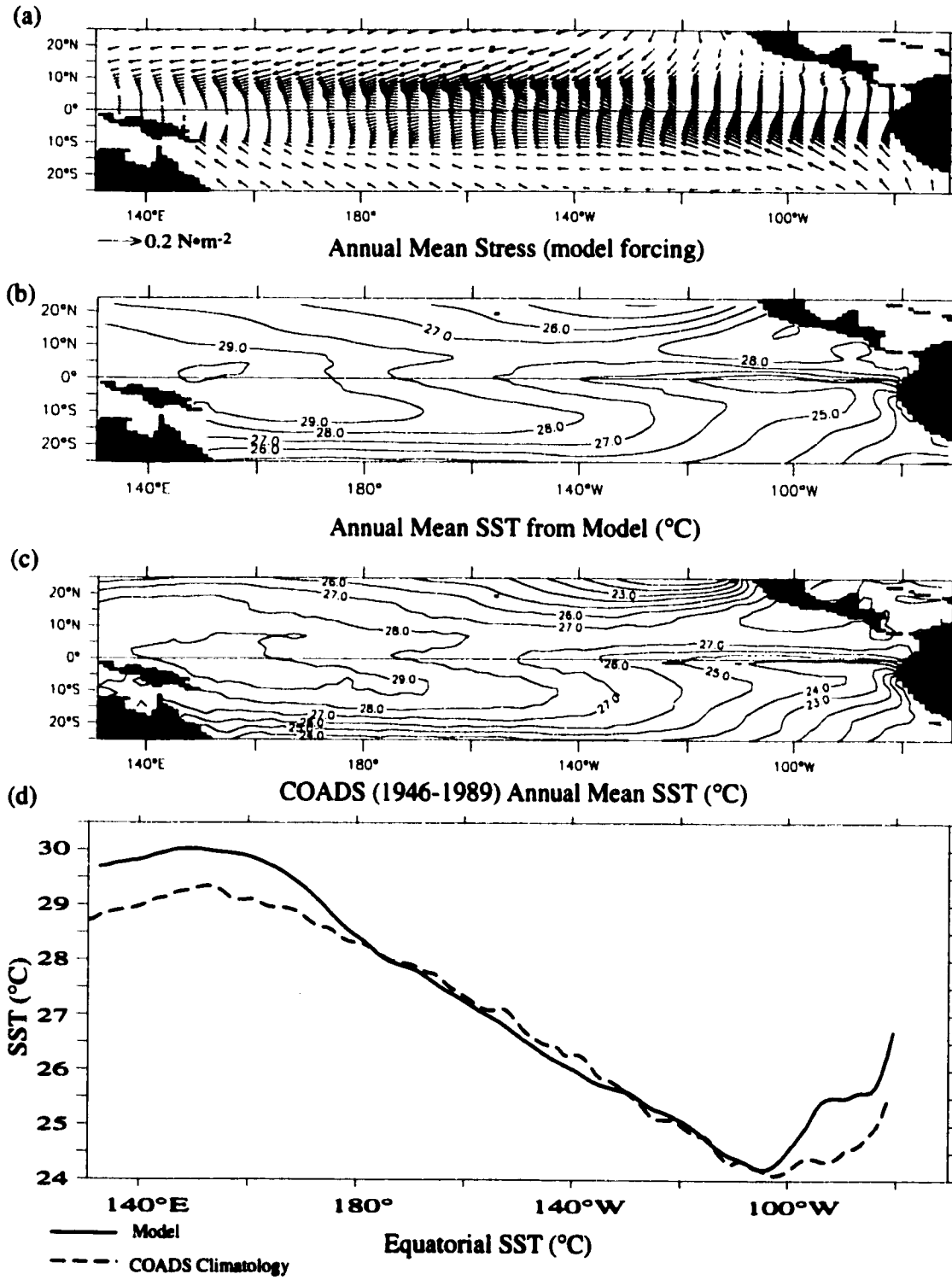

Figure V.1: (a) Annual mean surface wind stress used to initialize the model. (b) Annual mean SST from the OGCM. (c) Annual mean climatological SST. (d) Line plot of model and climatological SST along equatorial Pacific.

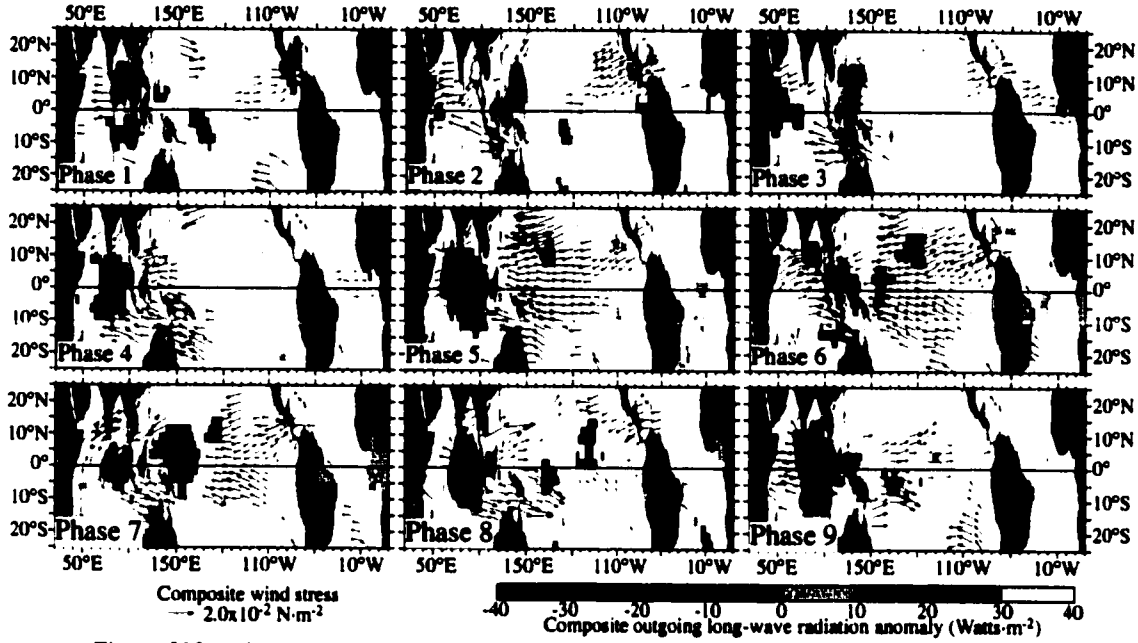

Figure V.2: All-event MJO composite surface wind stress and OLR anomalies for each of the 9 Phases defined by Maloney and Hartman (1998). Vectors show the compositestress values for which eitther the zonal or meridional component is significant at the 99% level. Shading indicates values of OLRA significant at the 99% confidence level.

Notice that the near equatorial SST in the central Pacific between 180° and 110°W is well reproduced by the model; while the negative zonal SST gradient between 160°E and 180° and the positive zonal SST gradient between 100°W and the coast are both too large in the model (Figure V.1.d). However, the SST gradients and current fields across most of the central and eastern Pacific, giving a realistic enough background state for these experiments.

The MJO experiments are forced by adding the 99% statistically significant all-event composite zonal stress anomaly field to the climatological stress field. The composite is evaluated as in Chapter IV, using the MJO list as defined using the Maloney and Hartmann (1998) MJO index, and the European Centre for Medium Range Weather Forecasts (ECMWF) 2.5°×2.5° gridded 12-hourly operational surface wind-stress analysis from 1986-1998 (ECMWF 1989). Anomalies were computed from a monthly climatology, 1986-1996. Figure V.2 shows a vector map of the 99% significant surface wind-stress fields associated with the MJO, and Figure V.3 shows a shaded plot of the evolution of the 99% significant

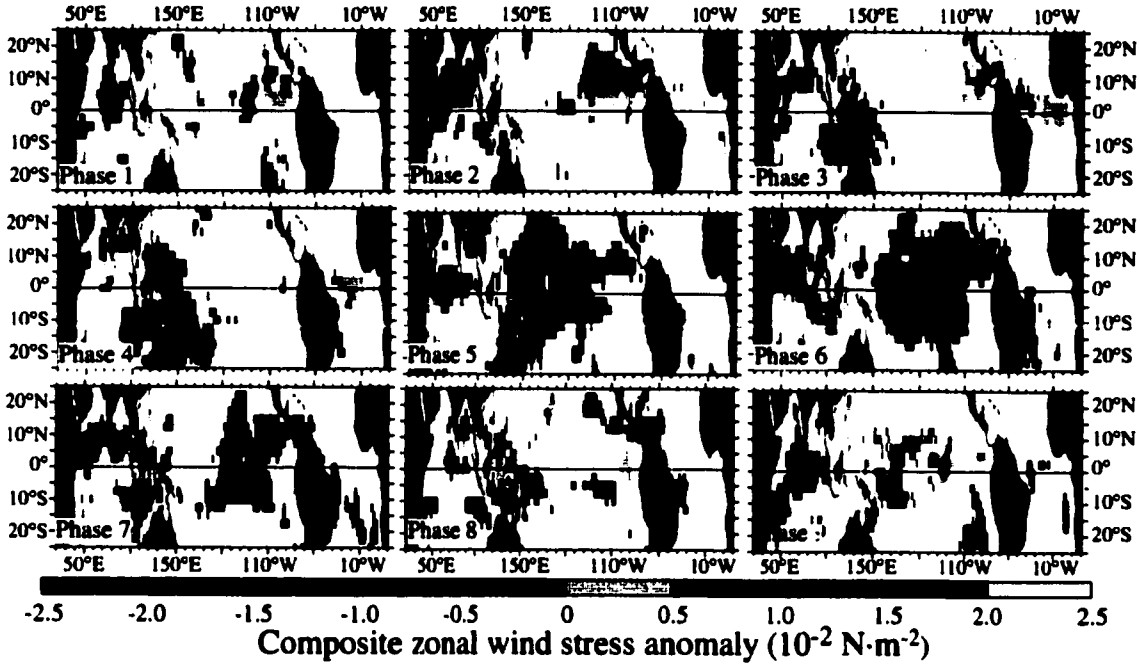

Figure V.3: Shaded plots of the evolution of the 99% significant all-event MJO composite zonal stress anomaly field. Only values for which the zonal stress anomaly is significantly different from zero at the 99% confidence level are shown.

zonal stress fields. Notice how, as in the MJO surface wind fields, the composite is dominated by easterly stress anomalies over the eastern and central Pacific. Through the lifetime of an MJO event, the western Pacific stress anomalies exhibit periods of both easterly and westerly stress.

Five MJO forcing experiments were performed (M1-M5), and are summarized in Table V.1; three examine the effect of a single MJO period on the tropical Pacific, and the fourth examines the effect of four sequential MJOs. The fifth experiment removes the mean

Table V.1: List of MJO experiments used in this Chapter.

Experiment #	*Anomalous surface zonal stress forcing used*
M1	*1 Period of 99% significant composite zonal stress anomaly.*
M2	*1 Period of 99% significant composite zonal stress anomaly west of 165°E, zero east of 165°E.*
M3	*1 Period of 99% significant composite zonal stress anomaly east of 165°E, zero west of 165°E.*
M4	*4 Periods of 99% significant composite zonal stress anomaly.*
M5	*4 Periods of 99% signficant composite zonal stress anomaly, with the mean over one MJO period removed.*

stresses associated with the MJO and examines the ocean response. For the experiments shown here each MJO Phase was taken to be 5 days long (using Phase lengths 7 and 10 days, or using 3 consecutive MJOs, did not affect the main results). To minimize transients, I begin each MJO on Phase 3 and run through Phase 2 - the Phases with smallest equatorial Pacific zonal stress associations (see Figure V.2 and V.3; starting the MJO on Phase 1 does not alter the main results).

To examine the response to the OGCM to Type C WWEs, I run a series of experiments using the Gaussian zonal stress anomaly model, with the scales described in Chapter II. The zonal *e*-folding scale is 18°, the meridional *e*-folding scale is 5° and the temporal *e*-folding scale is 3.5 days (see Table II.3). The composite Type C WWE stress has an amplitude near 0.06 $N \cdot m^{-2}$, I use three different amplitude WWEs to test the amplitude dependence of the solutions: 0.06 $N \cdot m^{-2}$, 0.1 $N \cdot m^{-2}$ and 0.2 $N \cdot m^{-2}$. Table V.2 summarizes the experiments run. Experiments C1 through C3 examine the effect of a single Type C WWE on the annual mean ocean; Experiments C4 through C6 examine the effect of multiple WWEs. Experiment CM explores the response of the Tropical Pacific to a Type C WWE superimposed on a composite MJO.

Table V.2: List of the Type C WWE experiments discussed in this Chapter.

Experiment #	*Anomalous surface zonal stress forcing used*
C1	*One Gaussian Type C WWE (0.06 $N \cdot m^{-2}$), centered on Jan-15.*
C2	*One Gaussian Type C WWE (0.1 $N \cdot m^{-2}$), centered on Jan-15.*
C3	*One Gaussian Type C WWE (0.2 $N \cdot m^{-2}$), centered on Jan-15.*
C4	*Three Gaussian Type C WWEs (0.06 $N \cdot m^{-2}$), centered on Jan-15, Feb-4, and Feb-24.*
C5	*Three Gaussian Type C WWEs (0.1 $N \cdot m^{-2}$), centered on Jan-15, Feb-4, and Feb 24.*
C6	*Three Gaussian Type C WWEs (0.2 $N \cdot m^{-2}$), centered on Jan-15, Feb-4 and Feb-24.*
C7	*Type C WWEs (0.1 $N \cdot m^{-2}$), every 20 days starting on Jan-15 and continuing through run.*
CM	*One Composite MJO + 1 Type C (0.06 $N \cdot m^{-2}$) WWE centered on Phase 6 of the MJO.*

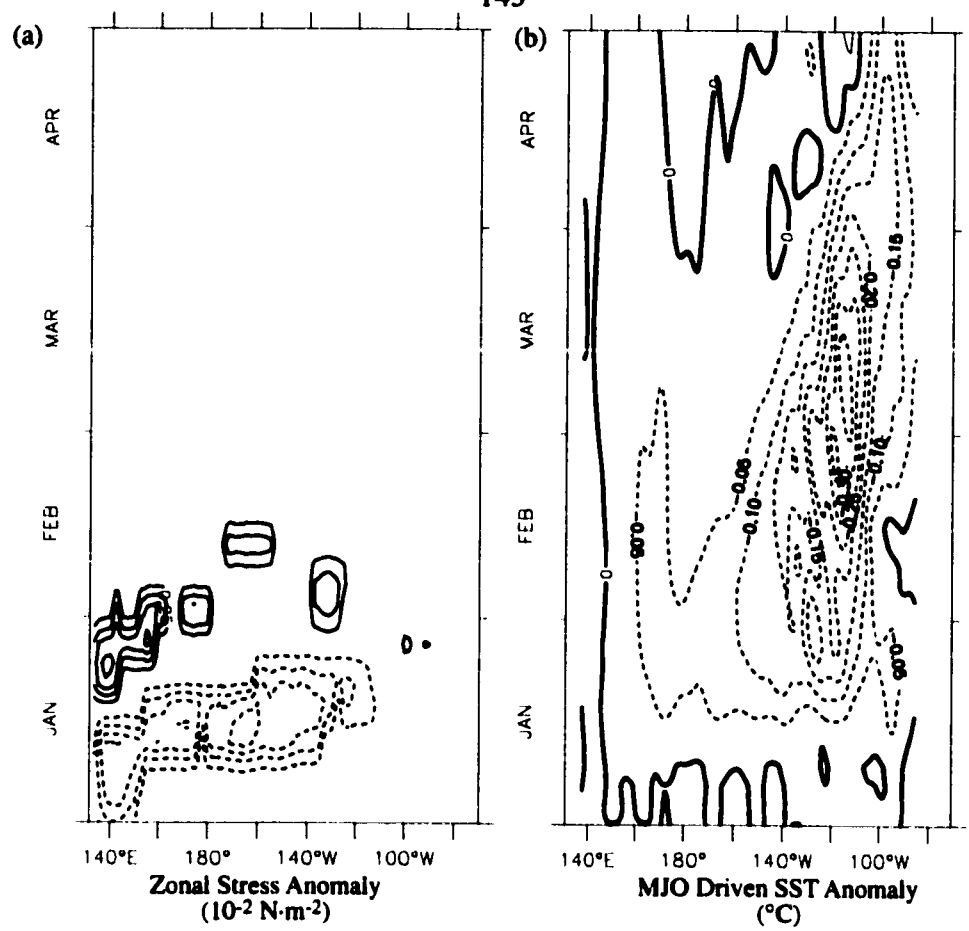

Figure V.4: (a) Zonal stress anomaly at the equator from Experiment M1. Contour interval is 0.25×10^{-2} NÆm (b) MJO-driven SSTA along the equator, from Experiment M1. Notice how the composite MJO drives central and eastern Pacific surface cooling during and following the wind anomalies. SSTA is zonally smoothed with an 11° cosine filter in longitude to remove TIWs. Contour interval is 0.05°C.

3. Ocean Response to the MJO:

Because easterly stress anomalies are very effective at cooling local SST by horizontal and vertical advection, and because the MJO-related easterly stress anomalies exceed the westerly stress anomalies in space and intensity, one should expect the MJO composite zonal wind-stress anomaly to cool the equatorial Pacific. The OGCM results confirm that expectation. The response of the equatorial Pacific SSTA to a single period of composite MJO zonal stress anomaly (Experiment M1) is shown in Figure V.4. As expected from the composite zonal stress fields, the surface of the eastern and central Pacific weakly cools

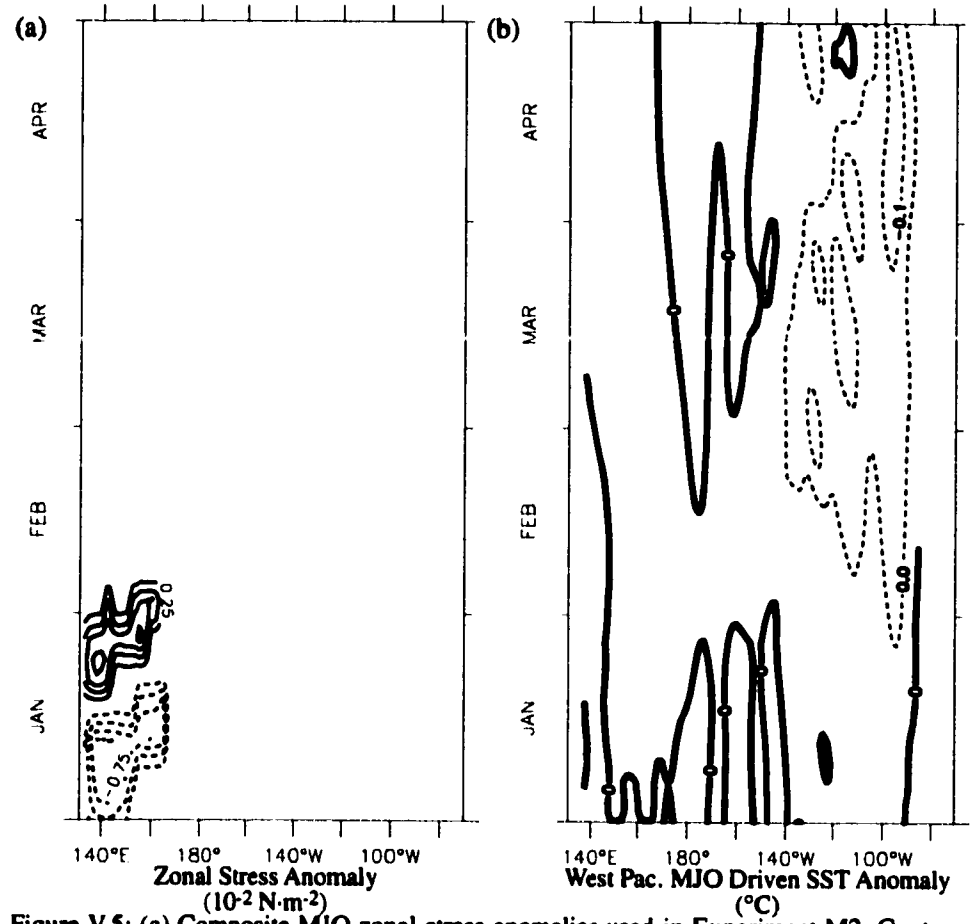

Figure V.5: (a) Composite MJO zonal stress anomalies used in Experiment M2. Contour interval is 0.25×10^{-2} N/m^2. (b) SSTA deiven by the western Pacific part of the MJO zonal wind stress forcing (Experiment M2). SSTA is zonally smoothed with an 11° cosine filter in longitude to remove TIWs. Contour interval is 0.05°C.

during the lifetime of the MJO. There is also weak warming following the event, which does not exceed 0.1°C. The cooling occurs during the MJO Phases with easterly stress anomalies over the eastern and central Pacific (Phases 5-7) under the stress anomalies. The cooling enhances in the eastern Pacific (between 140°W and 100°W) in the month that follows the anomalous forcing, and then begins to disappear.

To parse the effects of the near-sinusoidal western Pacific stress anomaly fields, and the easterly stress surge in the central and eastern Pacific, I ran experiments M2 and M3. Experiment M2 is run with only the western Pacific zonal stress anomaly field (west of 170°E), while M3 is run with only the eastern Pacific zonal stress anomaly field (east of 170°W). The SST changes driven by the western Pacific part of the MJO anomalies are

shown in Figure V.5, and Figure V.6 shows the response to the central and eastern Pacific part of the MJO. The response to the entire MJO forcing resembles a superposition of the response to the western Pacific forcing and the eastern Pacific forcing, since the magnitude of the stress anomalies is small, the linear character of the response is not unexpected.

The western Pacific part of the MJO zonal stress anomaly forcing drives weak eastern Pacific SST cooling (Figure V.5). The cooling in the far eastern Pacific is weak (less than 0.1°C) and begins about 30 days after the beginning of the anomalous zonal stress in the western Pacific. The SSTA cooling driven by the western Pacific zonal stress anomalies accounts for approximately one third the far eastern Pacific cooling; the western Pacific zonal stress anomalies have little effect on the central Pacific SST. It must be noted that the zonal SST gradients in the region of largest west-Pacific-MJO SST response (the far-eastern Pacific) are overestimated in the background state when compared with COADS climatology (see Figure V.1). The response of the model ocean to the western Pacific part of the MJO is likely overestimated due to this.

The equatorial SSTA driven by the central and eastern Pacific part of the MJO zonal stress anomaly field is dominated by cooling through the event (Figure V.6). There is very little western Pacific SSTA associated with the stress anomalies from Experiment M3, the main changes occur underneath and to the east of the easterly surge. The cooling begins across the central and eastern part of the basin upon the arrival of the easterly stress anomalies, A front develops and moves east over the months following the forcing, with cooled SST to the east of it, and normal SST to the west of it. The front reaches the far eastern Pacific by mid-April, about two and a half months after the end of the easterly anomalies. The central and eastern Pacific part of the MJO forcing is responsible for practically all the cooling in the central part of the basin (between 165°E and 140°W), and about two thirds of the surface cooling east of 140°W.

Because the effect of one MJO event is to cool the eastern Pacific SST with weak

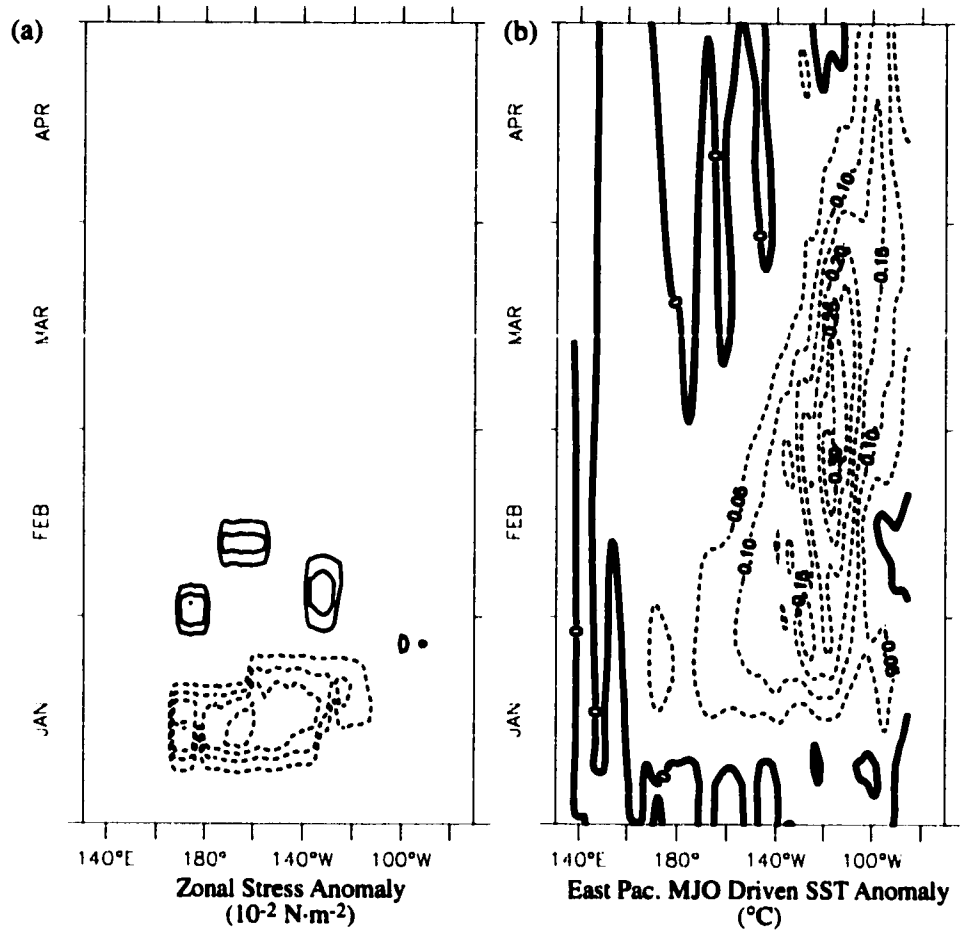

Figure V.6: (a) zonal stress anomalies used in Exp M3. Contour interval is 0.25×10^{-2} N/m^2. (b) SSTA deiven by the central and eastern Pacific part of the MJO zonal wind stress forcing (Experiment M3). SSTA is zonally smoothed with an 11° cosine filter in longitude to remove TIWs. Contour interval is 0.05°C.

warming following the event, I expect a sequence of MJO events to lead to cooling of the eastern equatorial Pacific. The OGCM confirms this expectation, Figure V.7 shows the SSTA result of forcing with four consecutive cycles of the MJO composite zonal wind stress anomalies (smoothed in longitude with an 11° cosine filter to remove tropical instability waves). Cooling prevails over the central and eastern equatorial Pacific during the period in which MJO forcing was imposed. Subsequent to the MJO forcing interval very weak central or eastern Pacific warming occurs which does not extend across any large band of the Pacific. Rather than warm the eastern equatorial Pacific, as has been suggested recently, the effect of a sequence of composite MJO events is to weakly cool the surface of

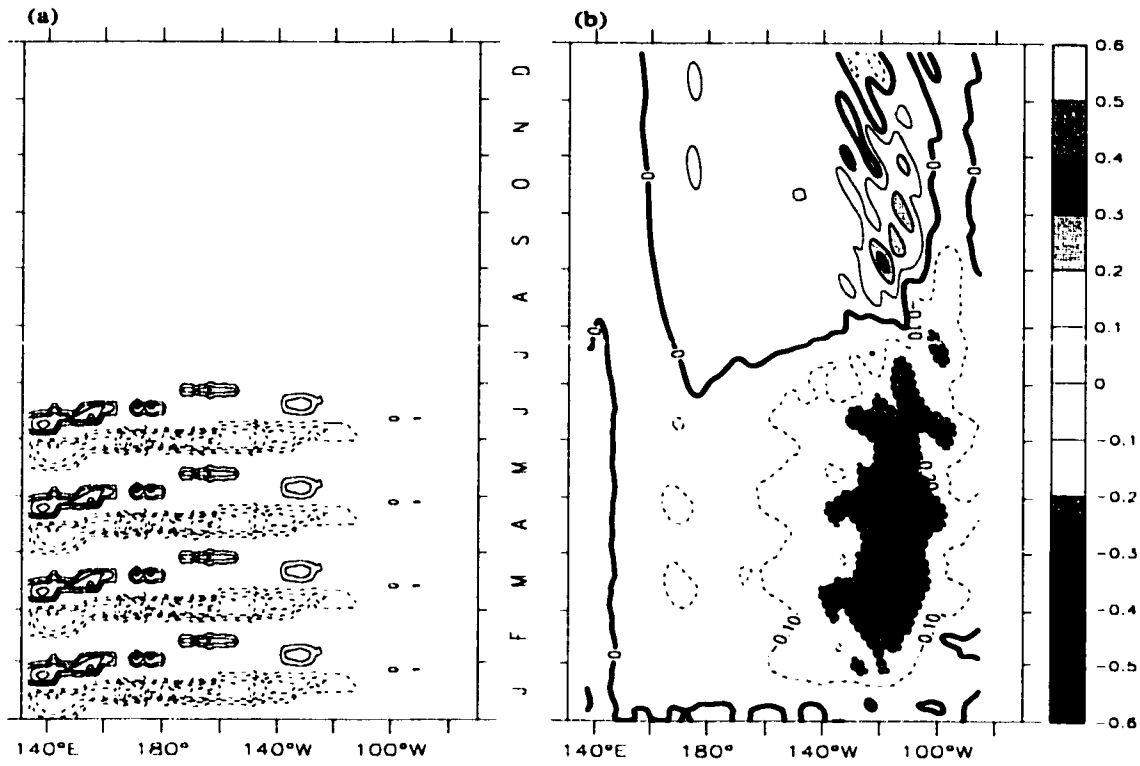

Figure V.7: (a) Four periods of composite MJO surface zonal stress anomaly forcing (Experiment M4). Contour interval is 0.25×10^{-2} N/m^2. (b) SSTA response to the four periods of composite MJO surface zonal stress anomaly forcing. SSTA is zonally smoothed with an 11° cosine filter in longitude to remove TIWs.

the eastern equatorial Pacific.

The mean equatorial easterlies in the central and eastern Pacific, which appear in the MJO composite are possibly an artifact of the MJO compositing technique or the climatoloy used. It is important to consider the effect of the MJO composite zonal stress fields which do not have a net momentum flux into the eastern and central equatorial Pacific. Experiment M5 examines the effect of driving the OGCM with four cycles of the MJO composite zonal stress, with its mean subtracted. Figure V.8 shows the SSTA and the zonal stress anomalies from experiment M5. These should be contrasted with those shown in Figure V.7. Notice how the SSTA changes in the eastern and central Pacific in the presence of the MJO anomalies is still not for warming; there is very weak cooling in the eastern and central equatorial Pacific. Following the MJO forcing there is some weak warming in the central Pacific. This warming is localized, and is associated with the termination of the

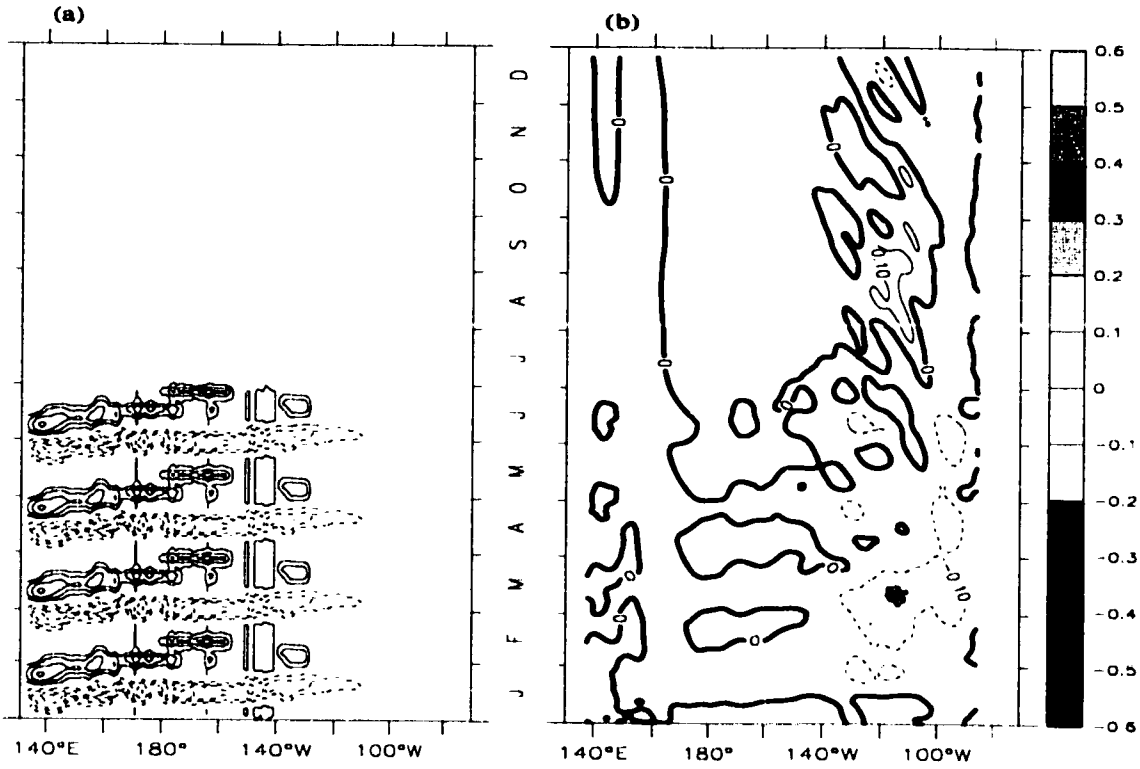

Figure V.8: (a) Four periods of composite MJO surface zonal stress anomaly forcing with the mean over an MJO removed (Experiment M5). Contour interval is 0.25×10^{-2} N/m^2. (b) SSTA response to the four periods of composite MJO surface zonal stress anomaly forcing. SSTA is zonally smoothed with an 11° cosine filter in longitude to remove TIWs.

MJO forcing. Even with the mean eastern and central equatorial Pacific easterlies removed, the composite MJO suraface zonal stress anomalies do not drive warming in the model.

Figure V.9 shows the thermocline anomalies, approximated as the depth of the 20°C isotherm, driven by the four period composite MJO zonal stress anomalies (Experiment M4). Notice how during the period of anomalous forcing (January through June) the western and central Pacific thermocline anomaly evolution is dominated by a series of eastward propagating pulses of alternating shoaling and deepening. Meanwhile, the eastern Pacific thermocline is dominated by a shoaling through the forcing period, with slight variability at the period of the MJO. West of 140°W, the SSTA changes driven by the MJO are not a direct representation of the MJO driven thermocline changes; while the MJO driven thermocline changes are primarily oscillatory, the SSTA is dominated by cooling with a superimposed oscillation. In the eastern Pacific, the SSTA and thermocline depth anomaly patterns corre-

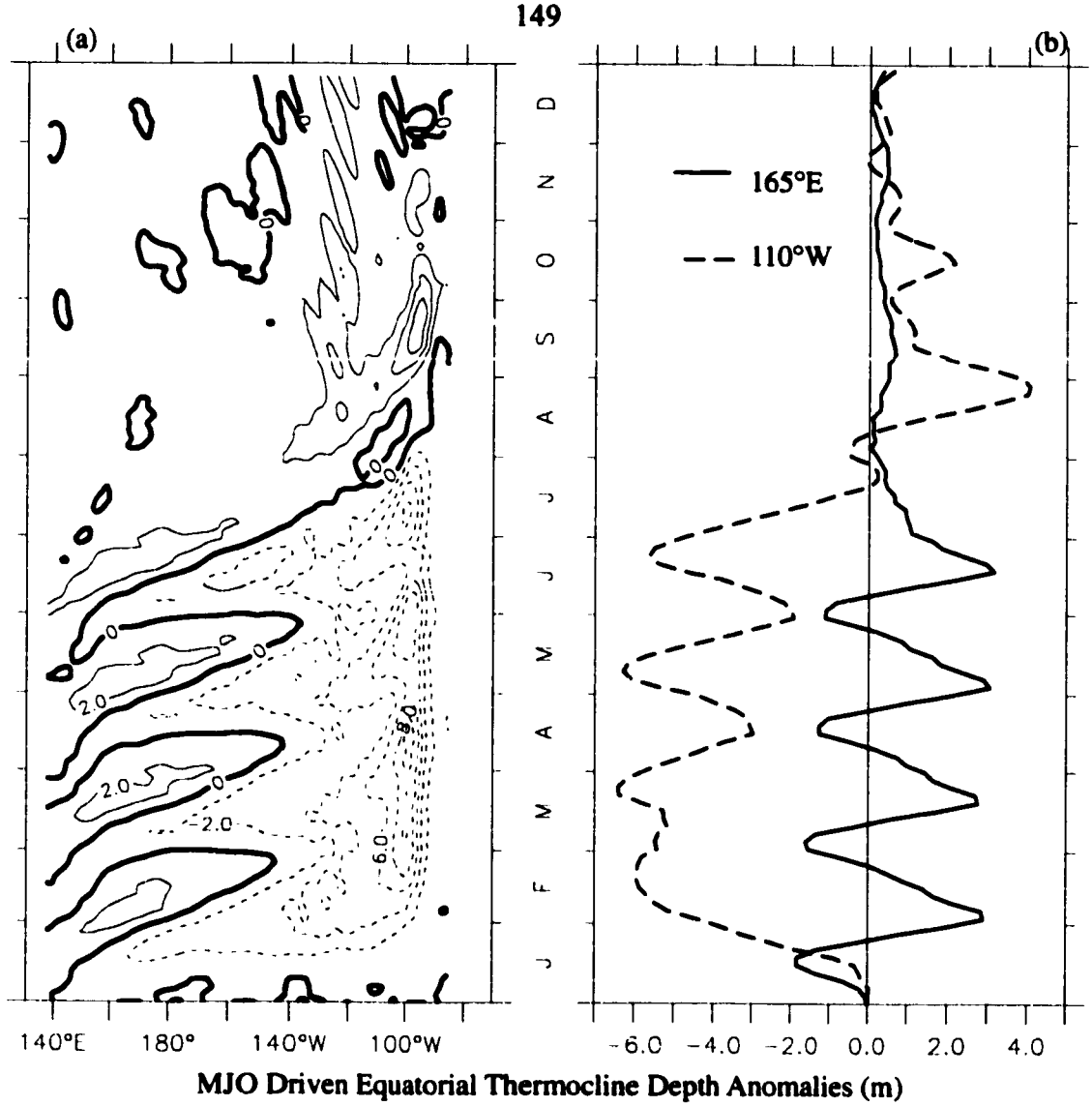

Figure V.9: (a) Time-longitude contour plot of the 15° cosine smoothed (in longitude - to remove TIWs) equatorial thermocline depth anomaly driven by four consecutive MJOs (Experiment M4). Contour interval is 2 meters. (b) Time-series of the 15° cosine smoothed thermocline depth anomalies at (165°E,0°) and (110°W,0°).

spond more closely. Following the final MJO event in the series there is a pulse of thermocline deepening which propagates east across the basin. These relationships between SSTA and thermocline depth anomalies are consistent with the long-term SSTA/thermocline depth anomaly correlations, which show that only in the eastern Pacific there are statistically significant correlations between SSTA and thermocline depth anomaly (see Harrison and Vecchi 2000). The arrival of the pulse of downwelling corresponds with the return of SST to normal in the eastern Pacific.

4. Ocean Response to Type C WWEs:

I now examine the response of the OGCM to the Type C WWE forcing experiments. First I attempt to reproduce the SSTA changes which appear in the Type C WWE composite (see Section III.3). I then examine the mechanisms responsible for the SSTA changes in the model.

a. Comparison to Data:

The composite SSTA changes following Type C WWEs were dominated by warming of the eastern and central equatorial Pacific, and by weak cooling along the western edge of the WWE (see Chapter III). The OGCM forced with the idealized (using realistic scales) zonal stress anomaly fields for the Type C WWE reproduce many of the characteristics of the composite SSTA change fields. Figure V.10 shows the composite SSTA change 60 days after the WWE center date for Experiments C1,C2 and C3, and from the Case REGULAR Type C composite. Model data are smoothed with a 30-day boxcar filter to remove TIWs.

The structure of the model SST changes agree with the composite structures in the region 160°W to 100°W, with the amplitude being best reproduced by Experiment C3. The model warming in the central Pacific is concentrated east of 160°W, as in the composite. The model gives weak warming in the far eastern Pacific and along the coast of South America, consistent with the compositing results.

The main qualitative differences are west of the Dateline and east of 100°W, where the initial model SST gradients were larger than climatology. The model zonal SST gradient between 160°E and the Dateline is about twice climatology; if the anomalous zonal advection term in that area is halved (after the model is run) and the temperature tendency is recomputed, there is no equatorial warming west of the Dateline. Similarly, if the zonal SST gradient east of 100°W is artificially reduced after the model is run, the warming in the far-

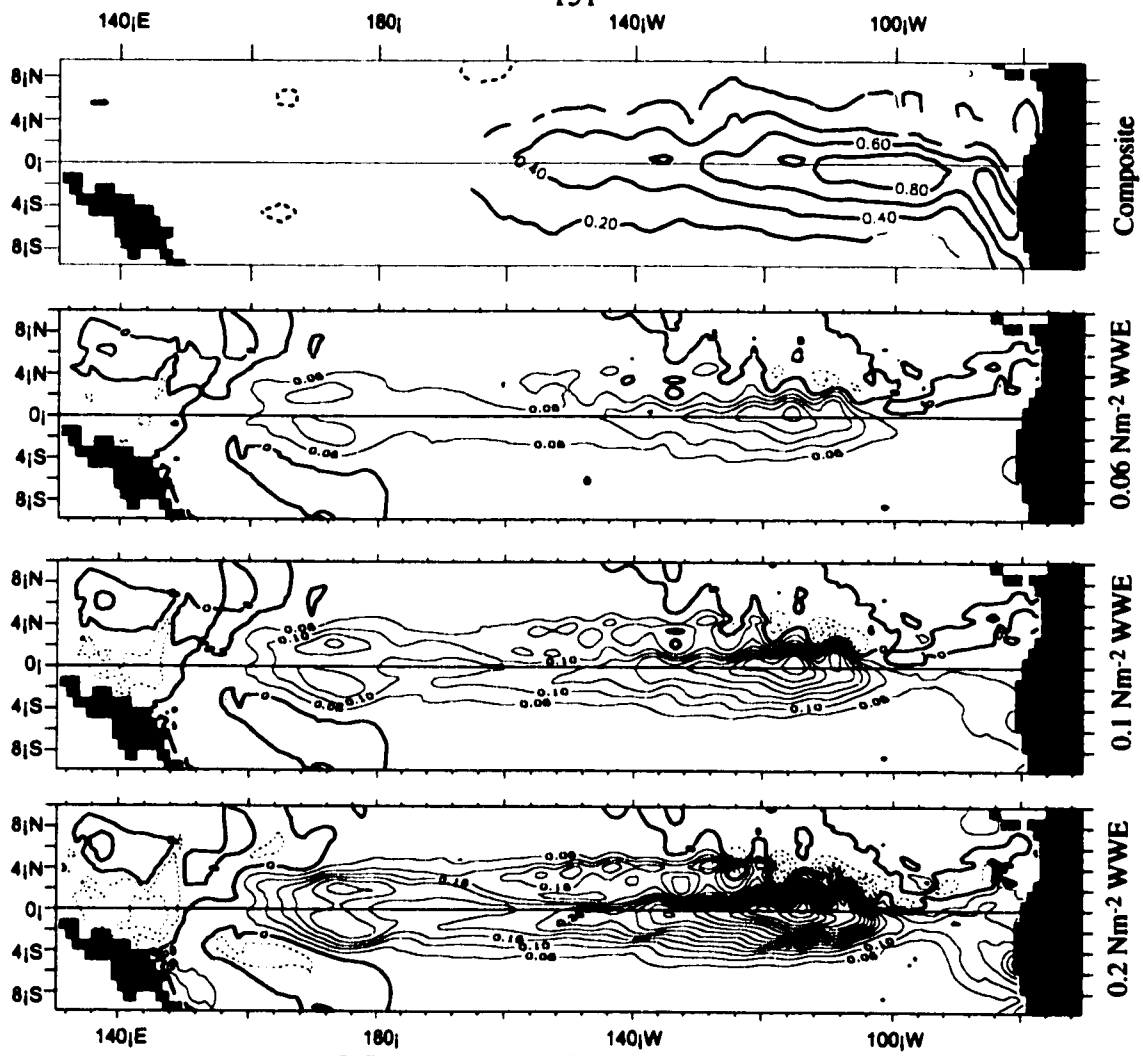

Figure V.10: SSTA Change 60 days after a Type C WWE from: (a) the 95% signficant ΔSSTA composite (contour interval 0.2°C), (b) Experiment C1 (countour interval 0.05°C), (c) Experiment C2 (contour interval 0.05°C), and (d) Experiment C3 (contour interval 0.05°C). Notice that the composite structure and the model structure are qualitatively similar in the region 165°W-100°W, where the initial conditions have a realistic zonal SST gradient.

eastern Pacific is increased to levels comparable to that near 110°W. The model reproduces the characteristics of the composite warming, within the limits of the model initial conditions.

A process which the model lacks, and could help explain some of the differences from observations, is coupling between the WWE driven SSTA response and the eastern and central Pacific surface stress fields and responsive clouds. ENSO is a coupled phenomenon characterized be wind and temperature changes across the basin (Rasmusson and Car-

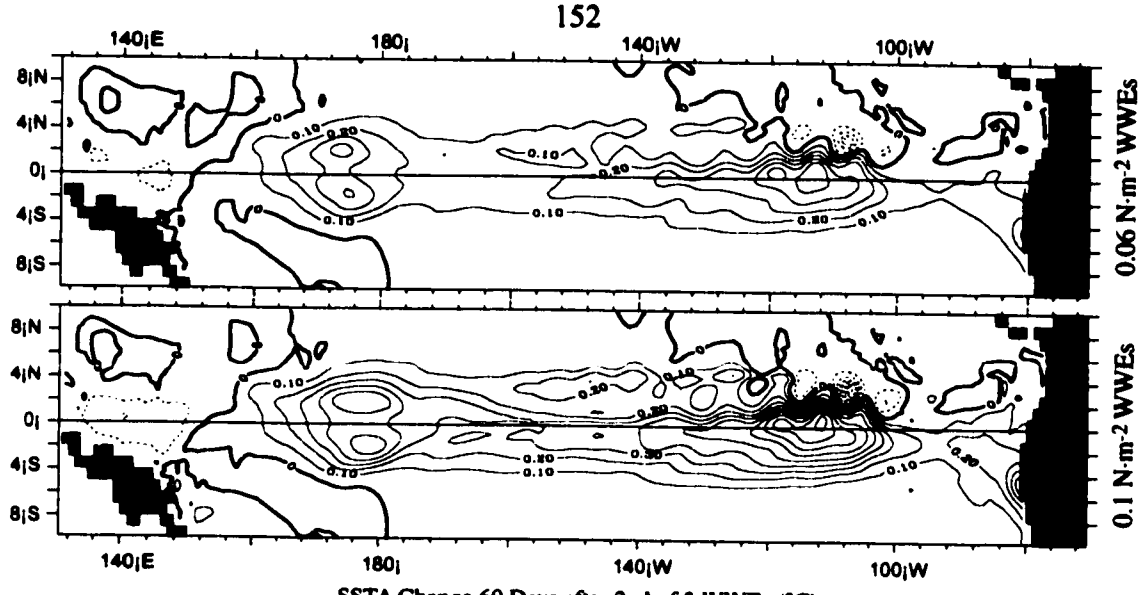

Figure V.11: SSTA Changes 60 Days after the seond event in a series of three events, for (a) Experiment C4, and (b) Experiment C5. Contour interval is 0.1°C. Notice how the warming along the coast of South America is more prominent, and the amplitude of the changes has increased, relative the single-WWE experiments. (Figure V.9)

penter 1982, Harrison and Larkin 1996, 1998.a), as well as changes in incoming solar radiation due to changes in stratus clous (Klein and Hartmann 1993). These experiments, with their prescribed eastern Pacific winds and clouds, will be unable to capture any coupling. This coupling would tend to produce enhancement of the of the warming through reduction of the intensity of the easterly equatorial trade winds, and the upwelling and vertical mixing driven by them. Also reduced by warming of the eastern equatorial Pacific is the stratus cloud coverage (Klein and Hartmann 1993), which would tend to enhance warming by allowing more incoming solar radiation to reach the far eastern Pacific.

In Section IV.4, it was noted that WWEs often occurred less than 40 days apart. Experiments C4-7 examine the effect of sequencing WWEs. The result is increased warming following each WWE. Also, for each WWE after the first, the warming along the coast of South America is enhanced relative the single event results. Figure V.10 shows the SSTA changes 60 days after the second of three WWEs for Experiments C4 and C5.

Sequencing the WWEs increases the anomalies changes after each WWE, and changes the structure of the anomalies after the second and third events to resemble the

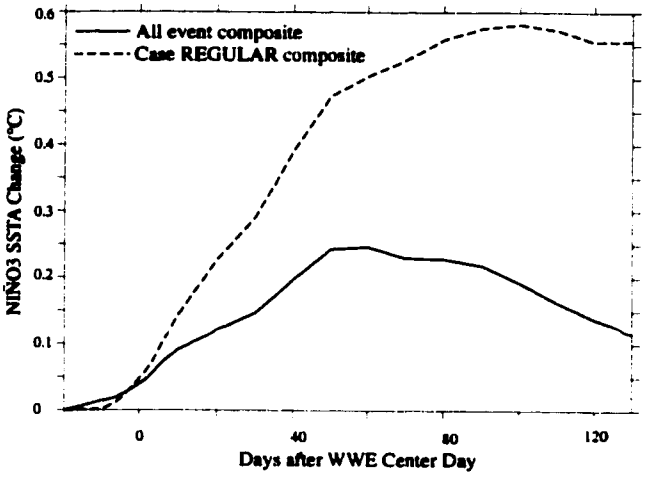

Figure V.12: Composite NIÑO3 SSTA Change (from Day (-20)) for the Type C all-event (solid line), and Case REGULAR (dashed line) composites. Units are °C.

composite more closely. Notice how the amplitude and structure of the east-of-dateline SSTA 60 days after the second and third events (Figure V.11.a-.b) is qualitatively similar to that of the composite (Figure V.10.a). The composite is still more diffuse in the meridional, a feature due to the smudging effects of averaging. The west of dateline anomalies are still stronger than expected from the composite; this additional warming is due to the incorrect SST gradient in the model. A sequence of three average amplitude WWEs (Experiment C4, Figure V.11.a) produces central Pacific equatorial warming of about a third the amplitude as that in the composite (Figure V.10.c); three stronger than average WWEs (Experiment C5, Figure V.11.b) produce central Pacific SSTA changes on the order of the composite.

A quantity of interest in the study of El Niño is the NIÑO3 SSTA index (SSTA averaged over the region 150°W-90°W, 5°S-5°N), and Type C WWEs are associated with warming of the NIÑO3 index (see Section III.4). Figure V.12 shows the Type C WWE composite change of the NIÑO3 SSTA index (from Day(-20)) for all events (solid line) and for Case REGULAR events (see Chapter III, dashed line). In both composites the index warms quickly following the WWE center day, reaching its maximum value somewhere between Day(40) and Day(60) for the all-event composite, and between Day(80) and Day(100) for the Case REGULAR composite. In the Case REGULAR composite the warm-

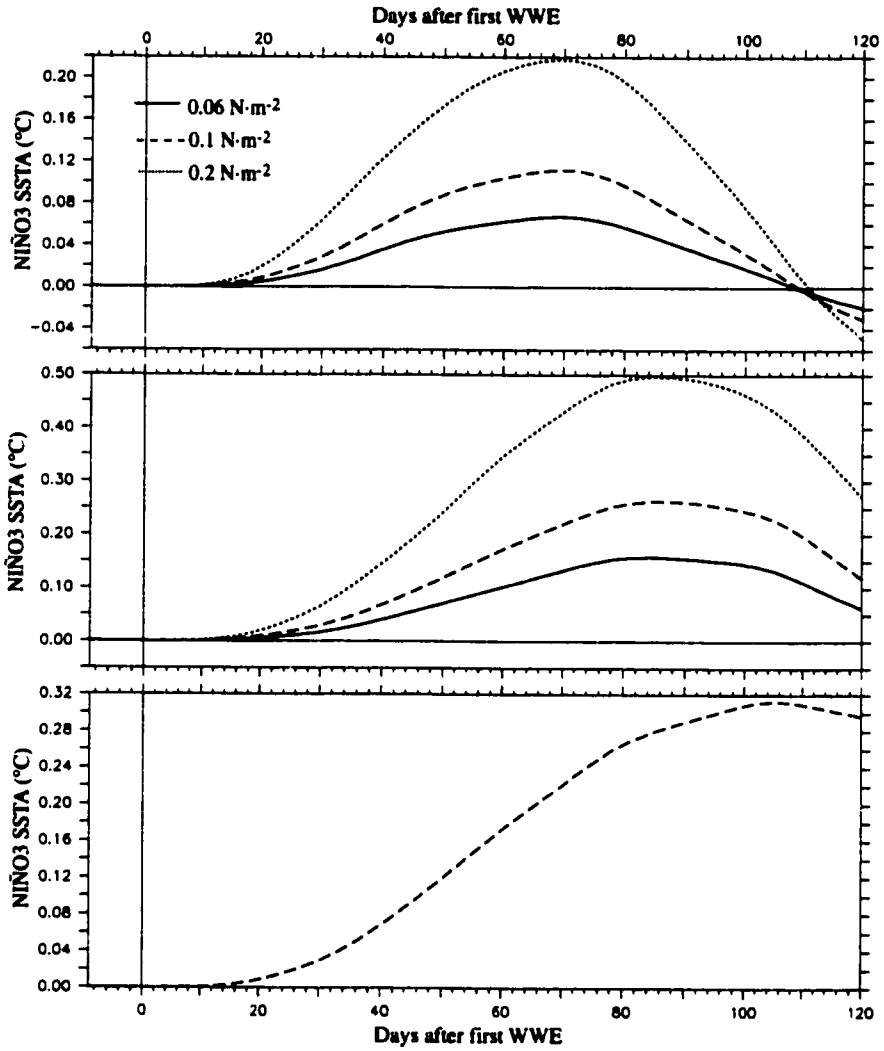

Figure V.13: NIÑO3 SSTA Change following (a) the single WWE experiments (C1-3), (b) the first event of the three WWE experiments (C4-6), and (c) the first event of the ten WWE experiment. In panels (a) and (b) the solid lines denote the 0.06 N·m^{-2} experiments, the dashed line denotes the 0.1 N·m^{-2} experiments, and the dotted line denotes the 0.2 N·m^{-2} experiments. Units are °C.

ing remains through Day(125).

Figure V.13 shows the NIÑO3 SSTA Index evolution for the single WWE cases (Experiments C1-3; upper panel), the three WWE cases (Experiments C4-6; middle panel), and for the ten WWE case (Experiment C7; lower panel). Notice how the amplitude of the NIÑO3 SSTA changes following the single WWEs (Figure V.13.a) appears to be relatively proportional to the WWE amplitude, with a 0.11°C maximum warming following the 0.1 N·m^{-2} burst and a 0.22°C maximum warming following the 0.2 N·m^{-2} burst. In the single

burst experiments, the timing of the maximum more closely resembles that of the all-event composite, occurring near Day(70); the warming disappears by Day(100). In the Experiments C1 and C2, the warming is fastest between Day(20) and Day (40) and slows, until the maximum is reached. In Experiment C3, a larger proportion of the warming happens before Day(40) than in the two weaker experiments.

For the three event experiments (Figure V.13.b), the amplitude of the maximum is increased, occurs later and lasts longer than for the single event experiments. The amplitude of the warming still appears to be somewhat linear, with a 0.25°C warming following the 0.1 $N \cdot m^{-2}$ bursts and a 0.5°C maximum warming following the 0.2 $N \cdot m^{-2}$ bursts. The effect of multiple WWEs is to raise and maintain NIÑO3 SSTA. The maximum in the three WWE experiments (Figure V.13.b), occurs near Day (90) and in the continued WWE experiment, the maximum occurs near Day(100). The continued WWEs in Experiment C7 maintain the NIÑO3 SSTA anomaly through Day(120), similar to the Case REGULAR composite.

In Chapter IV it was shown that the expected NIÑO3 SSTA changes following equatorial WWEs were independent to their association to the MJO (see Figure IV.21), and that the NIÑO3 SSTA changes following an MJO with an associated equatorial WWE were towards warming (see Figure IV.20). Experiment CM examines the SSTA changes following an MJO with a Type C event superimposed on it, in an attempt to reproduce the statistical relationships. Figure V.14 shows the equatorial SSTA in experiment CM. Notice how, as opposed to the MJO experiments (Exps. M1-4), the central and eastern equatorial Pacific warm following the termination of the MJO. The structure of the SSTA changes is similar to that following the Type C WWE (see Figure V.15,V.16). The character of the response is dominated by the WWE part, since the surface stress anomalies associated with the WWE are impulsive and much larger than those associated with the MJO. The model comfirms that the SSTA changes following an MJO with an equatorial WWE are similar to those following an equatorial WWE.

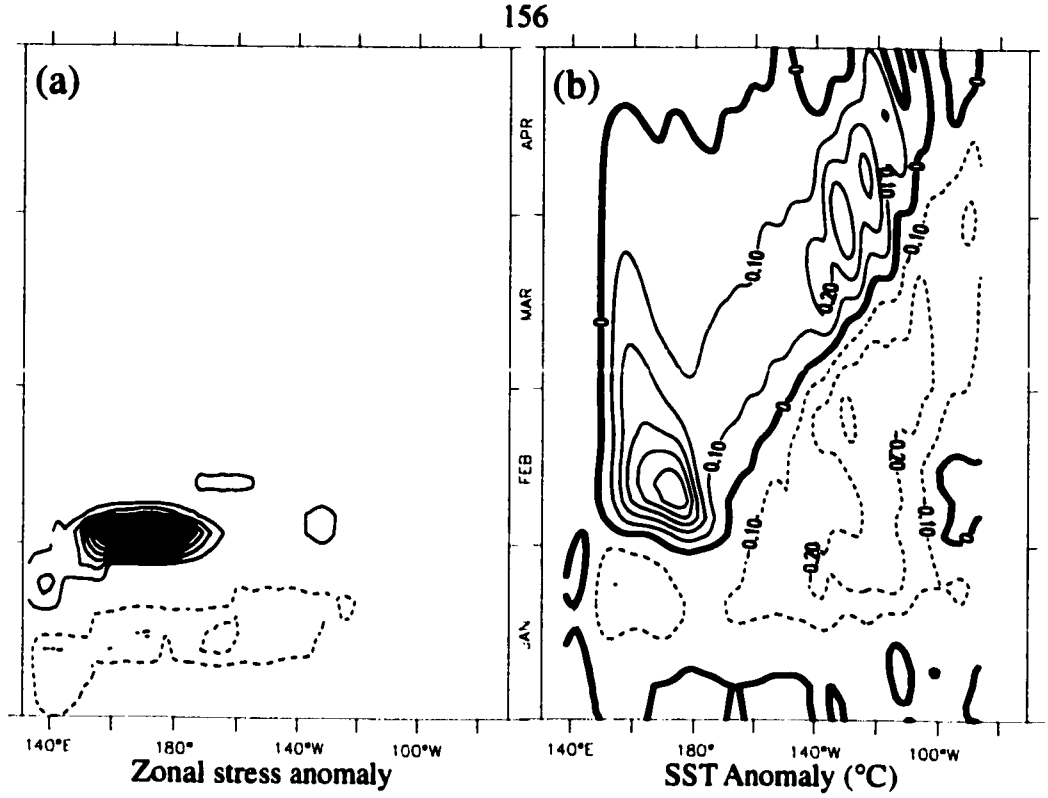

Figure V.14: Equatorial (a) Zonal stress anomaly ($N \cdot m^{-2}$), and (b) SST anomaly (°C), for Experiment CM. Contour interval in (a) is 0.5×10^{-2} $N \cdot m^{-2}$, contour interval in (b) is 0.1°C. Notice how the central equatorial Pacific warms following the WWE embedded in the MJO.

b. Mechanisms for SST Change:

In this section I examine the mechanisms which led to the WWE-driven equatorial SST changes in the OGCM. From Experiment C2, figure V.15 shows the time-longitude evolution of the 3-day-sampled equatorial: (a) Sea level height anomaly field, (b) SST anomaly field, (c) the thermocline depth field, and (d) the surface current anomaly field. The background shading indicates the expected 1st baroclinic and 2nd baroclinic Kelvin mode envelopes forced by the WWE; darker shading indicates the overlap between the two envelopes. Notice how the deepening of the thermocline, the raising of sea level height and the initial surface eastward acceleration coincide with the passage of the 1st baroclinic Kelvin pulse. Coincident with the 2nd baroclinic mode is a modification of the TIW field, and the largest amplitude SST anomalies. The modification of the TIW field leads to large amplitude meridional velocity anomalies, which overwhelm the WWE-forced signal, and pro-

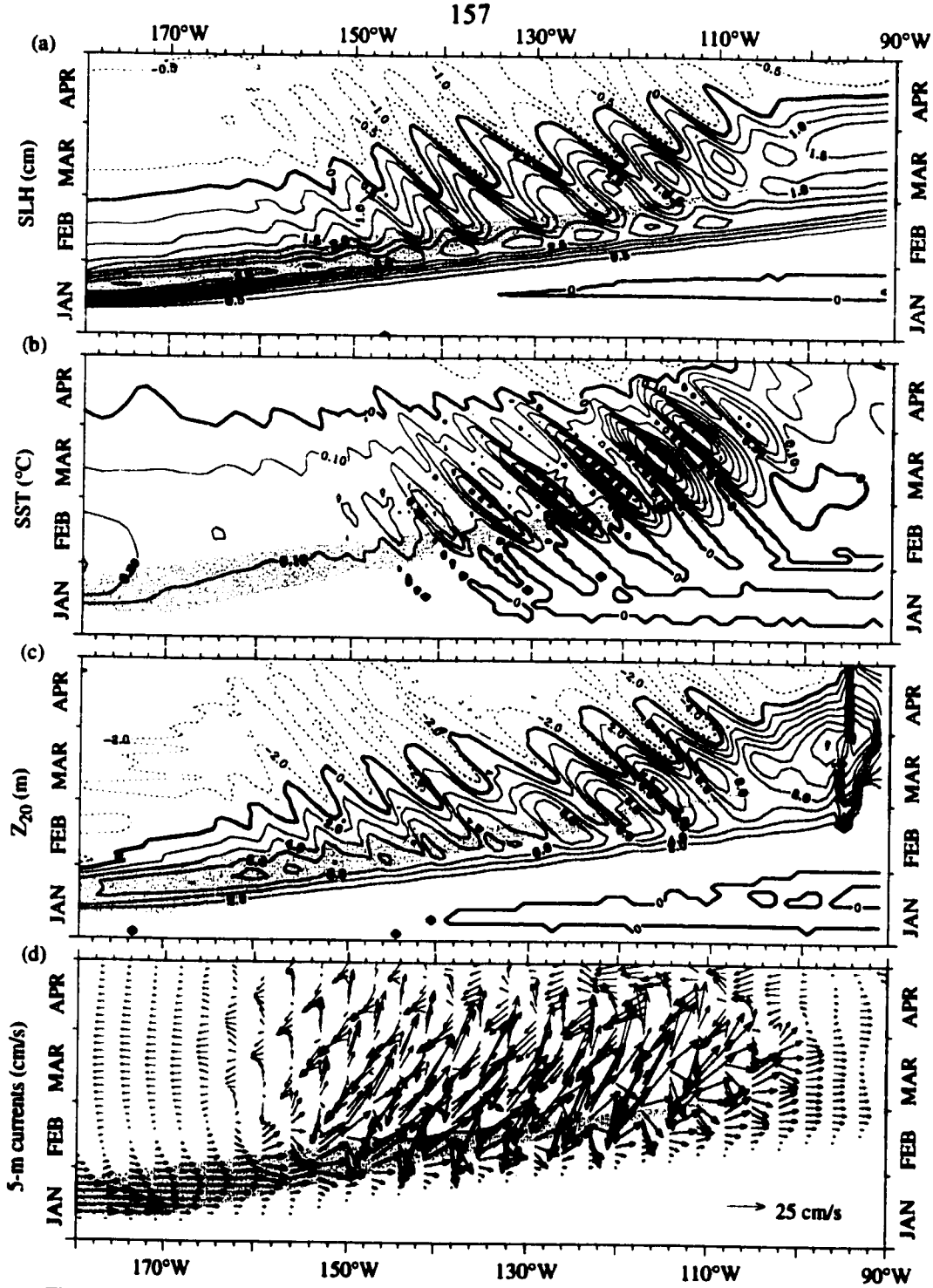

Figure V.15: East-of-dateline evolution of the 3-day sampled WWE driven anomalies along the equator, from experiment C2. (a) Sea level height anomalies in centimeters, (b) 5-meter temperature anomalies in °C, (c) thermocline depth (depth of 20°C isotherm) anomalies in meters, and (d) 5-meter current anomalies in cm/s. Shading in the background indicates first and second baroclinic mode envelopes, darker shading indicates the overlap between the two envelopes.

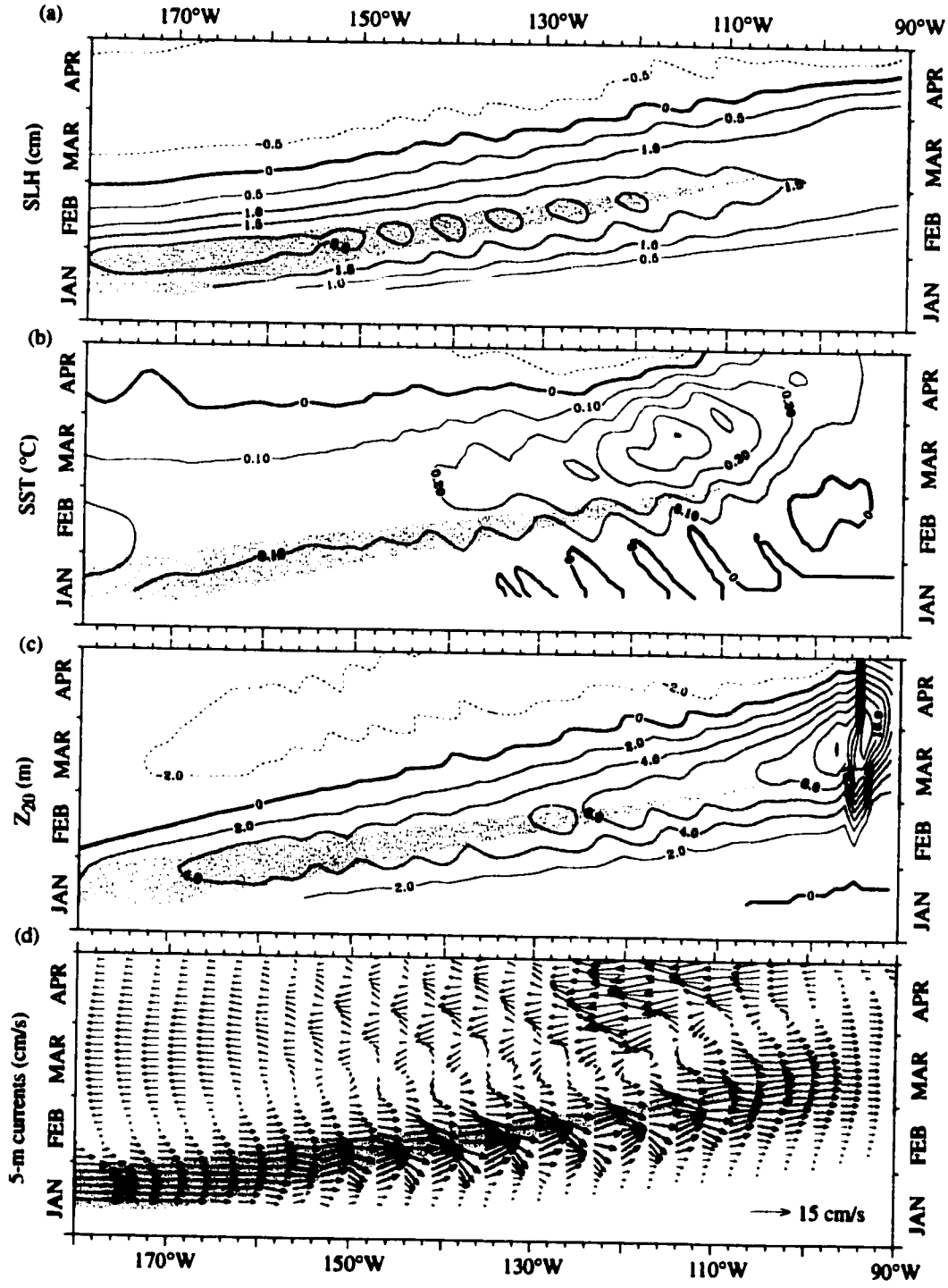

Figure V.16: East-of-dateline evolution of the 30-day boxcar smoothed WWE driven anomalies along the equator, from experiment C2. (a) Sea level height anomalies in centimeters, (b) 5-meter temperature anomalies in °C, (c) thermocline depth (depth of 20°C isotherm) anomalies in meters, and (d) 5-meter current anomalies in cm/s. Shading in the background indicates first and second baroclinic mode envelopes, darker shading indicates the overlap between the two envelopes.

duce large amplitude anomalies in all the plotted quantities.

To understand the evolution following the WWE it more useful to examine the 30-day boxcar smoothed evolution of the same anomalies.; these are shown in Figure V.16. Notice how the sea level height and thermocline depth anomalies appear with the 1st baroclinic mode, and return to zero as the 2nd mode passes. The surface current anomaly field is largely zonal, with eastward acceleration following the 1st baroclinic mode, but continuing into the 2nd. The maximum eastward currents correspond to the overlap between the 1st and 2nd mode envelopes, and in the far eastern Pacific where the two modes separate there appear to be two zonal current maxima. In the central Pacific sea level rising, thermocline deepening, zonal acceleration and SST warming reach a maximum at the overlap between the 1st and 2nd mode. While the 1st baroclinic mode propagates at ~2.8 ms^{-1} and the 2nd mode propagates at ~1.8 ms^{-1}, the maximum anomalies propagate at ~2.4 ms^{-1}. This propagation speed is the speed of the overlap between the two baroclinic modes.

The relative timing of the various quantities in the surface layer are more clearly seen in timeseries across the basin. Figure V.17 shows timeseries of the evolution of the uppermost layer of the model in Experiment C1-3. Each column is a separate location along the equator, from 155°W to 95°W (corresponding to the location of the TAO buoys). The rows show the 30-day boxcar smoothed evolution of anomalies in SST, thermocline depth, surface zonal current, surface meridional current, and 20-m vertical velocity. As in Figures V.15 and V.16, the envelopes of the 1st and 2nd baroclinic Kelvin pulses are shown by the background shading, with the dark shading indicating the overlap between the two modes. The solid line is for experiment C1, the dashed line is for experiment C2, and the dotted line is for experiment C3.

Notice, in Figure V.17, that the initial thermocline deepening and zonal current acceleration is coincident with the arrival of the 1st baroclinic mode, while the main surface warming generally occurs with both the 1st and 2nd baroclinic mode. The surface current is

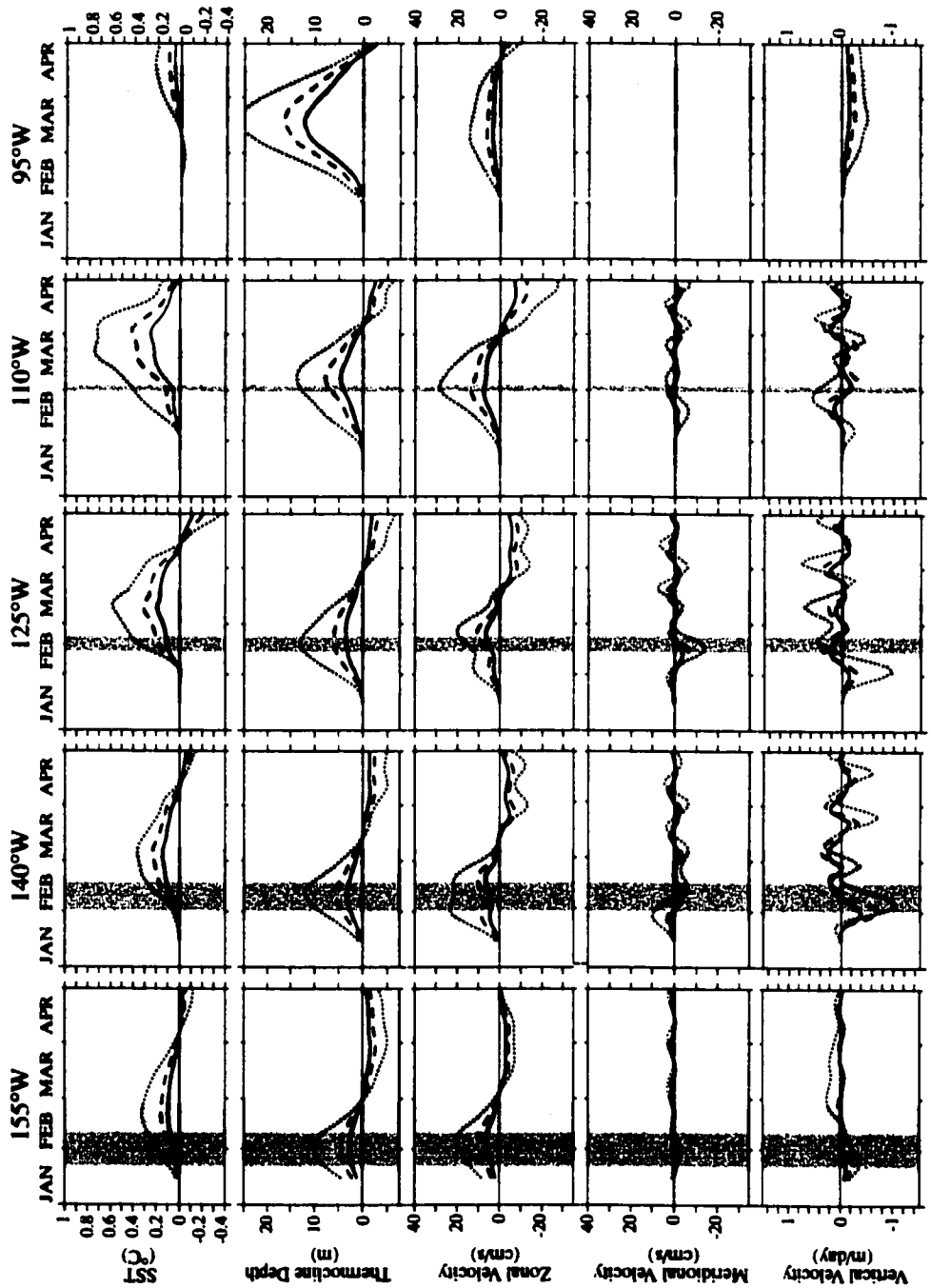

Figure V.17: Timeseries of the 30-day boxcar smoothed evolution of the the model for experiments C1-3 across the equator from 155°W to 95°W. Starting at the top row: 5-meter temperature anomalies, Thermocline depth anomalies, 5-meter zonal current anomalies, 5-meter meridional velocity anomalies, and 20-meter vertical velocity anomalies. Solid line is for experiment C1, dashed line for experiment C2, and dotted line for experiment C3.

accelerated eastward and thermocline is deepened by the first and second baroclinic mode passes,with the maximum anomalies in the overlap of the first two modes. Notice how even with the 30-day boxcar smoother, between 140°W and 110°W the main meridional and vertical velocity anomalies have a period similar to the TIWs, and result due to differences in the TIW fields. It would be difficult to measure differences such as these, because they result from differences between two instability wave fields. At 95°W the vertical velocity field is dominated by downwelling begining with the arrival of the 1st baroclinic mode and continuing with the 2nd baroclinic mode.

Timeseries of the 30-day boxcar smoothed anomalous balance of terms for temperature averaged over the top 20 meters across the equator is shown in Figure V.17, for Experiments C1-C3. The first column shows the temperature tendency term ($\partial T/\partial t$), the second column shows the negative advection of temperature, and the third column shows the diffusive including the surface heat flux anomaly. Notice how the warming is generally related to anomalous temperature advection, and after there has been some warming, there begins to be diffusive and heat-flux anomalies. The diffusive anomalies in most locations (except in February at 140°W and 125°W) are dominated by the tendency of the surface heat-flux to oppose the anomalous warming, thus the term appears as a cooling term.

Figure V.19 parses the advective term into its components, at each location I show: the total negative advection anomaly, the negative zonal advection anomaly, the negative meridional advection anomaly and the negative vertical advection anomaly. The intial dominant advective term in the heat balance varies with location: zonal advection dominates in the central basin (155°W and 140°W), vertical advection dominate in the eastern basin (125°W and 110°W), and in the far west warming due to vertical advection is opposed by cooling due to zonal advection (95°W). Between 155°W and 110°W meridional advection is an important term following the initial warming; this is a region with TIW activity in the model. There is warming due to meridional advection at 155°W and 110°W,cooling due to

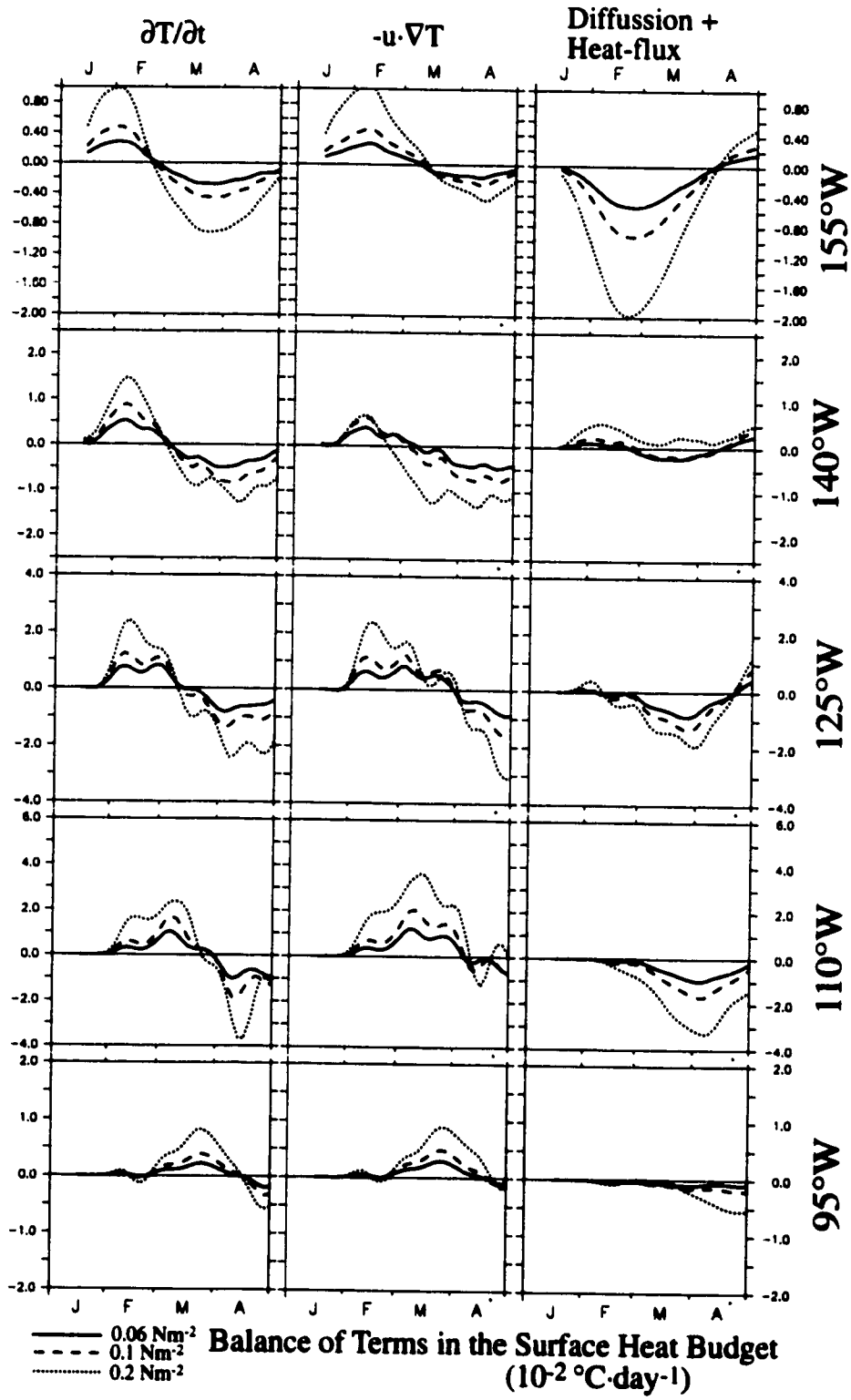

Figure V.18: Heat balance of the upper 20 meters for Experiments C1-3 along the Equator from 155°W through 95°W. Units are 0.1°C/day. Notice that the vertical axes are different for each longitude.

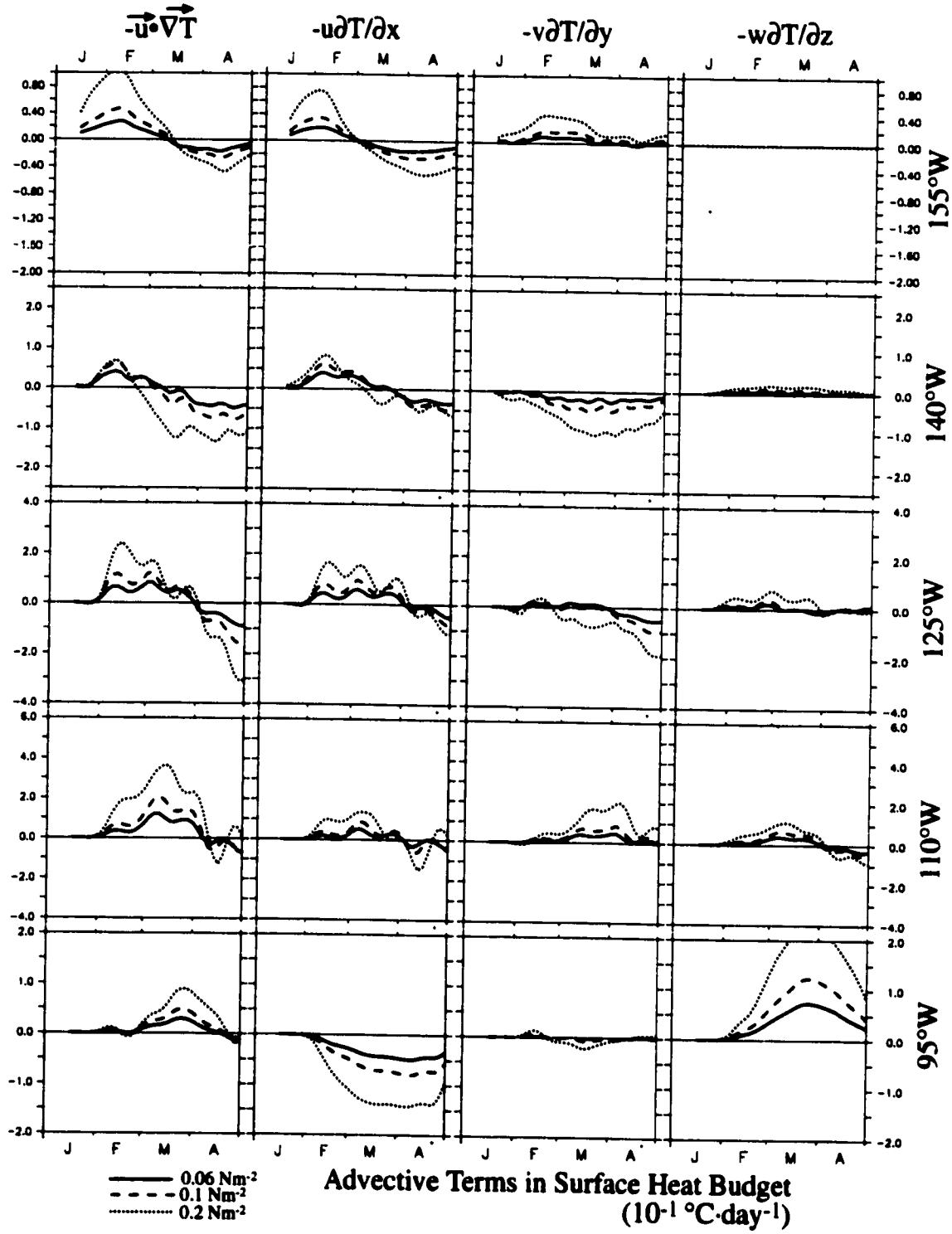

Figure V.19: Breakdown of the advective terms in the hear balance of the upper 20meters for Experiments C1-3 along the Equator from 155°W through 95°W. Solid line is for experiment C1, dashed line for experiment C2, and dotted line for experiment C3. Units are 0.1°C/day. Notice that the vertical axes are different for each longitude.

anomalous meridinal advection at 140°W and 125°W.

Anomalous advection of temperature has three components: advection of the background temperature gradient by the anomalous currents ($\mathbf{u}'\cdot\nabla T$), advection of the anomalous temperature gradient by the background currents ($\mathbf{u}\cdot\nabla T'$), and advection of the anomalous temperature gradient by the anomalous currents ($\mathbf{u}'\cdot\nabla T'$). At none of the locations is the third term ($\mathbf{u}'\cdot\nabla T'$) dominant to the anomalous SST. In most locations the main SST warming is initiated by advection by anomalous currents ($\mathbf{u}'\cdot\nabla T$); a notable exception is 95°W where vertical advection of the anomalous temperature gradient leads to the main surface warming. In the central Pacific, the SST warming is dominated by ($\mathbf{u}'\cdot\nabla T$), since the termocline is generally deeper than the background meridional upwelling cell (~50 m). In the eastern Pacific, since the thermocline is often shallower than the meridional upwelling cell,vertical advection of anomalously warm water becomes an important term (a dominant one at 95°W). Except in the far eastern Pacific, thermocline deepening occurs prior the SST warming forced by WWEs (see Figure V.15-V.17), however this thermocline deepening is not driving the warming. Rather, the surface warming is being driven by anomalous currents, whose convergence causes the thermocline to deepen.

5. Summary and Conclusions:

I have attempted to reproduce the SSTA changes statistically associated with the MJO and WWEs in the eastern and central Pacific using an OGCM. I also examined the mechanisms responsible for those changes. The composite MJO zonal stress anomalies do not drive eastern Pacific waveguide warming during the lifetime of the event. Equatorial WWEs drive circulation changes which result in eastern and central equatorial Pacific SST warming resembling that observed in the SSTA composites (see Chapter III). WWEs provide a mechanism for the onset of El Niño SSTA, through advection of the backgroud SST gradient.

MJO-driven surface wind variability over the western and central Pacific has been suggested as an important mechanism for waveguide SST warming during El Niño (Lau and Chan 1986, 1988, Lau and Shen 1988, Weickman 1991, Kessler *et al.* 1995, Moore and Kleeman 1999). The surface wind structure of the MJO has been idealized as a sinusoid confined to the western Pacific warm pool (Kessler *et al.* 1995, Kessler and Kleeman 2000). These idealizations are inconsistent with the composite surface wind structure of the MJO using the Maloney and Hartmann (1998) MJO index (see Chapter IV), and with the MJO-related equatorial surface zonal stress described by Hendon *et al.* (1998).

The absence of correlation between El Niño waveguide warming and enhanced MJO activity is consistent with the results of forcing the OGCM with composite MJO surface wind stress. There is no correlation between enhanced MJO activity and El Niño waveguide warming (Slingo *et al.* 1999, Hendon *et al.* 1999, Harrison and Vecchi 2000, Figure IV.2). Certain MJO events, which co-occur with equatorial WWEs, tend to be followed by equatorial waveguide warming (see Figure IV.19), yet this warming is not significantly different from that which follows equatorial WWEs which occur without the MJO. The warming is a feature of the WWEs, not of the MJO.

A significant feature of the surface wind and wind-stress field associated with the MJO is periods of easterly and westerly flow across most of the equatorial Pacific (Figure V.2-.3). When the model is forced with the statistically significant MJO zonal stress anomalies, the eastern and central equatorial Pacific SST cools. The central Pacific cooling is driven by the central Pacific easterlies which dominate the composite, while the eastern Pacific cooling is forced by both the central Pacific and western Pacific wind stress anomalies (Section V.3). A sequence of MJOs produces cooling in excess of 0.3°C across most of the eastern and central equatorial Pacific, during and in the month following the MJOs (Figure V.11). When the mean over the period of an MJO is removed from the zonal stress anomaly field, the effect of the MJO on the model is to produce very small cooling during

the forcing period. The composite MJO zonal stress field is not suggestive of the MJO driving eastern and central Pacific waveguide warming during the onset of El Niño. These experiments lack coupling of the ocean and atmosphere, which has been suggested as an important mechanism for the evolution of the SSTA field following the MJO (Kessler *et al.* 1995, Kessler and Kleeman 2000), their results idicate that there is a coupling between the MJO driven SSTA changes and the location of the maximum westerlies in the surccessive MJO events. It would be of interest to repeat the coupled experiments of Kessler *et al.* (1995) and Kessler and Kleeman (2000) with the MJO forcing derived using the MH98 MJO index, which exhibits zonal stress anomalies far beyond the eastern edge of the warm pool.

Prior to the return of SST to normal at the end of recent El Niño events, there has been a shoaling of the eastern equatorial Pacific thermocline to normal or shallower than normal depths; this thermocline shoaling makes cool water available to be upwelled by equatorial easterly winds (Harrison *et al.* 1990, Kessler and McPhaden 1995, Harrison and Vecchi 1999, 2000, McPhaden 1999, McPhaden and Yu 1999). This thermocline shoaling might be due to "delayed-oscillator" type mechanisms (see Suarez and Schopf 1988, Battisti and Hirst 1989, Neelin *et al.* 1998), or to the interaction of the seasonal cycle with anomalous El Niño conditions (Harrison and Vecchi 1999), or a combined effect of the two. During weak or moderate El Niño events, such as 1986-7 or 1991-2, when easterly trade winds remain present to some degree through the event, the shoaling thermocline makes cool subsurface water available to the shallow upwelling circulation and returns eastern Pacific SST towards climatology. In extreme El Niño events – such as 1982-3 or 1997-8 – during which the easterly trade winds weaken and even disappear across the Pacific, the cool subsurface waters, brought close to the surface by the thermocline shoaling, do not break through to the surface until equatorial easterlies return. The presence of equatorial easterlies in the MJO-composite, when NIÑO3 SST is warmer than normal (see Section IV.3.a), suggests

the MJO as a potential mechanism for eastern Pacific SST cooling at the end of major El Niño events.

Takayabu *et al.* (1999) have suggested that the abrupt termination of the 1997-8 El Niño event was related to central equatorial Pacific easterly winds associated with an MJO in May 1998. Figure IV.2 shows that MJO events passed across the tropical Pacific in June 1983 and May 1998, coincident with the rapid cooling to normal SST at the end of these to major El Niño events (during which the easterly trade winds became extremely weak and even disappeared; see Harrison *et al.* 1990, McPhaden 1999, McPhaden and Yu 1999). As the thermocline shoaled at the end of these major El Niño events, horizontal surface temperature gradients were weak and there was little evidence for equatorial upwelling. Once the thermocline shoaled, a large vertical temperature gradient was set up in the central/ eastern equatorial Pacific; and since the entire equatorial Pacific had SST in excess of 28°C the MJO-related stresses over the entire Pacific should be in the convective regime. The convective regime is characterized by a quasi-oscillatory propagating zonal stress variability (see Figures 4,5,7). Westerly stress anomalies over the equatorial Pacific tend to lead to warming, primarily through advective processes; in the absence of horizontal gradients and background upwelling one would expect the effects to be small. Easterly stress anomalies over the equatorial Pacific tend to drive surface cooling through advective, heat-flux and mixing processes; since the vertical temperature gradient is the dominant temperature gradient across the equatorial Pacific, one would expect the effect of the easterly Phases of the MJO to be cooling of the eastern and central equatorial Pacific. Thus, the MJO provides a mechanism for the return of SSTA to normal when the background easterly trades are weak.

Equatorial WWEs have been suggested as a mechanism for the onset of El Niño waveguide warm anomalies. WWEs are observed to precede El Niño (Keen 1982, Luther *et al.* 1983, Harrison and Giese 1989,1990, Harrison and Vecchi 1997) and are linked with the onset and maintenance of warm conditions (Vecchi and Harrison 2000, Chapter III). Ocean

general circulation model (OGCM) experiments have suggested that equatorial WWEs can drive El Niño eastern and central equatorial Pacific SST changes (Harrison and Giese 1988, Giese and Harrison 1990,1991, Kindle and Phoebus 1995). WWEs with realistic (x,y,t) scales drive SSTA changes consistent with the observed associations (Chapter III).

The central equatorial Pacific SSTA driven by individual WWEs is similar to that in the associations, however the amplitude for average amplitude WWEs is much smaller than the associated changes. However, when WWEs are placed in succession, they reproduce the amplitude and the structure of the composite SSTA changes. Since WWEs often occur within 40 days of each other (see Figures IV.15-.16), the composites represent the effect of more than one WWE. The OGCM is unable to reproduce any ocean/atmosphere coupling in the eastern and central Pacific; this coupling would strengthen the warming response of the system.

Following the WWE, theermocline deepens, sea level height rises, surface zonal current accelerates and SST warms in association with both the first and the second baroclinic modes. The maxima in zonal current, thermocline depth and sea level height anomaly occurs at the overlap between the first and second baroclinic wave envelopes. The maximum propagates eastward at the speed of the overlap of the first and second mode ($\sim 2.4 ms^{-1}$), which does not correspond to the speed of the first or second mode envelopes ($\sim 2.8 ms^{-1}$, and $\sim 1.8 ms^{-1}$, respectively). In the far eastern Pacific (95°W), there is almost no SST signal until the expected arrival of the second baroclinic mode. However, most of the warming in the far eastern Pacific is not driven directly by the pulse, but rather results from thermocline deepening associated with the current pulse.

The warming following the WWE is initially driven by SST advection, after which vertical mixing and anomalous heat flux become important terms. There are three regimes in the eastern and eastern-central Pacific, based on which advective term which initiates the warming. In the central Pacific (155°W and 140°W) zonal advection by the WWE driven

pulses drive the initial warming. Near 125°W and 110°W zonal and vertical advection are important for the initial warming. In the far eastern Pacific (~95°W) warming is dominated by vertical advection, and opposed by zonal advection of the background positive $\partial SST/\partial x$; the warming is associated both with advection of the background temperature gradient by the anomalous vertical currents and advection of the anomalous temperature gradient by the background upwelling circulation. Between 155°W and 110°W meridional advection is a significant term following the initial warming, this is a region of strong TIW activity.

The results for the WWE experiments using realistic zonal scales are consistent with those of Harrison and Giese (1988) and Giese and Harrison (1990, 1991). The character of the SSTA changes following WWEs with a zonal length scale of ~30° and with a zonal length scale of ~20° is similar. Both suggest that WWEs drive eastern and central Pacific SST warming similar to that seen during El Niño.

Equatorial WWEs, with duration typically in the 6-20 day range, have been strongly associated with equatorial SSTA warming (if the initial state of the ocean was normal or cooler than normal) and with the maintenance of warm SSTA (if the ocean was already significantly warmer than normal). OGCM experiments have established mechanisms by which WWEs cause SSTA to increase or maintain warm SSTA. WWEs are a fundamental mechanism in El Niño waveguide SST warming and warm anomaly maintenance. The surface wind anomaly field associated with the MJO is dominated by eastern and central Pacific easterlies, providing a potential mechanism for the return to normal SST at the end of extreme El Niño events and for cooling during La Niña events. Equatorial SSTA changes following an MJO with a superimposed equatorial WWE are of similar character to those following an equatorial WWE (Figure V.13). The surface stress anomaly associated with an average WWE (0.06 $N \cdot m^{-2}$) overwhelms the surface stress anomaly associated with the average MJO (0.01 $N \cdot m^{-2}$).

The importance of sub-seasonal atmospheric variability in ENSO is apparent: WWEs

are a fundamental mechanism for the onset and maintenance of El Niño warming, and the MJO may be important in the termination of certain extreme El Niño events. Because there is so much energy in the sub-seasonal band, and because westerly wind events have been strongly connected with the onset and maintenance of El Niño, further study of the sub-seasonal band is important for understanding the life-cycle of El Niño. In particular, improvement in our ability to predict the onset and amplitude of El Niño warming is likely to come from improved understanding of the entire sub-seasonal band of tropical Pacific wind variability. Improved forecasts of the onset, amplitude and termination of El Niño events will likely depend on improved understanding and prediction of WWEs, the MJO, cyclones, cold surges and convective superclusters, and their interconnections.

Bibliography

Anderson, D.L.T., and A.E. Gill, 1976: Spin-up of a stratified ocean, with applications to upwelling. *Deep Sea. Res.*, **22**(9), 583-596.

Barber, R.T., and F.P. Chavez, 1983: Biological Consequences of El Niño. *Science*, **222**, 1195-1202.

Battisti, D.S., and E.S. Sarachik, 1995: Understanding and predicting ENSO. *Rev. Geophys.*, **33**(Suppl.), 1367-1376.

Battisti, D.S. and A.C. Hirst, 1989: Interannual variability in a tropical ocean-atmosphere model: influence of basic state, ocean geometry and nonlinearity. *J. Atmos. Sci.*, **46**(12), 1687-1712.

Bickel, P.J., and K.A. Doksum, 1977: Mathematical Statistics: Basic Ideas and Selected Topics. Holden-Day Inc., 492 pp.

Bjerkness, J., 1961: "El Niño" study based on analysis of ocean surface temperatures 1935-1957. *Inter. Am. Trop. Tuna Comm. Bull.*, **5**, 219-271.

Bjerkness, J., 1966: A possible response of the atmospheric Hadley circulation to anomalies of ocean temperature. *Tellus*, **18**, 820-829.

Bjerkness, J., 1969: Atmospheric teleconnections from the equatorial Pacific. *Mon. Wea. Rev.*, **97**, 163-172.

Busalacchi, A.J., and J.J. O'Brien, 1980: The seasonal variability in a model of the tropical Pacific. *J. Phys. Oceanogr.*, **10**, 1929-1951.

Cane, M.A., 1977: Forced baroclinic ocean motions, Pt.1, Linear equatorial unbounded case. *J. Marine Res.*, **34**(4), 629-665.

Cane, M.A., 1983: Oceanographic Events During El Niño. *Science*, **222**(4629), 1189-1194.

Cane, M.A., and S.E. Zebiak, 1985: A theory for El Niño and the Southern Oscillation. *Science*, **228**, 113-127.

Chavez, F.P., P.G. Strutton, and M.J. McPhaden, 1998: Biological-physical coupling in the central equatorial Pacific during the onset of the 1997-8 El Niño. *Geophys. Res. Lett.*, **25**(19), 3543-3546.

Chen, S.S., R.A. Houze, and B.E. Mapes, 1996: Multiscale Variability of Deep Convection in Relation to Large-Scale Circulation in TOGA COARE. *J. Atmos. Sci.*, **53**(10), 1380-1409.

Chu, P.S., 1988: Extratropical Forcing and the Burst of Equatorial Westerlies in the Western Pacific: A Synoptic Study. *J. Met. Soc. Japan*, **66**(4), 549-564.

Chu, P.S., and J. Frederick, 1990: Westerly Wind Bursts and Surface Heat Fluxes in the Equatorial Western Pacific in May 1982. *J. Met. Soc. Japan*, **68**(5), 523-536.

Cronin, M.F., and M.J. McPhaden, 1997: The upper ocean heat balance in the western equatorial Pacific warm pool during September-December 1992. *J. Geophys. Res.*, **102**(C4), 8,533-8,553.

Delcroix, T., G. Eldin, M. McPhaden, and A. Morliere, 1993: Effects of Westerly Wind Bursts Upon the Western Equatorial Pacific Ocean, February-April 1991. *J. Geophys. Res.*, **98**, 16,379-16,385.

Donguy, J.R., and C. Hénin, 1980: Climatic Teleconnections in the Western South Pacific with El Niño Phenomenon. *J. Phys. Oceanogr.*, **10**, 1952-1958.

Efron, B., and R. Tibshirani, 1991: Statistical Data Analysis in the Computer Age. *Science*, **253**, 390-395.

Eldin, G., T. Delcroix, C. Hénin, K. Richards, Y. Du Penhoat, J. Picaut, and P. Rual, 1994: Large-Scale Current and Thermohaline Structures Along 156°E During the COARE Intensive Observational Period. *Geophys. Res. Lett.* **21**(24), 2,681-2,684.

Eriksen C.C, M.B. Blumenthal, S.P. Hayes, and P. Ripa, 1983: Wind-Generated Kelvin Waves Observed Across the Pacific Ocean. *J. Phys. Oceanogr.*, **13**, 1622-1640.

European Centre for Medium Range Weather Forecasts, 1989: The desciption of the ECMWF/WCRP level III-A global atmospheric data archive, technical attachment, 72 pp. [Avaliable from ECMWF, Shinfield Park, reading RG2, 9AX, United Kingdom].

Feng, M., P. Hacker, and R. Lukas, 1998: Upper ocean heat and salt balances in response to a westerly wind burst in the western equatorial Pacific during TOGA COARE. *J. Geophys. Res.*, **103**(C5), 10,289-10,311.

Giese, B.S., 1989: Equatorial Response to Forcing on Time Scales from Days to Months. NOAA Technical Memorandum ERL PMEL-87, 99 pp.

Giese, B.S., and D.E. Harrison, 1990: Aspects of Kelvin Wave Response to Episodic Wind Forcing. *J. Geophys. Res.*, **95**(C5), 7,289-7,312.

Giese, B.S., and D.E. Harrison, 1991: Eastern Equatorial Pacific Response to Three Composite Westerly Wind Types. *J. Geophys. Res.*, **96**(Supp.), 3,239-3,248.

Gill, A.E., 1982: Atmosphere-Ocean Dynamics. Academic Press, 662 pp..

Global Tropical/Extratropical Cyclone Climatic Atlas, 1996. CD-ROM Version 2.0, Jointly produced by the Fleet Numerical Meteorology and Oceanography Detachment and the National Climatic Data Center.

Godfrey, J.S., 1975: On Ocean Spindown I: A Linear Experiment. *J. Phys. Oceanogr.*, **5**, 399-409.

Godfrey, J.S., R.A. Houze Jr., R.H. Johnson, R. Lukas, J.-L. Redelsperger, A. Sumi, and R. Weller, 1998: Coupled Ocean-Atmosphere Response Experiment (COARE): An interim report. *J. Geophys Res.*, **103**(C7), 14,395-14,450.

Harrison, D.E., 1984: On the Appearance of Sustained Equatorial Westerlies During the 1982 Pacific Warm Event. *Science*, **225**, 1099-1102.

Harrison, D.E., 1987: Monthly mean island surface winds in the central tropical Pacific and El Niño. *Mon. Wea. Rev.*, **115**, 3,133-3,145.

Harrison, D.E., 1989: On climatological monthly mean wind stress and wind stress curl fields over the world ocean. *J. Climate*, **2**, 57-70.

Harrison, D.E., 1991: Equatorial sea surface temperature sensitivity to net surface heat flux: Some ocean circulation model results. *J. Climate*, **4**, 539-549.

Harrison, D.E., 1996: Vertical velocity variability in the tropical Pacific - a circulation model perspective of JGOFS. *Deep-Sea Res.*, **II, 43**, 687-705.

Harrison, D.E., and A. Craig, 1993: Ocean model studies of upper ocean variability at (0°N,160°W) during the 1982-83 ENSO; local and remote forcing. *J. Phys. Oceanogr.*, **23**, 427-451.

Harrison, D.E., and B.S Giese, 1988: Remote westerly wind forcing of the eastern equatorial Pacific; some model results. *Geophys. Res. Lett.*, **15**, 804-807.

Harrison, D.E., and B.S. Giese, 1989: Comments on "The Response of the Equatorial Pacific Ocean to a Westerly Wind Burst on May 1986" by M.J. McPhaden *et al.*. *J. Geophys. Res.*, **94**(C4), 5,024-5,026.

Harrison, D.E., and B.S. Giese, 1991: Episodes of surface westerly winds as observed from islands in the western tropical Pacific. *J. Geophys. Res.*, **96**, 3,221-3,237.

Harrison, D.E., and D.S. Luther, 1990: Surface Winds from Tropical Pacific Islands - Climatological Statistics. *J. Climate*, **3**(2), 251-271.

Harrison, D.E., and G.A. Vecchi, 1997: Surface westerly wind events in the tropical Pacific: 1986-1995. *J. Climate*, **10**(12), 3,131-3,156.

Harrison, D.E., and G.A. Vecchi, 1999: On the termination of El Niño. *Geophys. Res. Lett.*, **26**, 1593-1596.

Harrison, D.E., and G.A. Vecchi, 2000: El Niño and La Niña - Equatorial Pacific termocline depth and sea surface temperature anomalies, 1986-1998. *Geophys. Res. Lett., submitted.*

Harrison, D.E., and N.K. Larkin, 1996: The COADS Sea Level Pressure Signal: A Near-Global El Niño Composite and Time Series View, 1946-1993. *J. Climate,* **9**(12), 3,025-3,055.

Harrison, D.E., and N.K. Larkin, 1998.a: The ENSO Surface Temperature and Wind Signal: A Near-Global Composite and Time-Series View, 1946-1995. *Rev. Geophys.*, **36**(3), 353-399.

Harrison, D.E., and N.K. Larkin, 1998.b: Seasonal U.S. temperature and precipitation anomalies associated with El Niño: Historical results and comparissons with 1997-98. *Geophys. Res. Lett.*, **25**(21), 3,959-3,962.

Harrison, D.E., and P.S. Schopf, 1984: Kelvin wave induced anomalous advection and the onset of SST warming in El Niño events. *Mon. Wea. Rev.*, **112**, 923-933.

Harrison, D.E., B.S. Giese and E.S. Sarachik, 1990: Mechanisms of SST change in the equatorial waveguide during the 1982-83 ENSO. *J. Climate,* **3**, 173-188.

Harrison, D.E., W. Kessler and B. Giese, 1989: Hindcasts of the 1982-3 El Niño: Thermal and dynamical height variability along ship of opportunity XBT tracks. *J. Phys. Oceanogr.*, **19** 397-418.

Hartmann, D.L., M.L. Michelsen, and S.A. Klein, 1992: Seasonal Variations of Tropical Intraseasonal Oscillations: A 20-25-Day Oscillation in the Western Pacific. *J. Atmos. Sci.*, **49**(14), 1277-1289.

Hartten, L.M., 1996: Synoptic settings of westerly wind bursts. *J. Geophys. Res.*, **101**(D12), 16,997-17,019.

Hayes, S.P., P. Chang, and M.J. McPhaden, 1991: Variability of the Sea Surface Temperature in the Eastern Equatorial Pacific During 1986-1988. *J. Geophys. Res.*, **98**(C6), 10,553-10,566.

Hendon, H.H. and M.L. Salby, 1994: The Life Cycle of the Madden-Julian Oscillation. *J. Atmos. Sci.*, **51**(15), 2,225-2,237.

Hendon, H.H. B. Liebmann, and J.D. Glick, 1998: Oceanic Kelvin Waves and the Madden-Julian Oscillation. *J. Atmos. Sci.*, **55**, 88-101.

Hendon, H.H., C. Zhang, and J.D. Glick., 1999: Interannual Variation of the Madden-Julian Oscillation during Austral Summer. *J. Climate,* **12**(12), 2,538-2,550.

Ji, M., A. Leetmaa, and J. Derber, 1995: An ocean analysis system for seasonal to interannual climate studies. *Mon. Wea. Rev.*, **123**(2), 460-481.

Joint Typhoon Warning Center, 1994.a: Western North Pacific Typhoons - 1994. *Mar. Wea. Log,* **38**(1), 34-40.

Joint Typhoon Warning Center, 1994.b: Western North Pacific Typhoons - 1993. *Mar. Wea. Log,* **38**(4), 16-23.

Journal of Geophysical Research, 1998. **103**(C7).

Kalnay, E. and coauthors, 1996: The NCEP/NCAR 40-year reanalysis project. *Bull. Amer. Meteor. Soc.*, **77**, 437-471.

Keen, R.A., 1982: The role of cross-equatorial cyclone pairs in the Southern Oscillation. *Mon. Wea. Rev.*, **110**, 1405-1416.

Kessler, W.S. and M.J. McPhaden, 1995: Oceanic Equatorial Waves and the 1991-3 El Niño. *J. Climate,* **8**, 1757-1774.

Kessler, W.S., M.J. McPhaden, and K.M. Weickmann, 1995: Forcing of intraseasonal Kelvin waves in the equatorial Pacific. *J. Geophys. Res.*, **100**(C6), 10,613-10,631.

Kessler, W.S., and R. Kleeman, 2000: Rectification of the Madden-Julian Oscillation into the ENSO cycle. *J. Climate*, in press.

Kiladis, G.N., G.A. Meehl, and K.M. Weickmann, 1994: Large-scale circulation associated with westerly wind bursts and deep convection over the western equatorial Pacific. *J. Geophys. Res.*, **99**(D9), 18,527-18,544.

Kindle, J.C., and P.A. Phoebus, 1995: The ocean response to operational winds bursts during the 1991-2 El Niño. *J. Geophys. Res.*, **100**(C3), 4,803-4,920.

Klein, S.A., and D.L. Hartmann, 1993: The Seasonal Cycle of Low Stratiform Clouds. *J. Climate*, **6**, 1587-1606.

Kousky, V.E., and A. Leetmaa, 1989: The 1986-87 Pacific Warm Episode: Evolution of Oceanic and Atmospheric Anomaly Fields. *J. Climate*, **2**, 254-267.

Large, W.G. and S. Pond, 1981: Open Ocean Momentum Flux Measurments in Moderate to Strong Winds. *J. Phys. Oceanogr.*, **11**, 324-336.

Lau, K.H., and N.C. Lau, 1992: The energetics and propagation dynamics of tropical summertime synoptic-scale disturbances. *Mon. Wea. Rev.*, **120**, 2,523-2,539.

Lau, K.M., and P.H. Chan, 1986: The 40-50 Day Oscillation and the El Niño/Southern Oscillation: A New Perspective. *Bull. Amer. Meteor. Soc.*, **67**(5), 533-534.

Lau, K.M., and P.H. Chan, 1988: Intraseasonal and Interannual Variations in Tropical Convection: A possible Link between the 40-50 Day Oscillation and ENSO?. *J. Atmos. Sci.*, **45**(3), 506-521.

Lau, K.M., L. Peng, C.H. Sui, and T. Nakazawa, 1989: Dynamics of Super Cloud Clusters, Westerly Wind Bursts, 30-60 Day Oscillations and ENSO: An Unified View. *J. Meteorol Soc. Japan,* **67**(2), 205-219.

Levitus, S., 1982: Climatological Atlas of the World Ocean, NOAA/ERL GFDL Professional Paper 13, Princeton, NJ, 173 pp. (NTIS PB83-184093)

Liebmann, B., H.H. Hendon, and J.D. Glick, 1994: The relationship between tropical cyclones of the western Pacific and Indian oceans and the Madden-Julian oscillation. *J. of the Meteorol. Soc. of Japan*, **72**(3), 401-412.

Lin, X., and R.H. Johnson, 1996: Kinematic and Thermodynamic Characteristics of the Flow over the Western Pacific Warm Pool during TOGA COARE. *J. Atmos. Sci.*, **53**(5), 695-715.

Love, G., 1985.a: Cross-equatorial influence of winter hemisphere subtropical cold surges. *Mon Wea. Rev.*, **113**, 1487-1498.

Love, G., 1985.b: Cross-equatorial Interactions during Tropical Cyclogenesis. *Mon Wea. Rev.*, **113**, 1499-1509.

Lukas, R., P.J. Webster, M. Ji, and A. Leetmaa, 1995: The Large-Scale Context for the TOGA Coupled Ocean-Atmosphere Response Experiment. *Met. Atmos. Phys.*, **56**, 3-16.

Luther, D.S., and D.E. Harrison, 1984: Observing Long-Period Fluctuations of Surface Winds in the Tropical Pacific: Initial Results from Island Data. *Mon. Wea. Rev.*, **112**(2), 285-302.

Luther, D.S., D.E. Harrison, and R.A. Knox, 1983: Zonal Winds in the Central Equatorial Pacific and El Niño. *Science*, **222**, 814-837.

Madden, R.A., and P.R. Julian, 1972: Description of Global-Scale Circulation Cells in the Tropics with a 40-50 Day Period. *J. Atmos. Sci.*, **29**, 1109-1123.

Madden, R.A., and P.R. Julian, 1994: Observations of the 40-50 Day Tropical Oscillation - A Review. *Mon. Wea. Rev.*, **122**, 814-837.

Maes, C., P. Delecleuse, and G. Madec, 1998: Impact of westerly wind bursts on the warm pool of the TOGA-COARE domain in an OGCM. *Climate Dynamics*, **14**, 55-70.

Maloney, E.D., and D.L. Hartmann, 1998: Frictional Moisture Convergence in Composite Life Cycle of the Madden-Julian Oscillation. *J. Climate*, **11**, 2,387-2,403.

Mangum, L.J., H.P. Freitag, and M.J. McPhaden, 1994: TOGA-TAO Array Sampling Schemes and Sensor Evaluations. *Proceedings of the Oceans '94*, OASTES, v.II, 402-406.

McBride, J.L., N.E. Davidson, K. Puri, and G.C. Tyrell, 1995: the Flow during TOGA COARE as Diagnosed by the BMRC Tropical Analysis and Prediction System. *Mon. Wea. Rev.*, **123**, 717-736.

McCreary, J.P., 1976: Eastern Tropical Ocean Response to Changing Wind Systems: with Application to El Niño. *J. Phys. Oceanogr.*, **6**, 632-645.

McPhaden, M.J., 1993: TOGA-TAO and the 1991-3 El Niño Southern Oscillation Event. *Oceanography*, **6**, 36-44.

McPhaden, M.J., 1999: Genesis and Evolution of the 1997-98 El Niño. *Science*, **283**, 951-954.

McPhaden, M.J. and X. Yu, 1999: Equatorial Waves and the 1997-98 El Niño. *Geophys. Res. Lett.*, **26**(19), 2,961-2,964.

McPhaden, M.J., F. Bahr, Y. Du Penhoat, E. Firing, S.P. Hayes, P.P. Niiler, P.L. Richardson, and J.M. Toole, 1992: The Response of the Western Equatorial Pacific Ocean to Westerly Wind Bursts During November 1989 to January 1990. *J. Geophys. Res.*, **97**, 14,289-14,303.

McPhaden, M.J., H.P. Freitag, S.P. Hayes, B.A. Taft, Z. Chen, and K. Wyrtki, 1988: The Response of the Equatorial Pacific Ocean to a Westerly Wind Burst in May 1986. *J. Geophys. Res.*, **93**(C9), 10,589-10,603.

Meehl, G.A., G.N. Kiladis, K.M. Weickmann, M. wheeler, D.S. Gutzler, and G.P Compo, 1986: Modulation of equatorial subseasonal convective episodes by tropical-extratropical interactions in the Indian and Pacific Ocean regions. *J. Geophys. Res.*, **101**(D10), 15,033-15,049.

Meyers, G., J.R. Donguy, and R.K. Reed, 1986: Evaporative cooling of the western equatorial Pacific ocean by anomalous winds. *Nature*, **323**, 523-526.

Moore, A.M., and R. Kleeman, 1999: Stochastic Forcing of ENSO by the Intraseasonal Oscillation. *J. Climate*, **12**, 1199-1220.

Moore, D.W. and S.G.H. Philander, 1977: Modeling of the tropical oceanic circulation. In The Sea, Vol. 6, Ch. 8, Goldberg *et al.* (eds.), New York, Interscience.

Murakami, T., and W.L. Sumathipala, 1989: Westerly Bursts during the 1982/83 ENSO. *J. Climate*, **2**, 71-85.

Neelin, J.D., D.S. Battisti, A.C. Hirst, F.F. Jin, Y. Wakata, T. Yamagata, and S.E. Zebiak, 1998: ENSO theory. *J. Geophys. Res.*, **103**(C7), 14,261-14,290.

Nicholls, N., and A. Kariko, 1993: East Australian Rainfall Events: Interannual Variations, Trends and Relationship to the Southern-Oscillation. *J. Clim.*, **6**, 1141-1152.

Pacanowski, R.C., and S.G.H. Philander, 1981: Parametrizations of Vertical Mixing in Numerical Models of Tropical Oceans. *J. Phys. Oceanogr.*, **11**, 1443-1451.

Penland, C., K. Weickmann, and C. Smith, 1995: Forecasts of Pacific-Indian Ocean SST

using linear inverse modeling. *Experim. Long Lead Forecast Bull.*, **4**(2), 26-28.

Penland, C., and P.D. Sardeshmukh, 1995: The optimal growth of tropical sea surface temperature anomalies. *J. Climate*, **8**, 1999-2024.

Penland, C., and T. Magorian, 1993: Predicting Niño 3 sea surface temperature anomalies using linear inverse modeling. *J. Climate*, **6**, 1067-1076.

Philander, S.G.H., A.D. Seigel, 1985: Simulation of the El Niño of 1982-1983. *Coupled Ocean Atmosphere Models*, edited by J. Nihoul, Elsevier. 517-541.

Philander, S.G.H., W.J. Hurlin, and A.D. Seigel, 1989: Simulation of the seasonal cycle of the tropical Pacific Ocean. *J. Phys. Oceanogr.*, **17**(11), 1986-2002.

Philander, S.G.H., W.J. Hurlin, and R.C. Pacanowski, 1987: Initial Conditions for a General Circulation Model of Tropical Oceans. *J. Phys. Oceanogr.*, **17**, 147-157.

Ralph, E.A., K. Bi, P.P. Niiler, and Y. Du Penhoat, 1997: A Lagrangian Description of the Western Equatorial Pacific Response to the Wind Burst of December 1992: Heat Advection in the Warm Pool. *J. Climate*, **10**, 1706-1721.

Rasmusson, E.M., and J.M. Wallace, 1983: Meteorological aspects of the El Niño/Southern Oscillation. *Science*, **222**(4629), 1195-1202.

Rasmusson, E.M., and T.H. Carpenter, 1982: Variations in Tropical Sea Surface Temperature and Surface Wind Fields Associated with the Southern Oscillation/El Niño. *Mon. Wea. Rev.*, **110**, 354-384.

Reynolds, R.W. and T.M. Smith, 1994: Improved global sea surface temperature analyses using optimum interpolation. *J. Clim.*, **7**(6), 1195-1202.

Rui, H., and B. Wang, 1990: Development Characteristics and Dynamic Structure of Tropical Intraseasonal Convection Anomalies. *J. Atmos. Sci.*, **47**, 357-379.

Schopf, P.S., and D.E. Harrison, 1983: On oceanic Kelvin waves and El Niño, I, Influence of initial states and wave induced current and warming. *J. Phys. Oceanogr.*, **13**, 936-948.

Schopf, P.S., and M.J. Suarez, 1990: Ocean Wave Dynamics and the Time Scale of ENSO. *J. Phys. Oceanogr.*, **20**, 629-645.

Slingo, J. D.P. Rowell, K.R. Sperber, and F. Nortley, 1999: On the predictability of the interannual behavior of the Madden-Julian Oscillation and its relationship to El Niño. *Q. J. R. Meteorol. Soc.*, **125**, 583-609.

Smyth, W.D., D. Herbert, and J.N. Moum, 1996.a: Local ocean response to a multiphase westerly wind burst. 1. Dynamic response. *J. Geophys. Res.*, **101**(C10), 22,495-22,512.

Smyth, W.D., D. Herbert, and J.N. Moum, 1996.b: Local ocean response to a multiphase westerly wind burst. 1. Thermal and freshwater responses. *J. Geophys. Res.*, **101**(C10), 22,513-22,533.

Speigel, M.R., 1994: Theory and Problems of Statistics. Schaum's Outline Series, McGraw-Hill Inc.

Suarez, M.J., and P.S. Schopf, 1988: Delayed action oscillator for ENSO. *J. Atmos. Sci.*, **45**(21), 3,283-3,287.

Sui, C.H.,and K.M. Lau, 1992: Multiscale Phenomena in the Tropical Atmosphere over the Western Pacific. *Mon. Wea. Rev.*, **120**(3), 407-430.

Takayabu, Y.N., T. Iguchi, M. Kachi, A. Shibata, and H. Kanzawa, 1999: Abrupt termination of the 1997-8 El Niño in response to the Madden-Julian oscillation. *Nature*, **402**, 279-282.

Thompson, C.J., and D.S. Battisti, 2000: A Linear Stochastic Dynamical Model of ENSO, Part II: Analysis. *J. Climate*, submitted.

Tsutsui, J., and A. Kasahara, 1996: Simulated tropical cyclones usng the National Center for Atmospheric Research community climate model. *J. Geophys. Res.*, **101**(D10), 15,013-15,032.

Vecchi, G.A., and D.E. Harrison, 1997: Westerly Wind Events in the Tropical Pacific, 1986-1995; an Atlas. NOAA/PMEL Technical Memorandum.

Vecchi, G.A., and D.E. Harrison, 2000: Tropical Pacific sea surface temperature anomalies, El Niño and equatorial westerly wind events. *J. Clim.*, **13**(*in press*).

Weare, B.C., A.R. Navato, and R.E. Newell, 1976: Empirical Orthogonal Analysis of Pacific Sea Surface Temperatures. *J. Phys. Oceanogr.*, **6**, 671-678.

Webster, P.J. and R. Lukas, 1992: TOGA COARE: The Coupled Ocean-Atmosphere Response Experiment. *Bull. Amer. Meteor. Soc.*, **73**(9), 1377-1416.

Weickmann, K.M., 1991: El Niño/Southern Oscillation and the Madden-Julian (30-60 Day) Oscillations During 1981-1982. *J. Geophys. Res.*, **96**(supp.), 2,187-2,195.

Woodruff, S.D., R.J. Slutz, R.L. Jenne, and P.M. Steurer, 1987: A Comprehensive Ocean-Atmosphere Data Set. *Bull. Amer. Meteor. Soc.*, **68**, 1239-1250.

Wyrtki, K., 1975: El Niño - The Dynamic Reponse of the Equatorial Pacific Ocean to Atmospheric Forcing. *J. Phys. Oceanogr.*, **5**, 572-584.

Yu, L., and M.M. Rienecker, 1998: Evidence of extratropical atmospheric influence during the onset of the 1997-8 El Niño. *Geophys. Res. Lett.*, **18**, 3,537-3,540.

Zebiak, S.E. and M.A. Cane, 1987: A model El Niño-Southern Oscillation. *Mon. Wea. Revi.*, **115**, 2,262-2,278.

Zhang, C., 1996: Atmospheric Variability at the Surface in the Tropical Western Pacific. *J. Atmos. Sci.*, **53**(5), 739-758.

Zhang, C., 1997: Intraseasonal variability of the upper-ocean thermal structure observed at 0° and 165°E. *J. Climate*, **10**(12), 3,077-3,092.

Zwillinger, D. ed., 1996: CRC - Standard Mathematical Tables and Formulae, 30th Ed., CRC Press, 812 pp.

Appendix:
Statistical Significance Methods

In Chapter II, I used various methods to compute the significance of the statistically derived quantities. In this Appendix I describe the methods used to derive these significance statistics. For the computation of the significance of the composite anomaly winds and the significance of the correlation coefficients between SOI and number of events, I used standard statistical tests that assume our populations are normally distributed. To test the significance of the monthly distribution of the WWEs I used a bootstrap method.

A.1. Composite wind anomaly significance test

I use a Students-t test to estimate the statistical significance of the composite results, so I require the standard deviation of the zonal and meridional wind anomalies that make up each composite. In particular, I needed to know these standard deviations for every 12 hour period during the 19 days of the composite . These standard deviations were computed as follows:

$$\vec{\sigma}(x,y,t_n) = \left\{ \frac{\sum_{i=1}^{N} \left[\vec{U}(x,y,t_n) - \vec{u}(x,y,t_n + \tau_i) \right]^2}{N} \right\}^{1/2}$$

where σ is the standard deviation vector, **U**, **u**, x, y, t_n, and $\{\tau_i\}$ and N are the same as in Section II.2, and I define a vector power to be:

$$\vec{\xi} \equiv \begin{pmatrix} \xi_1 \\ \xi_2 \end{pmatrix} \Rightarrow \vec{\xi}^{\alpha} \equiv \begin{pmatrix} \xi_1^{\alpha} \\ \xi_2^{\alpha} \end{pmatrix}$$

I performed a Student's-t test (Bickel and Docksun, 1977, p.210-215) on each component of our composite vector wind anomaly field, to determine whether the true mean was distinguishable from zero, to the 99% confidence limit. I use a double sided significance test, since I are interested in wind components that are statistically significant, re-

gardless of the sign. I set the number of degrees of freedom in our test to be the number of individual events that went into generating the composite minus 1, using previous notation: N-1. According to the Student's-t test, our averages were significant to the 99% level if the following inequality was satisfied:

$$\left|\frac{\vec{U}(x,y,t_n)\cdot\hat{e}_j}{\vec{\sigma}(x,y,t_n)\cdot\hat{e}_j}\right| > \frac{t_{99.5\%,N}}{\sqrt{N-1}}$$

Where $\mathbf{U},\sigma$, x, y, t_n and N are as before; $\mathbf{e}_j$ is the unit vector in the zonal (j=1) or meridional (j=2) direction; $t_{99\%,N}$ is the double sided Student's-t coefficient at the 99% significance level for N degrees of freedom; and indicates the vector dot product operation. The values for $t_{99\%,N}$ are tabulated in most statistics or mathematical table handbooks, e.g. Speigel (1994), Zwillinger (1996).

A.2. Correlation coefficient significance test

I performed a Student's-t (Bickel and Docksun, 1977, p.220) test on our sample correlation coefficients, r, to evaluate whether the true correlation coefficient, r, approximated r was distinguishable from zero, to a prescribed significance level, l. I use a double sided significance test because I are interested in significant correlations regardless of the sign of the correlation. The following inequality had to be satisfied in this test:

$$r^2 > \frac{t_{l,N-2}^2}{N-2+t_{l,N-2}^2}$$

where $t_{l,N-2}$ is the double sided Student's-t coefficient for l significance level and for N-2 degrees of freedom. Since in our case N = 10, the threshold for 95% significance is $|r|>0.63$, and the threshold for 99% significance is $|r|>0.77$, for the zero lag correlation tests; while for the one year lagged case N=9, so the threshold for 90% significance is $|r|>0.58$, and for 95% significance $|r|>0.67$. The values for $t_{l,N-2}$ are tabulated in most statistics or mathematical table handbooks, e.g. Speigel (1994), Zwillinger (1996).

A.3. Monthly distribution significance test

I performed a bootstrap test (Efron and Tibshirani, 1991) on the monthly distribution data to find the probability, P, the "on" season I observed for each event had of occurring randomly. I then took the significance level of the seasonal distribution to be 100×(1-P) %. The probability was computed using a bootstrap method, with 100,000 bootstrap samples.

The procedure to determine the probability of N_{seas} events being distributed over a continuous L_{secs} month period on a random distribution of N events is as follows. I sample 100,000 times; at each sampling I randomly distribute the N events for the particular event type, into twelve equally likely months. I then test whether there exists a continuous period of L_{seas} months for which the total number of events randomly placed is equal to or greater to N_{seas}. I count the number of times the test turns out true in our bootstrap procedure, and define the bootstrap probability to be P = E/B; where E is the number of positive tests, and B is the number of bootstrap samples. The bootstrap probability converged for B > 1,000, but I took B = 100,000 for good measure.

A.4. Event sequencing significance test

I performed a bootstrap test (Efron and Tibshirani, 1991) to find the probability, P, the sequencing pattern I observed for each event pair had of occurring randomly. I then took the significance level of the event sequencing to be 100×(1-P) %. The probability was computed using a bootstrap method, with 10,000 bootstrap samples.

I determined the probability of distributing N_1 center days of type 1 and N_2 center days of type 2 on a ten year time axis semi-randomly, so that no two center days of the same type were within seven days of each other, and having M or more ordered pairs of events

(n_1,n_2) within three days of each other in the following manner. I sample 10,000 times, at each sampling step semi-randomly distributing N_1 and N_2 events as just described. I then test to see how many ordered pairs (n_1,n_2) are within 3 days of each other. I count the

Curriculum Vitae

Education

Ph.D. Physical Oceanography Apr.., 2000 University of Washington Seattle, WA

M.S. Applied Mathematics: Feb. 1999 University of Washington Seattle, WA

M.S. Physical Oceanography: Dec. 1996 University of Washington Seattle, WA

B.A. Mathematics: May 1994 Rutgers University New Brunswick, NJ

Professional experience

Sep. 1994 - Present Research Assistant Seattle, WA
University of Washington, School of Oceanography / Joint Institute for the Study of the Atmosphere and Oceans

- Extensive statistical analysis of large ocean and atmosphere data sets.
- Numerical modeling of the tropical Pacific, Atlantic and Indian Oceans, using a high-resolution finite difference scheme (GFDL MOM-2).

Sep. 1996 – Present Private Mathematics Tutor Seattle, WA

- Tutor high-school through college students in mathematics.

Sep. 1995 – Dec. 1995 Teaching Assistant Seattle, WA
University of Washington. Oceanography 504 – Fluid Dynamics.

- Conducted office hours and helped students.
- Graded assignments and exams.

Oct. 1993 – Sept 1994 Research Assistant New Brunswick, NJ
Institute for Marine and Coastal Sciences, Rutgers University

- Idealized numerical ocean modeling, using spectral finite element techniques.
- Developed grid generation and modification software, and grids to be used with the Rutgers Shallow Water Spectral Finite Element Model.

Summer 1993 Summer Research Fellow New Brunswick, NJ
Institute for Marine and Coastal Sciences, Rutgers University

- Awarded research fellowship for the summer.
- Idealized ocean modeling problems using a spectral finite element method.
- Developed software to ease model implementation.

Publications

Harrsion, D.E. and G.A. Vecchi (2000). El Niño and La Niña: Equatorial Pacific surface temperature and thermocline variability, 1986-98. *Geophys. Res. Lett.*, (in press).

Vecchi, G.A. and D.E. Harrison (2000). Tropical Pacific sea surface temperature anomalies, El Niño and equatorial westerly wind events. *J. Climate*, (in press).

Harrison, D.E. and G.A. Vecchi (1999). On the termination of El Niño. *Geophys. Res. Lett.* V.26 (11), 1593-7.

Vecchi, G.A. and D.E. Harrison (1997). Westerly wind events in the tropical Pacific, 1986-1995: An atlas from the ECMWF operational surface wind fields. NOAA Technical Memorandum ERL PMEL-109 (NTIS PB97-188213).

Harrison, D.E., and G.A. Vecchi (1997). Westerly wind events in the tropical Pacific, 1986-1995. *J. Climate*, V.10 (12), 3131-3156.

Conference Proceedings:

Vecchi, G.A., and D.E. Harrison (1999). Large-scale environmental associations with equatorial westerly wind events. In: Proceedings of a Conference on the TOGA coupled ocean-atmosphere response experiment (COARE). WCRP-107. WMO/TD-No. 940, pp 387-8.

Vecchi, G.A. , and D.E. Harrison (1998). Sea surface temperature and sub-surface temperature variability associated with equatorial westerly wind events. In: Proceedings from the 9th Conference on Air-Sea Interaction - American Meteorological Society.

Conference Presentations

November, 1999 - 24th Annual Climate Diagnostics Workshop.
Sub-seasonal atmospheric convection and equatorial westerly wind events.

November, 1999 - 24th Annual Climate Diagnostics Workshop.
Tropical Pacific SSTA changes, westerly wind events and El Niño.

November, 1999 - 24th Annual Climate Diagnostics Workshop.
Tropical Pacific seasonal cycle and the termination of El Niño.

August, 1998 - COARE98 Conference.
Large-scale environmental associations with equatorial westerly wind events.

January, 1998 - 9th Conference on Air-Sea Interaction (AMS).
Ocean temperature variability associated with westerly wind events.

Awards received

- NASA Space Grant Scholarship, 1994-1996.
- Cook College, Rutgers University Marine Sciences Student of the Year, 1994.

Professional memberships

- American Geophysical Union.
- American Meteorological Society.